Weighted Radon transforms and their applications

Fedor Goncharov

NNT : 2019SACLX029

THÈSE DE DOCTORAT

de

L'Université Paris-Saclay

École doctorale de mathématiques Hadamard (EDMH, ED 574)

Établissement d'inscription : École polytechnique

Laboratoire d'accueil : Centre de mathématiques appliquées de Polytechnique, UMR 7641 CNRS

Spécialité de doctorat : Mathématiques appliquées

Fedor Goncharov

Transformations de Radon pondérées et leurs applications

Date de soutenance : 15 juillet 2019

Après avis des rapporteurs : Jan BOMAN (Stockholm University)
Leonid KUNYANSKY (University of Arizona)

Jury de soutenance :

François ALOUGES	(Professeur, École polytechnique)	Président du jury
Jan BOMAN	(Professeur émérite, Stockholm University)	Rapporteur
Joonas ILMAVIRTA	(Professeur adjoint, University of Jyväskylä)	Examinateur
François JAUBERTEAU	(Professeur, Université de Nantes)	Examinateur
Leonid KUNYANSKY	(Professeur, University of Arizona)	Rapporteur
Mai NGUYEN-VERGER	(Professeur, Université de Cergy-Pontoise)	Examinatrice
Roman NOVIKOV	(Professeur, École polytechnique)	Directeur de thèse
Alexander SHANANIN	(Professeur, MIPT, MSU)	Examinateur

Weighted Radon transforms and their applications

PhD thesis of F. O. Goncharov under the supervision of R. G. Novikov
CMAP, École Polytechnique

Remerciements / Aknowledgements

First of all I want to thank Roman Novikov for his very pedagogical approach in supervising this thesis. Here the word pedagogical means a lot of things, which I don't precise, but it is obvious that managing a "fresh" master student to write articles is for sure a complicated thing. I am also very thankful for our countless discussions on mathematics, philosophy and history from which I have learned not only the research field but also got a good pile of reflections on how the world works.
I am also very thankful to all of the members of the jury who have agreed to come to my defense : François Alouges, Jan Boman, Joonas Ilmavirta, François Jauberteau, Leonid Kunyansky, Mai Nguyen-Verger, Alexander Shananin. For me it was hard to believe that we would manage to gather such professional jury from 5 different countries ! Of course, I could write a small "passage" on each member, instead I will just say that I am glad that I had met you at some points of my life and had a chance to have discussions with you.
In turn, the defense would not have happened if jury would have not been welcomed in École polytechnique. At this point I would like to thank the administration of CMAP for the hospitality and warm atmosphere : Anne de Bouard (for recommending me for this PhD position and accepting me during the "conseils du labo" when my french was not good at all), Naar Nasséra (for being so nice, so that I always preferred always to go an extra time to your office than sending emails), Alexandra Noiret (for coping with me and my jury who do not really followed the rules "comme il faut"). Additionally, thank you Alexandra for dealing with invitations, it was not easy at all !
It was very pleasant to work in my bureau because of my friends with whom we mostly did things in order not to work ! Thank you Martin for drugging me (and the whole lab) on chess, Heythem (for keeping the bureau in order and for our discussions on literature, so that you was reading russian authors and I started to read french ones), Celine (for feeding me with food intended for the PhD seminar), Juliette and Pierre (for being my personal maîtres of french language, literature and beer), Arthur (for explaining politics in France and the model of electric cars), Antoine and Hélène (for just being best friends in so many occasions), Kevish (for your stories about Mauritius Islands), Benoît (for discussions of history and future discussions of physics), Florian (for stories about trail running and football), Younes (for our math discussions), Étienne and Kuankuan (for being best and most non-trivial flat neighboors ever), Alexey (for millions of hours of discussions of mathematics, literature, philosophy and beers near the lake), Misha Isaev (for bringing me the idea to study tomography in France). I am also thankful to all members of the laboratory with whom I crossed in the cantine, seminars, football matches and evenings in Paris, I will keep these memories for a long time !

Finally, I want to thank my family : Yegor (in particular, for turning on the projector before the defense), my mother and father (for everything in my life), Marie-Christine (for providing the best paté for my "pôt de thèse"), Martine, Roger, Florent (for french-spiritual support).

However, all this work would not be possible without support of my lovely wife, her help with the french part of the thesis and, of course, her perfect dinners ! Thank you Marie-Liesse, you are the best I could ever have and I hope it won't be a second thesis !

P. S. Additionally I want to thank studio "Europacorp" of Luc Besson for financing the costume I was wearing during the defense.

Contents

Préface

Dans cette thèse, nous étudions différents aspects du problème inverse des transformations de rayon pondérées et de Radon dans les espaces euclidiens.

D'une part, nos études sont motivées par des applications des transformations de type Radon en tomographies, par exemple, en tomographie par rayons X, en tomographies d'émission (PET, SPECT), en tomographie optique, en tomographie de fluorescence et dans beaucoup d'autres domaines.

D'autre part, incidemment, nous avons obtenu des résultats surprenants sur l'injectivité et la non-injectivité pour le problème inverse mentionné ci-dessus pour une grande classe de poids et de fonctions test. Ces derniers résultats peuvent être considérés comme purement mathématiques au regard de nos résultats appliqués.

Le texte lui-même est basé sur cinq articles qui sont divisés en deux parties. Ces parties reflètent les deux pendants de la thèse - le côté orienté applications et le côté purement mathématique.

Les articles de la première partie sont les suivants :

1. Goncharov F. O., Novikov R. G., *An analog of Chang inversion formula for weighted Radon transforms in multidimensions*, EJMCA, 4(2): 23-32, 2016.
2. Goncharov F. O., *An iterative inversion of weighted Radon transforms along hyperplanes*, Inverse Problems, **33** 124 005, 2017.

Dans l'article 1, nous prouvons un résultat conceptuel qui peut s'entendre comme suit : *dans de nombreuses tomographies, les données fournies par les transformations des rayons pondérées admettent une réduction naturelle à des données fournie par des transformations de Radon pondérées (pour un autre poids) le long de plans en 3D.* Une telle réduction permet de reformuler le problème inverse d'origine pour les transformations des rayons pondérées en un autre problème inverse pour les transformations de Radon pondérées le long des hyperplans. Dans les articles 1, 2, nous développons plus avant cette idée et présentons deux nouvelles méthodes d'inversion des transformations de Radon pondérées en trois dimensions. Le résumé détaillé de nos résultats de la partie I avec expériences numériques est donné dans la sous-section 4.1 du chapitre 1. Les articles 1 et 2 sont présentés dans les chapitres 3 et 4.

Les articles de la deuxième partie sont les suivants :

3. Goncharov F. O., Novikov R. G., *An example of non-uniqueness for the weighted Radon transforms along hyperplanes in multidimensions*, Inverse Problems **34** 054001, 2018.
4. Goncharov F. O., Novikov R. G., *An example of non-uniqueness for Radon transforms with continuous positive rotation invariant weights*, Journal of Geometric Analysis 25(4): 3807-3828, 2018.
5. Goncharov F. O., Novikov R. G., *A breakdown of injectivity for weighted ray transforms in multidimensions*, (to appear) Arkiv för Matematik, hal-01635188v3, 2019

Dans les articles 3-5, nous donnons quelques contre-exemples de l'injectivité pour les transformations des rayons pondérées et de Radon en multidimensions. Bien sûr, un contre-exemple à l'injectivité pour ces transformations n'aide pas à résoudre directement un problème inverse particulier. Mais elle aide à mieux comprendre les limites de l'applicabilité des méthodes mathématiques et numériques pour résoudre ces problèmes. Un contre-exemple à l'injectivité est intéressant s'il semble "proche" d'un cas où une transformation de type Radon

devient injective. C'est le cas avec nos résultats. Dans la sous-section 4.2 du chapitre 1 nous donnons un résumé des contributions données par nos contre-exemples. Les articles 3-5 se trouvent dans les chapitres 5-7 de la partie II de la thèse.

Preface

In this thesis we study different aspects of the inverse problem for weighted ray and Radon transforms in Euclidean spaces.

On one hand, our studies are motivated by applications of Radon-type transforms in tomographies, for example, in X-ray tomography, emission tomographies (PET, SPECT), optical tomography, flourescence tomography and in many others.

On the other hand, by chance, we have obtained some surprising results on injectivity and non-injectivity for the aforementioned inverse problem for a large class of weights and test-functions. The latter results can be considered as purely mathematical in view of our applied-oriented results.

The text itself is based on five articles which are splitted in two parts. These parts reflect the two sides of the thesis – applications-oriented side and purely mathematical side.

The articles of the first part are the following:

1. Goncharov F. O., Novikov R. G., *An analog of Chang inversion formula for weighted Radon transforms in multidimensions*, EJMCA, 4(2): 23-32, 2016.
2. Goncharov F. O., *An iterative inversion of weighted Radon transforms along hyperplanes*, Inverse Problems, **33** 124 005, 2017.

In Article 1 we prove a conceptual result which may sound as follows: *in many tomographies the data given by weighted ray transforms admits a natural reduction to a data given by weighted Radon transforms (for another weight) along planes in 3D.* Such a reduction allows to reformulate the original inverse problem for weighted ray transforms to another inverse problem for weighted Radon transforms along hyperplanes. In Articles 1, 2 we develop further this idea and present two new methods for inversion of weighted Radon transforms in three-dimensions. The detailed resume of our results from Part I with numerical experiments is given in Subsection 4.1 of Chapter 2. Articles 1, 2 are presented in Chapters 3, 4.

The articles of the second part are the following:

3. Goncharov F. O., Novikov R. G., *An example of non-uniqueness for the weighted Radon transforms along hyperplanes in multidimensions*, Inverse Problems **34** 054001, 2018.
4. Goncharov F. O., Novikov R. G., *An example of non-uniqueness for Radon transforms with continuous positive rotation invariant weights*, Journal of Geometric Analysis 25(4): 3807-3828, 2018.
5. Goncharov F. O., Novikov R. G., *A breakdown of injectivity for weighted ray transforms in multidimensions*, (to appear) Arkiv för Matematik, hal-01635188v3, 2019

In Articles 3-5 we give some counterexamples to injectivity for weighted ray and Radon transforms in multidimensions. Of course, a counterexample to injectivity for these transforms does not help to solve directly a particular inverse problem. But, at the same time, it helps to understand better the limits of applicability of mathematical and numerical methods for solving these problems. A counterexample to injectivity is interesting if it appears to be "close" to a case when a Radon-type transform becomes injective. This is what happened to our results. In Subsection 4.2 of Chapter 2 we give resume of the contributions given by our counterexamples. Articles 3-5 are given in Chapters 5-7 of Part II of the thesis.

Introduction (en français)

1 Un intermède historique à la transformation de type Radon

Два чувства дивно близки нам —
В них обретает сердце пищу —
Любовь к родному пепелищу,
Любовь к отеческим гробам.

А. С. Пушкин (Pouchkine), 1830

Dans cette section, nous donnons un court aperçu historique de la suite d'événements qui mène au développement des transformations de type Radon. Nous croyons que cette suite a sa propre esthétique et peut bien servir d'introduction au contenu de cette thèse.

1.1 L'héritage de Minkowski-Funk-Radon

Les premiers résultats de ce que nous appelons maintenant les "transformations de type Radon" datent du début du 20ème siècle et apparoussent les publications de Hermann Minkowski [Mi04], Paul Funk [Fu13] et Johann Radon [Ra17]. En particulier, chacun de ces mathématiciens a examiné un problème géométrique conduisant à des considérations de transformations intégrales correspondantes. Celles-ci se sont finalement révélées fondamentales dans de nombreux domaines des mathématiques pures et appliquées.

[1]Par exemple, le travail original de Minkowski était lié à un problème de géométrie convexe dans lequel l'auteur a étudié des objets appelés *les corps de largeur constante*. De nos jours, le résultat de ce travail est aussi connu sous le nom de Théorème de Minkowski qui dit que *les corps de circonférence constante sont des corps de largeur constante*. Dans sa preuve Minkowski, en particulier, a utilisé la formule suivante

$$Mf(\theta) = \int\limits_{\mathbb{S}^2 \cap \Sigma(\theta)} f(\sigma)\, d\sigma,\ \theta \in \mathbb{S}^2, \tag{1.1}$$

où $\Sigma(\theta) = \{x \in \mathbb{R}^3 : x \cdot \theta = 0\}$, $d\sigma$ est une mesure de longueur uniforme sur $\mathbb{S}^2$ et f est une fonction sur $\mathbb{S}^2$. De la formule (1.1) on peut voir que les intégration sont été realisées sur de grands cercles de $\mathbb{S}^2$ et, en fait, les deux fonctions f, Mf, n'étaient pas arbitraires et avaient un sens géométrique spécifique ; voir [Mi04] pour les détails. Ainsi, il était encore trop tôt

[1]Dans cette partie de l'exposition sur P. Funk et H. Minkowski nous avons utilisé, en particulier, un sympathique article [Da10].

pour parler de M comme d'une transformation intégrale jusqu'à l'œuvre de P. Funk en 1913. Désigné par son encadrant de thèse, David Hilbert, pour examiner le travail de Minkowski, Paul Funk a considéré le problème suivant :

$$\text{reconstruire la fonction } f \text{ sur } \mathbb{S}^2 \text{ à partir de ses intégrales } Mf \text{ définies dans (1.1).} \quad (1.2)$$

Une telle formulation a évidemment fait apparaître M comme une transformation des fonctions sur $\mathbb{S}^2$ et elle a été étudiée par Funk dans sa thèse de doctorat et dans sa publication ultérieure [Fu13]. En particulier, une des applications de M présentées dans [Fu13] était une dérivation simple et élégante du théorème de Minkowski. De nos jours, la transformation M avec ses généralisations à des dimensions plus élevées est connue sous le nom de transformation de Funk-Minkowski et elle est utilisée, par exemple, en géométrie convexe et intégrale, en analyse harmonique, en équations différentielles et dans certains domaines connexes des mathématiques appliquées, par exemple, en tomographie photo-acoustique (PAT) ; voir [Ka18] et ses références.

[2]Après les travaux de Minkowski et Funk, le mathématicien autrichien Johann Radon, motivé par des applications en physique mathématique, a considéré un problème similaire :

$$\begin{array}{l}\text{reconstruire la fonction } f \text{ sur } \mathbb{R}^2 \text{ à partir de ses intégrales}\\ \text{le long de toutes les droites dans } \mathbb{R}^2.\end{array} \quad (1.3)$$

En d'autres termes, Radon a étudié l'inversion de la transformation R donnée par la formule suivante[3] :

$$Rf(s,\theta) = \int_{-\infty}^{+\infty} f(s\theta + t\theta^{\perp})\, dt,\ s \in \mathbb{R},\ \theta = (\cos\varphi, \sin\varphi) \in \mathbb{S}^2,\ \varphi \in [0, 2\pi], \quad (1.4)$$

où $\theta^{\perp} = (-\sin\varphi, \cos\varphi)$ et où la fonction f est suffisamment régulière sur $\mathbb{R}^2$ avec une décroissance adéquate à l'infini. Dans son travail, Radon a résolu le problème (1.3) en proposant des formules d'inversion analytiques exactes pour R^{-1} qui sont maintenant connues sous le nom de *formules d'inversion classiques de Radon* ; voir [Ra17] pour les détails. Par ailleurs, outre les formules d'inversion, Radon a proposé la généralisation suivante de (1.2) et (1.3) :

$$\begin{array}{l}\text{reconstruire la fonction } f \text{ sur une surface } S \text{ à partir}\\ \text{de ses intégrales sur une famille de courbes } C \text{ sur } S.\end{array} \quad (1.5)$$

Dans les considérations de Funk et Minkowski la surface S était la sphère $\mathbb{S}^2$ et les courbes C étaient des géodésiques (ou, également, des grands cercles). De même, dans les considérations de Radon, les courbes C étaient les géodésiques mais sur le plan $\mathbb{R}^2$. Une autre direction proposée était d'envisager des généralisations de R à partir de (1.4) en dimension plus élevée[4], où les intégrations seraient prises le long des hyperplans de $\mathbb{R}^d$, $d > 2$. Cela était donc une étape philosophique importante : passer des considérations particulières de Minkowski en

[2]Il y a aussi une remarque de Bockwinkel [Bo06], disant qu'une transformation de l'intégration d'une fonction sur $\mathbb{R}^3$ sur des plans bidimensionnels était déjà connue de H. Lorentz. En outre, il est attesté que Lorentz avait une formule d'inversion pour cette transformation dans ses notes de cours.

[3]Ici nous présentons les transformations de Funk-Minkowski et de Radon comme deux applications différentes. Mais, en fait, les deux sont des versions différentes de la *transformation projective de Radon* ; voir [G+03].

[4]Dans le travail original de Radon, l'auteur dérive aussi des formules d'inversion exactes pour toute dimension $d \geq 2$, quand les intégrations sont prises le long des hyperplans.

géométrie convexe à une volonté d'étudier une toute nouvelle classe de transformations de type intégral que nous appelons maintenant - transformations de type Radon.

Il est intéressant de noter que l'article [Ra17], considéré comme central, le plus honoré aujourd'hui par les spécialistes dans de nombreux domaines des mathématiques pures et appliquées, ne semblait pas être si important pour Radon lui-même ; voir aussi [RaSch18]. En particulier, dans la nécrologie de son collègue Paul Funk au professeur Radon [Fu13a], l'auteur a mentionné des réalisations mathématiques exceptionnelles de Radon (nombres de Radon, Théorème de Radon-Nykodim, Théorème de Radon-Riesz) mais ignoré la transformation de Radon. Cela n'a rien d'étonnant, puisqu'au début du XXe siècle, il n'y avait pas d'idées d'application des transformations de Radon et, du point de vue mathématique, ces résultats n'étaient pas considérés comme une avancée capitale.

Néanmoins, le développement mathématique de ces transformations s'est poursuivi. En 1927, le mathématicien allemand Philomena Mader a publié de nouvelles formules d'inversion pour R^{-1} en dimensions $d \geq 2$; voir [Ma27]. Un travail très important a été fait par Fritz John dans son livre [Jo55], où il a appliqué la transformation de Radon pour construire des solutions pour les problèmes de Cauchy pour les équations hyperboliques et elliptiques aux dérivées partielles. Les formules résultantes étaient basées sur la décomposition des fonctions en ondes planes, mais contrairement à la "méthode de Fourier", des intégrales planes au sens de J. Radon ont été utilisées. De plus, il semble aussi que F. John ait été le premier à proposer d'appeler les transformations intégrales "transformations de Radon" ; voir p.2 dans l'Introduction de [Jo55]. Entre les années 60 et 70, grâce aux travaux d'Israel Gelfand et de ses co-auteurs, de Harish-Chandra et de Sigurdur Helgason, les transformations de Radon ont commencé à apparaître dans les études des fonctions généralisées, la théorie de la représentation des groupes de Lie et en analyse harmonique ; voir [G+59], [G+69], [G+62], [HC58], [HC58a], [He65], [He65a], [He66], [He70]. La philosophie de ces études consiste en une approche théorique de groupe à la transformation de Radon où elle est définie comme une application entre une paire d'espaces homogènes pour un certain groupe de Lie G qui admet ce qui est appelé *une double fibration*. Cette approche a également été généralisée par Gelfand et son école pour le cas des variétés sans action d'un groupe de Lie mais avec une structure de double fibration. Une très bonne référence sur les transformations de Radon qui suit cette approche est un livre de Sigurdur Helgason [He99].

Le but des références données ci-dessus est d'expliquer l'intérêt grandissant pour les transformations de type Radon chez les mathématiciens. Partant d'exemples très concrets à l'origine les transformations ont très vite été étudiées d'un point de vue beaucoup plus général à l'aide nombreuses théories modernes. Cependant, ce n'est qu'une facette de l'histoire. Les mathématiques contiennent une quantité énorme de beaux résultats et du récit de leur découvertes, et dans ce sens, les transformations de Radon ne sont pas uniques. Nous aurions pu continuer ici l'exposition du développement mathématique de la transformation de Radon jusqu'à nos jours (ce qui ne serait pas facile non plus), mais il y aurait une faille chronologique. La raison en est une série de redécouvertes inattendues de ces derniers dans des domaines complètement nouveaux dont nous parlons dans la sous-section suivante.

1.2 Redécouvertes, les Beatles et le prix Nobel

Bien que les transformations de Radon aient été connues de nombreux mathematiciens dans les années 50 du siècle dernier, elles ont émergé de manière inattendues dans un tout nouveau domaine d'application – la tomographie assistée par ordinateur.

Le résultat pionnier appartient ici à un physicien sud-africain et américain Allan MacLeod

Cormack[5]. Dans les années 1950, il était chargé de cours au département de physique de l'Université du Cap et il menait également ses propres recherches en physique nucléaire. En fait, comme Cormack l'a décrit lui-même [Co80a], le travail à l'Université du Cap à cette époque était assez solitaire puisqu'il y avait très peu de physiciens nucléaires dans le pays. À la fin de 1955, en raison de la démission d'un physicien hospitalier local, Cormack s'est vu proposé de prendre sa place dans le département de radiologie jusqu'à ce qu'un nouveau spécialiste soit trouvé. Selon les lois sud-africaines, seule une personne qualifiée pouvait donner l'autorisation d'utiliser des isotopes radioactifs sur les patients et, par chance, Cormack semblait être la seule personne de l'université à manipuler de tels isotopes. Travaillant quelques heures par semaine pendant six mois à l'hôpital Groot Schurr, il a eu l'occasion de voir des procédures diagnostiques et radiologiques.

En particulier, l'un des problèmes importants pour les médecins était de contrôler la quantité de radiations délivrées à un patient en utilisant une telle procédure. Encore une fois, d'après les souvenirs de Cormack [Co80a], les pratiques de l'époque étaient plutôt grossières, il était donc nécessaire d'améliorer ces procédures. Pour mieux contrôler la dose de rayonnement délivrée, il faut au moins connaître les valeurs d'atténuation des tissus dans les régions traversées par les rayons X. Le problème initial considéré par Cormack était donc de reconstruire l'application d'atténuation à l'aide de radiographies.

En 1956, la loi exponentielle d'atténuation dans les milieux homogènes (la loi de Beer) était connue depuis près de 60 ans déjà. Ayant cela à l'esprit et remarquant que les tissus sont caractérisés par leur atténuation, Cormack a rapidement compris que le problème était en fait mathématique.

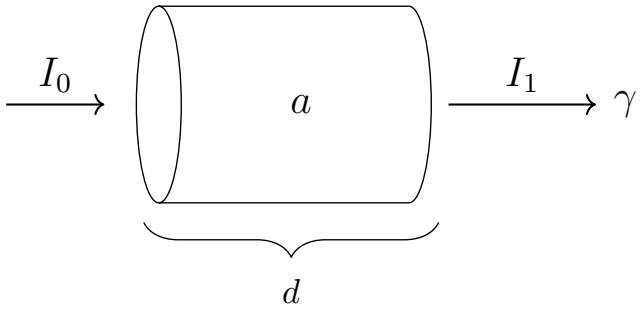

Figure 1.1 Loi d'atténuation de Beer

La loi d'atténuation de Beer a la forme suivante : si un rayon d'intensité I_0 est émis dans une région de longueur d avec atténuation constante a, alors l'intensité du rayon à la sortie I_1 est donnée par la formule (voir la figure 1.1)

$$I_1 = I_0 e^{-d \cdot a}. \tag{1.6}$$

D'après (1.6) il est évident que pour les milieux hétérogènes avec atténuation $a = a(x)$, $x \in \mathbb{R}^2$, les intensités I_0, I_1 seront liées par la formule suivante :

$$I_1 = I_0 \exp\left(- \int_\gamma a(x)\, dx \right), \tag{1.7}$$

où l'élément dx désigne la mesure de Lebesgue uniforme le long du rayon γ. Ayant obtenu

[5]Dans cette partie de l'exposition, nous nous référons principalement à ses notes biographiques [Co80], [Co80a] et à ses publications phares [Co63], [Co64] sur la tomographie assistée par ordinateur.

la formule (1.7), Cormack a réduit le problème de reconstruction de $a = a(x)$ au suivant :

reconstruire la fonction $a = a(x)$ sur $\mathbb{R}^2$ à partir de ses intégrales Pa, avec

$$Pa(\gamma) \stackrel{\text{def}}{=} \int_\gamma a(x)\,dx, \text{ où } \gamma \text{ est un rayon sur } \mathbb{R}^2; \tag{1.8}$$

de plus, il est supposé que a est à support dans le domaine fixe ouvert délimité D.

Bien que les transitions de (1.6) à (1.8) puissent sembler assez naturelles au lecteur, ce n'était pas le cas au moment des événements. En particulier, dans ses notes sur la tomographie assistée par ordinateur [Co80], [Co80a], Cormack a fait remarquer qu'il ne trouvait la formule (1.7) dans aucune des références à sa disposition. Il a également consulté des mathématiciens du Cap, des États-Unis et du Royaume-Uni pour voir si le problème (1.8) était déjà résolu.

Notez que le problème (1.8) était exactement le même que (1.3) considéré par Radon en 1917 ! Cependant, la motivation de A. Cormack était complètement différente de celle de Radon : l'application $a = a(x)$ était le coefficient d'atténuation des tissus, les rayons γ représentaient les trajectoires de propagation des rayons gamma émis et, finalement, le "domaine fixe" D était une tranche d'une région dans laquelle la "procédure d'analyse" devait avoir lieu. Quelle chance de trouver le même problème, mais dans un domaine complètement différent !

Malheureusement ou heureusement pour Cormack, il n'a pas réussi à trouver des résultats mathématiques déjà existants sur ce problème, il a alors cherché à résoudre (1.8) lui-même. Et une solution a été trouvée et publiée dans [Co63], [Co64]. La solution de Cormack était différente de celle de J. Radon, en particulier, dans son approche du problème[6]. Pour résumer, il a décomposé la fonction a en une série de composantes radiales et angulaires et a établi leurs relations avec Pa à partir de (1.8) ; pour les détails, voir [Co63]. En outre, pour cette publication, Cormack, avec ses collègues, a réalisé la premiere véritable expérience tomographique sur un modèle synthétique à symétrie sphérique de bois et d'aluminium. Les résultats de la reconstruction ont montré la précision de sa méthode. Dans la publication suivante [Co64], Cormack a modifié certaines de ses formules d'inversion et a également présenté de nouveaux résultats numériques pour une expérience plus élaborée sur un modèle synthetique non sphérique. Les résultats étaient encore une fois très prometteurs, de sorte que d'autres tentatives ont été faites pour intéresser les physiciens hospitaliers à sa méthode. Malheureusement, comme Cormack l'a lui-même fait remarquer, ses résultats ont suscité très peu d'intérêt jusqu'en 1971, année où un premier scanner tomographique commercial est apparu sur le marché. Alors comment a-t-il pu apparaître si ce n'est pas par l'intermédiaire des travaux de A. Cormack ?

La raison en était un travail remarquable et indépendant d'une autre personne – Ingénieur électricien britannique, Sir Godfrey Newbold Hounsfield[7].

Après la Seconde Guerre mondiale, au cours de laquelle Hounsfield a servi dans l'armée de l'air britannique comme instructeur en mécanique radar, et avec l'aide de contacts établis lors de son service militaire, il a obtenu une bourse pour étudier au Faraday House Electrical Engineering College à Londres ; voir [Ho80], [Pi19]. Après y avoir obtenu son diplôme, il a travaillé chez Electronic and Musical Industries (EMI, Ltd.) dans le Middlesex où il

[6]Si on regarde attentivement [Co63] on constate que l'auteur a obtenu à un moment donné une version de la formule de J. Radon (formule (26) dans le texte original) qui ne donne une reconstruction exacte que pour les fonctions symétriques sphériques. En particulier, dans [Ra17] cela a été utilisé pour obtenir la formule d'inversion pour des fonctions arbitraires, mais cet argument était absent du travail de Cormack.

[7]Godfrey Hounsfield a été fait chevalier en 1981.

développait des systèmes d'armes téléguidées et des radars. Puis, après un certain temps, il s'est intéressé à la conception d'ordinateurs qui en étaient à leurs premiers balbutiements à l'époque. Par exemple, on compte au nombre de ses réalisations au sein de l'EMI le premier ordinateur britannique tout transistors – EMIDEC 1100.

L'entreprise avait confiance en ses capacités créatives et après l'échec d'un projet pour des raisons commerciales, on lui a proposé de choisir un nouveau projet de recherche en fonction de ses propres goûts. Notons qu'il est surprenant qu'une entreprise investisse de l'argent dans la recherche pure.

Comme son nom l'indique, EMI ne produisait et ne vendait pas seulement des équipements électroniques (tels que des équipements de télévision, des radars ou des ordinateurs), mais était en fait une société d'enregistrement musical ; voir [EMI]. Parmi les stars de la musique qui ont été enregistrées à EMI, on peut citer : *Frank Sinatra*, *Nat King Cole*, *Peggy Lee*, *Adam Faith*, *Frankie Vaughan*, *Alma Cogan* et enfin *Les Beatles*. En 1963, le premier single des Beatles 'Love Me Do' n'était classé qu'au 17e rang des palmarès britanniques, mais le suivant 'Please, Please Me' est rapidement devenu deuxième et cela a complètement changé le monde de la musique. La période suivante dans le monde de la musique est connue sous le nom de 'Beatlemania'[8] et dans l'histoire, il n'y a pas d'équivalent de tels succès. Évidemment, ce succès a fait d'EMI une entreprise extrèmement riche qui avait assez d'argent pour investir dans des projets de recherche audacieux. C'est le cas pour un de ces projets accordé à Hounsfield ; voir [Pi19] pour plus de détails.

D'après les souvenirs de G. Hounsfield [Ho80], durant la période de travail sur 'Sergeant Pepper's Lonely Heart's Club Band' des Beatles, de manière inattendue, il a eu l'idée suivante :

> si le principe des radars est de les placer au centre de la région
> d'intérêt et d'analyser la périphérie, pourquoi ne pas essayer d'inverser ce modèle ?
> Simplement, pour reconstruire la partie intérieure d'un objet inconnu, (1.9)
> par exemple, d'une boîte tridimensionnelle en utilisant uniquement
> des mesures extérieures.

Développant cette idée, il a décidé d'utiliser des rayons X et de considérer le modèle d'atténuation de la même manière que Cormack dans (1.8). Hounsfield ne connaissant pas les œuvres de Radon et Cormack, il s'agissait encore une fois d'une nouvelle redécouverte indépendante des transformations de Radon ! La solution du problème de Hounsfield (1.8), publiée en 1971 dans son brevet [Ho71], était très simple et correspondait parfaitement à l'esprit d'un ingénieur de talent.

[8] De 1963, et au cours des huit années suivantes Les Beatles ont enregistré et sorti des albums tels que : 'Sergent Peppers Lonely Hearts Club Band', 'Rubber Soul', 'Abbey Road' et 'The While Album'.

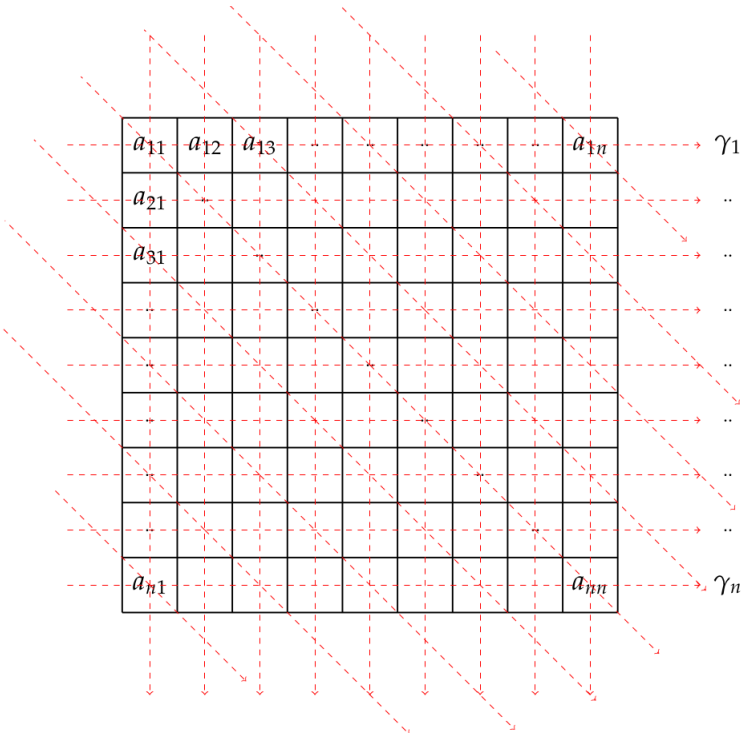

Figure 1.2 Idée de Hounsfield pour résoudre le problème (1.8)

Hounsfield a compris qu'en pratique, il fallait seulement considerer une image plane d'atténuation $a = a(x)$. Parce qu'une image n'est qu'un tableau bidimensionnel de pixels, alors la fonction a pouvait être supposée localement constante dans chaque pixel avec les valeurs correspondantes $\{a_{ij}\}_{i,j=1}^n$; voir la figure 1.2. Dans ce modèle, la formule pour Pa de (1.8) se réduit à la suivante :

$$Pa(\gamma) = \sum_{i,j=1}^{n} a_{ij} L_{ij}(\gamma), \tag{1.10}$$

où $L_{ij}(\gamma)$ sont les longueurs des intersections de rayon γ avec les cellules de pixels ; voir la figure 1.2. La formule (1.10) peut être vue comme une équation linéaire sur les coefficients $\{a_{ij}\}_{i,j=1}^n$ qui sont inconnus. Donc, en prenant suffisamment de rayons différents pour le modèle (1.10) on obtient un système linéaire d'équations résoluble sur $\{a_{ij}\}$. Cette idée simple et naturelle a été mise en pratique par Hounsfield et, plus tard, publiée sous forme de brevet. Fait intéressant, A. Cormack, dans l'introduction de son article original [Co63], a également considéré l'équation (1.10), mais il n'a pas vu l'argument selon lequel il suffisait de prendre suffisamment de rayons différents pour composer un système complet d'équations[9].

Des tests sur des cerveaux d'animaux[10] ont montré que la méthode de Hounsfield fonctionnait et de nouveaux tests cliniques sur des êtres humains étaient nécessaires. En 1971, le premier prototype, appelé scanner cérébral EMI, a été installé à l'hôpital Morley d'Atkinson et le premier patient a été examiné le 1er octobre 1971. Le processus d'examen ne prenait que 4,5 minutes pour les mesures et 20 secondes pour la reconstruction. Les images produites

[9]En fait, G. Hounsfield a pris plus de rayons dans (1.10) que le nombre de coefficients $\{a_{ij}\}$. Ce faisant, il a obtenu un système linéaire surdéterminé d'équations $Aa = Pa$, où A est une matrice de taille $N \times n^2$, $N > n^2$. Un tel système a été résolu dans le sens des moindres carrés $A^T A = A^T Pa$, ce qui correspond à la minimisation en norme ℓ_2 de l'erreur $\varepsilon(a) = \|Aa - Pa\|_2^2$. Cette approche est tout à fait naturelle pour réduire l'impact des erreurs de mesure.

[10]Les premières expériences ont été effectuées sur des cerveaux de taureau que G. Hounsfield achetait lui-même dans une boucherie à Londres ; voir [Pi19] et ses références.

avaient une résolution de 80 x 80 pixels et c'était déjà un résultat révolutionnaire pour les diagnostics radiologiques. Après quelques présentations de ces résultats lors de conférences (qui se sont terminées par des ovations [Pi19]), un grand nombre de mathématiciens, médecins et ingénieurs ont participé au développement de méthodes et d'appareils pour la reconstruction tomographique par rayons X. En deux ans, la résolution avait déjà atteint 320 x 320 pixels et les scanners ont maintenant une résolution d'environ 2048 x 2048 pixels.

Enfin, en 1979, A. Cormack et G. Hounsfield ont tous deux reçu le prix Nobel de physiologie et de médecine et il est à noter qu'ils ne se sont rencontrés que lors de cette cérémonie ; voir aussi [Ag14]. En outre, au moment de l'attribution du prix Nobel, les travaux de Radon et de Cormack étaient déjà concordants et maintenant il est reconnu le travail de Radon dans les tomographies basées sur les inversions des transformations du type Radon fut pionnier.

1.3 Remarques finales

Après l'invention de la tomographie informatisée, l'intérêt pour les transformations de type Radon a été renouvelé. Bien que les premières applications des transformations de Radon aient été en médecine, leur succès a inspiré l'application de techniques similaires dans d'autres domaines appliqués. Par exemple, les transformations de Radon et leurs généralisations sont maintenant utilisées en médecine, en optique, en géophysique, en astronomie, en économie et dans d'autres domaines appliqués ; voir [Br56], [Na86], [De07], [Ku14], [HeSh90], [Ag+18]. [Qu80], [Qu06], [Na86], [BQ87], [No02], [Il16], [RaSch18] et leurs références. En particulier, parmi les exemples de transformations de type Radon, certaines d'entre elles s'appellent *transformations de Radon pondérées* (ou *transformations de Radon généralisées*[11]) et sont aussi l'objet central de ce travail ; voir par exemple, [Qu80], [Be84].

Dans la section suivante nous définissons avec précision les transformations de Radon pondérées et donnons des références à des résultats déjà classiques.

2 Préliminaires pour les transformations de type Radon pondérées

Définition 1. *La transformation de Radon pondérée n-dimensionnelle* $R_W^{d,n}$ est définie par

$$R_W^{d,n} f(P) = \int_P f(x) W(x,P)\, dx,\ P \in \mathcal{P}^{d,n},\ 1 \le n < d, \tag{1.11}$$

où $W(x,P)$ est *le poids*, $f = f(x)$ est *une fonction test* sur $\mathbb{R}^d$,

$$\begin{aligned} &\mathcal{P}^{d,n} \text{ la variété de tous les plans orientés } n\text{-dimensionels dans } \mathbb{R}^d, \\ &\dim \mathcal{P}^{d,n} = (n+1)(d-n). \end{aligned} \tag{1.12}$$

Dans la formule (1.11), l'élément dx désigne la mesure de Lebesgue uniforme sur $P \in \mathcal{P}^{d,n}$. Pour f et W nous supposons que

$$f \text{ est continue et à support compact sur } \mathbb{R}^d, \tag{1.13}$$

$$W \text{ est à valeurs réelles, } W \ge c > 0,\ W \in L^\infty_{\text{loc}}(Z), \tag{1.14}$$

[11] Néanmoins, le terme *transformations de Radon généralisées* est souvent utilisé dans un contexte plus général, y compris les transformations de Radon non abeliennes [No02a] et les transformations de Radon le long des courbes sur des variétés pas nécessairement plates [Ku06], [Ba05], [Ba09], [Pa+12], [Gu+16]. Dans notre travail, nous n'avons pas étudié ce cas, ainsi nous utiliserons toujours le terme *transformations de Radon pondérées*.

où c est une constante, Z est une sous-variété fermée de $\mathbb{R}^d \times \mathcal{P}^{d,n}$ définie par

$$Z = \{(x, P) \in \mathbb{R}^d \times \mathcal{P}^{d,n} : \text{ le point } x \text{ appartient géometriquement au plan } P\}. \quad (1.15)$$

Dans la définition ci-dessus, nous ne détaillons pas la structure des variétés $\mathcal{P}^{d,n}$ et Z sauf deux cas $n \in \{1,\ d-1\}$; pour plus de détails voir, par exemple, [He99], [Fr89]. C'est parce que nous sommes principalement intéressés par des études de $R_W^{d,n}$ seulement pour ces deux cas. Pour tout n différent de $\{1,\ d-1\}$ nous spécifierons $\mathcal{P}^{d,n}$ et Z, où cela sera nécessaire.

Considérant la définition 1 pour $n = \{1, d-1\}$ on peut la réécrire comme suit.

Définition 2. Soit f une fonction continue à support compact sur $\mathbb{R}^d$ et (un poids) W une fonction sur $\mathbb{R}^d \times \mathbb{S}^{d-1}$ (i.e., $W = W(x, \theta)$) satisfaisant (1.14) avec $\mathbb{R}^d \times \mathbb{S}^{d-1}$ au lieu de Z. Alors, on désigne par *transformation de Radon pondérée de f pour le poids W*, la fonction suivante

$$R_W f(s, \theta) = \int\limits_{x\theta=s} f(x)W(x, \theta)\, dx,\ (s, \theta) \in \mathbb{R} \times \mathbb{S}^{d-1}, \quad (1.16)$$

où l'intégrale ci-dessus est prise au sens de Lebesgue uniforme sur l'hyperplan $\{x \in \mathbb{R}^d : x\theta = s\}$.

Définition 3. Soit f une fonction continue à support compact sur $\mathbb{R}^d$ et W une fonction sur $\mathbb{R}^d \times \mathbb{S}^{d-1}$ (i.e., $W = W(x, \theta)$) satisfaisant (1.14) avec $\mathbb{R}^d \times \mathbb{S}^{d-1}$ au lieu de Z. Alors, on désigne par *transformation des rayons pondérée de f pour le poids W*, la fonction suivante

$$P_W f(x, \theta) = \int\limits_{-\infty}^{+\infty} f(x + t\theta)W(x + t\theta, \theta)\, dt,\ (x, \theta) \in T\mathbb{S}^{d-1}, \quad (1.17)$$

où $T\mathbb{S}^{d-1}$ est la fibration tangente de la sphère unitaire $\mathbb{S}^{d-1}$ et est définie par

$$T\mathbb{S}^{d-1} = \{(x, \theta) \in \mathbb{R}^d \times \mathbb{S}^{d-1} : x\theta = 0\}. \quad (1.18)$$

Dans les définitions ci-dessus, la continuité de f n'est pas essentielle, et pour chaque cas particulier, nous préciserons la régularité des fonctions test considérées.

Notons que les définitions 2, 3 correspondent à la définition 1 pour $n = d-1$ et $n = 1$, respectivement. En effet, pour $n = d-1$ les intégrales dans (1.11) sont effectuées le long d'hyperplans orientés dans $\mathbb{R}^d$, exactement comme dans (1.16). Les variétés $\mathcal{P}^{d,1}$ et Z de (1.12), (1.15), sont isomorphes à $\mathbb{R} \times \mathbb{S}^{d-1}, \mathbb{R}^d \times \mathbb{S}^{d-1}$ respectivement, où

$$\begin{aligned} &(s, \theta) \in \mathbb{R} \times \mathbb{S}^{d-1} \text{ correspond à l'hyperplan } \{x \in \mathbb{R}^d : x\theta = s\}, \text{ où} \\ &\text{la normale } \theta \in \mathbb{S}^{d-1} \text{ donne l'orientation;} \end{aligned} \quad (1.19)$$

$$(x, \theta) \in \mathbb{R}^d \times \mathbb{S}^{d-1} \text{ correspond à } (x, (x\theta, \theta)) \in Z \text{ de (1.15) pour } n = d-1. \quad (1.20)$$

Pour $n = 1$ les intégrales dans (1.11) sont effectuées le long des rayons (lignes droites orientées) dans $\mathbb{R}^d$ comme dans (1.17). Les variétés $\mathcal{P}^{d,1}$ et Z de (1.12), (1.15) sont isomorphes à $T\mathbb{S}^{d-1}$, $\mathbb{R}^d \times \mathbb{S}^{d-1}$, respectivement, où

$$\begin{aligned} &(x, \theta) \in T\mathbb{S}^{d-1} \text{ correspond au rayon } \gamma(x, \theta) = \{y \in \mathbb{R}^d : y = x + t\theta,\ t \in \mathbb{R}\}, \\ &\theta \in \mathbb{S}^{d-1} \text{ donne l'orientation au rayon;} \end{aligned} \quad (1.21)$$

$$(x, \theta) \in \mathbb{R}^d \times \mathbb{S}^{d-1} \text{ correspond à } (x, (x - (x\theta)\theta, \theta)) \in Z \text{ de (1.15) pour } d = 1. \quad (1.22)$$

Notons également que en dimension $d = 2$ les transformations P_W et R_W sont équivalentes au changement de variables près :

$$\begin{aligned} &\mathbb{R} \times \mathbb{S}^1 \to T\mathbb{S}^1 : (s, \theta) \mapsto (s\theta, \theta^\perp), \\ &\theta = (\theta_1, \theta_2),\ \theta^\perp = (-\theta_2, \theta_1). \end{aligned} \quad (1.23)$$

Les transformations P_W, R_W, et certaines de leurs généralisations apparaissent dans de nombreux domaines des mathématiques pures et appliquées. Par exemple, elles apparaissent dans les études de groupes ([G+59], [G+62], [HC58a], [He65], [He99], [Il16]), l'analyse harmonique ([St82], [St91]), les EDPs ([Be84], [Jo55]), la géométrie intégrale ([Sh12]), l'analyse microlocale ([Qu+14], [Qu+18]), elles peuvent aussi être étudiées en propre ([Qu80], [Fri+08], [Bo11], [Il19]) et, enfin, elles sont largement utilisées en tomographies par l'ordinateur ([Qu83], [Na86], [Mi+87], [Ku14], [No02], [Qu06], [De07], [Ngu+09], [Ba09], [MiDeP11]). La liste de références ci-dessus est loin d'être exhaustive et il faut également considérer les références qu'elles contiennent.

Dans la section suivante, nous décrivons notre motivation pour ce travail et les problèmes mathématiques associés à P_W et R_W.

3 Problèmes et motivation

Dans cette thèse, nous poursuivons l'étude des transformations de type Radon pondérées pour des applications aux problèmes inverses. En particulier, nous étudions le problème inverse suivant

Problème 1. *Étant donné W et $P_W f$, trouver f.*

Comme on l'a remarqué dans la section 2, pour les dimensions $d = 2, 3$, ce problème se pose en tomographie, en particulier en tomographie à rayons X, en SPECT et en PET. Résoudre le problème 1 pour des poids apparaissant en SPECT était la motivation initiale de cette thèse. Dans les tomographies susmentionnées, le problème 1 se pose habituellement pour la dimension $d = 2$, dans l'approche de reconstruction tranche par tranche ; voir aussi la sous-section 4.1 pour les détails. Dans cette thèse, nous proposons une autre approche pour trouver f à partir de $P_W f$, qui consiste principalement en une réduction du problème 1 pour $d = 2$ sur plusieurs "tranches" bidimensionnelles à un problème inverse pour $R_{W'}$ pour $d = 3$, où W' est un autre poids construit avec W. En d'autres termes, nous considérons également le problème inverse suivant

Problème 2. *Étant donné W et $R_W f$, trouver f.*

La réduction susmentionnée est le principal argument de nos résultats de la partie I. En fait, il est bien connu qu'en dimension $d = 2$, le problème 1 pour des poids W survenant en SPECT est parfaitement soluble ; voir [No02], [Kun01] et la sous-section 4.1. En particulier, pour l'opérateur P_W^{-1} il existe une formule d'inversion analytique exacte [No02], qui admet également des implémentations numériques très efficaces [Kun01]. Cependant, en SPECT, en pratique, les données mesurées ne sont pas données par $P_W f(\gamma)$, $\gamma \in T\mathbb{S}^{d-1}$, mais elles sont données par le nombre de photons $N(\gamma)$, $\gamma \in T\mathbb{S}^{d-1}$, qui sont des réalisations d'un processus de Poisson sur $T\mathbb{S}^{d-1}$ avec des intensités proportionnelles à $P_W f(\gamma)$, $\gamma \in T\mathbb{S}^1$; voir aussi la sous-section 4.1. La présence de bruit est un problème sérieux pour la stabilité des reconstructions en SPECT, car, en réalité, le problème 1 est initialement *mal-posé* et, en fait, en présence de bruit, la formule explicite de [No02] devient instable dans certains régimes [GuNo05], [GuNo08], [GuNo12]. Dans cette dernière optique, nos contributions de la partie I de la thèse peuvent être considérées comme une tentative d'augmenter la stabilité des reconstructions de f à partir de $P_W f$ en SPECT. Après avoir reformulé le problème original, nous proposons deux nouvelles méthodes d'inversion pour résoudre le problème 2, et nous les testons sur des données synthétiques et réelles de SPECT.

Le résumé de ces résultats est donné dans la sous-section 4.1.

En même temps, les problèmes 1, 2 peuvent être traités d'une manière très générale, sans hypothèses sur la structure particulière du poids W comme c'était le cas pour le scanner à rayons X, la PET ou la SPECT. Dans ce cas, la première question qui se pose est de savoir si les problèmes ci-dessus peuvent être résolus. Sur un plan mathématique, cela se réduit au problème de l'injectivité et de la non-injectivité pour P_W, R_W. La partie II de cette thèse est consacrée à ce sujet.

Il existe de nombreux résultats sur l'injectivité et la non-injectivité pour P_W et R_W, par exemple, [Ra17], [Co63], [BQ87], [Bo11], [LaBu73], [MaQu85], [Fi86], [No02a], [No14], [Qu83], [Ku92], [K+95] [Il16] et ses références. Notre motivation initiale était de poursuivre les études d'injectivité et de non-injectivité pour ces dernières transformations. En particulier, nous pensons que nous y sommes parvenus, car nous avons trouvé de nouveaux contre-exemples d'injectivité intéressants pour P_W, R_W à partir du célèbre contre-exemple de Boman dans [Bo93]. Notre premier résultat en ce sens a été obtenu dans l'article 4, où nous avons montré que $R_W^{d,2}$ (voir la définition (1.11)) peut ne pas être injective en dimensions $d \geq 3$ sur $C_c^\infty(\mathbb{R}^d)$ pour un W satisfaisant (1.14) et continu. Ce résultat n'était pas si surprenant en dimension $d = 3$, étant donné que le problème inverse pour $R_W^{3,2}$ est non surdéterminé. Par contre, pour $d > 3$ le problème inverse pour $R_W^{d,2}$ est strictement surdéterminé, et compte tenu de ce fait, notre résultat est complètement nouveau et déjà étonnant. En nous basant sur les développements de ce travail, nous avons construit dans l'article 5 un autre exemple de non-injectivité pour P_W sur $C_c^\infty(\mathbb{R}^d)$ pour $d \geq 2$, pour des poids satisfaisant (1.14) et étant Hölderiens (mais pas encore de classe C^1). Ce résultat semble très inattendu compte tenu des nombreux résultats d'injectivité existants pour P_W pour $d \geq 3$ pour des poids de classe C^1, par exemple, [Fi86], [Il16]. En particulier, intuitivement, c'était inattendu à cause de la *boundary stripping method* bien connue pour prouver l'injectivité de P_W en dimension $d \geq 3$ pour les poids W satisfaisant (1.14).

Pour conclure nos études d'injectivité et de non-injectivité pour P_W, R_W, dans l'article 3 nous avons construit des analogues du contre-exemple de Boman pour R_W en dimension $d \geq 3$. Fait intéressant, pour obtenir ces résultats, nous avons adapté le contre-exemple de J. Boman [Bo93] et notre méthode de réduction du problème 1 au problème 2 du premier article. Le seul inconvénient de nos constructions est que les poids construits W ne semblaient pas être de classe C^∞ mais seulement presque partout sur $\mathbb{R}^d \times \mathbb{S}^{d-1}$, contrairement à l'exemple de Boman pour $d = 2$. Le résultat peut sembler encore peu satisfaisant, car le problème inverse pour R_W n'est pas surdéterminé, et on pourrait s'attendre à ce que R_W ne soit pas injective pour toutes les dimensions $d \geq 3$ pour un W satisfaisant (1.14) et aussi être infiniment lisse partout sur $\mathbb{R}^d \times \mathbb{S}^{d-1}$. D'autre part, nous n'avons jamais rencontré auparavant dans la littérature de contre-exemples à l'injectivité globale pour R_W pour $d \geq 3$, donc ce résultat peut être considéré comme un premier pas dans cette direction.

Les contre-exemples susmentionnés à l'injectivité pour P_W, R_W sont valables dans le cadre des poids généraux W, qui ne satisfont que (1.14). De telles considérations générales n'aident pas directement à résoudre des problèmes inverses réels, mais elles aident à mieux comprendre les limites de l'applicabilité des méthodes mathématiques qui sont utilisées pour résoudre ces problèmes. Nous voyons les résultats de la partie II de la thèse exactement dans cette optique.

Le résumé des résultats sur la non-injectivité de P_W, R_W est donné dans la sous-section 4.2.

4 Résumé de nos résultats

4.1 Résumé des résultats de la partie I

Nous commençons l'exposition en rappelant le cadre de plusieurs tomographies conventionnelles. Ensuite, nous expliquons la réduction du problème 1 à problème 2 dans le cadre des tomographies d'émission (article 1), et nous présentons également deux nouvelles méthodes pour résoudre le problème 2 (articles 1, 2). A la fin, nous donnons des exemples numériques de reconstructions pour nos méthodes.

Les saveurs de différentes tomographies

La tomographie ($\tau o \mu o \sigma$ – tranche et $\gamma \rho a \phi \omega$ - écrire) peut être considérée comme une collection de techniques et de méthodes pour la reconstruction des propriétés intérieures d'objets à partir de leurs mesures extérieures. On pourrait également dire que la tomographie fait partie d'un domaine plus vaste appelé *Sciences de l'Imagerie*, qui est consacré à diverses formes de construction et d'analyse d'images ; voir [BM04].

Une caractéristique importante des techniques tomographiques est qu'elles sont non invasives, non destructrices. Cela les rend très attrayants pour de nombreux problèmes d'imagerie médicale, de diagnostic technique, de contrôle de qualité et d'autres domaines. Dans cette thèse, nous nous concentrons sur les applications médicales de la tomographie et en particulier, sur la tomographie à rayons X, les tomographie par émission de positrons et monophotonique (PET et SPECT).

D'un point de vue mathématique, le choix de ce triplet - tomographie à rayons X, PET et SPECT - est agréable car il repose sur le même objet mathématique – *les transformations des rayons pondérées* P_W en trois dimensions, où W est le poids qui dépend du type de tomographie considérée.

Ensuite, nous rappelons les cadres des tomographies susmentionnées.

CT à rayons X

Pour les applications médicales, l'objectif principal de la tomographie à rayons X est de reconstruire l'image anatomique dans la région donnée du corps humain.

La méthode de reconstruction est basée sur la mesure des pertes d'intensité des rayons X émis traversant la région d'intérêt ; voir la figure 1.3. Comme les tissus du corps peuvent être caractérisés par la force d'atténuation des rayons X, le problème se réduit à trouver le coefficient d'atténuation $a = a(x)$, $x \in \mathbb{R}^3$.

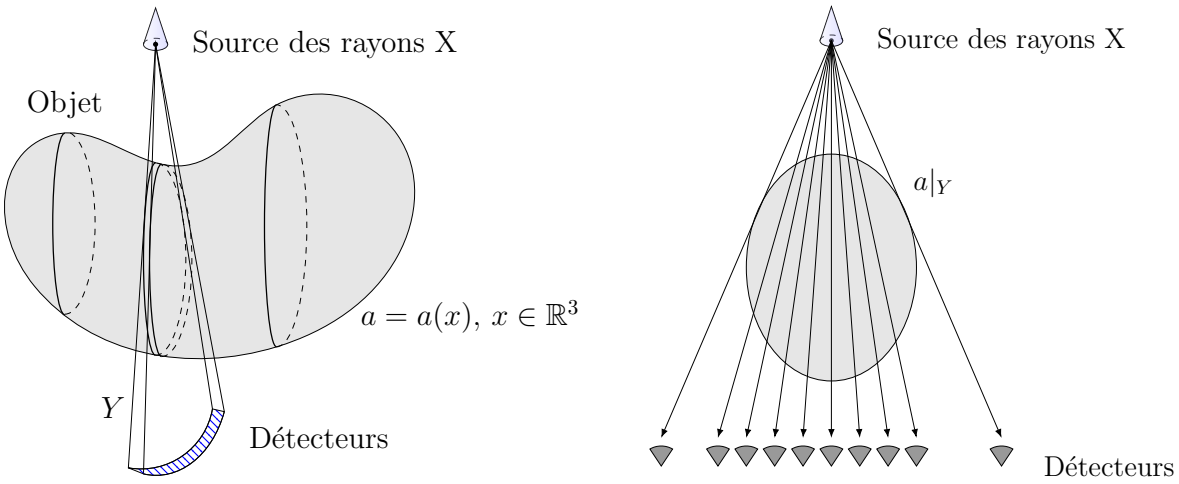

Figure 1.3 Tomographie à rayons X

En mesurant les pertes d'intensité pour de nombreux rayons et en appliquant la loi d'atténuation de Beer (voir la formule (1.7)), on peut calculer la transformée des rayons classique Pa, qui est donnée par la formule suivante

$$Pa(x,\theta) = \int_{-\infty}^{+\infty} a(x+t\theta)\,dt,\ \gamma = \gamma(x,\theta) \in T\mathbb{S}^2, \tag{1.24}$$

où $a = a(x)$, $x \in \mathbb{R}^3$, est le coefficient d'atténuation à reconstruire. Par conséquent, sur un plan mathématique, le problème de reconstruction est réduit au problème 1 pour $W \equiv 1$ en dimension $d = 3$.

Bien que le but soit de reconstruire l'atténuation a en trois dimensions, pour des raisons pratiques, il est souvent résolu comme un ensemble de problèmes 1 en dimension $d = 2$, dans ce qu'on appelle l'approche *reconstruction tranche par tranche*. Dans cette approche, le support de la fonction inconnue a est découpé en un ensemble de plans parallèles, et la réduction $a|_Y$ à chaque plan Y est reconstruite ; voir la figure 1.3.

Pour le problème réduit, il est bien connu que

$$Pa\big|_{T\mathbb{S}^1(Y)} \text{ détermine } a\big|_Y \text{ uniquement}, \tag{1.25}$$

où $T\mathbb{S}^1(Y)$ est l'ensemble des rayons en Y. De plus, la détermination de $a\big|_Y$ peut être implémentée via les formules d'inversion classiques de Radon [Ra17] :

$$f(x) = \frac{1}{4\pi}\int_{\mathbb{S}^1} \theta^\perp \nabla \tilde{q}_\theta(x\theta^\perp)\,d\theta,\ x \in \mathbb{R}^2, \tag{1.26}$$

$$\tilde{q}_\theta(s) = \frac{1}{\pi} p.v. \int_{-\infty}^{+\infty} \frac{q_\theta(t)}{s-t}\,dt, \tag{1.27}$$

$$q_\theta(s) = Pf(s\theta^\perp, \theta),\ s \in \mathbb{R},\ \theta = (\theta_1,\theta_2) \in \mathbb{S}^1,\ \theta^\perp = (-\theta_2,\theta_1), \tag{1.28}$$

où Pa est donné dans (1.24).

D'après les considérations qui précèdent, il est évident que le problème mathématique de la tomographie est parfaitement résoluble. Nous notons également qu'il existe de nombreuses autres méthodes de reconstruction de a à partir de Pa qui diffèrent principalement dans le schéma d'acquisition des données Pa. Par exemple, les scanners modernes peuvent de ne

pas effectuer des reconstructions tranche par tranche, mais mesurer Pa sur un ensemble plus complexe de rayons (par exemple, méthodes de Katsevich et de Grangeat) et effectuer des reconstructions directement en 3D ; pour plus de détails voir [Gr91], [Na99], [Kat02], [Va+16].

Dans la pratique, outre l'inversion réelle de P, il y a beaucoup d'autres questions importantes, par exemple : la stabilité des reconstructions, la dépendance aux données finies (échantillonnage, données incomplètes).

- Stabilité des reconstructions: la transformation P est un opérateur lissant et pour $d = 2$ agit, par exemple, de $H_0^s(\Omega)$ à $H_0^{s+1/2}([-1,1] \times \mathbb{S}^1)$, $s \geq 0$, où Ω est une boule unitaire dans $\mathbb{R}^2$, H_0^s est l'espace de Sobolev standard avec condition aux limites nulle. Pour cette raison, le problème réel d'inversion de P est *mal-posé* (pour être rigoureux, cela se prouve en analysant les valeurs singulières de P), et c'est un problème très important dans les applications ; voir aussi [La+86]. Dans une procédure réelle de tomographie par rayons X, les données mesurées sont le nombre de photons $N(\gamma)$ dans un temps donné pour chaque rayon $\gamma \in T\mathbb{S}^1$. Ce nombre de photons $N(\gamma)$ peut être modélisé comme un processus de Poisson, [Wa08], avec une intensité égale à $CPa(\gamma)$, où C est une constante dépendant de l'installation. Par conséquent, l'application de formules inverses directes (par exemple, (1.26)-(1.28)) à des données bruitées et brutes peuvent causer des artefacts et des erreurs dans les images reconstruites. Un moyen de stabiliser les reconstructions est de *régulariser* les données, soit par un traitement de données, [HoWe16], soit en acquérant une bonne statistique pour les données ou en faisant les deux.

- Méthodes d'inversion de P: en dehors des formules d'inversion (1.26)-(1.28) il existe de nombreuses autres formules et méthodes pour trouver f à partir de Pf (algébrique, itérative, statistique) ; voir, par exemple, [Na99], [AdOk17]. L'avantage d'utiliser des formules d'inversion exactes est que beaucoup d'entre elles admettent des implémentations très efficaces en termes de vitesse, appelées *filtered backprojection algorithms* (ou - FBP). D'autre part, ces formules contiennent toujours des opérations qui peuvent être considérées instables du point de vue des méthodes numériques - dérivations ou intégrations avec des noyaux singuliers. Pour cette raison et parce que les données mesurées sont toujours obtenues pour un nombre fini de rayons et qu'elles sont corrompues par le bruit, les implémentations numériques exigent une modification soigneuse des formules analytiques en leurs analogues discrets.

Toutes les questions ci-dessus sont étudiées depuis longtemps et il y a déjà d'énormes progrès dans toutes les modalités de la tomographie à rayons X ; voir [Na86], [Ku14] et ses références. Comme nous le verrons plus loin, les parties mathématiques et numériques correspondantes des problèmes inverses pour la PET et la SPECT sont beaucoup moins simples.

PET

La tomographie par émission de positrons (PET) est aussi un type de tomographie utilisé en médecine nucléaire (également sous forme de tomographie à rayons X et SPECT); [Na86], [To96], [Ku14]. D'un point de vue médical, elle se concentre principalement sur la représentation de l'activité physiologique, du métabolisme ou des niveaux d'activités chimiques dans une région d'intérêt à l'intérieur du corps, tandis que la tomographie à rayons X se concentre sur l'imagerie de l'anatomie. Pour étudier les activités susmentionnées, un patient reçoit une injection d'un médicament spécial appelé *traceur*, dont le composant principal est un isotope qui a une courte demi-vie. Ensuite, à l'aide d'un scanner PET spécial, le rayonnement émis par les isotopes est mesuré et à partir de ces données, la distribution des isotopes, et donc

du médicament, est reconstruite. Enfin, la distribution du médicament est interprétée par des spécialistes afin d'établir un diagnostic.

Sur le plan physique, le rayonnement émis est représenté par des photons gamma, qui sont produits par les réactions nucléaires à l'intérieur du corps du patient. En particulier, en raison de la désintégration nucléaire de l'isotope, un positron est d'abord émis et peu de temps après il est annihilé par un électron voisin. Le produit de l'anéantissement sont deux photons gamma qui voyagent dans des directions opposées ; voir la figure 1.4.

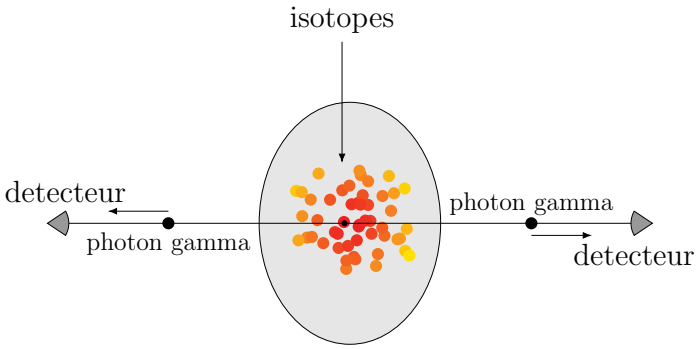

Figure 1.4 Mesures en PET

Pour chaque rayon $\gamma \in T\mathbb{S}^2$, le nombre de paires de photons $N(\gamma)$ qui ont atteint les détecteurs le long de γ pendant une période de temps fixe t constitue les données initiales (données d'émission) en PET.

Sur un plan mathématique, le nombre de photons mentionnés ci-dessus $N(\gamma)$ est lié aux transformations de type Radon par la formule suivante :

$$N(\gamma) \sim \mathrm{Po}(CtP_{\omega_a} f(\gamma)),\ \gamma \in T\mathbb{S}^2, \tag{1.29}$$

où

$\mathrm{Po}(\lambda)$ désigne la distribution de Poisson d'intensité λ,

C est une constante positive qui dépend des paramètres de l'installation, (1.30)

$t > 0$ est le temps d'acquisition par rayon,

P_{ω_a} est la transformation des rayons pondérée définie dans (1.17) pour $d = 3$, (1.31)

$f = f(x)$, $x \in \mathbb{R}^3$ est la distribution de densité de l'isotope. (1.32)

Le poids ω_a est donné par la formule suivante

$$\omega_a(x, \theta) = \exp\left(-Pa(x, \theta)\right),\ x \in \mathbb{R}^3,\ \theta \in \mathbb{S}^2, \tag{1.33}$$

où $a = a(x)$, $x \in \mathbb{R}^3$ est l'atténuation, P est la transformation des rayons classique, définie dans (1.17) pour $W \equiv 1$. Dans le cadre de la PET les valeurs pour C, t et d'atténuation $a = a(x)$, $x \in \mathbb{R}^3$ sont supposés être connus *a priori*. En fait, l'application a est habituellement reconstruite à l'aide de tomographie à rayons X avant la procédure de PET proprement dite. En outre, dans la procédure de PET réelle, le nombre de photons $N(\gamma)$ de (1.29) n'est souvent connu que sur un sous-ensemble de $T\mathbb{S}^2$ qui correspond au cadre de reconstruction tranche par tranche[12] (voir aussi le paragraphe précédent sur la tomographie à rayons X).

Des formules (1.29)-(1.33) et de leurs interprétations on peut conclure ce qui suit :

[12]En fait, il existe des scanners PET qui produisent les données d'émission quadridimensionnelles [To96]. Ceci, en particulier, est motivé par la réduction de l'impact du bruit fort dans les données mesurées.

1. Les données mesurées $N(\gamma)$, $\gamma \in T\mathbb{S}^2$ sont des réalisations d'un processus de Poisson avec intensités proportionnelles à $P_{\omega_a} f(\gamma), \gamma \in T\mathbb{S}^2$. Du point de vue des transformations de type Radon, les données obtenues via $P_{\omega_a} f$ correspondent à la version non-bruitée des données réelles d'émission. En effet, d'après (1.29) et les propriétés de la distribution de Poisson

$$\mathbb{E}N(\gamma) = CtP_{\omega_a} f(\gamma),\ \gamma \in T\mathbb{S}^2. \tag{1.34}$$

   Par conséquent, la résolution du problème 1 pour PET, où $W = w_a$ défini dans (1.33), correspond à la reconstruction de f à partir des données "idéales".

2. De (1.33) il s'ensuit que $\omega_a(x, \theta)$ est constant pour $x \in \gamma(x, \theta) \in T\mathbb{S}^2$ pour $\theta \in \mathbb{S}^2$ fixé. Cela rend l'inversion de P_{ω_a} triviale. En effet, de la définition 3 et de la formule (1.33), il résulte que

$$P_{\omega_a} f(x, \theta) = \exp\left(-Pa(x, \theta)\right) Pf(x, \theta),\ (x, \theta) \in T\mathbb{S}^2, \tag{1.35}$$

   où P – est la transformation des rayons classique de $\mathbb{R}^3$, a est l'application d'atténuation. Alors, la reconstruction de f à partir de $P_{\omega_a} f$ et a peut être implémentée via la formule suivante :

$$f(x) = P^{-1}(\exp(Pa)P_{w_a} f)(x),\ x \in \mathbb{R}^3, \tag{1.36}$$

   où P^{-1} est l'inversion de la transformation des rayons classique.

A partir des considérations ci-dessus, on peut voir que le problème 1 pour la PET en 3D est facilement résoluble via la formule (1.36). De plus, de (1.36), il s'ensuit que toutes les techniques qui sont applicables pour l'inversion de P peuvent être appliquées en PET. D'autre part, à l'instar de la tomographie par rayons X, l'un des principaux problèmes de la PET est la stabilité des reconstructions. En effet, de (1.29) il s'ensuit que le problème 1 pour la PET est beaucoup plus mal posé que celui de la tomographie à rayons X. En particulier, on le voit déjà à partir de la formule (1.36), qui peut être interprétée de manière informelle comme suit : le caractère mal-posé de l'inversion de P_{ω_a} est égal au caractère mal-posé de l'inversion de P fois le facteur exponentiel $\exp(-Pa)$. Par conséquent, une forte atténuation augmente l'instabilité des reconstructions en PET ; pour plus de détails voir [Na86], [Ku14]. En même temps, dans la pratique, les données d'émission contiennent un bruit issu d'un processus de Poisson très fort qui affecte beaucoup plus la stabilité des reconstructions que le caractère mal posé. En présence d'un fort bruit, les méthodes statistiques basées sur *la maximization de vraisemblance* sont utilisées ; voir, par exemple, [Ka93], [V-Sl+15].

Malgré les problèmes susmentionnés, les modalités technologiques de la PET ont beaucoup progressé et c'est désormais d'un outil standard pour le diagnostic en médecine.

SPECT

La tomographie par émission monophotonique (SPECT) appartient également au domaine de la médecine nucléaire et ses objectifs principaux sont très similaires à ceux de la PET.

Sur le plan médical, l'application principale de la SPECT est l'analyse de la circulation sanguine dans le cerveau. Comme pour la PET, lors d'une SPECT un traceur intégré à un isotope est injecté dans la circulation sanguine et diffusé dans l'organisme. En fait, le traceur est chimiquement conçu pour se concentrer principalement dans le cerveau. En raison de la désintégration radioactive des isotopes, des photons gamma sont émis dans différentes directions et sont enregistrés par les détecteurs du scanner spécial. En mesurant ce rayonnement dans de nombreuses directions différentes, on peut reconstruire la distribution

du traceur dans le cerveau. La distribution peut être utilisée, par exemple, pour détecter des zones du cerveau présentant un débit sanguin réduit ou des lésions.

Sur le plan physique, la principale différence entre la PET et la SPECT est qu'en SPECT, en raison d'une désintégration nucléaire de l'isotope, un seul photon gamma est émis par réaction ; voir la figure 1.5.

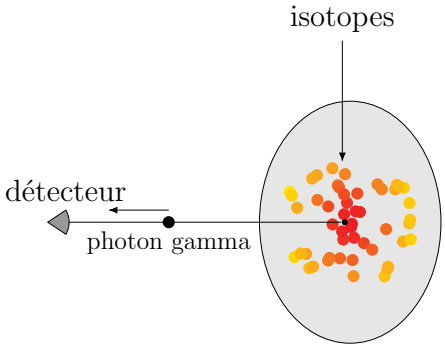

Figure 1.5 Mesures en SPECT

En même temps, les données mesurées sont à nouveau obtenues par le nombre de photons $N(\gamma)$, $\gamma \in T\mathbb{S}^2$ et un analogue de la formule (1.29) est vérifie. En particulier, dans la SPECT, l'intensité du processus de Poisson dans (1.29) est proportionnelle à $P_{W_a} f$, où $f = f(x)$, $x \in \mathbb{R}^3$ est la densité du traceur et le poids W_a est donné par les formules :

$$W_a(x,\theta) = \exp(-Da(x,\theta)), \tag{1.37}$$

$$Da(x,\theta) = \int_0^{+\infty} a(x+t\theta)\,dt,\ x \in \mathbb{R}^3,\ \theta \in \mathbb{S}^2, \tag{1.38}$$

où $a = a(x)$, $x \in \mathbb{R}^3$ est l'atténuation.

La transformation P_W pour le poids W_a de (1.37), (1.38) est aussi connu comme *la transformation des rayons X atténuée*. Il y a une longue histoire de l'étude de cette transformation; voir, par exemple, [TM80], [Ma84], [Fi86], [Sh93], [Na86], [Ar+98] et références y figurant. En particulier, dans les publications ci-dessus, les résultats ont porté principalement sur l'injectivité de P_{W_a} (locale, puis globale) et aussi sur les méthodes d'inversions basées sur des schémas itératifs. Il n'y a pas si longtemps, Novikov a réalisé un grand progrès en proposant des formules d'inversion analytiques et exactes pour $P_{W_a}^{-1}$; [No02]. La grande différence de ces formules par rapport aux résultats précédents et, en particulier, aux résultats de [Ar+98] est que les formules de Novikov présentent la même structure que les formules d'inversion de Radon [Ra17] ; voir également la discussion dans [Fi03]. Les nouvelles formules sont, en particulier, très importantes pour les applications, car leur structure permettent de mettre en œuvre des reconstructions en termes d'algorithme FBP très efficace [Kun01].

En particulier, l'inversion de P_{W_a} est donnée par les formules suivantes ([No02]):

$$f(x) = \frac{1}{4\pi} \int\limits_{\mathbb{S}^1} \theta^\perp \nabla_x (\exp[-Da(x,-\theta)] \tilde{g}_\theta(\theta^\perp x))\, d\theta, \tag{1.39}$$

$$\begin{aligned} \tilde{g}_\theta(s) = &\exp(A_\theta(s)) \cos(B_\theta(s)) H(\exp(A_\theta) \cos(B_\theta) g_\theta)(s) + \\ &\exp(A_\theta(s)) \sin(B_\theta(s)) H(\exp(A_\theta) \sin(B_\theta) g_\theta)(s), \end{aligned} \tag{1.40}$$

$$A_\theta(s) = \frac{1}{2} Pa(s\theta^\perp, \theta),\ B_\theta(s) = HA_\theta(s), g_\theta(s) = P_{W_a} f(s\theta^\perp, \theta), \tag{1.41}$$

$$Hu(s) = \frac{1}{\pi} p.v. \int\limits_{-\infty}^{+\infty} \frac{u(t)}{s-t}\, dt, \tag{1.42}$$

$$x \in \mathbb{R}^2, \theta^\perp = (-\theta_2, \theta_1) \text{ for } \theta = (\theta_1, \theta_2) \in \mathbb{S}^1,\ s \in \mathbb{R}.$$

Une propriété importante de (1.39)-(1.42) est que pour un cas non atténué (i.e., $a = 0$), lorsque P_{W_a} se réduit à la transformation des rayons classique P, les formules réduisent à (1.26)-(1.28) pour P^{-1}. En outre, une forme plus simple de (1.39)-(1.42) peut être trouvée, par exemple, dans [Na01].

De la discussion ci-dessus on peut voir que le problème 1 pour la SPECT est parfaitement résoluble. Cependant, comme pour la PET, les formules exactes d'inversion ne constituent pas encore une solution complète au problème réel. Bien que les formules (1.39)-(1.42) aient été testées sur des données d'émission synthétiques et réelles [Kun01], [Gu+02], il est apparu que ces formules peuvent être instables en présence d'un fort bruit de Schottky dans les données d'émission [GuNo12]. A présent, les méthodes qui sont le plus souvent utilisées dans la SPECT sont des méthodes statistiques ; voir, par exemple, [CrDeP07].

Pour conclure, il existe encore des recherches très actives sur les différentes modalités de la SPECT ; voir aussi [BJ11], [Br00], [Ku14]. En particulier, beaucoup d'efforts se portent sur le développement de méthodes stables de reconstruction, y compris de nouvelles approches technologiques [Ngu+09].

Inversions des transformations de type de Radon pondérées en tomographies

D'après les paragraphes précédents, on a pu voir que les problèmes de reconstruction en tomographies se réduisent soit au problème 1, soit au problème 2. En fait, la première étape pour résoudre ces derniers est de voir s'ils sont résolubles en général.

Sur un plan mathématique, cela revient à poser la question de l'injectivité et de la non-injectivité de P_W, R_W sur certains espaces fonctionnels pour des poids W satisfaisant (1.14). En particulier, dans la tomographie à rayons X, PET et SPECT, la question de l'injectivité de P_W, R_W est résolue trivialement par les formules d'inversion analytiques exactes – formules classiques d'inversion de Radon (1.26)-(1.28) pour la tomographie à rayons X et PET et formules de Novikov (1.39)-(1.42) pour la SPECT.

Pour un poids général non constant W, la situation des inversions de P_W, R_W est très différente des cas précédents. Premièrement, il semble qu'il n'y ait pas de formule d'inversion analytique générale pour P_W, R_W, sauf dans certains cas particuliers où W a des symétries très spécifiques [Ra17], [TM80], [No02], [Bo04], [Gi10], [No11], [GN16]. Pour certains poids W satisfaisant (1.14) il y a même des contre-exemples à l'injectivité pour P_W, R_W pour $d \geq 2$; voir la sous-section 4.2 pour plus de détails.

Le premier exemple de tomographie où des transformations P_W avec des poids non triviaux W sont utilisés est la SPECT. Bien que dans ce cas il existe une formule d'inversion analytique pour P_W^{-1} pour $d = 2$ (formules (1.39)-(1.42)), elle n'est pas encore utilisée dans les applications tomographiques. Plus précisément, en cas de données non bruitées dans la

SPECT la formule de Novikov donne des reconstructions parfaites dans tous les modèles d'atténuation [Kun01], [Na01]. Mais en cas de fort bruit de Schottky dans les données d'émission, cela devient numériquement instable et produit des artefacts. Certaines tentatives ont déjà été faites pour appliquer des filtres de régularisation aux données d'émission [GuNo05], [GuNo08], [GuNo12], mais le problème de la stabilisation efficace de la formule reste ouvert [13].

Dans notre approche du problème inverse dans la SPECT, nous avons décidé de nous concentrer sur des méthodes d'inversion approximatives qui ont une meilleure stabilité en présence de bruit que les formules analytiques exactes. Pour les reconstructions tranche par tranche, ces méthodes sont la formule d'inversion approximative de Chang [Ch78], [No11] et l'algorithme itératif d'inversion de Kunyansky [Ku92], [GuNo14].

Formule de Chang. La formule d'inversion approximative de Chang (voir [Ch78]) est définie par :

$$f_{appr}(x) \stackrel{\text{def}}{=} \frac{1}{4\pi w_0(x)} \int\limits_{\mathbb{S}^1} h'(x\theta^{\perp}, \theta)\, d\theta,\ x \in \mathbb{R}^2, \tag{1.43}$$

$$\begin{aligned} h'(s,\theta) &= \frac{d}{ds} h(s,\theta), \\ h(s,\theta) &= \frac{1}{\pi} p.v. \int\limits_{-\infty}^{+\infty} \frac{P_W f(t\theta^{\perp}, \theta)}{s-t}\, dt,\ s \in \mathbb{R},\ \theta \in \mathbb{S}^1,\ x \in \mathbb{R}^2, \end{aligned} \tag{1.44}$$

où $P_W f$ pour $d = 2$ est défini dans (1.17) et w_0 est défini par la formule

$$w_0(x) \stackrel{\text{def}}{=} \frac{1}{2\pi} \int\limits_{\mathbb{S}^1} W(x,\theta)\, d\theta,\ w_0(x) \neq 0 \text{ pour tout } x \in \mathbb{R}^2. \tag{1.45}$$

Notez que les formules (1.43)-(1.44) sont essentiellement des formules d'inversion de Radon (1.26)-(1.28) appliquées à P_W avec un facteur de pondération supplémentaire w_0.

Bien que la formule proposée ne donne qu'une inversion approximative de P_W, elle semble très efficace en SPECT [Mu+87], et elle a également été utilisée comme point de départ pour des schémas itératifs plus complexes ; voir, par exemple, [Ku92].

Très naïvement, la formule de Chang peut être vue comme une méthode pour trouver f approximativement à partir de $P_W f$, quand $W \approx w_0$. En effet, pour $W(x,\theta) \equiv w_0(x)$ nous avons :

$$P_W f = P_{w_0} f = P(w_0 f) \Rightarrow f = \frac{P^{-1} P_W f}{w_0}, \tag{1.46}$$

où P^{-1} est l'inverse de la transformation de Radon classique pour $d = 2$. Il n'y a pas si longtemps, dans [No11], on a réalisé que l'efficacité de la formule de Chang est due à une hypothèse plus faible sur W que $W \approx w_0$.

[13] Possiblement, il sera résolu à l'avenir avec des progrès technologiques dans la construction des scanners. De nos jours, dans les mesures en SPECT, presque tous les photons émis sont perdus en raison de l'effet de collimation. Une nouvelle approche possible pour surmonter ce problème est le développement de *Gamma-cameras de Compton* ; voir [Ngu+09] et ses références.

Théorème 1 (Novikov, 2011). *On suppose que les hypothèses de* (1.14) *pour* $d = 2$ *sont vérifiées et que* W *est également continu sur* $\mathbb{R}^2 \times \mathbb{S}^1$. *Soit* f_{appr} *donnée par* (1.43)-(1.45). *Alors*

$$f_{appr} = f \text{ (au sens des distributions) sur } \mathbb{R}^2 \text{ pour tout } f \in C_c(\mathbb{R}^2) \tag{1.47}$$

si et seulement si

$$w_0(x) \equiv \frac{1}{2}(W(x,\theta) + W(x,-\theta)),\ x \in \mathbb{R}^2,\ \theta \in \mathbb{S}^1, \tag{1.48}$$

où $C_c(\mathbb{R}^2)$ *désigne l'espace des fonctions continues à support compact sur* $\mathbb{R}^2$.

Un façon simple d'interpréter le théorème 1 est de regarder la condition (1.48) en termes de développement de W en harmoniques sphériques sur $\mathbb{S}^1$. Soit

$$W(x,\theta) = \sum_{k\in\mathbb{Z}} w_k(x) Y_k(\theta),\ x \in \mathbb{R}^2,\ \theta \in \mathbb{S}^1, \tag{1.49}$$

$$w_k(x) = \frac{1}{2\pi} \int_{\mathbb{S}^1} W(x,\theta) Y_{-k}(\theta)\, d\theta,\ k \in \mathbb{Z}, \tag{1.50}$$

$$Y_k(\theta(\varphi)) = (\theta_1(\varphi) + i\theta_2(\varphi))^k = e^{ik\varphi},\ \theta(\varphi) = (\cos\varphi, \sin\varphi) \in \mathbb{S}^1,\ \varphi \in [0, 2\pi). \tag{1.51}$$

De (1.49)-(1.51) il est facile de voir que la condition (1.48) est équivalente à la suivante

$$w_{2k} \equiv 0 \text{ on } \mathbb{R}^2, \text{ for } k \in \mathbb{Z}\backslash\{0\}. \tag{1.52}$$

Une caractéristique importante de (1.52) est qu'elle ne contient aucune condition sur w_k pour k impair. Par conséquent, pour W tel qu'il manque beaucoup de termes w_k dans (1.49) pour k pair et que tous les termes w_k sont donnés pour k impair, la formule de Chang donnera des reconstructions presque parfaites ! Ceci explique l'efficacité des formules (1.43)-(1.45) en SPECT même si elles sont seulement approximatives. En même temps, il est bien connu qu'en cas de forte atténuation en SPECT, la formule de Chang produit des artefacts ; voir la figure 1.6. Dans ce cas, des méthodes de reconstruction plus complexes devraient être utilisées, par exemple, la méthode de Kunyansky dont nous parlons dans le paragraphe suivant.

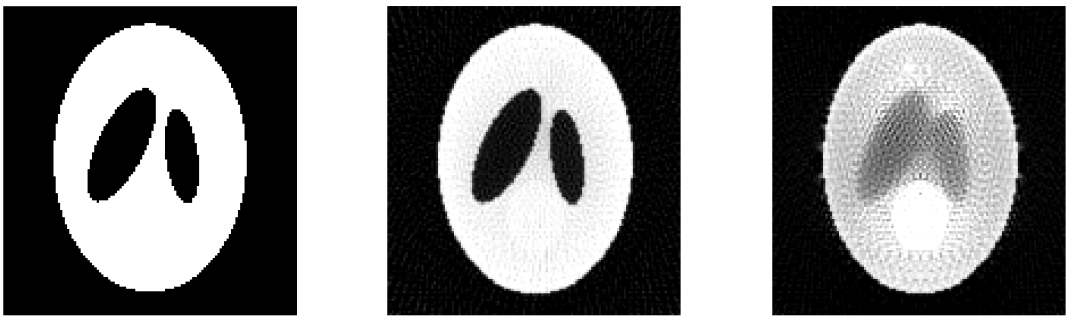

(a) fonction f (b) f_{appr}, atténuation faible (c) f_{appr}, atténuation forte

Figure 1.6 Reconstructions dans le cadre de la SPECT en utilisant la formule de Chang ; pour l'atténuation $a = a(x)$, $x \in \mathbb{R}^2$ (voir les formules (1.37), (1.38)) nous avons utilisé le modèle Shepp-Logan 3D [Ga+08]

Méthode de Kunyansky. Une amélioration de la méthode de Chang est l'algorithme itératif de Kunyansky [Ku92], [No14], [GuNo14][14]. L'idée principale de la méthode est de

[14]En particulier, dans [GuNo14], [No14] les auteurs relâchent les hypothèses sur W selon lesquelles l'algorithme itératif de Kunyansky [Ku92] converge.

considérer plus de termes pairs w_{2k} dans le développement (1.49) que dans la formule de Chang. Dans ce cas, l'inversion de R_W n'est pas donnée par une formule analytique mais comme une solution d'une certaine équation intégrale.

Nous expliquons brièvement la méthode suivant la notation de [GuNo14], car elle sera similaire aux notations de nos résultats de l'article 2. De la présentation ci-dessous, dans un premier temps, nous ne nous intéressons pas aux hypothèses de régularité ou aux conditions de convergences de séries, nous expliquons uniquement le concept principal. Ensuite, nous présentons des théorèmes qui soutiennent nos développements. Rappelons aussi que pour $d = 2$ les transformations P_W, R_W sont équivalentes et nous allons utiliser les notations pour R_W au lieu de P_W.

Soit

$$D \text{ un domaine fixé ouvert et borné dans } \mathbb{R}^2, \tag{1.53}$$

$$f \in L^\infty(\mathbb{R}^2), \operatorname{supp} f \subset D. \tag{1.54}$$

Considérons A_W défini par

$$A_W f \stackrel{\text{def}}{=} R^{-1} R_W f, \tag{1.55}$$

où R^{-1} est l'inverse de la transformation de Radon classique pour $d = 2$ (voir les formules (1.26)-(1.28)). Il a été démontré dans [Ku92] et [GuNo14] que

$$A_W f = R^{-1} R_{W_{sym}} f, \tag{1.56}$$

$$R_{W_{sym}} f(s,\theta) = \frac{1}{2}(R_W f(s,\theta) + R_W f(-s,-\theta)),\ (s,\theta) \in \mathbb{R} \times \mathbb{S}^1, \tag{1.57}$$

où W_{sym} est défini par la formule suivante

$$W_{sym}(x,\theta) \stackrel{\text{def}}{=} \frac{1}{2}(W(x,\theta) + W(x,-\theta)),\ x \in \mathbb{R}^2,\ \theta \in \mathbb{S}^1. \tag{1.58}$$

En développant W_{sym} de (1.58) dans une série d'harmoniques sphériques sur $\mathbb{S}^1$ nous avons que

$$W_{sym}(x,\theta) = \sum_{l \in \mathbb{Z}} w_{2l}(x) Y_{2l}(\theta),\ x \in \mathbb{R}^2,\ \theta \in \mathbb{S}^1, \tag{1.59}$$

où les w_{2k} sont définis dans (1.50), les Y_{2k} sont définis dans (1.51).

Remarque 1. Notons aussi que la condition de suffisante dans le théorème 1 résulte directement de (1.48) et de (1.55)-(1.59).

De (1.16), (1.59) il s'ensuit que

$$R_{W_{sym}} f(s,\theta) = R(w_0 f)(s,\theta) + \sum_{\mathbb{Z}\setminus\{0\}} Y_{2k}(\theta) R(w_{2k} f)(s,\theta),\ (s,\theta) \in \mathbb{R} \times \mathbb{S}^1. \tag{1.60}$$

En appliquant R^{-1} aux deux côtés de (1.60) et en utilisant la formule (1.56) on obtient l'identité suivante :

$$(I + Q_{W,D,\infty})(w_0 f) = R^{-1} R_W f, \tag{1.61}$$

où I est l'opérateur identité, $Q_{W,\,D,\,\infty}$ est un opérateur intégral défini par la formule

$$Q_{W,\,D,\,\infty}u \stackrel{\text{def}}{=} R^{-1}\left(\sum_{k\in\mathbb{Z}\setminus\{0\}} Y_{2k}(\theta)\int\limits_{x\theta=s}\frac{w_{2k}(x)}{w_0(x)}\chi_D(x)u(x)\,dx\right), \tag{1.62}$$

où $\chi_D = \chi_D(x)$ est la fonction caractéristique du domaine D.

L'idée principale de la méthode de Kunyansky est de considérer l'identité (1.61) comme une équation intégrale sur f, où $R^{-1}R_W f$ est connu. Alors, si l'opérateur $I + Q_{W,\,D,\,\infty}$ de (1.61) est inversible, f peut être trouvée à partir de $R_W f$ par la formule suivante :

$$f = (w_0)^{-1}(I + Q_{W,\,D,\,\infty})^{-1}R^{-1}R_W f. \tag{1.63}$$

Maintenant, pour donner un sens rigoureux aux formules (1.58)-(1.63), il faut introduire des espaces fonctionnels sur lesquels les opérateurs intégrants précités sont bien définis. Les résultats suivants sont issus de [Ku92], [GuNo14].

Théorème 2 (Kunyansky 1992, Guillement-Novikov 2014)**.** *Soient D, f comme dans* (1.53), (1.54)*, $W \in C(\mathbb{R}^2\times\mathbb{S}^1)\cap L^(\mathbb{R}^2\times\mathbb{S}^1)$, w_0, w_{2k}, $k\in\mathbb{Z}$ définis par* (1.49)-(1.51) *et $w_0(x)\neq 0$ pour tout $x\in\mathbb{R}^2$. Supposons également que*

$$\sum_{k\in\mathbb{Z}\setminus\{0\}}\left\|\frac{w_{2k}}{w_0}\right\|_{L^2(D)} < +\infty. \tag{1.64}$$

Alors, $R^{-1}R_W f\in L^2(\mathbb{R}^2)$. De plus, si

$$\sigma_{W,\,D,\,\infty} \stackrel{\text{def}}{=} \sum_{k\in\mathbb{Z}\setminus\{0\}}\sup_{x\in D}\left|\frac{w_{2k}}{w_0}\right| < +\infty, \tag{1.65}$$

alors l'opérateur $Q_{W,\,D,\,\infty}$ de (1.62) *est un opérateur borné linéaire sur $L^2(\mathbb{R}^2)$ et on obtient la majoration suivante*

$$\|Q_{W,\,D,\,\infty}\|_{L^2(\mathbb{R}^2)\to L^2(\mathbb{R}^2)} \le \sigma_{W,\,D,\,\infty}. \tag{1.66}$$

En outre, l'opérateur $Q_{W,,D,\,\infty}$ de (1.62) admet une forme plus simple.

Lemme 1 (Kunyansky 1992, Guillement-Novikov 2014)**.** *Supposons les hypothèses du théorème 2 vérifiées et, de plus, la condition* (1.65) *satisfaite. Alors, l'opérateur $Q_{W,\,D,\,\infty}$ de* (1.62) *peut être réécrit sous la forme suivante :*

$$Q_{W,\,D,\,\infty}u = \sum_{k\in\mathbb{Z}\setminus\{0\}} d_{2k} * \frac{w_{2k}}{w_0}\chi_D u,\ u\in L^2(\mathbb{R}^2), \tag{1.67}$$

où $*$ – indique la convolution dans $\mathbb{R}^2$ et les fonctions d_{2k} définies par

$$d_{2k}(x(r,\varphi)) \stackrel{\text{def}}{=} (-1)^k\frac{|k|}{\pi}\frac{e^{2ki\varphi}}{r^2},\ x = (r\cos\varphi, r\sin\varphi),\ r>0,\ \varphi\in[0,2\pi). \tag{1.68}$$

De plus, pour d_{2k} comme dans (1.68) *la propriété suivante est vérifiée :*

$$F[d_{2k}](\xi(\rho,\psi)) = e^{2ki\psi},\ \xi = (\rho\cos\psi, \rho\sin\psi),\ \rho>0,\ \psi\in[0,2\pi), \tag{1.69}$$

où $F[\cdot]$ est la transformation de Fourier bidimensionelle.

Le théorème 2 et le lemme 1 sont le fondement de la méthode itérative de Kunyansky. Après avoir précisé $Q_{W,\,D,\,\infty}$ comme opérateur linéaire continu dans $L^2(\mathbb{R}^2)$ on peut étudier les conditions pour que l'équation (1.61) soit résoluble.

(1) Supposons que

$$\sigma_{W,\,D,\,\infty} < 1, \tag{1.70}$$

où $\sigma_{W,\,D,\,\infty}$ est défini dans (1.65). Puis, de (1.66) du théorème 2 il vient que l'opérateur $I + Q_{W,\,D,\,\infty}$ est continuellement inversible. De plus, dans ce cas, l'opérateur $(I + Q_{W,\,D,\,\infty})^{-1}$ peut être donné par la série de Neumann :

$$(I + Q_{W,\,D,\,\infty})^{-1} = \sum_{k=0}^{\infty} (-Q_{W,\,D,\,\infty})^k, \tag{1.71}$$

où $Q_{W,\,D}$ est donné par (1.62) ou par (1.67). Notez que l'hypothèse (1.70) et les formules (1.63), (1.71) peuvent être utilisées pour construire le modèle itératif suivant :

$$\begin{cases} u^{(k+1)} = R^{-1} R_W f - Q_{W,\,D,\,\infty} u^{(k)},\ k \geq 1, \\ u^{(0)} = R^{-1} R_W f, \end{cases}, \ u^{(k)} \xrightarrow{L^2(\mathbb{R}^2)} w_0 f. \tag{1.72}$$

Par conséquent, f peut être bien approximée par $w_0^{-1} u^{(N)}$ pour N assez grand. En pratique, seulement quelques itérations du schéma (1.72) sont nécessaires, car l'hypothèse (1.70) implique que la convergence dans (1.72) est géométrique.

(2) Supposons que la condition (1.70) n'est pas satisfaite. C'est-à-dire

$$\sigma_{W,\,D,\,\infty} \geq 1, \tag{1.73}$$

où $\sigma_{W,,D,\,\infty}$ est défini dans (1.65). Alors, l'opérateur $I + Q_{W,\,D,\,\infty}$ n'est pas nécessairement continuellement inversible, et même s'il l'était, il ne serait pas possible d'utiliser la série Neumann pour $(I + Q_{W,\,D,\,\infty})^{-1}$ comme dans le cas précédent. Cependant, une inversion approximative de R_W peut être définie de la manière suivante.

Soit W_m, $m \geq 0$ un "seuillage de W" (voir la formule (1.49)) définie par la formule :

$$W_m(x, \theta) \stackrel{\text{def}}{=} \sum_{k=-2m}^{2m} w_k(x) Y_k(\theta),\ x \in \mathbb{R}^2,\ \theta \in \mathbb{S}^1. \tag{1.74}$$

Alors, il y a des analogues directs des formules (1.55)-(1.63), du théorème 2 et du lemme 1 pour W_m au lieu de W. En particulier, on peut définir un opérateur $Q_{W,\,D,\,m}$ sur $L^2(\mathbb{R}^2)$ de la manière suivante

$$Q_{W,\,D,\,m} u = \sum_{k=-m,\,k\neq 0}^{m} d_{2k} * \frac{w_{2k}}{w_0} \chi_D u,\ u \in L^2(\mathbb{R}^2), \tag{1.75}$$

$$\|Q_{W,\,D,\,m}\|_{L^2(\mathbb{R}^2) \to L^2(\mathbb{R}^2)} \leq \sigma_{W,\,D,\,m}, \tag{1.76}$$

où les d_{2k} sont les fonctions de (1.68), (1.69), les w_{2k} sont les fonctions de (1.50) et $\sigma_{W\ D,\,m}$ est défini par

$$\sigma_{W,\,D,\,m} \stackrel{\text{def}}{=} \sum_{k=-m,\,k\neq 0}^{m} \sup_{x \in D} \left| \frac{w_{2k}}{w_0} \right|,\ \sigma_{W,\,D,\,0} = 0. \tag{1.77}$$

On appelle f_m, $m \geq 0$ par *la m-ième approximation de f* ($f_m \approx f$), si c'est une solution de l'équation intégrale suivante :

$$(I + Q_{W,\,D,\,m})(w_0 f_m) = R^{-1} R_W f, \tag{1.78}$$

où l'opérateur $Q_{W,\,D,\,D,\,m}$ est défini dans (1.75). Notons que cette équation est complètement analogue à (1.61) avec le même membre à droite $R^{-1}R_W f$ qui est supposé connu.

Le but du seuillage est de choisir $m \in \mathbb{N} \cup \{0\}$ pour s'assurer que l'équation (1.78) est résoluble par la méthode des approximations successives :

$$\begin{array}{l} \text{trouver le plus grand } m,\ m \geq 0, \text{ tel que} \\ \text{la condition } \sigma_{W,\,D,\,m} < 1 \text{ est effectivement satisfaite.} \end{array} \tag{1.79}$$

D'après (1.77) on peut voir qu'il est toujours possible de trouver m tel que (1.79) sera satisfaite. En particulier, pour $m = 0$, l'opérateur $Q_{W,\,D,\,m}$ est égal à zéro et l'équation (1.79) devient triviale :

$$w_0 f_0 = R^{-1}R_W f \Rightarrow f_0 = \frac{R^{-1}R_W}{w_0}. \tag{1.80}$$

On peut noter ici que la formule pour f_0 dans (1.80) est exactement la formule de Chang de (1.43)-(1.44). En choisissant m de sorte que la condition (1.79) soit satisfaite, on peut à nouveau utiliser la série de Neumann pour $(I + Q_{W,\,D,\,m})^{-1}$ pour construire un schéma itératif afin de trouver f_m :

$$\left\{ \begin{array}{l} u_m^{(k+1)} = R^{-1}R_W f - Q_{W,\,D,\,m} u_m^{(k)},\ k \geq 1, \\ u_m^{(0)} = R^{-1}R_W f, \end{array} \right. , \ u_m^{(k)} \xrightarrow{L^2(\mathbb{R}^2)} w_0 f_m. \tag{1.81}$$

Dans ce cas, l'approximation f_m peut être donnée par $u_m^{(N)}/w_0$ pour N assez grand. Comme dans le cas précédent, le choix de m selon (1.79) implique que seulement quelques étapes d'itération sont nécessaires.

Les considérations ci-dessus expliquent la méthode itérative de Kunyansky et, en particulier, la méthode peut être considérée comme une extension directe de la formule originale de Chang. Dans la figure 1.7 on peut voir que f_1 donne une meilleure approximation (c) de la fonction d'intérêt originale (a), que la méthode de Chang (b).

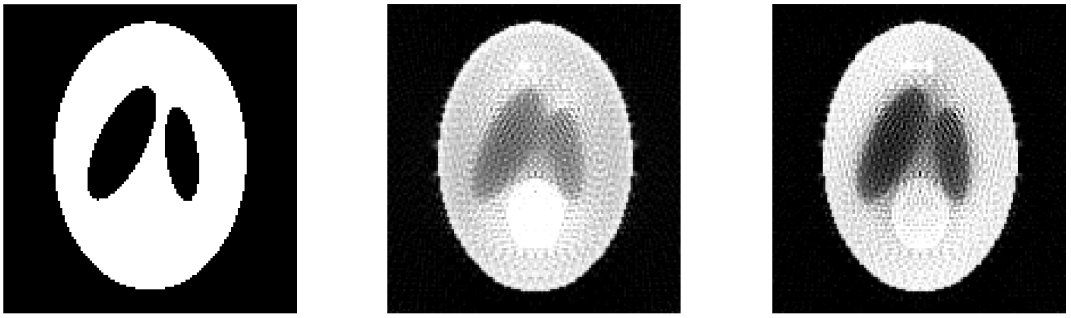

(a) fonction f (b) f_{appr}, méthode de Chang (c) f_1 méthode de Kunyansky

Figure 1.7 Reconstructions dans le cadre de la SPECT en utilisant la formule de Chang et la méthode de Kunyansky pour $m = 1$; pour le modèle d'atténuation $a = a(x)$, $x \in \mathbb{R}^2$ (voir les formules (1.37), (1.38)) nous avons utilisé le modèle Shepp-Logan 3D [Ga+08] avec des paramètres pour une forte atténuation ; voir aussi la figure 1.6

Outre la méthode de Kunyansky pour l'inversion de R_W pour des poids généraux W, il existe d'autres méthodes itératives, par exemple, la méthode de Beylkin [Be84].

Dans la méthode de Beylkin, la reconstruction de f à partir de W et $R_W f$ revient également à résoudre une équation intégrale sur f. Cependant, l'équation intégrale dans [Be84] est très différente de (1.61). Plus précisément, dans la méthode de Beylkin, l'équation intégrale est de type Fredholm, alors que dans (1.61) ce n'est pas le cas car il y a des singularités non-intégrables dans les noyaux des expressions (1.67), (1.68) pour les opérateurs $Q_{W,D,\infty}$, $Q_{W,D,m}$. L'approche de la construction d'une équation intégrale de type Fredholm sur f à partir de W, $R_W f$ est issue de la théorie des opérateurs pseudo-différentiels elliptiques, et consiste principalement à construire *une paramétrix* pour un opérateur elliptique associé à R_W. Une telle approche [15] permet, par exemple, d'effectuer des reconstructions "locales" à partir de $R_W f$, c'est-à-dire reconstruire f ayant un support suffisamment petit ; voir [Be84], [AG07].

Une caractéristique importante de la méthode de Kunyansky est qu'elle est assez robuste en présence de bruit dans les données mesurées ; voir [GuNo14]. Aussi, notons que la formule de Chang et la méthode de Kunyansky sont applicables pour tous les poids W satisfaisant (1.14) et les hypothèses de régularité correspondantes (1.64), (1.70), (1.79). Ces deux caractéristiques nous ont permis d'introduire de nouvelles méthodes d'inversion pour différentes tomographies.

Résumé de l'article 1. Dans cet article nous considérons le problème 1 pour $d = 3$, où

$$\begin{aligned} &\text{les transformées } P_W f \text{ sont connues pour tous les rayons} \\ &\text{parallèles à un plan bidimensionnel fixe } \Sigma_\eta = \{x \in \mathbb{R}^3 : x\eta = 0\}. \end{aligned} \tag{1.82}$$

Ce cadre correspond à l'approche de reconstruction tranche par tranche utilisée dans les tomographies comme la tomographie à rayons X, PET ou SPECT ; voir la figure 1.8.

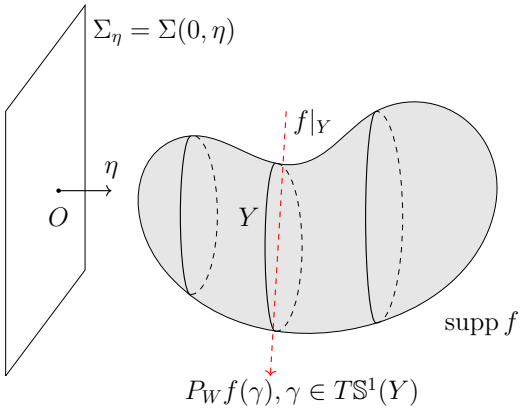

Figure 1.8 Reconstructions tranche par tranche

Au lieu de résoudre le problème inverse tranche par tranche, nous proposons une autre approche basée sur la construction géométrique simple suivante.

Soit $\Sigma = \Sigma(s,\theta)$ un plan bidimensionnel arbitraire qui n'est pas parallèle à Σ_η. Notons que le plan Σ peut être "tranché" dans un ensemble de rayons parallèles qui sont parallèles à Σ_η ; voir la figure 1.9.

[15] La construction d'une paramétrix pour un opérateur pseudodifferentiel elliptique associé à R_W permet, par exemple, de reconstruire des singularités de f à partir de $R_W f$. La reconstruction des singularités de f à partir de R_Wf est aussi connue sous le nom de *tomographie pseudo-locale* et, de l'avis de l'auteur, c'est le plus bel exemple des applications du calcul pseudo-différentiel en imagerie ; voir [Qu93], [Fa+01].

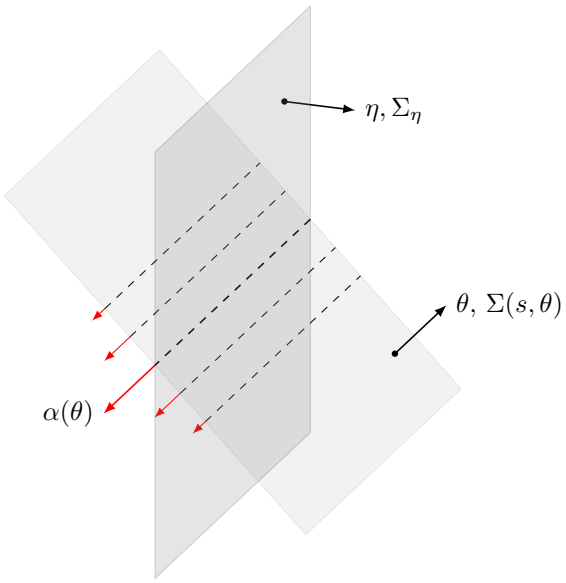

Figure 1.9

De plus, la direction $\alpha \in \mathbb{S}^2$ des rayons qui tranchent Σ est définie uniquement par $\eta, \theta \in \mathbb{S}^2$:

$$\alpha = \alpha(\theta) = \frac{[\eta, \theta]}{|[\eta, \theta]|} \in \mathbb{S}^2, \tag{1.83}$$

où $[\cdot, \cdot]$ désigne le produit vectoriel standard de $\mathbb{R}^3$. Alors, les formules suivantes sont valables :

$$\begin{aligned} &R_w f(s,\theta) = \int_{-\infty}^{+\infty} P_W f(s\theta + \tau[\theta,\alpha],\, \alpha)\, d\tau,\ (s,\theta) \in \mathbb{R} \times \mathbb{S}^2, \\ &w(x,\theta) = W(x, \alpha(\theta)),\ [\eta,\theta] \neq 0,\ x \in \mathbb{R}^3. \end{aligned}, \tag{1.84}$$

où R_w est la transformation de Radon pondérée standard pour le poids w le long des plans de $\mathbb{R}^3$, $\alpha(\theta)$ est donné en (1.83).

En raison des formules de (1.84) les données tomographiques modélisées par $P_W f$ peuvent être réduites aux données modélisées par $R_w f$. L'intuition derrière une telle réduction est de réduire l'impact du bruit sur les reconstructions, par exemple, dans les tomographies d'émission. En effet, dans les reconstructions tranche par tranche pour chaque plan bidimensionnel, la réduction $f|_Y$ est reconstruite à partir de $P_W f|_{T\mathbb{S}^1(Y)}$ et le reste des données est complètement ignoré (voir la figure 1.8) alors que la réduction de (1.84) contient une intégrale qui peut être interprétée comme une régularisation du bruit. Comme nous le verrons plus loin, en appliquant les méthodes d'inversion appropriées à $R_w f$, on obtient des reconstructions plus stables que leurs analogues dans une approche tranche par tranche.

Compte tenu de ce qui précède, nous proposons le schéma suivant pour trouver f à partir de $P_W f$:

(i) En utilisant (1.84) réduire les données fournies par le poid W, $P_W f$ en tout rayon parallèle à Σ_η, à w et $R_w f$ sur tous les plans, sauf les plans parallèles à Σ_η. (1.85)

(ii) Appliquer une méthode d'inversion pour R_w pour $d = 3$ pour trouver f à partir de $R_w f$.

Remarque 2. Il est intérresant de noter que, les formules de (1.84) pour $W \equiv 1$ sont triviales et peuvent être considérées comme un cas particulier du théorème de Fubini : une intégrale $Rf(s,\theta)$ sur un plan $\Sigma(s,\theta)$ peut être vue comme une intégrale des intégrales des rayons $Pf(\cdot,\alpha(\theta))$ le long des rayons qui coupent ce plan. Néanmoins, pour les poids non constants, de telles formules n'existaient pas jusqu'à notre résultat de l'article 1.

Après avoir introduit une méthode pour réduire le problème 1 au problème 2 pour $d = 3$, il est nécessaire d'avoir une méthode pour résoudre le problème 2. Comme nous sommes motivés par des applications tomographiques, nous sommes également intéressés par des méthodes approximatives mais efficaces. Une méthode simple à proposer consiste en un analogue des formules d'inversion approximatives de Chang pour $d \geq 3$.

Compte tenu de (1.43)-(1.45), nous définissons les formules d'inversion approximative suivantes pour R_W pour $d \geq 2$:

$$f_{appr}(x) = \begin{cases} \dfrac{(-1)^{(d-2)/2}}{2(2\pi)^{d-1} w_0(x)} \displaystyle\int_{\mathbb{S}^{d-1}} \mathbb{H}\left[R_W f\right]^{(d-1)}(x\theta,\theta)\, d\theta, \ d \text{ est pair}, \\ \dfrac{(-1)^{(d-1)/2}}{2(2\pi)^{d-1} w_0(x)} \displaystyle\int_{\mathbb{S}^{d-1}} \left[R_W f\right]^{(d-1)}(x\theta,\theta)\, d\theta, \ d \text{ est impair}, \end{cases} \tag{1.86}$$

où

$$w_0(x) \stackrel{\text{def}}{=} \frac{1}{\text{Vol}(\mathbb{S}^{d-1})} \int_{\mathbb{S}^{d-1}} W(x,\theta)\, d\theta, \ w_0(x) \neq 0, \ x \in \mathbb{R}^d, \tag{1.87}$$

$$\begin{aligned} &\left[R_W f\right]^{(d-1)}(s,\theta) = \left(\frac{d}{ds}\right)^{(d-1)} R_W f(s,\theta), \\ &\mathbb{H}g(s) \stackrel{\text{def}}{=} \frac{1}{\pi} p.v. \int_{\mathbb{R}} \frac{g(t)}{s-t} dt, \ s \in \mathbb{R}, \ \theta \in \mathbb{S}^{d-1}. \end{aligned} \tag{1.88}$$

De plus, nous supposons que les formules (1.86)-(1.88) sont définies seulement pour W satisfaisant (1.14).

Remarque 3. En notation générique pour les transformations de Radon pondérées et leurs inversions, la formule (1.86) a la forme suivante :

$$f_{appr}(x) = \frac{R^{-1} R_W f(x)}{w_0(x)}, \ x \in \mathbb{R}^d, \tag{1.89}$$

où R^{-1} est l'inverse de la transformation de Radon classique, $w_0(x)$, $x \in \mathbb{R}^d$ est défini dans (1.87). De (1.46), (1.89) il est clair que les formules (1.86)-(1.88) sont des extensions directes de la formule de Chang à $d \geq 3$.

De plus, nous avons étendu le théorème 1 aux dimensions supérieures $d \geq 3$, et en combinaison avec cela nous avons obtenu le résultat suivant

Théorème 3. *Considerons W satisfaisant* (1.14) *et continu sur $\mathbb{R}^d \times \mathbb{S}^{d-1}$, $d \geq 2$. Soit f_{appr} défini par* (1.86)-(1.88) *au regard de $R_W f$ et w_0. Alors*

$$f_{appr} = f \ \textit{(au sens des distributions) sur } \mathbb{R}^d \textit{ pour tout } f \in C_c(\mathbb{R}^d) \tag{1.90}$$

si et seulement si

$$w_0(x) \equiv \frac{1}{2}\left(W(x,\theta) + W(x,-\theta)\right),\ x \in \mathbb{R}^d,\ \theta \in \mathbb{S}^{d-1}, \tag{1.91}$$

où $C_c(\mathbb{R}^d)$ désigne l'espace des fonctions continues à support compact sur $\mathbb{R}^d$.

Remarque 4. Notons que le poids w apparaissant dans (1.84) n'est pas continu, en général. La discontinuité de w est liée à la non-unicité du "découpage" pour les plans parallèles à Σ_η. D'autre part, l'ensemble de discontinuité de w est de mesure nulle sur $\mathbb{R} \times \mathbb{S}^2$ ce qui rend le théorème 3 toujours applicable pour w de (1.84).

Le résultat du théorème 3 soutient l'intuition que les analogues (1.86)-(1.88) de la formule de Chang de (1.43), (1.44) pourraient être efficaces pour les applications tomographiques. Cette intuition a également été confirmée par nos expériences numériques qui sont présentées plus loin.

Enfin, du point de vue mathématique, le théorème 3 pourrait aussi être intéressant comme extension du théorème 1 aux dimensions impaires, puisqu'on sait que les inversions des transformations de Radon sont très différentes pour les dimensions paires et impaires ; voir [Na86].

Les détails de construction de (1.84) et la preuve du théorème 3 sont présentés au chapitre 3.

Bien qu'avec les formules d'inversion approximatives de Chang pour $d \geq 3$ on puisse tester la nouvelle méthode d'inversion proposée pour P_W, ces formules étaient encore trop simples et heuristiques pour conclure nos études. Par la suite, dans l'article 2, nous développons notre nouvelle méthode d'inversion en étendant l'algorithme de Kunyansky à $d \geq 3$.

Résumé de l'article 2. Dans cet article, nous continuons à développer les résultats de l'article 1 et des articles [Ku92], [No14], [GuNo14]. En particulier, nous proposons une extension de l'algorithme itératif de Kunyansky de $d = 2$ à $d \geq 3$. Pour la dimension $d = 3$ notre extension est d'importance pour les applications tomographiques compte tenu de la nouvelle méthode de reconstruction de l'article 1.

Nous considérons le problème 2 et nous supposons que

$$W \in C(\mathbb{R}^3 \times \mathbb{S}^2) \cap L^\infty(\mathbb{R}^3 \times \mathbb{S}^2), \tag{1.92}$$

$$w_{0,0}(x) \stackrel{\text{def}}{=} \frac{1}{4\pi} \int\limits_{\mathbb{S}^2} W(x,\theta)\, d\theta,\ w_{0,0}(x) \neq 0,\ x \in \mathbb{R}^3, \tag{1.93}$$

$$f \in L^\infty(\mathbb{R}^3),\ \operatorname{supp} f \subset D, \tag{1.94}$$

où W, f sont à valeurs complexes, $d\theta$ est un élément de mesure uniforme sur $\mathbb{S}^2$, D est un domaine borné ouvert (qui est fixé *à priori*).

De la même manière que [Ku92], [GuNo14], nous réduisons le problème d'inversion de R_W pour $d = 3$ à la résolution d'une certaine équation intégrale linéaire. En particulier, nous montrons que si la partie paire de W en θ (i.e., $\frac{1}{2}(W(x,\theta) + W(x,-\theta))$) est proche de $w_{0,0}$, l'équation intégrale peut être résolue avec des méthodes d'approximations successives. Par contre, si l'approximation ci-dessus n'est pas vérifiée, on définit une série d'approximations $f_m \approx f$, $m \in \mathbb{N} \cup \{0\}$, où m est choisi en fonction de W. Cela correspond à (1.70), (1.73) pour l'algorithme bidimensionnel original de Kunyansky.

Ci-dessous nous expliquons l'extension de l'algorithme de Kunyansky à $d = 3$. Les détails de nos extensions à $d > 3$ peuvent être trouvés dans le chapitre 4.

De la même manière que les développements bidimensionnels (1.56)-(1.81), nous considérons les développements suivants:

$$W(x,\theta(\gamma,\varphi)) = \sum_{k=0}^{\infty}\sum_{n=-k}^{k} w_{k,n}(x)Y_k^n(\gamma,\varphi), \tag{1.95}$$

$$W_m(x,\theta(\gamma,\varphi)) \stackrel{\text{def}}{=} \sum_{k=0}^{m}\sum_{n=-k}^{k} w_{2k,n}(x)Y_{2k}^n(\gamma,\varphi),\ x\in\mathbb{R}^3,\ m\in\mathbb{N}\cup\{0\}, \tag{1.96}$$

$$Y_k^n(\gamma,\varphi) \stackrel{\text{def}}{=} p_k^{|n|}(\cos(\gamma))e^{in\varphi},\ k\in\mathbb{N}\cup\{0\},\ n=-k,\dots k, \tag{1.97}$$

$$\theta(\gamma,\varphi) = (\sin\gamma\cos\phi, \sin\gamma\sin\varphi, \cos\gamma)\in\mathbb{S}^2,\ \gamma\in[0,\pi],\ \varphi\in[0,2\pi], \tag{1.98}$$

où $p_k^n(x)$, $x\in[-1,1]$, sont des polynômes associés de Legendre semi-normalisés (voir [SW16]). En particulier, les fonctions Y_k^n de (1.97) constituent la base des harmoniques sphériques dans $L^2(\mathbb{S}^2)$ avec la paramétrisation de (1.98). Les coefficients $w_{k,n}$ de (1.95) sont donnés par les formules suivantes :

$$\begin{aligned} w_{k,n} &= c(k,n)\int_0^{2\pi} e^{-in\varphi}\,d\varphi\int_0^{\pi} W(x,\theta(\gamma,\phi))p_k^{|n|}(\cos\gamma)\sin\gamma\,d\gamma,\\ c(k,n) &= \frac{2k+1}{8\pi},\ k\in\mathbb{N}\cup\{0\},\ n=-k,\dots k. \end{aligned} \tag{1.99}$$

Compte tenu des développements bidimensionnelles (1.55)-(1.81) on définit les objets suivants :

$$Q_{W,D,\infty}u(x) \stackrel{\text{def}}{=} R^{-1}(R_{W,D,\infty}u)(x),\ x\in\mathbb{R}^3, \tag{1.100}$$

$$Q_{W,D,m}u(x) \stackrel{\text{def}}{=} R^{-1}(R_{W,D,m}u)(x),\ m\in\mathbb{N},\ Q_{W,D,m}u(x)=0 \text{ pour } m=0, \tag{1.101}$$

$$\sigma_{W,D,\infty} \stackrel{\text{def}}{=} \sum_{k=1}^{\infty}\sum_{n=-2k}^{2k}\sup_{x\in D}\left|\frac{w_{2k,n}(x)}{w_{0,0}(x)}\right|, \tag{1.102}$$

$$\sigma_{W,D,m} \stackrel{\text{def}}{=} \sum_{k=1}^{m}\sum_{n=-2k}^{2k}\sup_{x\in D}\left|\frac{w_{2k,n}(x)}{w_{0,0}(x)}\right|,\ \text{pour } m\in\mathbb{N}, \tag{1.103}$$

où R^{-1} est l'inversion classique des transformations de Radon pour $d=3$ (voir [Ra17], [Na86]), les coefficients $w_{0,0}, w_{2k,n}$ sont définis dans (1.93), (1.99) et

$$R_{W,D,\infty}u(s,\theta(\gamma,\varphi)) \stackrel{\text{def}}{=} \sum_{k=1}^{\infty}\sum_{n=-2k}^{2k} Y_{2k}^n(\gamma,\varphi)R(\chi_D u)(s,\theta(\gamma,\varphi)), \tag{1.104}$$

$$R_{W,D,m}u(s,\theta(\gamma,\varphi)) \stackrel{\text{def}}{=} \sum_{k=1}^{m}\sum_{n=-2k}^{2k} Y_{2k}^n(\gamma,\varphi)R(\chi_D u)(s,\theta(\gamma,\varphi)), \tag{1.105}$$

$$x\in\mathbb{R}^3,\ s\in\mathbb{R},\ \theta(\gamma,\varphi)\in\mathbb{S}^2,$$

où Y_k^n sont définis dans (1.97), R est la transformation de Radon classique pour $d=3$, $\chi_D=\chi_D(x)$ est la fonction caractéristique du domaine D de (1.94), u est une fonction test sur $\mathbb{R}^3$.

Notons que les formules (1.100)-(1.105) sont des analogues directs de (1.62), (1.65), (1.75), (1.77) de la méthode Kunyansky pour $d=2$. La seule différence est que les développements

de W, W_m, les nouveaux opérateurs $Q_{W,D,\infty}$, $Q_{W,D,m}$ et les coefficients $w_{2k,n}$ sont réécrits en termes d'harmoniques sphériques Y_k^n sur $\mathbb{S}^2$. Notons aussi que dans les formules (1.100)-(1.105) parmi les termes $w_{k,n}$, Y_k^n seuls ceux avec des indices k pairs sont présents. Cela est similaire à (1.55), (1.56) et, en particulier, parce que $R^{-1}R_W f = R^{-1}R_{W_{sym}} f$, où W_{sym} est la partie paire W en θ (c'est-à-dire $W_{sym}(x,\theta) = \frac{1}{2}(W(x,\theta) + W(x,-\theta))$).

Ensuite, nous montrons que $Q_{W,D,\infty}$, $Q_{W,D,m}$ sont des opérateurs linéaires bornés dans $L^2(\mathbb{R}^2)$.

Lemme 2. *Soit $Q_{W,D,\infty}$, $Q_{W,D,m}$ les opérateurs définis par* (1.100), (1.101), *respectivement, et u une fonction test sur $\mathbb{R}^3$. Alors*

$$Q_{W,D,\infty}u = \sum_{k=1}^{\infty}\sum_{n=-2k}^{2k} d_{2k,n} * \frac{w_{2k,n}}{w_{0,0}}\chi_D u, \tag{1.106}$$

$$Q_{W,D,m}u = \sum_{k=1}^{m}\sum_{n=-2k}^{2k} d_{2k,n} * \frac{w_{2k,n}}{w_{0,0}}\chi_D u, \tag{1.107}$$

où les coefficients $w_{k,n}$ sont définis dans (1.99), *$*$ désigne la convolution dans $\mathbb{R}^3$, $d_{2k,n}$ sont définis par la formule :*

$$d_{2k,n}(x(r,\gamma,\varphi)) = (-1)^k \frac{2^{1/2}\Gamma(\frac{3}{2}+k)}{\pi\Gamma(k)} \frac{Y_{2k}^n(\gamma,\varphi)}{r^3},\ r>0, \tag{1.108}$$

où $\Gamma(\cdot)$ est la fonction Gamma, $x(r,\gamma,\varphi)$ est défini par la formule :

$$x(r,\gamma,\phi) = (r\sin\gamma\cos\varphi, r\sin\gamma\sin\varphi, r\cos\gamma) \in \mathbb{R}^3,\ \gamma\in[0,\pi],\ \varphi\in[0,2\pi],\ r\geq 0. \tag{1.109}$$

En outre, pour $d_{2k,n}$ dans (1.108) *la propriété suivante est satisfaite:*

$$F[d_{2k,n}](\xi) = Y_{2k,n}\left(\frac{\xi}{|\xi|}\right),\ \xi\in\mathbb{R}^3\backslash\{0\}, \tag{1.110}$$

où $F[\cdot]$ est la transformation de Fourier dans $\mathbb{R}^3$.

Lemme 3. *Les opérateurs linéaires $Q_{W,D,\infty}$, $Q_{W,D,m}$ définis dans* (1.106), (1.107), *sont des operateurs linéaires bornés dans $L^2(\mathbb{R}^2)$ et les estimations suivantes sont satisfaites :*

$$\|Q_{W,D,\infty}\|_{L^2(\mathbb{R}^2)\to L^2(\mathbb{R}^2)} \leq \sigma_{W,D,\infty}, \tag{1.111}$$

$$\|Q_{W,D,m}\|_{L^2(\mathbb{R}^2)\to L^2(\mathbb{R}^2)} \leq \sigma_{W,D,m},\ m\in\mathbb{N}\cup\{0\}, \tag{1.112}$$

où $\sigma_{W,D,\infty}$, $\sigma_{W,D,m}$ sont définis dans (1.102), (1.103).

De la même manière que la méthode originale de Kunyansky, nous réduisons le problème d'inversion de R_W à la résolution d'une équation intégrale linéaire. En particulier, cette équation est obtenue en appliquant R^{-1} à $R_W f$ et en exprimant l'opérateur $R^{-1}R_W$ en termes de $Q_{W,D,D,\infty}$.

Lemme 4. *Soit*

$$\sum_{k=1}^{\infty}\sum_{n=-2k}^{2k} \left|\left|\frac{w_{2k,n}}{w_{0,0}}\right|\right|_{L^2(D)} < +\infty, \tag{1.113}$$

où les $w_{k,n}$ sont définis dans (1.99). *Alors*

$$R^{-1}R_W f \in L^2(\mathbb{R}^3). \tag{1.114}$$

De plus, la formule suivante s'applique :

$$R^{-1}R_W f = w_{0,0}f + \sum_{k=1}^{\infty}\sum_{n=-2k}^{2k} d_{2k,n} * w_{2k,n}f = (I + Q_{W,D,\infty})(w_{0,0}f), \tag{1.115}$$

où f satisfait (1.94)*, R^{-1} est l'inversion de la transformation de Radon classique et $Q_{W,D,\infty}$ est donné par* (1.100)*.*

Compte tenu de la méthode de Kunyansky susmentionnée et des résultats des lemmes 2-4 nous proposons la méthode suivante de reconstruction de f à partir de $R_W f$:

(1) Soit

$$\sigma_{W,D,\infty} < 1. \tag{1.116}$$

L'inégalité (1.116) et l'estimation (1.111) impliquent que $I + Q_{W,D,\infty}$ est continuellement inversible et l'identité suivante est vérifiée (au sens de norme d'opérateur dans $L^2(\mathbb{R}^3)$) :

$$(I + Q_{W,D,\infty})^{-1} = \sum_{j=0}^{\infty}(-Q_{W,D,\infty})^j. \tag{1.117}$$

Théorème 4. *Supposons que les conditions* (1.92)-(1.94)*,* (1.116) *soient remplies. Alors, R_W est injective dans $L^2(\mathbb{R}^2)$ et l'inversion peut être exprimée par la formule suivante :*

$$f = w_{0,0}^{-1}(I + Q_{W,D,\infty})^{-1}R^{-1}R_W f. \tag{1.118}$$

où $w_{0,0}$ est défini dans (1.93)*, R^{-1} est l'inversion de la transformation de Radon classique, l'opérateur $(I + Q_{W,D,\infty})^{-1}$ est donné dans* (1.117)*.*

La formule (1.118) peut être considérée comme une équation intégrale pour $w_{0,0}f$ et sous l'hypothèse (1.116) elle peut être résolue par la méthode des approximations successives :

$$\begin{cases} u^{(k+1)} = R^{-1}R_W f - Q_{W,D,\infty}u^{(k)},\ k \geq 1, \\ u^{(0)} = R^{-1}R_W f, \end{cases}, \ u^{(k)} \xrightarrow{L^2(\mathbb{R}^2)} w_{0,0}f. \tag{1.119}$$

En choisissant N assez grand dans (1.119) on prend f comme $u^{(N)}/w_{0,0}$. En pratique, seulement quelques itérations du schéma susmentionné sont nécessaires, car sous l'hypothèse (1.116) la convergence de (1.119) vers $w_{0,0}f$ est géométrique.

En pratique, l'hypothèse (1.116) n'est pas toujours satisfaite [GuNo14], donc, nous proposons une série d'inversions approximatives $f_m \approx f$, $m \in \mathbb{N} \cup \{0\}$.

(2) Soit

$$\begin{aligned} &\sigma_{W,D,m} < 1, \text{ pour } m \in \mathbb{N} \cup \{0\}, \\ &\sigma_{W,D,\infty} < +\infty, \end{aligned} \tag{1.120}$$

où $\sigma_{W,D,\infty}, \sigma_{W,D,m}$ sont définis dans (1.102), (1.103), respectivement.

L'hypothèse de (1.120) et l'inégalité (1.112) dans le lemme 3 implique que $I + Q_{W,D,m}$ est continuellement inversible et son inverse peut être donné (au sens de norme d'opérateur dans $L^2(\mathbb{R}^3)$):

$$(I + Q_{W,D,m})^{-1} = \sum_{j=0}^{\infty}(-Q_{W,D,m})^j, \tag{1.121}$$

où I est l'opérateur identité dans $L^2(\mathbb{R}^3)$.

Théorème 5. *Supposons que les conditions* (1.92)-(1.94), (1.120) *soient satisfaites. Alors*

$$f \approx f_m \stackrel{\text{def}}{=} (w_{0,0})^{-1}(I + Q_{W,\,D,\,m})^{-1}R^{-1}R_W f, \tag{1.122}$$

$$f = f_m - (w_{0,0})^{-1}(I + Q_{W,\,D,\,m})^{-1}R^{-1}R_{\delta W_m} f, \tag{1.123}$$

$$\|f - f_m\|_{L^2(D)} \leq \frac{\|f\|_\infty}{c(1 - \sigma_{W,\,D,\,m})} \sum_{k=m+1}^{\infty} \sum_{n=-2k}^{2k} \|w_{2k,n}\|_{L^2(D)} < +\infty, \tag{1.124}$$

où

$$c = \min_{x \in D} |w_{0,0}(x)|,\ c > 0, \tag{1.125}$$

$$\delta W_m(x, \theta(\gamma, \varphi)) \stackrel{\text{def}}{=} W(x, \theta(\gamma, \varphi)) - \sum_{k=0}^{2m+1} \sum_{n=-k}^{k} w_{k,n}(x) Y_k^n(\gamma, \varphi), \tag{1.126}$$

$$x \in \mathbb{R}^3,\ \gamma \in [0, \pi],\ \varphi \in [0, 2\pi],\ m \in \mathbb{N} \cup \{0\}, \tag{1.127}$$

$w_{0,0}$ *est définie dans* (1.93), $\theta(\gamma, \phi)$ *est défini dans* (1.98), *les* Y_k^n *sont définis dans* (1.97), *l'opérateur* $(I + Q_{W,\,D,\,m})^{-1}$ *est défini dans* (1.121).

Remarque 5. La formule (1.122) peut être considérée comme l'équation intégrale linéaire suivante sur $w_{0,0} f_m$:

$$w_{0,0} f_m + Q_{W,\,D,\,m}(w_{0,0} f_m) = R^{-1} R_W f. \tag{1.128}$$

Les inégalités de (1.120) et l'identité (1.121) impliquent que l'équation (1.128) est résoluble par la méthode des approximations successives :

$$\begin{cases} u_m^{(k+1)} = R^{-1}R_W f - Q_{W,\,D,\,m} u_m^{(k)},\ k \geq 1, \\ u_m^{(0)} = R^{-1}R_W f, \end{cases},\ u_m^{(k)} \xrightarrow{L^2(\mathbb{R}^2)} w_{0,0} f. \tag{1.129}$$

En fait, la condition $\sigma_{W,\,D,\,\infty} < +\infty$ peut être relâchée de la façon suivante :

$$\sum_{k=1}^{\infty} \sum_{n=-2k}^{2k} \left\| \frac{w_{2k,n}}{w_{0,0}} \right\|_{L^2(D)} < +\infty, \tag{1.130}$$

où $w_{k,n}$ sont définis dans (1.99).

La formule (1.122) est une extension de la formule bidimensionelle de Chang de [Ch78], [No11], [GuNo14] pour $d = 2$ et aussi une extension de la formule de type Chang de l'article 1, où cette formule était donnée pour $m = 0$.

Comme $m \geq 0$ peut être choisi de sorte que l'inégalité (1.120) soit satisfaite, nous proposons la reconstruction approximative suivante de f à partir de $R_W f$:

$$\begin{aligned} &(i) \text{ trouver } m \text{ maximal tel que (1.120) soit satisfaite,} \\ &(ii) \text{ reconstruire } f \text{ par approximations via } f_m \text{ en utilisant (1.122).} \end{aligned} \tag{1.131}$$

Remarque 6. Pour les applications pratiques, il est évident qu'il n'est jamais possible de considérer un nombre infini de termes dans (1.106), même si l'inégalité (1.116) est satisfaite. Par conséquent, l'approche de (1.131) est toujours utilisée. L'implémentation numérique

de la méthode de (1.131) est directe suivant les formules (1.95)-(1.98), (1.103), (1.120)-(1.122). De plus, l'implémentation des opérateurs $Q_{W,D,\infty}$, $Q_{W,D,m}$ est est très simple grâce à la formule (1.110). Au vu de ces formules, les opérateurs $Q_{W,D,\infty}$, $Q_{W,D,m}$ peuvent être réécrits sous la forme suivante :

$$\begin{aligned} Q_{W,D,\infty}u &= \mathcal{F}_\xi^{-1}\left(\sum_{k=1}^{\infty}\sum_{n=-2k}^{2k} Y_{2k}^n\left(\frac{\xi}{|\xi|}\right)\mathcal{F}_x\left(\frac{w_{2k,n}}{w_{0,0}}\chi_D u\right)(\xi)\right), \\ Q_{W,D,m}u &= \mathcal{F}_\xi^{-1}\left(\sum_{k=1}^{m}\sum_{n=-2k}^{2k} Y_{2k}^n\left(\frac{\xi}{|\xi|}\right)\mathcal{F}_x\left(\frac{w_{2k,n}}{w_{0,0}}\chi_D u\right)(\xi)\right), \end{aligned} \tag{1.132}$$

où $u \in L^2(\mathbb{R}^3)$, $\mathcal{F}_\xi^{-1}$, $\mathcal{F}_x$ sont les transformations de Fourier inverse et directe pour les variables ξ, $x \in \mathbb{R}^3$, respectivement. Les formules de (1.132) sont beaucoup plus faciles à implémenter numériquement que (1.106), (1.106), car les premières sont seulement les compositions de transformations de Fourier et les multiplications par des harmoniques sphériques Y_{2k}^n. Les détails et commentaires de nos implémentations peuvent être trouvés dans le prochain paragraphe concernant la simulation numérique.

Pour conclure l'exposé des résultats de l'article 2, nous mentionnons également que les formules et méthodes de (1.92)-(1.132) permettent des extensions simples à $d > 3$. Les détails de ces extensions sont donnés dans le chapitre 4.

Nous testons ensuite numériquement la formule de type Chang en trois dimensions et également la méthode de type Kunyansky de (1.131).

Simulation numérique

Nous présentons ici des tests numériques de nos méthodes d'inversion des articles 1, 2. Tous nos tests ont été réalisés dans le cadre de SPECT en 3D, où les données ont été modélisées par $P_W f$ dans le cadre de reconstructions tranche par tranche. Plus précisément, notre simulation numérique comportait les étapes suivantes :

1. Pour un modèle d'atténuation donné $a = a(x)$ et une distribution $f = f(x)$, $x \in \mathbb{R}^3$, simuler les données $P_{W_a} f(\gamma)$, $\gamma \in \Gamma$, où W_a est donné par (1.37), (1.38), Γ est une grille discrète dans $T\mathbb{S}^2$ qui correspond aux acquisitions dans les reconstructions tranche par tranche.

2. En utilisant les développements de l'article 1 (formules (1.83)-(1.84)), réduire les données d'émission $P_{W_a} f(\gamma)$, $\gamma \in \Gamma$ aux $R_W f(s,\theta)$, $(s,\theta) \in \Pi$, où Π est une grille discrète sur $\mathbb{R} \times \mathbb{S}^2$, le poids W est construit à partir de W_a et en utilisant les formules (1.84).

3. Appliquer nos méthodes d'inversion des articles 1, 2 (les analogues de la formule de Chang et de l'algorithme itératif de Kunyansky pour $d = 3$) pour reconstruire f à partir de $R_W f(s,\theta)$, $(s,\theta) \in \Pi$.

Pour la simulation des données synthétiques, notre choix de modèles d'atténuation, de distributions de nucléotide et de grilles Γ, Π est décrit ci-dessous en détail. L'objectif de la simulation sur des données synthétiques est de montrer qu'en effet, la réduction proposée apporte plus de stabilité aux reconstructions, indépendamment de la méthode utilisée - formule de type Chang ou méthode itérative plus avancée de type Kunyansky.

En plus des expériences sur des données synthétiques, nous avons également appliqué nos méthodes d'inversion sur des données réelles obtenues du *Service Hospitalier Frédéric Joliot, CEA (Orsay)*. Plus précisément, l'expérience réelle a été réalisée sur un singe qui a été

soumis à une procédure SPECT standard. Les détails de cette expérience sont décrits plus loin dans le texte. Dans l'expérience sur des données réelles, comme la distribution réelle du nucléotide n'était pas connue, il n'a pas été possible de mesurer quantitativement la qualité des reconstructions. Le but de cette expérience était de démontrer que notre méthode est applicable, en principe, dans des procédures SPECT réalistes.

Le contenu de cette sous-section est organisé comme suit. Tout d'abord, nous décrivons l'expérience sur les données synthétiques. Nous décrivons les modèles de l'atténuation, des distributions de nucléotides et le processus de simulation des données d'émission (géométrie des acquisitions de $P_{W_a} f$, modélisation du bruit). Nous présentons par la suite les reconstructions des distributions nucléotidiques à l'aide de la formule de Chang et de la méthode itérative de Kunyansky en 3D. Nous comparons visuellement et numériquement la qualité de nos reconstructions avec des méthodes bidimensionnelles basées sur la formule d'inversion de Chang et l'algorithme itératif de Kunyansky. Ensuite, nous présentons les résultats des reconstructions pour l'expérience réelle sur le singe. Dans ce cas, nous ne présentons que des images de reconstructions pour notre méthode tridimensionnelle basée sur la formule de Chang. Enfin, nous commentons nos implémentations et fournissons un lien vers celles-ci.

Modèle d'atténuation

Dans nos expériences pour le modèle d'atténuation, nous avons utilisé l'extension du célèbre modèle Shepp-Logan en 3D ([Ga+08], [SL74]) ; voir la figure 1.10. Ce modèle imite la tête humaine et est standard pour tester les algorithmes de reconstruction dans le domaine des tomographies.

(a) $i_z = 40$ (b) $i_z = 64$ (c) $i_z = 80$

Figure 1.10 Application d'atténuation : Coupe transversale du modèle de Shepp-Logan par plans $z = const$

Le modèle se compose d'un grand ellipsoïde qui représente le cerveau et de plusieurs petits ellipsoïdes qui représentent ses caractéristiques. La couche ellipsoïdale externe avec des axes de 13.8 cm, 18 cm et 18.4 cm de longueur correspond à l'os du crâne ; l'atténuation standard du matériau osseux est égale à 0.17 cm^{-1}. L'atténuation à l'intérieur d'un ellipsoïde interne plus petit représentant le matériau cérébral est égale à 0.15 cm^{-1}. Les sphères plus petites (sphères gris foncé sur la figure 1.10) représentent des inclusions dans le cerveau et ont une atténuation de 0.10 cm^{-1}. Le modèle inclut également des cavités qui sont données par deux régions ellipsoïdales près du centre (voir les ellipsoïdes en couleur noire, figure 1.10. (b), (c))). Dans ces régions, l'atténuation a été fixée à zéro.

La caractéristique quantitative qui décrit l'intensité de l'atténuation est la longueur optique de l'atténuation le long de certains trajets sélectionnés (la longueur optique le long d'un trajet est une intégrale du coefficient d'atténuation le long de ce chemin). Dans le modèle donné, les longueurs optiques suivant les axes X, Y et Z sont égales respectivement à 2.44, 3.89 et 4.81. D'un point de vue pratique, ces valeurs correspondent à une forte atténuation.

Pour étudier l'efficacité de nos méthodes de reconstruction pour différents régimes, nous avons utilisé deux modèles. Le premier, qui est référencé par a_1 ou *"atténuation forte"*, est le modèle de Shepp-Logan avec les paramètres décrits ci-dessus. Le second modèle, appelé a_2 ou *"atténuation faible"*, correspond au même modèle que le premier mais les valeurs d'atténuation ont été multipliées par un facteur de 1/10 ($a_2 = 10^{-1}a_1$). Ainsi, les longueurs optiques le long de l'axe X, Y, Z pour le deuxième modèle d'atténuation a_2 sont égales à 0.244, 0.389 et 0.481, respectivement. Du point de vue pratique, cela correspond au cas d'une très faible atténuation.

Avant de poursuivre, nous notons que toutes les images de cette sous-section seront présentées dans une échelle de gris linéaire, où les couleurs plus foncées correspondent à des valeurs plus petites (la couleur noire correspond à zéro).

Modèle pour la distribution des nucléotides

Nous avons utilisé deux modèles pour la distribution des nucléotides. Le premier, désigné par f_1 ou *modèle 1*, est décrit par une fonction caractéristique de l'ellipsoïde interne du modèle de Shepp-Logan du paragraphe précédent, voir la figure 1.11 (a).

(a) modèle 1, f_1 (b) modèle 2, f_2

Figure 1.11 Distribution des nucléotides

Le but du modèle 1 est de tester la capacité à reconstruire des distributions du nucléotide uniformes dans l'espace et variant lentement.

En même temps, il est important de tester les algorithmes lorsque la distribution de l'activité a une distribution très non uniforme dans l'espace. Pour ces raisons, nous utilisons le modèle f_2 ou *modèle 2*, qui est décrit par une couche sphérique placée presque au centre de l'application d'atténuation ; voir la figure 1.11. (b) (le modèle de fond en gris est placé uniquement pour la visualisation de la position de f_2 par rapport au modèle d'atténuation). Le rayon extérieur de la couche sphérique est de 4 cm et le rayon de l'intérieur est égal à 2 cm. En particulier, le modèle 2 est utilisé pour simuler le réglage classique en SPECT : reconstruire la distribution d'un nucléotide qui a tendance à se concentrer dans le cerveau d'un patient.

Enfin, notons que sur la figure 1.11 seules des tranches de modèles 1, 2 sont présentées, alors que ces derniers sont des objets complets en trois dimensions.

Simulation des données sans bruit

Rappelons que dans la SPECT, les données d'émission sont modélisées par $P_{W_a} f(\gamma)$ pour les rayons γ qui correspondent au cadre des reconstructions tranche par tranche ; voir aussi la figure 1.12.

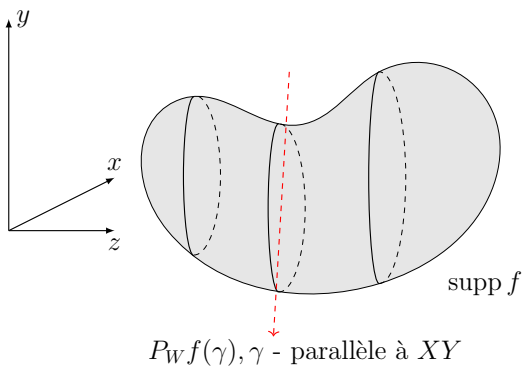

Figure 1.12

Plus précisément, cela signifie que

$$\begin{aligned} &P_{W_a} f(\gamma) \text{ sont donnés pour tous les rayons } \gamma \\ &\text{qui sont parallèles au plan } XY \text{ ; voir la figure 1.12,} \end{aligned} \tag{1.133}$$

où

1. les fonctions test $f = f(x)$, $x \in \mathbb{R}^3$, sont données par f_1, f_2.
2. le poids W_a est donné par les formules (1.37), (1.38), où a est donné par a_1, a_2.

Les modèle d'activité f_1, f_2 et les applications d'atténuation a_1, a_2 sont donnés par leurs valeurs sur la grille cartésienne du cube unitaire $[-1,1]^3$ et on suppose que ces fonctions ont leur supports dans la boule centrée de rayon $R = 1.0$.

En particulier, la grille cartésienne Ω_N sur $[-1,1]^3$ est définie comme suit

$$\begin{aligned} &\Omega_N = \{(x_i, y_j, z_k) : x_i = -R + i\Delta x,\ y_j = -R + j\Delta y,\ z_k = -R + k\Delta z\}, \\ &\Delta x = \Delta y = \Delta z = 2R/(N-1),\ i,\ j,\ k \in \{0, \dots N-1\}, \end{aligned} \tag{1.134}$$

où N est le nombre de points dans la grille dans une direction. Dans tous nos calculs nous avons pris $N = 129$ ce qui correspond à la résolution standard en SPECT. Pour les évaluations de $P_{W_a} f$ pour les poids W_a donnés par (1.37) sur ces grilles discrètes, nous avons supposé que les fonctions f_1, f_2 et a_1, a_2 étaient linéaire et continues par morceaux entre les points de la grille.

Pour faire une version discrétisée de (1.133) nous avons utilisé la grille Γ dans l'ensemble des rayons qui correspond au cadre des reconstructions tranche par tranche, où dans chaque plan $z = const$ les données d'émission $P_{W_a} f$ sont modélisées pour la géométrie de faisceau parallèle ; [Na86]. Selon cette grille de configuration, Γ se compose d'une grille de rayons dont chaque plan est parallèle à XY (i.e., $z = const$) et d'une grille suivante la coordonnée Z dans l'intervalle $[-1,1]$. Plus précisément, la grille Γ a été définie comme suit :

$$\begin{aligned} &\Gamma = \{\gamma = \gamma(z_i, s_j, \varphi_k) : z_i = -R + i\Delta z,\ s_j = -R + j\Delta s,\ \varphi_k = k\Delta\varphi\}, \\ &i = 0, \dots n_z - 1,\ j = 0, \dots n_s - 1,\ k = 0, \dots n_\varphi - 1, \\ &\Delta z = 2R/(n_z - 1),\ \Delta s = 2R/(n_s - 1),\ \Delta\varphi = 2\pi/n_\varphi, \end{aligned} \tag{1.135}$$

où $\gamma(z, s, s, \varphi)$ est donné par les formules

$$\begin{aligned} &\text{le rayon } \gamma = \gamma(z, s, \varphi) \text{ pour } (z, s, \varphi) \in [-1,1] \times [-1,1] \times [0, 2\pi] \text{ est définie par} \\ &\gamma(z, s, \varphi) = \{(x_1, x_2, x_3) : x_1 = s\cos(\varphi) - t\sin(\varphi),\ x_2 = s\sin(\varphi) + t\cos(\varphi),\ x_3 = z,\ t \in \mathbb{R}\}. \end{aligned} \tag{1.136}$$

Pour nos expériences, nous avons utilisé $n_z = n_s = 129$. Le nombre de projections n_φ a été choisi égal à 128. Notons que ce nombre est inférieur à celui de la formule [Kun01] ($n_\varphi = 400$), où la valeur de n_φ a été choisie en fonction de la condition d'échantillonnage de type Shannon-Nyquist pour les transformations des rayons (voir chapitre 3 dans [Na86]). Notre choix pour $n_\varphi = 128$ a été motivé par l'expérience sur des données réelles dans lesquelles nous n'avions que ce nombre de directions dans chaque plan de coupe.

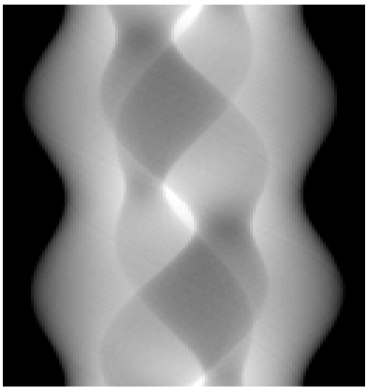

(a) $P_{W_a} f_1$, atténuation faible

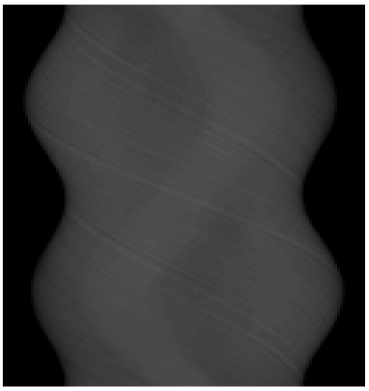

(b) $P_{W_a} f_1$, atténuation forte

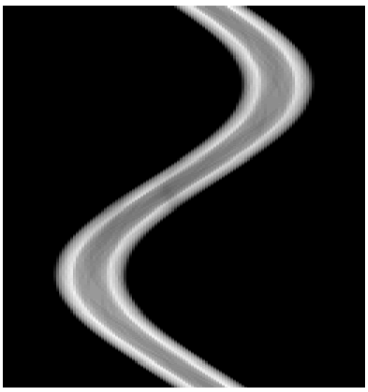

(a) $P_{W_a} f_2$, atténuation faible

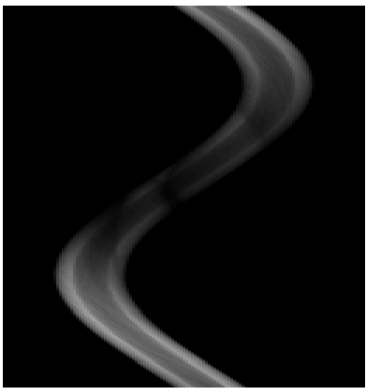

(b) $P_{W_a} f_2$, atténuation forte

Figure 1.14 Données des rayons $P_{W_a} f$ dans le plan $z = 0$

Dans la figure 1.14 nous donnons des exemples pour les valeurs des transformations des rayons pondérés $P_{W_a} f(z, s, \varphi)$ en tranche $z = 0$ (ces images sont aussi appelées *sinogrammes*) ; ces axes horizontal et vertical correspondent aux variables $(s, \varphi) \in [-1, 1] \times [0, 2\pi]$, respectivement. On peut déjà voir d'ici que, dans certaines directions, une forte atténuation peut causer une diminution significative ou une perte complète du signal.

Tester un algorithme de reconstruction sur les données d'émission données par $P_{W_a} f$ sans bruit ne peut être considéré que comme une première étape. Un fort bruit de Schottky dans les données d'émission est le principal problème mathématique et pratique en SPECT et en PET. Par conséquent, la stabilité contre le bruit de tout algorithme de reconstruction pour SPECT et PET doit être testée. Pour effectuer de tels tests, nous avons modélisé le bruit de Schottky à partir des données d'émission $P_{W_a} f(\gamma)$, $\gamma \in \Gamma$.

Dans le paragraphe suivant, nous expliquons comment nous avons modélisé le bruit dans les données de rayon $P_{W_a} f(\gamma)$, $\gamma \in \Gamma$.

Modélisation du bruit

Les mesures réelles en SPECT consistent en le nombre de photons enregistrés $N(\gamma)$ qui ont atteint un détecteur le long du rayon $\gamma \in \Gamma$, où Γ est la grille de (1.135). Avec une bonne approximation, $N(\gamma)$ a une distribution de Poisson avec une intensité $\lambda(\gamma)$ donnée par la formule

$$\lambda(\gamma) = CtP_{W_a} f(\gamma),\ \gamma \in \Gamma,\ C > 0,\ t > 0, \tag{1.137}$$

où C est une constante dépendant de la configuration, t est le temps d'exposition par projection, $P_{W_a} f$ est la transformée des rayons pondérée définie par (1.37), (1.38).

En utilisant la formule (1.137) et les considérations du paragraphe précédent, nous avons modélisé le bruit dans les données d'émission de la manière suivante.

Premièrement, pour les modèles d'atténuation et d'activité donnés (modèles d'atténuation a_1, a_2, modèles d'activité f_1, f_2) nous avons calculé les données non-bruitées $P_{W_a} f(\gamma)$, $\gamma \in \Gamma$. Ensuite, nous avons choisi une constante de normalisation $C = C_n$ telle que

$$C_n \max_{\gamma \in \Gamma} P_{W_a} f(\gamma) = n, \tag{1.138}$$

où n est une constante correspondante au nombre maximal de photons enregistrés le long des rayons dans Γ si le temps d'exposition était $t = 1$ pour tous les rayons. Dans nos expériences, nous avons utilisé deux valeurs différentes pour n : $n_1 = 50$ et $n_2 = 500$ qui correspondaient respectivement à des niveaux de bruit fort et faible (voir aussi remarques 7, 8 ci-dessous).

Ensuite, selon (1.137), nous avons défini les intensités $\lambda(\gamma)$, $\gamma \in \Gamma$, pour le processus de Poisson selon la formule

$$\lambda(\gamma) = C_n P_{W_a} f(\gamma), \tag{1.139}$$

où C_n est la constante de (1.138). Enfin, pour chaque $\gamma \in \Gamma$ nous avons généré indépendamment $N(\gamma) \sim \mathrm{Po}(\lambda(\gamma))$, où $\mathrm{Po}(\lambda)$ représente la distribution de Poisson d'intensité λ.

Remarque 7. Dans les expériences réelles, la constante C dépendant de la configuration et le temps d'exposition t de (1.137), sont connus. De ce fait, pour l'expérience sur les données synthétiques, il est bon de supposer que C_n est également connue et elle peut être utilisée pour prétraiter les données. Plus précisément, en utilisant C_n et en connaissant $N(\gamma)$, $\gamma \in \Gamma$, les valeurs réelles de $P_{W_a} f(\gamma)$ peuvent être approximées comme suit :

$$P_{W_a} f(\gamma) \approx \frac{N(\gamma)}{C_n},\ \gamma \in \Gamma. \tag{1.140}$$

Ici, nous rappelons que, dans l'expérience, après avoir modélisé le bruit pour les données d'émission, nous ne pouvons plus supposer $P_{W_a} f$ connu. En particulier, l'approximation (1.140) est basée sur la propriété suivante de la distribution de Poisson :

$$\text{Soit } N(\gamma) \sim \mathrm{Po}\left(C_n P_{W_a} f(\gamma)\right),\ \text{alors } \mathbb{E}\left(\frac{N(\gamma)}{C_n}\right) = P_{W_a} f(\gamma),\ \gamma \in \Gamma, \tag{1.141}$$

où $\mathrm{Po}(\lambda)$ désigne la distribution de Poisson, $\mathbb{E}$ - désigne l'espérance mathématique.

Remarque 8. Le choix de n constant dans (1.138) permet de contrôler le niveau du bruit dans les données d'émission générées. Plus précisément, en choisissant les intensités $\lambda(\gamma)$ comme dans (1.139) nous avons

$$\mathrm{Var}\left(\frac{N(\gamma)}{C_n}\right) = \frac{P_{W_a}f(\gamma)}{C_n} = \frac{P_{W_a}f(\gamma)\max\limits_{\gamma\in\Gamma} P_{W_a}f(\gamma)}{n},\ \gamma\in\Gamma, \tag{1.142}$$

où $\mathrm{Var}(\cdot)$ indique la variance. L'identité (1.142) est basée sur sur la propriété suivante de la distribution de Poisson : $\xi \sim \mathrm{Po}(\lambda)$, $\mathrm{Var}(\xi) = \lambda$. De (1.139)-(1.142) il vient que n plus grand correspond à de meilleures approximations dans (1.140). En particulier, notre choix $n_1 = 50$ correspond au cas d'un bruit fort et est en fait proche du cadre de notre expérience sur données réelles ; voir [GuNo08]. Enfin, à partir de (1.137), (1.138) on peut voir que choisir n plus grand peut être interprété comme ayant un temps d'acquisition t plus long, ce qui n'est pas toujours possible en raison des limitations pratiques en SPECT.

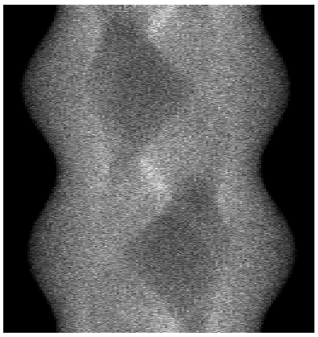

(a) $P_{W_a}f_1$, atténuation faible

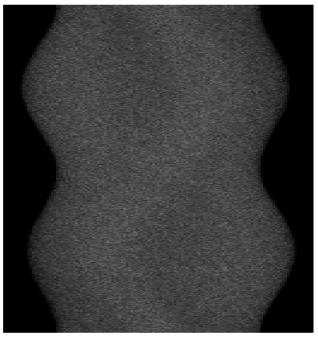

(b) $P_{W_a}f_1$, atténuation forte

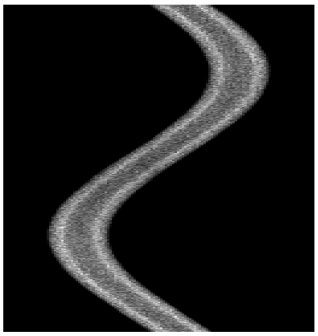

(a) $P_{W_a}f_2$, atténuation faible

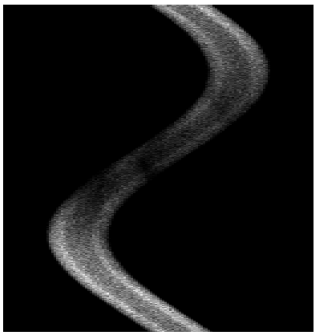

(b) $P_{W_a}f_2$, atténuation forte

Figure 1.16 Modélisation d'un bruit fort $n = n_1 = 50$

Dans la figure 1.16, la modélisation des données $N(\gamma), \gamma \in \Gamma$ pour des rayons dans le plan $z = 0$ est donnée.

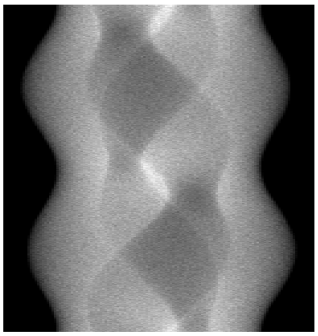

(a) $P_{W_a} f_1$, atténuation faible

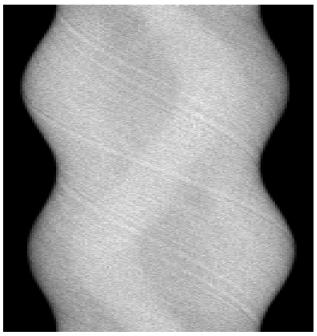

(b) $P_{W_a} f_1$, atténuation forte

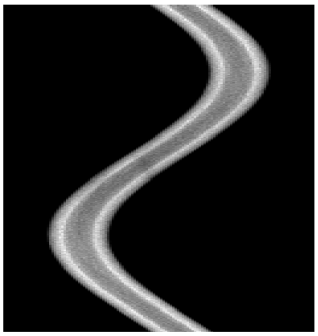

(a) $P_{W_a} f_2$, atténuation faible

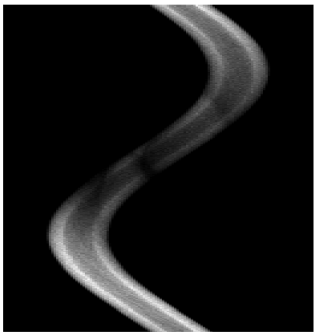

(b) $P_{W_a} f_2$, atténuation forte

Figure 1.18 Modélisation d'un bruit faible $n = n_2 = 500$

Notons que dans le cas d'un bruit faible ($n_2 = 500$), les images ne diffèrent presque pas des originaux sans bruit de la figure 1.14. Ceci a été expliqué dans la remarque 8, le niveau de bruit diminue avec l'augmentation du nombre de photons enregistrés (i.e., avec l'augmentation de n).

Réduction des données le long des rayons à des données le long des plans

Notre méthode d'inversion des articles 1, 2 est basée sur la réduction des données d'émission $P_{W_a} f$ à $R_W f$ le long des plans en 3D. Plus précisément, la réduction est décrite par les formules (1.83), (1.84), à partir desquelles on peut voir que les nouvelles données sont fournies par $R_W f$ pour tous les plans bidimensionnels, sauf ceux qui sont parallèles à XY ; voir aussi la figure 1.12.

Pour nos calculs, nous avons utilisé la grille suivante dans l'ensemble des plans orientés

$$\Pi = \{(s_i, \theta(\varphi_j, \psi_k)) : s_i - \text{ grille sur } [-1,1],\ \theta(\varphi_j, \psi_k) - \text{grille sur } \mathbb{S}^2\}, \tag{1.143}$$

où

$$\begin{aligned} &s_i = -R + i\Delta s,\ i = 0, \dots n_s - 1,\ \Delta s = 2R/(n_s - 1),\ R = 1.0, \\ &\varphi_j = j\Delta\varphi,\ j = 0, \dots n_\varphi - 1,\ \Delta\varphi = 2\pi/n_\varphi, \\ &\psi_k = \arccos(t_k),\ k = 0, \dots, n_\psi - 1, \\ &\{t_k\}_{k=0}^{n_\psi - 1} - \text{ points pour la quadrature de Gauss-Legendre sur } [-1,1] \end{aligned} \tag{1.144}$$

et $\theta(\varphi,\psi) = (\sin(\psi)\cos(\varphi), \sin(\psi)\sin(\varphi), \cos(\psi)) \in \mathbb{S}^2$. En particulier, dans toutes nos expériences numériques, nous avons utilisé $n_s = 129$, $n_\varphi = 128$, $n_\psi = 128$.

Pour réduire $P_{W_a} f(\gamma)$, $\gamma \in \Gamma$ à $R_W f(s,\theta)$, $(s,\theta) \in \Pi$, on réécrit (1.84) comme suit :

$$\begin{aligned} &R_W f(s,\theta(\varphi,\psi)) = \int\limits_{-\sqrt{1-s^2}}^{\sqrt{1-s^2}} P_{W_a} f(\gamma(z(s,\varphi,\psi,\tau),\varphi,\, \sigma(s,\varphi,\psi,\tau))\, d\tau, \\ &\gamma = \gamma(z,\sigma,\varphi) \text{ est donné dans (1.136) pour } z \in [-1,1],\ \sigma \in [-1,1],\ \varphi \in [0,2\pi), \\ &z(s,\varphi,\psi,\tau) = s\cos(\psi) + \tau\sin(\psi), \\ &\sigma(s,\varphi,\psi,\tau) = s\sin(\psi) - \tau\cos(\psi), \end{aligned} \tag{1.145}$$

où W est donné par la formule

$$W(x,\theta(\varphi,\psi)) = W_a\left(x, \theta\left(\varphi + \frac{\pi}{2}, \frac{\pi}{2}\right)\right) \text{ pour } W_a(x,\theta) \text{ définie par (1.37), (1.38).} \tag{1.146}$$

Le paramètre τ dans (1.145) joue le rôle de paramétrisation des rayons $\gamma(z,\sigma,\varphi)$ qui "fibrent" le plan orienté $(s,\theta(\varphi,\psi))$ et satisfont l'hypothèse dans (1.133). Aussi, pour obtenir (1.145), (1.146), (1.83), (1.84) nous avons utilisé le fait que $\eta = (0,0,1)$ et que la fonction f est supportée dans la boule unitaire centrée.

Enfin, pour réduire les données initiales $P_{W_a} f(\gamma)$, $\gamma \in \Gamma$ à $R_W f(s,\theta)$, $(s,\theta) \in \Pi$ nous utilisons de simples discrétisations de (1.145),(1.146). En particulier, dans (1.145) pour calculer $P_{W_a} f(\gamma)$ pour les rayons $\gamma(z,\sigma,\varphi)$ qui ne sont pas dans la grille Γ nous avons utilisé l'interpolation quadratique en la variable z et l'interpolation de splines en la variable σ (l'interpolation en φ était inutile puisque les angles $\{\varphi_j\}_{j=0}^{n_\varphi - 1}$ dans la grille Γ et Π étaient identiques). Nous aimerions noter ici que mathématiquement de telles interpolations ne sont pas correctes, parce que rigoureusement on doit faire l'interpolation en l'image de P_{W_a}. Une telle interpolation est compliquée du fait que l'image de la transformation de Radon atténuée est décrite par un nombre infini d'identités intégrales (Théorème de Paley-Wiener pour les transformations de Radon ; voir [G+03], [Na86]), qui semble difficile à utiliser dans les applications. En fait, on a utilisé des ordres d'interpolations aussi élevés à cause des artefacts dans le cas d'interpolations linéaires par morceaux. Ceci pourrait s'expliquer par la propriété que P_W, en général, est un opérateur de lissage (voir [Na86] pour le cas de $W \equiv 1$). Par conséquent, l'image de l'opérateur P_{W_a} contient des fonctions plus lisses et des ordres d'interpolations plus élevés doivent être utilisés.

Maintenant, ayant toute la description ci-dessus sur la simulation de nos données, nous présentons les reconstructions, où les atténuations sont a_1, a_2 et les distributions nucléotidiques sont f_1, f_2.

Reconstructions à partir de formules de type Chang en 2D et 3D

Cas non-bruité

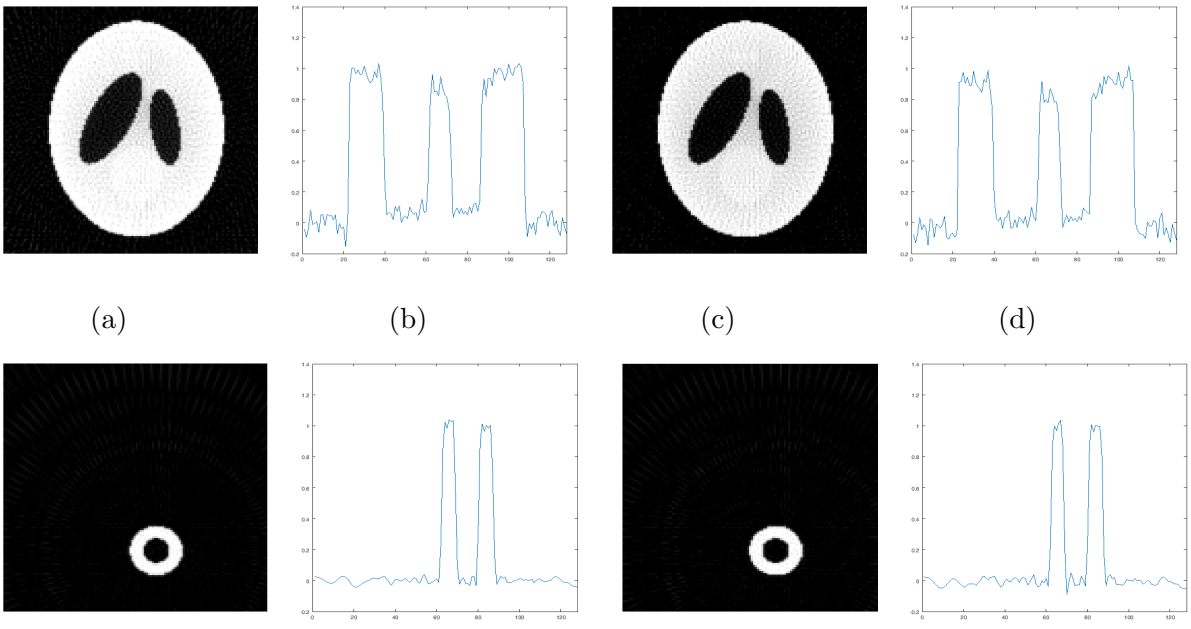

(a) (b) (c) (d)

(e) (f) (g) (h)

Figure 1.19 : Atténuation faible, pas de bruit ; reconstructions de f_1, f_2 par les formules de type Chang en 3D (a), (e) et en 2D (c), (g) ; (b), (d), (f), (h) – sections le long l'axe X

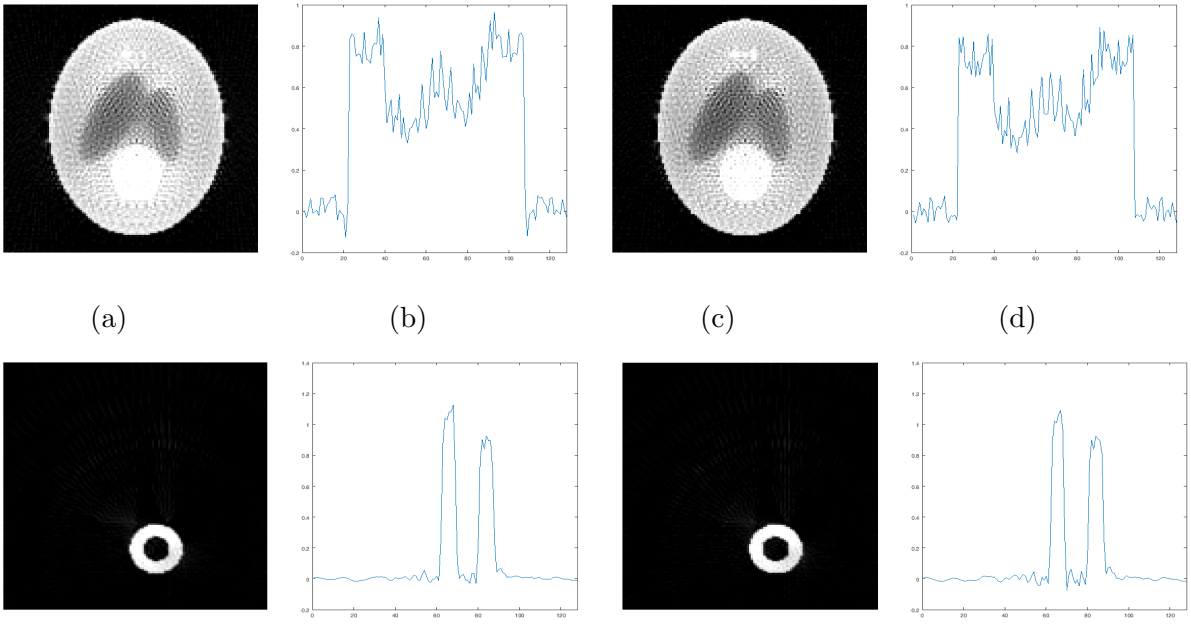

(a) (b) (c) (d)

(e) (f) (g) (h)

Figure 1.20 : Atténuation forte, pas de bruit ; reconstructions de f_1, f_2 à l'aide de formules de type Chang en 3D (a), (e) et en 2D (c), (g) ; (b), (d), (f), (h) – sections le long l'axe X

Cas bruité

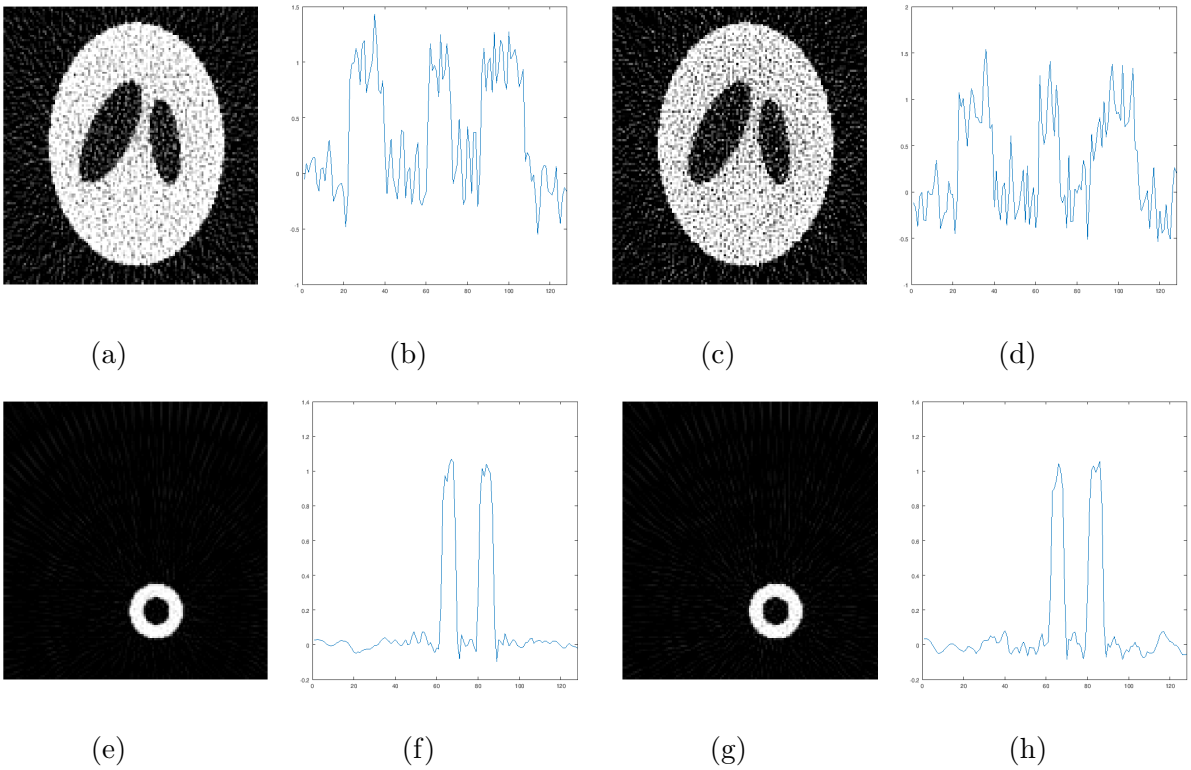

(a) (b) (c) (d)

(e) (f) (g) (h)

Figure 1.21 : Atténuation faible, bruit faible ($n_2 = 500$) ; reconstructions de f_1, f_2 en utilisant des formules de type Chang en 3D (a), (e) et en 2D (c), (g) ; (b), (d), (f), (h) – sections le long l'axe X

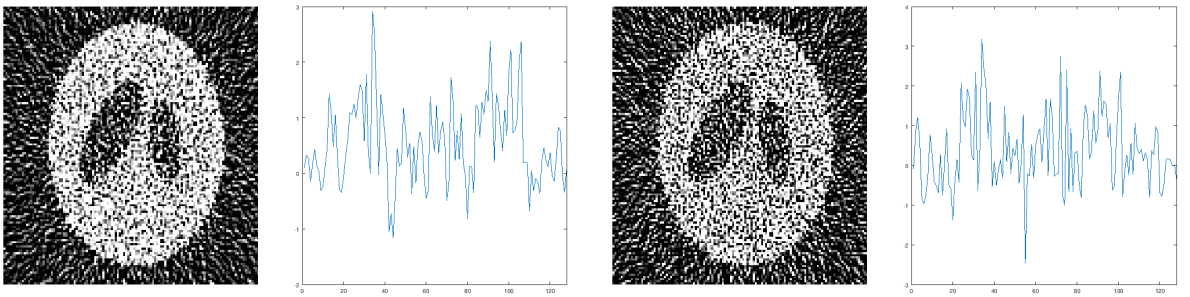

(a) (b) (c) (d)

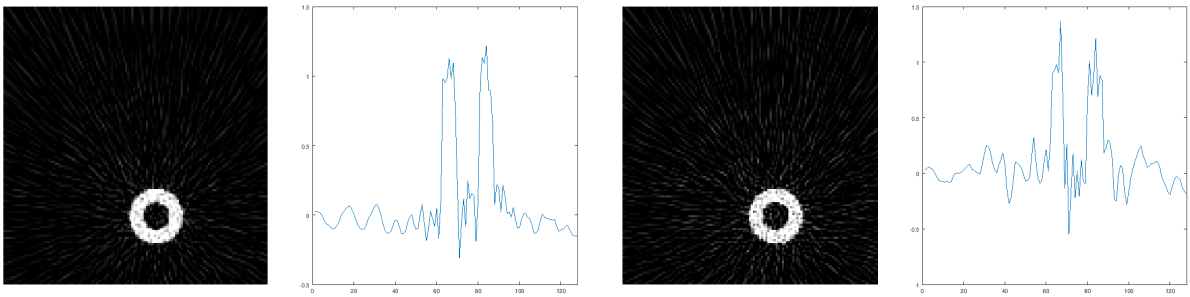

(e) (f) (g) (h)

Figure 1.22 : Atténuation faible, bruit fort ($n_1 = 50$) ; reconstructions de f_1, f_2 en utilisant des formules de type Chang en 3D (a), (e) et en 2D (c), (g) ; (b), (d), (f), (h)-sections le long l'axe X

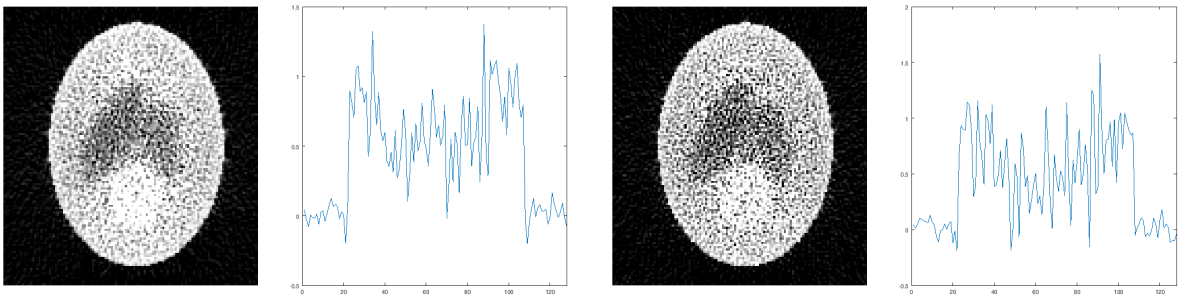

(a) (b) (c) (d)

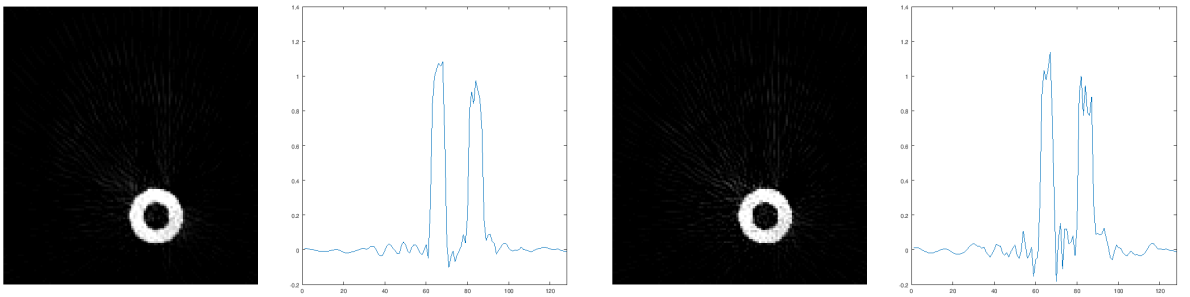

(e) (f) (g) (h)

Figure 1.23 : Atténuation forte, bruit faible ($n_2 = 500$) ; reconstructions de f_1, f_2 en utilisant des formules de type Chang en 3D (a), (e) et en 2D (c), (g) ; (b), (d), (f), (h) – sections le long l'axe X

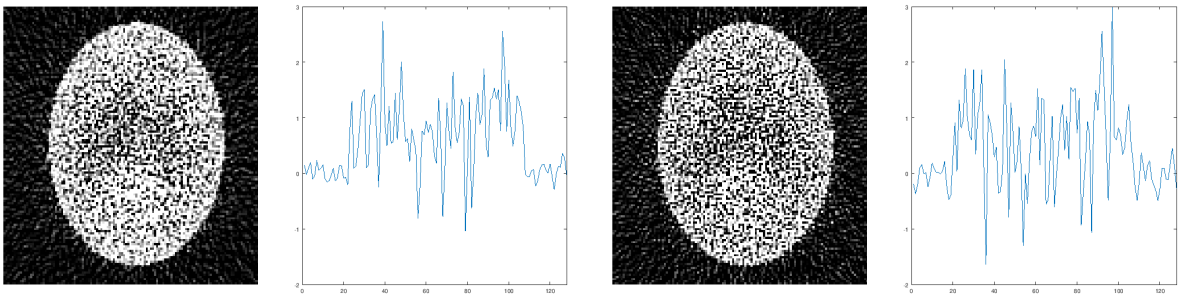

(a) (b) (c) (d)

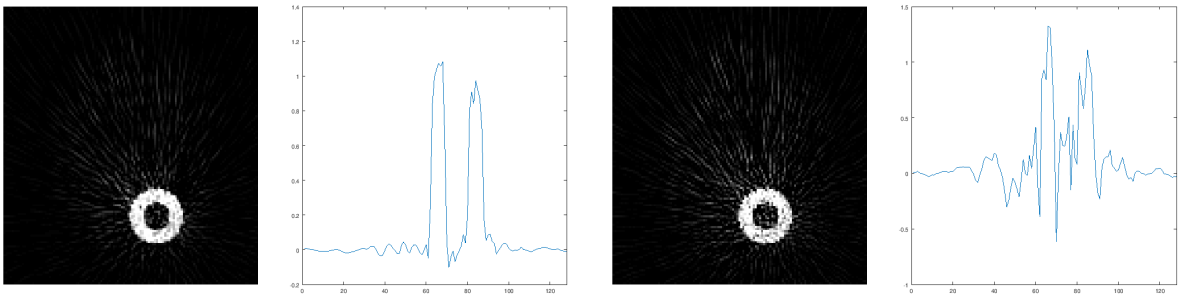

(e) (f) (g) (h)

Figure 1.24 : Atténuation forte, bruit fort ($n_1 = 50$) ; reconstructions de f_1, f_2 en utilisant des formules de type Chang en 3D (a), (e) et en 2D (c), (g) ; (b), (d), (f), (h) – sections le long l'axe X

Pour nos reconstructions, nous avons utilisé les formules (1.86)-(1.88) pour $d = 2, 3$ de l'article 1. Notons que dans la figure 1.20 il n'y a presque aucune différence entre les reconstructions utilisant des formules bidimensionnelles ou tridimensionnelles de type Chang. En même temps, dans les figures 1.21-1.24 les reconstructions obtenues en utilisant la formule de Chang pour $d = 3$ semblent déjà moins bruitées que leurs analogues pour $d = 2$. Cela confirme l'intuition selon laquelle notre réduction de l'article 1 fonctionne comme une régularisation du bruit.

Pour mesurer l'effet du bruit sur les reconstructions, nous avons calculé la distance au carré relative entre les images correspondant aux reconstructions avec bruit et leurs versions non-bruitées.

Soit

$$\begin{aligned} &\tilde{f}_i^{a_j},\ i = 1, 2,\ j = 1, 2,\ \text{les reconstructions de } f_1, f_2 \text{ pour} \\ &\text{l'atténuation forte et faible } a_1, a_2, \text{ en l'abscence de bruit et} \\ &\text{réduites au plan } z = 0 \text{ (voir les figures 1.19, 1.20).} \end{aligned} \tag{1.147}$$

Les reconstructions à partir des données avec bruit seront indiquées comme suit :

$$\begin{aligned} &\tilde{f}_i^{a_j, n_k},\ i = 1, 2,\ j = 1, 2,\ k = 1, 2,\ \text{les reconstructions de } f_1, f_2 \text{ pour} \\ &\text{l'atténuation forte et faible } a_1, a_2, \text{ en présence de bruit } n_1, n_2, \text{ et} \\ &\text{réduites au plan } z = 0 \text{ (voir les figures 1.27-1.30).} \end{aligned} \tag{1.148}$$

Alors, l'erreur de reconstruction $\varepsilon_{f_i, a_j, n_k}$ est définie par la formule

$$\varepsilon_{f_i, a_j, n_k} = \frac{\|\tilde{f}_i^{a_j, n_k} - \tilde{f}_i^{a_j}\|_2}{\|\tilde{f}_i^{a_j}\|_2},\ i = 1, 2,\ j = 1, 2,\ k = 1, 2, \tag{1.149}$$

où $\|\cdot\|_2$ indique la norme de Frobenius des images bidimensionnelles vues comme des matrices de taille $N \times N$, où N est le nombre de pixels dans une direction. La raison pour laquelle on calcule les erreurs à l'aide de la formule (1.149) est que les formules de type Chang ne fournissent que des reconstructions approximatives. Pour mesurer l'effet du bruit, il faut comparer des reconstructions approximatives à partir de données bruitées seulement avec des reconstructions approximatives à partir de données non-bruitées.

Pour nos reconstructions par des formules de type Chang nous avons obtenu les erreurs suivantes :

Méthode / Erreur	$\varepsilon_{f_1,a_1,n_1}$	$\varepsilon_{f_1,a_2,n_1}$	$\varepsilon_{f_1,a_1,n_2}$	$\varepsilon_{f_1,a_2,n_2}$	$\varepsilon_{f_2,a_1,n_1}$	$\varepsilon_{f_2,a_2,n_1}$	$\varepsilon_{f_2,a_1,n_2}$	$\varepsilon_{f_2,a_2,n_2}$
2D-méthode	1.193	1.340	0.377	0.434	0.644	0.625	0.211	0.202
3D-méthode	0.779	0.942	0.251	0.299	0.438	0.432	0.137	0.135

Table 1.1 Erreurs relatives pour les reconstructions via les formules de type Chang

De la table 1.1, on peut voir que notre méthode tridimensionnelle utilisant la formule de type Chang surpasse son analogue bidimensionnel pour tous les modèles d'activité, d'atténuation et de niveaux de bruit. De plus, le gain de stabilité dans les reconstructions est déjà visible dans les figures 1.21-1.24.

Inversions itératives

Pour les reconstructions itératives, nous avons utilisé l'algorithme itératif de type Kunyansky de l'article 2 en dimension $d = 3$ et l'algorithme bidimensionnel original de [Ku92]. En particulier, nous avons utilisé les schémas de (1.79), (1.131) pour les inversions approximatives pour $m = 1$. Notre choix de $m = 1$ a été motivé par les conditions de convergence (1.79), (1.120) en deux et trois dimensions, respectivement. Plus précisément, pour l'atténuation faible a_2, les formules de type Chang donnaient déjà des reconstructions presque parfaites de f_1, f_2 (modulo le bruit) (voir la figure 1.19 (a), (c), (e), (e), (g)), cependant, pour l'atténuation forte a_1, les formules de type Chang produisaient des artefacts non négligable (voir la figure 1.20 (a), (c), (e), (g)). Pour une forte atténuation a_1, la condition (1.120) est à peine satisfaite ($\sigma_{W,D,1} = 0.89$ pour $d = 3$ et 0.52 pour $d = 2$) donc, pour pouvoir comparer les algorithmes bidimensionnels et tridimensionnels nous conservons $m = 1$. Enfin, pour l'atténuation faible a_2, les conditions (1.79), (1.120) sont efficacement satisfaites ($\sigma_{W,D,1} = 0.17$ pour $d = 3$ et 0.11 pour $d = 2$). Le choix $m = 1$ était donc dû, en effet, au cas d'une forte atténuation.

Cas non-bruité

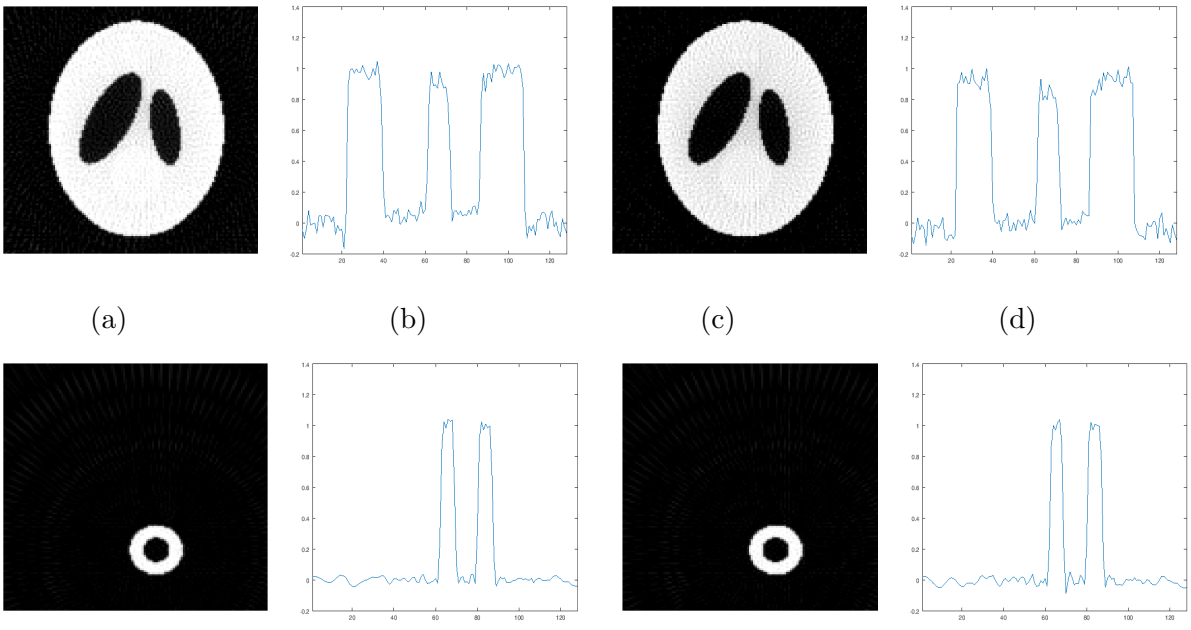

(a) (b) (c) (d)

(e) (f) (g) (h)

Figure 1.25 : Atténuation faible a_2, pas de bruit ; reconstructions de f_1, f_2 via des algorithmes itératifs de type Kunyansky en 3D (a), (e) et en 2D (c), (g) ; (b), (d), (f), (h) – sections le long l'axe X

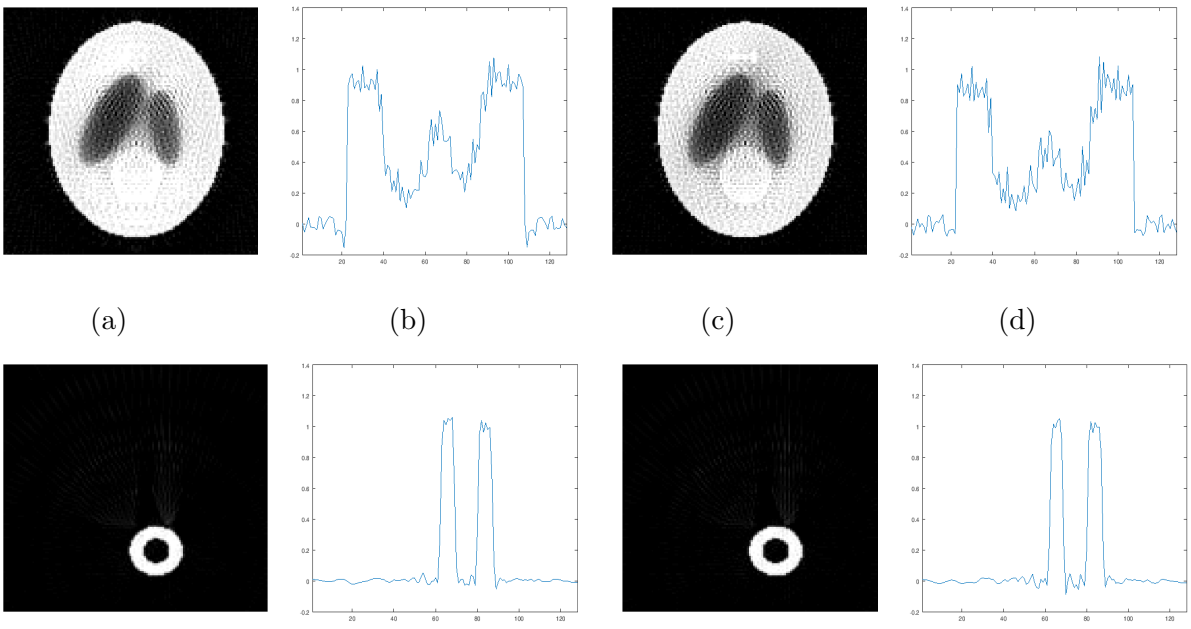

(a) (b) (c) (d)

(e) (f) (g) (h)

Figure 1.26 : Atténuation forte a_1, pas de bruit ; reconstructions de f_1, f_2 via des algorithmes itératifs de type Kunyansky en 3D (a), (e) et 2D (c), (g), (b), (d), (f), (h) – sections le long l'axe X

Cas bruité

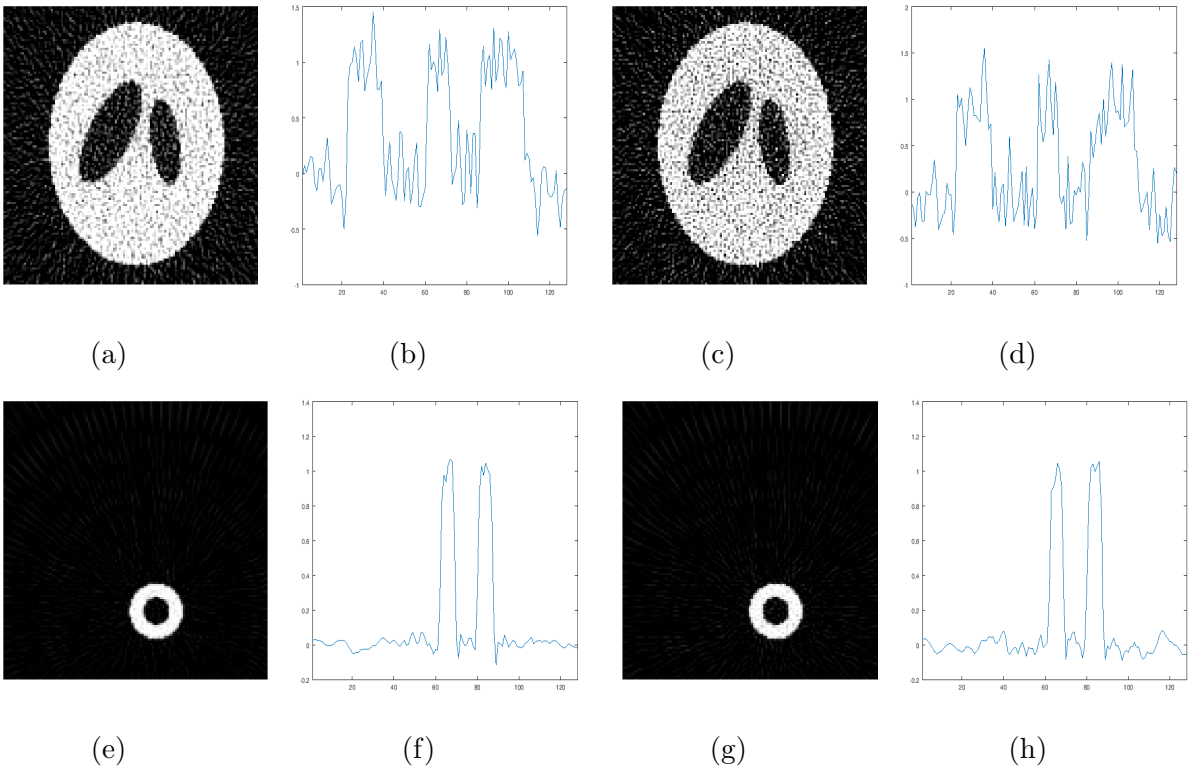

(a) (b) (c) (d)

(e) (f) (g) (h)

Figure 1.27 : Atténuation faible a_2, bruit faible ($n_2 = 500$) ; reconstructions de f_1, f_2 via des algorithmes itératifs de type Kunyansky en 3D (a), (e) et en 2D (c), (g) ; (b), (d), (f), (h) – sections le long l'axe X

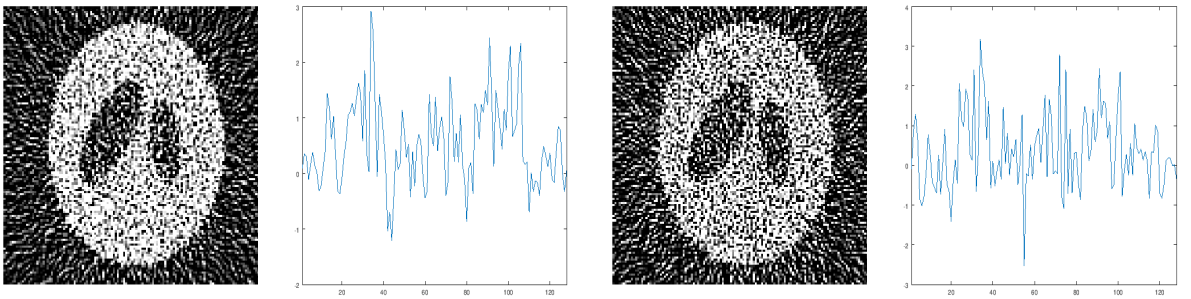

(a) (b) (c) (d)

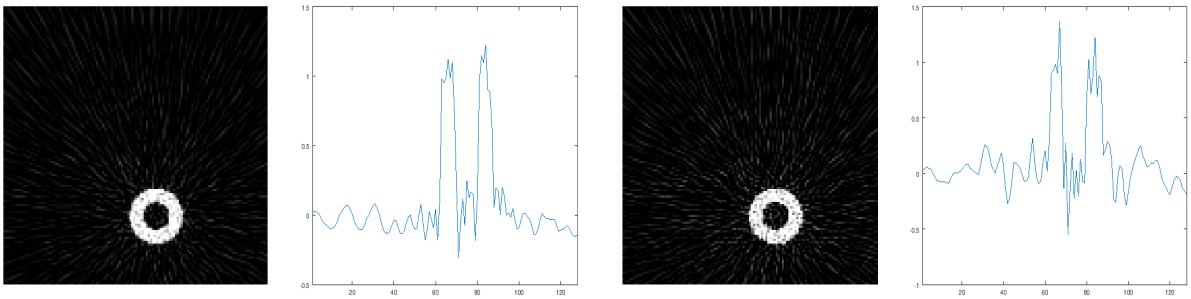

(e) (f) (g) (h)

Figure 1.28 : Atténuation faible a_2, bruit fort ($n_1 = 50$) ; reconstructions de f_1, f_2 via des algorithmes de type Kunyansky en 3D (a), (e) et en 2D (c), (g) ; (b), (d), (f), (h) – sections le long l'axe X

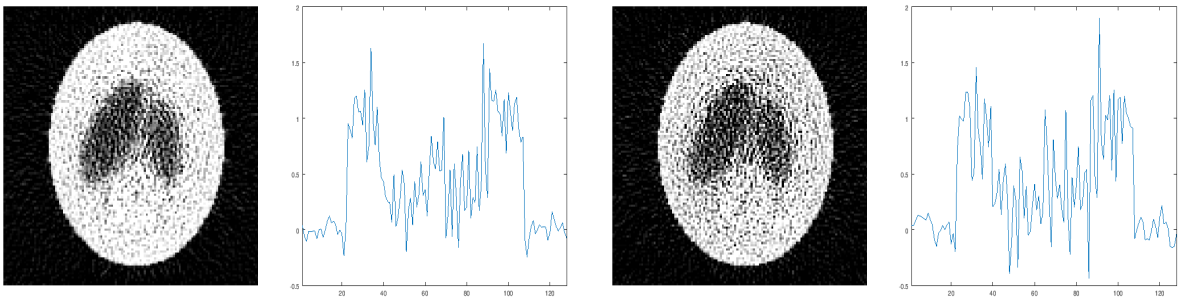

(a) (b) (c) (d)

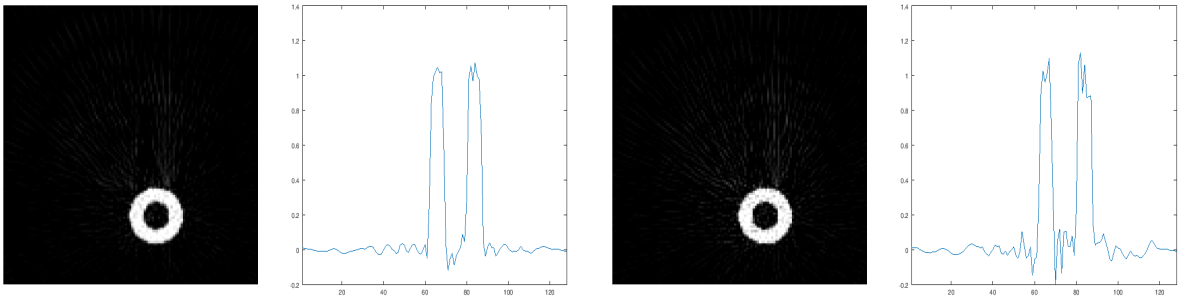

(e) (f) (g) (h)

Figure 1.29 : Atténuation forte a_1, bruit faible ($n_2 = 500$) ; reconstructions de f_1, f_2 via des algorithmes de type Kunyansky en 3D (a), (e) et en 2D (c), (g) ; (b), (d), (f), (h) – sections le long l'axe X

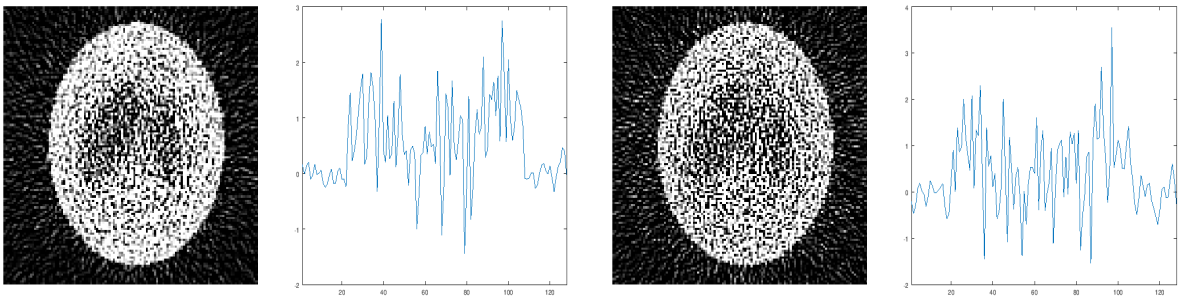

(a) (b) (c) (d)

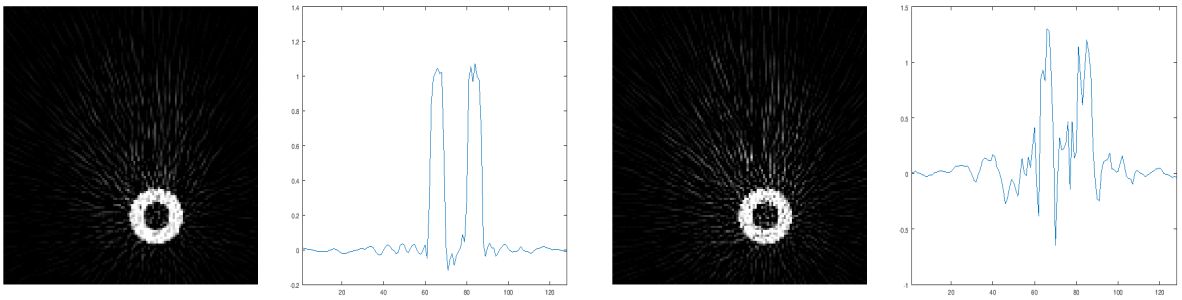

(e) (f) (g) (h)

Figure 1.30 : Atténuation forte a_1, bruit fort ($n_1 = 50$) ; reconstructions de f_1, f_2 via des algorithmes de type Kunyansky en 3D (a), (e) et en 2D (c), (g) ; (b), (d), (f), (h) – sections le long l'axe X

De plus, comme pour l'expérience des formules de type Chang, nous avons également calculé les erreurs relatives des reconstructions bidimensionnelles et tridimensionnelles.

Soit

$$\begin{aligned} &\hat{f}_i^{a_j},\ i = 1, 2,\ j = 1, 2,\ \text{les reconstructions de } f_1, f_2 \text{ pour} \\ &\text{l'atténuation forte et faible } a_1, a_2 \text{ sans bruit} \\ &\text{et réduites au plan } z = 0 \text{ (voir les figures 1.25, 1.26).} \end{aligned} \tag{1.150}$$

Les fonctions ci-dessus peuvent être considérées comme des "reconstructions idéales" pour les méthodes itératives utilisées. Les reconstructions en présence de bruit sont définies comme suit :

$$\begin{aligned} &\hat{f}_i^{a_j, n_k},\ i = 1, 2,\ j = 1, 2,\ k = 1, 2,\ \text{désignent les reconstructions de } f_1, f_2 \text{ pour} \\ &\text{l'atténuation forte et faible } a_1, a_2 \text{ en présence de bruit } n_1, n_2, \text{ respectivement, et} \\ &\text{réduites au plan } z = 0 \text{ (voir les figures 1.27-1.30).} \end{aligned} \tag{1.151}$$

L'erreur $\varepsilon_{f_i, a_j, n_k}$ des reconstructions est définie par la formule suivante :

$$\varepsilon_{f_i, a_j, n_k} = \frac{\|\hat{f}_i^{a_j, n_k} - \hat{f}_i^{a_j}\|_2}{\|\hat{f}_i^{a_j}\|_2},\ i = 1, 2,\ j = 1, 2,\ k = 1, 2, \tag{1.152}$$

où $\|\cdot\|_2$ indique la norme de Frobenius des images bidimensionnelles vues comme des matrices de taille $N \times N$, où N est le nombre de pixels dans une direction.

Pour nos reconstructions itératives, nous avons obtenu les erreurs suivantes :

Méthode / Erreur	$\varepsilon_{f_1,a_1,n_1}$	$\varepsilon_{f_1,a_2,n_1}$	$\varepsilon_{f_1,a_1,n_2}$	$\varepsilon_{f_1,a_2,n_2}$	$\varepsilon_{f_2,a_1,n_1}$	$\varepsilon_{f_2,a_2,n_1}$	$\varepsilon_{f_2,a_1,n_2}$	$\varepsilon_{f_2,a_2,n_2}$
2D-méthode	1.279	1.415	0.437	0.438	0.714	0.634	0.254	0.205
3D-méthode	0.847	0.952	0.316	0.303	0.494	0.439	0.187	0.138

Table 1.2 Erreurs relatives dans les reconstructions utilisant des algorithmes itératifs

À partir de la table 1.2, on peut voir que notre méthode itérative tridimensionnelle surpasse la méthode bidimensionnelle pour tous les modèles d'activité, les modèles d'atténuation et les niveaux de bruit. De plus, le gain de stabilité dans les reconstructions est déjà visible dans les figures 1.27-1.30.

Expérience sur des données réelles

Dans cette expérience nous voulions montrer qu'en principe, notre approche de réduction du problème 1 pour $d = 2$ dans le cadre de reconstructions tranche par tranche au problème 2 pour $d = 3$ peut être utilisée dans des applications réelles en SPECT.

Une procédure SPECT a été effectuée sur un singe. Les données pour cette expérience ont été fournies par le *Service Hospitalier Frédéric Joliot, CEA (Orsay)*. Les données fournies comprenaient deux fichiers : le premier contenait l'application d'atténuation tridimensionnelle de la tête du singe et le second contenait les données d'émission en termes de nombre de photons $N(\gamma)$ le long des rayons γ, γ, où Γ était donné par (1.135) pour $n_z = n_s = n_\varphi = 128$. L'application d'atténuation fournie $a = a(x)$, $x \in \mathbb{R}^3$ a été donnée sous la forme d'une image volumétrique de $128 \times 128 \times 128$ pixels.

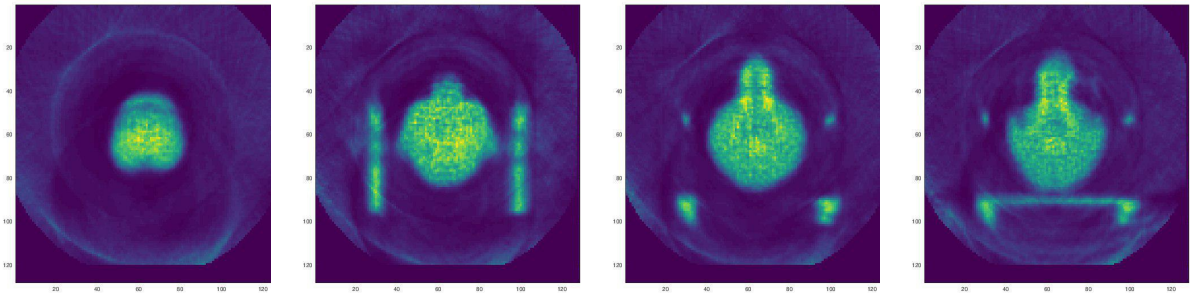

(a) $i_z = 45$ (b) $i_z = 60$ (c) $i_z = 70$ (d) $i_z = 80$

Figure 1.31 : Application d'atténuation de la tête du singe. Les sous-figures (a), (b), (c), (d) représentent l'application d'atténuation réduite à la séquence des plans $z = const$. La région verte au centre de l'image (a) correspond au matériau du cerveau, les lignes verticales et horizontales sur les images (b), (d) correspondent aux plaques qui ont servi à fixer la tête du singe.

Malheureusement, dans les données fournies, les unités de l'application d'atténuation n'ont pas été données, ce qui est crucial en raison de la dépendance non linéaire de la transformation P_{W_a} sur l'atténuation. Pour pallier ce manque d'information, nous avons multiplié l'application d'atténuation par une constante de sorte que le matériau cérébral de la figure 1.31 (a) corresponde à l'atténuation de l'eau 0.15 cm^{-1}. De plus, la constante C de (1.137) n'a pas été fournie, ce qui n'a permis de reconstruire la distribution des nucléotides

qu'à une constante multiplicative près[16]. Le temps d'acquisition pour une projection était de 14 secondes et le rayon de rotation des détecteurs était de 261 mm. Le nombre total de photons enregistrés était d'environ $4.6 \cdot 10^6$ et le nombre maximal de photons enregistrés par projection était de 60.

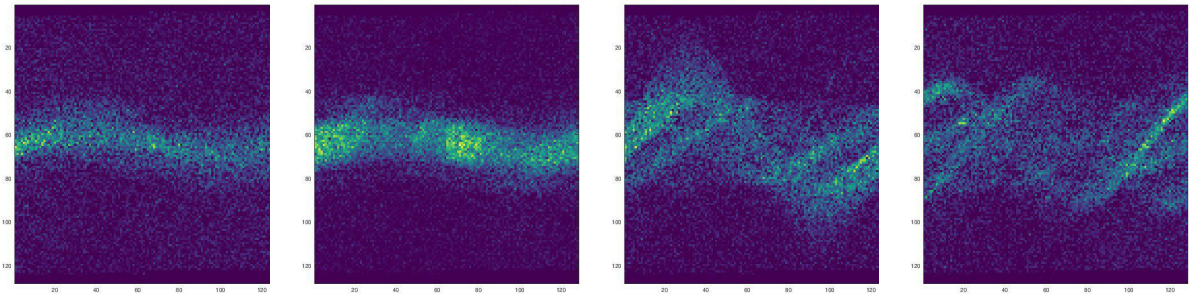

(a) $i_z = 42$ (b) $i_z = 53$ (c) $i_z = 63$ (d) $i_z = 95$

Figure 1.32 : Données d'émission dans l'expérience sur un singe. Les sous-figures (a) à (d) montrent le nombre de photons $N(\gamma)$, où les rayons γ appartiennent à différents plans $z = const$. Dans chaque plan $z = const$ les rayons sont paramétrés par (s, φ), $s \in [-1, 1]$, $\varphi \in [0, 2\pi]$ (voir la formule (1.136)). L'axe horizontal sur (a)-(d) correspond à la variable φ, l'axe vertical correspond à la variable s.

En appliquant la méthode de réduction et la formule de type Chang pour $d = 3$ de l'article 1, nous avons obtenu des reconstructions approximatives de la distribution des nucléotides dans le cerveau du singe.

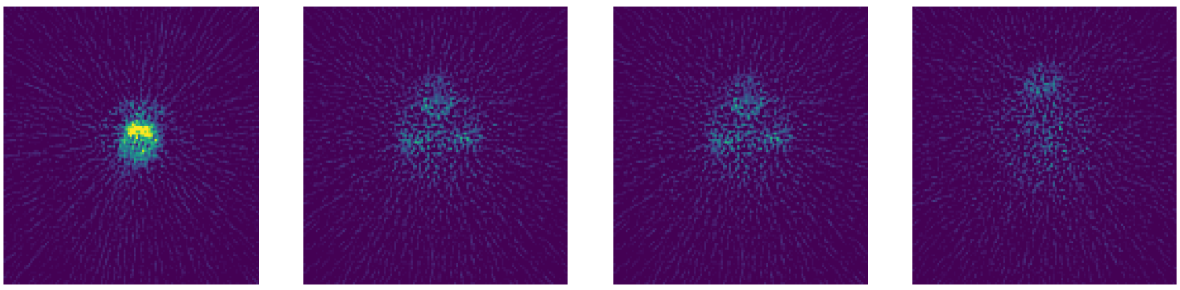

(a) $i_z = 45$ (b) $i_z = 60$ (c) $i_z = 70$ (d) $i_z = 89$

Figure 1.33 : Reconstruction de la distribution des nucléotides dans différents plans $z = const$. Notons que le plan $i_z = 45$ (a) correspond à la région du cerveau du singe.

Enfin, sur la figure 1.33(a) on peut voir une forte concentration de nucléotides. Cette zone correspondait géométriquement à la position du cerveau du singe (voir aussi la figure 1.31). En outre, pour le traceur en SPECT, on sait qu'il a tendance à se concentrer dans le cerveau, donc ce résultat soutient notre proposition que nos méthodes des articles 1, 2, en principe, peuvent être appliquées à des problèmes réels.

[16]Pour des raisons médicales, c'est encore suffisant, car en SPECT, seule une distribution relative du traceur est importante.

Quelques mots sur nos réalisations numériques

A partir des formules (1.83), (1.84), (1.86), (1.89) du résumé de l'article 1 et des formules (1.120)-(1.128) du résumé de l'article 2 on peut voir que nos applications numériques ne comprennent que deux étapes essentielles :

1. Réalisation numérique des formules (1.83), (1.84) pour la réduction de $P_{W_a} f$ à $R_w f$. Cette question a déjà été commentée dans (1.145). Nous avons utilisé des interpolations quadratiques et de splines en z, s, respectivement, pour échantillonner $P_{W_a} f$ pour les rayons manquants. Ce faisant, nous avons obtenus undubitablement des données qui n'appartenaient pas à l'image de l'opérateur P_W. A notre connaissance, l'interpolation efficace des données, même pour Pf, où P est la transformation des rayons classique, reste une question ouverte.

2. Inversion de la transformation de Radon classique R pour $d = 3$. Les méthodes de reconstruction des articles 1, 2 (formule de type Chang, méthode itérative de type Kunyansky) sont basées sur l'inversion de la transformation de Radon classique R^{-1} en dimension $d = 3$. Il existe de nombreuses bibliothèques en accès libre pour des calculs efficaces de R^{-1} pour $d = 2$ (par exemple, pour MATLAB/Octave, C, Python), mais pour $d = 3$ nous n'avons trouvé aucune bibliothèque accessible. Pour nos besoins, nous avons implémenté notre propre version numérique de R^{-1} en utilisant la transformée de Fourier et the Slice Projection Theorem (voir [Na86]) et aussi une très sympathique bibliothèque NFFT pour MATLAB/Octave développée dans TU Chemnitz [K+09].

Les détails de nos implémentations peuvent être trouvés dans le dépôt GitHub : github.com/fedor-goncharov/Weighted-ray-Radon-transforms-in-3D.

4.2 Résumé des résultats de la partie II

Si dans la partie I nous avons considéré les problèmes 1, 2 du point de vue des applications en tomographie, dans la partie II nous avons considéré ces problèmes en toute généralité. La première question à se poser dans ce cas est de savoir si les problèmes inverses susmentionnés peuvent être résolus en principe. Sur le plan mathématique, cela se réduit à l'étude des propriétés d'injectivité et de non-injectivité des transformations P_W, R_W. La partie II de cette thèse est consacrée à cette question.

Du point de vue de l'injectivité et de la non-injectivité, les problèmes inverses pour P_W et R_W (problèmes 1, 2 respectivement) sont très différents. Le problème 1 n'est pas surdéterminé pour la dimension $d = 2$ et est surdéterminé pour $d \geq 3$. En effet, la fonction $P_W f$ dépend de $2d - 2$ variables (en fonction de $T\mathbb{S}^{d-1}$) tandis que f dépend de d variables (en fonction de $\mathbb{R}^d$) et la formule suivante est vérifiée

$$2d - 2 = d \text{ seulement pour } d = 2 \text{ et } 2d - 2 > d \text{ pour } d \geq 3. \tag{1.153}$$

En même temps, le problème 2 est non surdéterminé dans toutes les dimensions $d \geq 2$. Ceci est dû au fait que $R_W f$ est une fonction de d variables (comme fonction sur $\mathbb{R} \times \mathbb{S}^{d-1}$, voir (1.16)), de même pour la fonction f. La surdétermination du problème 1 pour $d \geq 3$ donne l'intuition que les transformations des rayons pondérées devraient être injectives sous des hypothèses raisonnablement légères sur W et sur la classe des fonctions test. Cette intuition a également été soutenue par de nombreux résultats positifs, par exemple dans [Fi86], [Il16].

Théorème 6 (Finch, 1986, Ilmavirta, 2016)**.** *Soit $W \in C^{1+\varepsilon}(\mathbb{R}^d \times \mathbb{S}^{d-1})$, $d \geq 3$, où ε est strictement positif. Alors P_W est injective sur $L^p_c(\mathbb{R}^d)$, $p > 2$ ($L^p_c(\mathbb{R}^d)$ – fonctions p-intégrable à support compact dans $\mathbb{R}^d$).*

En particulier, l'injectivité de P_W pour $d \geq 3$ est basée sur le fait que P_W est localement injective pour $d = 2$, quand W satisfait (1.14) et est au moins de classe $C^{1+\varepsilon}$ pour $\varepsilon > 0$ arbitraire ; voir [LaBu73], [MaQu85], [LaBu73], [Il16].

Théorème 7 (Lavrent'ev, et. al., 1973, Markoe, Quinto, 1985, Ilmavirta, 2016a)**.** *Supposons que* $W \in C^{1+\varepsilon}(\mathbb{R}^2 \times \mathbb{S}^1)$ *pour* $\varepsilon > 0$ *arbitraire et*

$$W \geq c > 0, \ \|W\|_{C^{1+\varepsilon}(\mathbb{R}^2 \times \mathbb{S}^1)} \leq N, \tag{1.154}$$

pour des constantes c, N*. Alors, pour tout* $p > 2$*, il existe* $\delta = \delta(\varepsilon, c, N, p) > 0$ *tel que* P_W *est injective sur* $L^p(B(x, \delta))$ *pour tout* $x \in \mathbb{R}^2$*, où*

$$\begin{aligned} &L^p(B(x,\delta)) = \{f \in L^p(\mathbb{R}^2) : \operatorname{supp} f \subset \bar{B}(x,\delta)\}, \\ &\bar{B}(x,\delta) = \{x' \in \mathbb{R}^2 : |x - x'| \leq \delta\}. \end{aligned} \tag{1.155}$$

Les publications susmentionnées pour le théorème 7 diffèrent, en particulier, dans les hypothèses de régularité sur W, allant de C^∞ dans [LaBu73], à $C^{1+\varepsilon}$ dans [Il16].

Notons que le résultat du théorème 7 implique directement le résultat du théorème 6. La preuve est si courte et simple que nous la présentons ici :

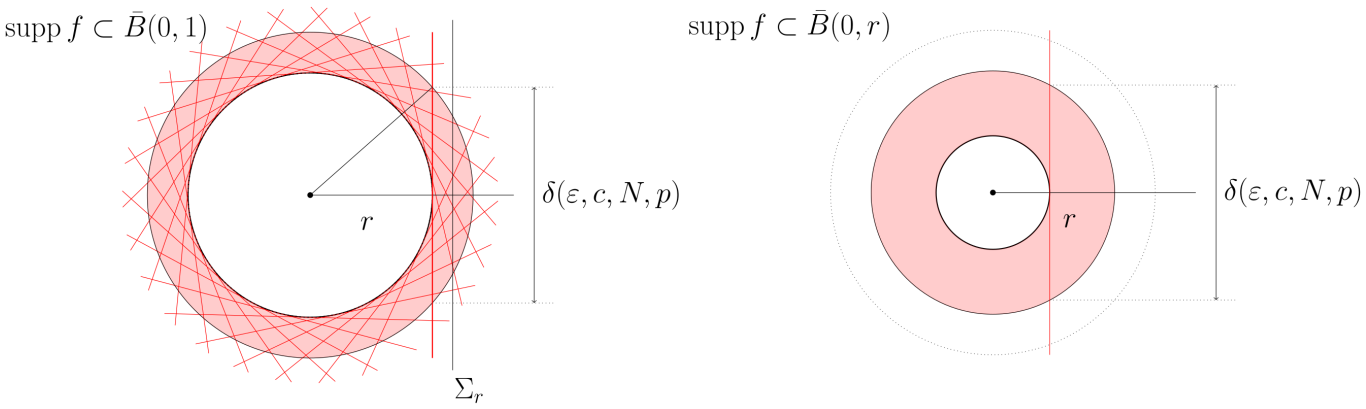

Figure 1.34 Boundary stripping method

Preuve. Soit $d \geq 3$ et supposons que $f \in \ker P_W$, $f \neq 0$, $f \in \operatorname{supp} \bar{B}(0,1)$. Tout plan bidimensionel Σ_r dont la distance à l'origine est $r > 0$ rencontre $\bar{B}(0,1)$ dans un sous-ensemble Ω_r dont le diamètre est limité par $d(r) \leq 2\sqrt{1 - r^2} > 0$. En choisissant r tel que $d(r) \leq \delta$ pour δ du théorème 7 nous avons que $f \equiv 0$ sur $\bar{B}(0,1) \backslash B(0,r)$. En itérant cet argument pour la boule $\bar{B}(0,r)$ et plus nous avons que $f \equiv 0$ sur $\mathbb{R}^d$. □

La méthode ci-dessus pour prouver l'injectivité de P_W pour $d \geq 3$ est connue sous le nom de *boundary stripping method* (voir aussi la figure 1.34) et elle est largement utilisée comme outil principal dans de nombreuses publications, par exemple, dans [Fi86], [Il16]. Notons également que l'argument de surdétermination du problème inverse pour P_W pour $d \geq 3$ est crucial ici. Dans le cas de R_W, lorsque le problème inverse n'est pas surdéterminé, la situation est complètement différente.

D'après le théorème 7 nous savons que R_W est *localement injective* pour $d = 2$ (en dimension $d = 2$ les transformations P_W et R_W sont équivalentes à changement de variables près). C'est-à-dire que l'hypothèse (1.14) sur W étant satisfaite avec une "régularité

supplémentaire", R_W est injective sur les fonctions avec un support suffisamment petit.

Mais que se passe-t-il si nous supposons un plus grand support pour les fonctions, ou de manière équivalente, y a-t-il *injectivité globale* de R_W pour $d \geq 2$ et pour W satisfaisant (1.14), peut-être avec quelques hypothèses de régularité supplémentaires ?

La première réponse à cette question pourrait être donnée par le célèbre résultat de J. Boman [Bo93] :

Théorème 8 (J. Boman, 1993)**.** *Il existe une fonction $f \in C_c^\infty(\mathbb{R}^2)$, $f \neq 0$ et un poids W satisfaisant* (1.14) *pour $d = 2$ infiniment lisse, tels que*

$$R_W f \equiv 0 \text{ sur } \mathbb{R} \times \mathbb{S}^1. \tag{1.156}$$

En particulier, ce résultat montre l'importance de la surdétermination sur les propriétés d'injectivité pour les problèmes inverses pour P_W, R_W. Il est également intéressant de noter que R_W pour le poids W construit dans [Bo93], n'est pas globalement injective sur $C_c^\infty(\mathbb{R}^2)$ mais est toujours localement injective du fait du théorème 7. La différence entre les injectivités locales et globales pour R_W peut être expliquée intuitivement en utilisant un argument de perturbation pour R_W. De manière informelle, pour les poids W satisfaisant (1.14) et "assez lisse"', l'action de R_W sur les fonctions de test avec un support "petit" peut être approchée par l'action de R plus un opérateur intégral K_W avec une petite norme pour les fonctions ayants un support suffisament petit (par exemple, des opérateurs intégraux avec des noyaux réguliers). Un exemple d'utilisation d'un tel argument avec des quantifications rigoureuses de toutes les étapes ci-dessus peut être trouvé, par exemple, dans [MaQu85].

Il est intéressant de noter que pour les poids W qui ont des "symétries", la transformation R_W peut être injective même avec des hypothèses de régularité raisonnablement faibles. Un exemple particulier est celui des poids *invariants par rotation* qui apparaissent également dans la PET ; voir [Qu83].

Définition 4 (Quinto, 1983)**.** Le poids $W = W(x, \theta)$ est appelé invariant par rotation s'il peut être écrit sous la forme suivante :

$$W(x, \theta) = U(|x - (x\theta)\theta|, x\theta),\ x \in \mathbb{R}^d,\ \theta \in \mathbb{S}^{d-1}, \tag{1.157}$$

où U est une fonction strictement positive, continue sur $\mathbb{R}^2$ telle que

$$U(r, s) = U(-r, s) = U(r, -s) \text{ pour tout } (r, s) \in \mathbb{R}^2. \tag{1.158}$$

Notons également que les symétries (1.157), (1.158) peuvent aussi être écrites comme

$$W(x, \theta) = \tilde{U}(|x|, x\theta),\ x \in \mathbb{R}^d,\ \theta \in \mathbb{S}^{d-1}, \tag{1.159}$$

$$\tilde{U}(r, s) = \tilde{U}(-r, s) = \tilde{U}(r, -s),\ (r, s) \in \mathbb{R}^2, \tag{1.160}$$

où $\tilde{U}$ est continu et strictement positif sur $\mathbb{R}^2$.

Pour la transformation de Radon pondérée R_W avec des poids invariants par rotation, le résultat suivant est valable

Théorème 9 (Quinto, 1983)**.** *Supposons que W satisfait* (1.14)*, $W \in C^\infty(\mathbb{R}^d \times \mathbb{S}^{d-1})$, $d \geq 2$ et est invariant par rotation. Alors, $R_W : L_c^2(\mathbb{R}^d) \to L^2(\mathbb{R} \times \mathbb{S}^{d-1})$ est injective.*

Remarque 9. En fait, dans l'hypothèse du théorème ci-dessus $W \in C^\infty(\mathbb{R}^d \times \mathbb{S}^{d-1})$ pourrait être remplacé par $W \in C^1(\mathbb{R}^d \times \mathbb{S}^{d-1})$ en dimensions $d = 2, 3$; voir [Qu83].

Bien que le problème inverse pour R_W pour les poids invariants par rotation ne soit pas surdéterminé, la symétrie de W compense le manque de lissage. En particulier, le poids W dans le contre-exemple de J. Boman n'était pas invariant par rotation.

Concluant l'exposition des résultats d'injectivité connus pour R_W pour $d \geq 2$, nous présentons le théorème suivant

Théorème 10 (Boman, Quinto, 1987)**.** *Supposons que* $(s_0, \theta_0) \in \mathbb{R} \times \mathbb{S}^{d-1}$ *et* $f \in \mathcal{E}'(\mathbb{R}^d)$ *(distributions sur* $\mathbb{R}^d$ *à support compact). Supposons aussi que* $W(x, \theta)$ *satisfait* (1.14) *est une function analytique à valeurs réelles sur* $\mathbb{R}^d \times \mathbb{S}^{d-1}$ *et est paire en* θ*, c'est-à-dire,* $W(x, \theta) = W(x, -\theta)$*. Soit* V *un voisinage ouvert de* θ_0*. Enfin, supposons que* $R_W f(s, \theta) = 0$ *pour* $s > s_0$ *et* $\theta \in V$*. Alors* $f = 0$ *sur le demi-espace* $x\theta_0 > s_0$*.*

Corollaire 10.1. *Soit* f *une fonction continue à support compact sur* $\mathbb{R}^d$ *et* W *satisfaisant aux conditions du théorème ci-dessus. Si* $R_W f(s, \theta) \equiv 0$ *sur* $\mathbb{R} \times \mathbb{S}^{d-1}$*, alors* $f \equiv 0$*.*

Il est intéressant qu'avec le contre-exemple de Boman, les résultats ci-dessus révèlent une autre phase de transition de l'injectivité de R_W. Bien que la C^∞-régularité n'était pas suffisante pour l'injectivité pour des poids généraux, l'analyticité de W étend l'injectivité pour R_W aux fonctions à support compact. La preuve du théorème 10 est basée sur la théorie des opérateurs pseudodifferentiels elliptiques analytiques et des ensembles de front d'ondes analytique [BQ87]. Des considérations similaires pourraient être effectuées pour des poids lisses non-analytiques, mais il est bien connu qu'un opérateur pseudo-differentiel elliptique général peut avoir une fonction lisse et à support compact dans son noyau.

Maintenant, ayant en main tous les résultats classiques ci-dessus, nous pouvons passer à nos contributions de la partie II. En particulier, nos contributions consistent en trois contre-exemples aux théorèmes d'injectivité ci-dessus, lorsque les hypothèses sur les poids sont légèrement assouplies. Tout d'abord, nous commençons par un contre-exemple de l'article 3 (chapitre 5), que nous considérons comme le plus simple. Ensuite, nous poursuivons avec nos résultats provenant des articles 4, 5 (chapitres 6, 7), où les contre-exemples construits sont plus intéressants et imprévus.

Résumé de l'article 3. Soit

$$(e_1, \dots e_d) \text{ la base canonique de } \mathbb{R}^d, \tag{1.161}$$

$$\Theta(v_1, v_2) = \{\theta \in \mathbb{S}^{d-1} : \theta \perp v_1,\, \theta \perp v_2\} \simeq \mathbb{S}^{d-3},\, v_1, v_2 \in \mathbb{R}^d,\, v_1 \perp v_2, \tag{1.162}$$

où $\perp$ désigne l'orthogonalité entre deux vecteurs de $\mathbb{R}^d$.

Théorème 11. *Pour* $d \geq 3$*, il exist* W *et* f*, tels que*

$$R_W f \equiv 0 \text{ sur } \mathbb{R} \times \mathbb{S}^{d-1}, \tag{1.163}$$

$$W \text{ satisfait } (1.14),\, f \in C_c^\infty(\mathbb{R}^d),\, f \neq 0. \tag{1.164}$$

De plus

$$W \text{ est de classe } C^\infty \text{ sur } \mathbb{R}^d \times (\mathbb{S}^{d-1} \backslash \Theta(e_1, e_2)), \tag{1.165}$$

où e_1, e_2 *et* $\Theta(e_1, e_2)$ *sont définis dans* (1.161), (1.162)*.*

Ce résultat peut être considéré comme une tentative de construire un exemple de non-injectivité pour R_W dans des dimensions supérieures $d \geq 3$, avec des propriétés similaires à W comme dans le théorème 8 de J. Boman. Nous rappelons que le problème inverse pour

R_W n'est pas surdéterminé, donc on pourrait s'attendre à ce que le théorème 8 admette des analogues directs dans des dimensions supérieures.

Dans le théorème 11, d'après (1.162), (1.165) on peut voir que W est infiniment lisse seulement presque partout en $\mathbb{R}^d \times \mathbb{S}^{d-1}$, alors que dans l'exemple de Boman le poids était de classe C^∞ dans tout l'espace. En fait, sur l'ensemble $\mathbb{R}^d \times \Theta(e_1, e_2)$ de (1.165) qui est de mesure nulle, le poids dans notre exemple a une discontinuité du deuxième type. Cette discontinuité est une propriété particulière de notre construction, et nous croyons qu'un autre exemple de non-injectivité de R_W avec W lisse partout pourrait être construit.

Résumé de l'article 4.

Théorème 12. *Il existe une fonction symétrique sphérique, non nulle $f \in C_c^\infty(\mathbb{R}^3)$ à support dans une boule unitaire fermée, et un poids W satisfaisant* (1.14) *et étant également invariant par rotation (voir la définition 4), tels que*

$$R_W f \equiv 0 \text{ sur } \mathbb{R} \times \mathbb{S}^2. \tag{1.166}$$

Ce résultat est déjà une amélioration du théorème 11 pour $d = 3$, où le poids satisfaisait (1.14) mais n'était pas encore continu en certains points. Notons aussi que R_W est injective sur $L_c^2(\mathbb{R}^3)$ si W satisfait (1.14) et est, au moins, de classe C^1 (par le théorème 9 pour $d = 3$). Le théorème ci-dessus rend l'hypothèse de régularité sur W cruciale pour ce résultat d'injectivité. Il est important de noter que la construction de W et f a été développée, en grande partie en adoptant le contre-exemple de Boman du théorème 8.

Bien que dans le théorème 12 le poids n'est pas infiniment lisse, comme dans l'exemple de Boman, l'invariance par rotation de W est le principal avantage de notre construction.

L'invariance par rotation de W et la symétrie sphérique de f permettent d'étendre le théorème 12 de la manière suivante.

Considerons $\tilde{U}$ et $\tilde{f}$ telles que

$$W(x, \theta) = \tilde{U}(|x|, |x\theta|),\ f(x) = \tilde{f}(|x|),\ x \in \mathbb{R}^3,\ \theta \in \mathbb{S}^2, \tag{1.167}$$

où W et f sont les fonctions du théorème 12. Nous avons utilisé ici le fait que W est invariant par rotation (voir les formules (1.159), (1.160)) et que f est symétrique sphérique.

Corollaire 12.1. *Soit W et f définis par les formules suivantes :*

$$W(x, P) = \tilde{U}(|x|, \operatorname{dist}(P, \{0\})),\ P \in \mathcal{P}^{d,2},\ x \in P, \tag{1.168}$$

$$f(x) = \tilde{f}(|x|),\ x \in \mathbb{R}^d, \tag{1.169}$$

où P est un plan orienté bidimensionnel dans $\mathbb{R}^d$, i.e., $P \in \mathcal{P}^{d,2}$, $\operatorname{dist}(P, \{0\})$ désigne la distance à l'origine $\{0\} \in \mathbb{R}^d$ au plan P, $\tilde{U}$ et $\tilde{f}$ sont les fonctions de (1.167)*, $d > 3$. Alors,*

$$R_W^{d,2} f \equiv 0 \text{ sur } \mathcal{P}^{d,2}. \tag{1.170}$$

De plus, le poids W est strictement positif continu et invariant par rotation, f est infiniment lisse à support compact dans $\mathbb{R}^d$ et $f \not\equiv 0$.

Dans ce cas, le contre-exemple obtenu est beaucoup plus intéressant, car le problème inverse pour $R_W^{d,2}$, $d > 3$, est déjà surdéterminé. En effet,

$$\dim \mathcal{P}^{d,2} = 3d - 6 > \dim \mathbb{R}^d = d \text{ pour } d > 3. \tag{1.171}$$

Cet exemple d'injectivité nous a donné l'intuition qu'un développement similaire pourrait être fait pour P_W pour $d \geq 3$. En particulier, on pourrait s'attendre à ce que P_W pour $d \geq 3$ ne soit pas injective si l'hypothèse de régularité pour W est réduite de $C^{1+\varepsilon}$ à, disons, continuité.

Résumé de l'article 5. En adoptant et développant les considérations de l'article 5 et de [Bo93] nous avons obtenu le résultat suivant.

Soit

$$\Omega = \mathbb{R}^d \times \mathbb{S}^{d-1}, \tag{1.172}$$

$$\Omega(\Lambda) = \{(x,\theta) \in \mathbb{R}^d \times \mathbb{S}^{d-1} : |x - (x\theta)\theta| \in \Lambda\},\ \Lambda \subset [0,+\infty). \tag{1.173}$$

Compte tenu de (1.15), (1.22) l'ensemble $\Omega(\Lambda)$ de (1.173) peut être interprété comme les points sur les rayons dans $\mathbb{R}^d$, où la valeur de la distance entre un rayon et l'origine $\{0\} \in \mathbb{R}^d$ appartient à $\Lambda \subset [0,+\infty)$.

Théorème 13. *Il existe un poids W satisfaisant* (1.14) *et une fonction non nulle $f \in C_c^\infty(\mathbb{R}^d)$, $d \geq 2$, tels que*

$$P_W f \equiv 0 \text{ sur } T\mathbb{S}^{d-1}, \tag{1.174}$$

où P_W est défini dans (1.17)*. En outre, W est invariant par rotation, i.e., qu'il satisfait* (1.157), (1.158)*, et f est symétrique sphérique à support dans une boule fermée. De plus,*

$$W \in C^\infty(\Omega \backslash \Omega(\{1\})), \tag{1.175}$$

$$W \in C^\alpha(\mathbb{R}^d \times \mathbb{S}^{d-1}) \text{ pour } \alpha \in (0,\alpha_0),\ \alpha_0 = 1/16, \tag{1.176}$$

$$W \geq 1/2 \text{ sur } \Omega \text{ et } W \equiv 1 \text{ sur } \Omega([1,+\infty)), \tag{1.177}$$

$$W(x,\theta) \equiv 1 \text{ pour } |x| \geq R > 1,\ \theta \in \mathbb{S}^{d-1}, \tag{1.178}$$

où $\Omega, \Omega(\{1\}), \Omega([1,+\infty))$ sont définis par (1.172), (1.173)*, R est une constante.*

Ce résultat est très surprenant pour plusieurs raisons. Tout d'abord, c'est déjà un contre-exemple au théorème 9 lorsque l'hypothèse de régularité sur W est légèrement relâchée de C^1 en dimensions $d = 2, 3$, et de C^2 pour $d > 3$ à C^α, $\alpha \in (0, 1/16)$. A part cela, l'exemple construit de non-injectivité pour P_W pour $d \geq 3$ est remarquable parce que le problème inverse pour P_W est surdéterminé (voir (1.153)) et injectif pour $W \in C^{1+\varepsilon}$, $\varepsilon > 0$, par le théorème 6. De plus, comme l'injectivité globale de P_W pour $d \geq 3$ est la conséquence de l'injectivité locale pour $d = 2$ (par le théorème 7 et la boundary stripping method), on obtient automatiquement un contre-exemple à l'injectivité locale.

Corollaire 13.1. *Pour tout $\alpha \in (0, 1/16)$ il existe $N > 0$ tel que pour tout $\delta > 0$ il existe W_δ, f_δ satisfaisant*

$$W_\delta \geq 1/2,\ W_\delta \in C^\alpha(\mathbb{R}^2 \times \mathbb{S}^1),\ \|W_\delta\|_{C^\alpha(\mathbb{R}^2 \times \mathbb{S}^1)} \leq N, \tag{1.179}$$

$$f_\delta \in C^\infty(\mathbb{R}^2),\ f_\delta \neq 0,\ \operatorname{supp} f_\delta \subset \bar{B}(0,\delta), \tag{1.180}$$

$$P_{W_\delta} f_\delta \equiv 0 \text{ sur } T\mathbb{S}^1. \tag{1.181}$$

La meilleure façon de comprendre le corollaire 13.1 est de réexpliquer le théorème 7. Selon ce théorème, P_W pour $d = 2$ est injective pour des fonctions avec un support suffisamment petit, à condition que W soit au moins de classe C^1. De plus, la "taille" du support dépend de la régularité du poids ; voir la définition de δ dans le théorème 7. Le corollaire ci-dessus indique exactement que l'injectivité locale de P_W pour $d = 2$ peut être violée si W est un peu moins lisse que C^1 ![17]

[17] À part l'interprétation géométrique directe donnée pour le corollaire 13.1, il est très intéressant de comprendre ce résultat en termes d'EDPs. Il est bien connu que P_W pour W satisfaisant (1.14) est lié à des opérateurs pseudodifferentiels elliptiques, pour lesquels on s'attend à ce qu'il ait une forme de *propriété de continuation unique* : essentiellement, si $Pu = 0$, où P est opérateur elliptique et u est égal à zero dans une boule, alors $u \equiv 0$ partout. Une étude de cette remarque pourrait faire l'objet de recherches futures.

Un autre corollaire intéressant du théorème 13 est lié à la propriété (1.178). En particulier, nous avons utilisé cette propriété et le support compact de f pour construire de nouveaux poids W tels que P_W agira sur les fonctions supportées dans des boules disjointes de la même manière que dans le théorème 13.

Théorème 14. *Pour tout $n \in \mathbb{N} \cup \{\infty\}$ il existe un poids W_n satisfaisant* (1.14) *tel que*

$$\dim \ker P_{W_n} \geq n \text{ sur } C_c^\infty(\mathbb{R}^d),\ d \geq 2, \tag{1.182}$$

où P_W est défini dans (1.17). *De plus,*

$$W_n \in C^\infty(\mathbb{R}^2 \times \mathbb{S}^1) \text{ pour } d = 2, \tag{1.183}$$

$$W_n \text{ est infiniment lisse presque partout sur } \mathbb{R}^d \times \mathbb{S}^{d-1}, \tag{1.184}$$

$$W_n \in C^\alpha(\mathbb{R}^d \times \mathbb{S}^{d-1}),\ \alpha \in (0, 1/16) \text{ pour } d \geq 3, \tag{1.185}$$

$$W_n(x, \theta) \equiv 1 \text{ pour } |x| \geq R > 1,\ \theta \in \mathbb{S}^{d-1} \text{ pour } n \in \mathbb{N},\ d \geq 2, \tag{1.186}$$

où R est une constante.

A notre connaissance, des exemples de W satisfaisant (1.14) tel que $\dim \ker P_W \geq n$ pour arbitraire $n \in \mathbb{N} \cup \{\infty\}$ n'ont pas été donnés dans la littérature avant notre travail même pour $n = 1$ en dimension $d \geq 3$ et même pour $n = 2$ en dimension $d = 2$.

En finalisant l'exposé de nos contributions de la partie II, nous voudrions noter que tous les résultats des articles 3-5 ont été obtenus en développant, en particulier, les considérations de Boman [Bo93]. Il semble que son contre-exemple initial présentait un certain degré de liberté dans la façon de commencer le processus de construction. Premièrement, nous avons observé ce degré de liberté dans l'article 4 et nous sommes parvenus à le développer dans l'article 5. En particulier, le titre de la partie II "A breakdown of injectivity for weighted Radon transforms" est consacré aux résultats de l'article 5. Les détails de nos preuves et constructions de la partie II sont présentés dans les chapitres 5-7.

5 Conclusions

Les principaux résultats du présent travail peuvent être résumés comme suit :

1. Nous présentons une nouvelle approche de résolution des problèmes inverses pour les transformations des rayons pondérées qui est basée sur la réduction à des problèmes inverses pour les transformations de Radon pondérées.

2. Nous appliquons l'approche susmentionnée aux problèmes inverses en tomographies. En particulier, nous montrons que les données tomographiques modélisées par transformations des rayons pondérées et acquises en reconstruction tranche par tranche peuvent être réduites aux nouvelles données modélisées par transformations de Radon pondérées (pour un autre poids) sur des plans en trois dimensions. Cette réduction est particulièrement importante pour les tomographies, car elle permet de réduire fortement l'impact du bruit sur les reconstructions.

3. Nous présentons deux nouvelles méthodes d'inversion pour les transformations de Radon pondérées en multidimensions : une méthode est une extension de la formule d'inversion approximative de Chang et l'autre est une extension de l'algorithme itératif de Kunyansky.

4. En utilisant l'approche susmentionnée basée sur la réduction des problèmes inverses en tomographies, nous présentons des tests numériques de nos nouvelles méthodes de reconstruction. En particulier, nous testons nos méthodes de reconstruction dans le cadre de la tomographie par émission monophotonique (SPECT). Nos tests incluent des expériences sur des données synthétiques et réelles. Dans le cas des données synthétiques, c'est-à-dire lorsqu'une comparaison entre reconstructions par différentes méthodes est possible, notre nouvelle approche semble numériquement plus stable contre le bruit que les méthodes de reconstruction conventionnelles utilisées pour la reconstruction tranche par tranche. Par le test numérique sur des données réelles, nous montrons que notre approche est également applicable aux procédures de SPECT réelles.

5. Nous poursuivons l'étude de l'injectivité et de la non-injectivité des transformations des rayons pondérées et de Radon pour des poids arbitraires strictement positifs. En particulier, nous établissons une série de nouveaux résultats sur la non-injectivité de ces derniers.

6. Nous construisons un exemple de non-injectivité pour les transformations de Radon pondérées en multidimensions avec un poids strictement positif qui est aussi infiniment lisse presque partout. Ce résultat peut être considéré comme une tentative d'étendre le célèbre contre-exemple d'injectivité de Boman (1993) à des dimensions supérieures $d \geq 3$.

7. Nous construisons un exemple de non-injectivité pour les transformations de Radon pondérées le long de plans bidimensionnels dans $\mathbb{R}^d$, $d \geq 3$, de sorte que le poids est continu, invariant par rotation et strictement positif. Ce résultat est déjà très inattendu pour deux raisons :

   (i). Quinto (1983) a prouvé que les transformations de Radon pondérées R_W pour des poids invariants par rotation positifs sont injectives si W est de classe C^∞ (C^1 en dimensions $d = 2, 3$). Notre résultat montre que l'hypothèse de régularité est cruciale pour ce résultat d'injectivité.

   (ii). Le problème inverse pour les transformations de Radon pondérées sur des plans bidimensionnels dans $\mathbb{R}^d$ est surdéterminé pour $d > 3$. Bien qu'il n'y ait pas eu de résultats sur l'injectivité et la non-injectivité dans un tel contexte, la surdétermination conduit généralement à l'injectivité de transformations de type Radon.

8. Nous construisons un contre-exemple à l'injectivité pour les transformations des rayons pondérées en dimensions $d \geq 2$, où le poids est positif, la rotation invariante et Hölder régulière. Ce résultat est très surprenant compte tenu des nombreux résultats d'injectivité connus pour les transformations des rayons pondérées lorsque W est au moins de classe C^1. De ce résultat, il s'ensuit que la régularité du poids est cruciale pour ces résultats d'injectivité, même si les problèmes inverses correspondants sont surdéterminés. De façon informelle, nous appelons un tel phénomène "brisure de l'injectivité" pour les transformations des rayons pondérées.

On peut proposer, en particulier, les développements possibles suivants des sujets étudiés dans la thèse :

1. Les formules de réduction du problème inverse pour les transformations des rayons pondérées au problème inverse pour les transformations de Radon pondérées de l'article 1

ne répondent pas complètement, d'un point vue mathématique, à la question de savoir pourquoi les reconstructions deviennent plus stables numériquement. L'effet de la régularisation du bruit pourrait être étudié plus en détail.

2. Le contre-exemple de l'article 3 pourrait éventuellement être adapté pour construire un nouveau contre-exemple à l'injectivité pour les transformations de Radon pondérées en multidimensions. En particulier, dans le nouvel exemple, il serait important de construire un poids qui soit strictement positif et infiniment lisse partout. Cela compléterait l'extension du contre-exemple de J. Boman (1993) aux dimensions $d \geq 3$.

3. Il est très intéressant de trouver une interprétation du contre-exemple à l'injectivité de l'article 5 en termes à EDPs et de théorie des opérateurs pseudo-différentiels elliptiques. En particulier, aux opérateurs P_W, R_W il est possible d'associer certains opérateurs pseudo-différentiels qui sembleront elliptiques dans l'hypothèse où le poids W est positif. L'injectivité des transformations pondérées de type Radon susmentionnées est étroitement liée aux propriétés de ces opérateurs elliptiques. En particulier, une fonction à support compact dans le noyau d'un opérateur différentiel elliptique signifie la violation de la propriété de continuation unique bien connue pour cette classe d'opérateurs. Un exemple d'une telle violation est particulièrement intéressant, construit par Pliś [Pl63]. En particulier, de l'exemple de Pliś il s'ensuit qu'il y a une rupture de la propriété de continuation unique pour les opérateurs elliptiques si les coefficients dans l'opérateur sont Hölder réguliers ou moins.

Introduction (in English)

1 A historical interlude to Radon-type transforms

In this section we give a short historical overview of the sequence of events that lead to development of Radon-type transforms. We believe that this sequence has its own esthetic beauty and may serve as a good introduction to the contents of this thesis.

1.1 Minkowski-Funk-Radon's heritage

First results on what we call now "Radon-type transforms" are going back to the beginning of the 20th century to publications of Hermann Minkowski [Mi04], Paul Funk [Fu13] and Johann Radon [Ra17]. In particular, each one of these mathematicians considered a certain geometrical problem that lead to considerations of some corresponding integral transformations. These finally appeared to be fundamental in many domains of pure and applied mathematics.

[1]For example, Minkowski's original work was related to a problem in convex geometry in which the author studied objects called *the bodies of constant width*. Nowadays, the result of this work is also known as Minkowski's Theorem which states that *bodies of constant circumference are bodies of constant width*. In his proof Minkowski, in particular, used the following formula

$$Mf(\theta) = \int\limits_{\mathbb{S}^2 \cap \Sigma(\theta)} f(\sigma)\, d\sigma,\ \theta \in \mathbb{S}^2, \tag{2.1}$$

where $\Sigma(\theta) = \{x \in \mathbb{R}^3 : x \cdot \theta = 0\}$, $d\sigma$ is a uniform length measure on $\mathbb{S}^2$ and f is some function on $\mathbb{S}^2$. From formula (2.1) one can see that integrations were taken over great circles of $\mathbb{S}^2$ and, actually, both functions f, Mf, were not arbitrary and had a specific geometric sense; see [Mi04] for details. The latter fact was making too early to speak of M as an integral transformation until the work of P. Funk in 1913. Assigned by his advisor – David Hilbert, to look at Minkowski's work, Paul Funk considered the following problem:

$$\text{reconstruct function } f \text{ on } \mathbb{S}^2 \text{ from all integrals } Mf \text{ of (2.1).} \tag{2.2}$$

Such formulation obviously made M seen as a transformation of functions on $\mathbb{S}^2$ and it was studied by Funk in his doctoral dissertation and in his further publication [Fu13]. In particular, one of the applications of M presented in [Fu13] was simple and elegant derivation of Minkowski's Theorem. Nowadays, transform M together with its generalizations to higher dimensions is known as Funk-Minkowski transform and it is used, for example, in convex and integral geometries, harmonic analysis, differential equations and in some related areas

[1]In this part of exposition on P. Funk and H. Minkowski we used, in particular, a nice review paper [Da10].

of applied mathematics, e.g., in photo-acoustic tomography (PAT); see [Ka18] and references therein.

[2]After the works of Minkowski and Funk the austrian mathematician Johann Radon, motivated by applications in mathematical physics, considered a similar problem:

$$\text{reconstruct function } f \text{ on } \mathbb{R}^2 \text{ from its integrals along all straight lines in } \mathbb{R}^2. \tag{2.3}$$

In other words, Radon studied the inversion of transform R given by the following formula[3]

$$Rf(s,\theta) = \int_{-\infty}^{+\infty} f(s\theta + t\theta^{\perp})\, dt,\ s \in \mathbb{R},\ \theta = (\cos\varphi, \sin\varphi) \in \mathbb{S}^2,\ \varphi \in [0, 2\pi], \tag{2.4}$$

where $\theta^{\perp} = (-\sin\varphi, \cos\varphi)$, function f is sufficiently regular on $\mathbb{R}^2$ with appropriate decay at infinity. In his work, Radon solved problem (2.3) by proposing exact analytic inversion formulas for R^{-1} which now are known as *classical Radon inversion formulas*; see [Ra17] for details. Also, apart of the inversion formulas, Radon proposed the following generalization of (2.2), (2.3):

$$\begin{gathered}\text{reconstruct function } f \text{ on a surface } S \text{ from} \\ \text{its integrals over a family of curves } C \text{ on } S.\end{gathered} \tag{2.5}$$

In considerations of Funk and Minkowski the surface S was the sphere $\mathbb{S}^2$ and curves C were the geodesics (or, equally, big circles) as well in considerations of Radon curves C were also geodesics but on the plane $\mathbb{R}^2$. Another proposed direction was to consider generalizations of R from (2.4) to higher dimensions[4], where the integrals will be taken along hyperplanes in $\mathbb{R}^d$, $d > 2$. So this was an important philosophical step from particular considerations of Minkowski in convex geometry to a proposition to studies of a whole new class of integral-type transforms which we call by now – Radon-type transforms.

Interestingly, paper [Ra17] which is considered central and the most honored now by specialists in many domains of pure and applied mathematics actually seemed to be not so significant for Radon by himself; see also [RaSch18]. In particular, in the obituary of his colleague Paul Funk to Prof. Radon [Fu13a], the author mentioned outstanding mathematical achievements of Radon (Radon-numbers, Theorem of Radon-Nykodim, Radon-Riesz Theorem) but ignored Radon transforms. This looks not so surprising, since at the beginning of the 20th century there were no ideas for applications of Radon transforms and from the mathematical point of view these results were not considered as a breakthrough.

Nevertheless, a mathematical development of these transforms was continued. In 1927 the German mathematician Philomena Mader published new inversion formulas for R^{-1} in dimensions $d \geq 2$; see [Ma27]. A very significant work was done by Fritz John in his book [Jo55], where he applied Radon transforms to build solutions for Cauchy problems for hyperbolic and elliptic partial differential equations. The resulting formulas were based on decompositions of functions into plane waves, however, to the contrast of "Fourier method", plane integrals in "the sense of J. Radon" were used. In addition, it appears also that F.

[2]There is also a remark of Bockwinkel [Bo06], that a transform of integrating a function on $\mathbb{R}^3$ over two-dimensional planes was already known to H. Lorentz. Moreover, it is claimed that Lorentz had an inversion formula for this transform in his lectures notes.

[3]Here we present Funk-Minkowski and Radon transforms as two different maps. But, in fact, both of them are different versions of the *projective Radon transform*; see [G+03].

[4]In the original Radon's work the author also derives exact inversion formulas in all dimensions $d \geq 2$, when the integrations are taken along hyperplanes.

John was the first who proposed to call the integral transforms by "Radon transforms"; see p.2 in the Introduction of [Jo55]. Between 60's and 70's, due to works of Israel Gelfand with his co-authors, of Harish-Chandra and of Sigurdur Helgason, Radon transforms started to appear in studies of generalized functions, representation theory of Lie groups and in harmonic analysis; see [G+59], [G+69], [G+62], [HC58], [HC58a], [He65], [He65a], [He66], [He70]. The philosophy of these studies consists in a group-theoretical approach to Radon transform where it is defined as a map between a pair of homogeneous spaces for a certain Lie group G that admits what is called *a double fibration*. This approach was also generalized by Gelfand and his school to the case of manifolds without action of a Lie group but still attaining a double fibration structure. A very good reference on Radon transforms that follows this approach is a book by Sigurdur Helgason [He99].

The purpose of references given above is to explain the growth of interest to Radon-type transforms among mathematicians. From the very concrete examples in the beginning the transforms were studied already in a full generality with help of many modern theories. However, it is only one side of the story. Mathematics contains an enormous amount of beautiful results and stories behind them, and in this sense Radon transforms are not unique. We could have continued here the exposition of mathematical development of Radon transforms up to present time (which would be also a not easy thing to do), but it would contain a chronological flaw. The reason for that is a series of unexpected rediscoveries of the latter in completely new domains about which we speak in the next subsection.

1.2 Rediscoveries, The Beatles and the Nobel Prize Award

Though the Radon transforms were known to many mathematicians by the 50's of the past century, it was only for them to reappear in a completely new field of applications – in computer-assisted tomographies (CAT or CT).

Pioneering result belongs here to a South African and American physicist Allan MacLeod Cormack[5]. In 1950's, he worked as a Lecturer at University of Cape Town at the Physics Department and he also conducted his own research in nuclear physics. In fact, as Cormack described by himself [Co80a], the work at University of Cape Town at that time was quite lonely since it were very few nuclear physicists in the whole country. In the end of 1955, due to resign of a local hospital physicist, Cormack was proposed to take his place in radiology department until a new specialist was found. By South African laws, only a qualified person could give permission to use radioactive isotopes on patients and, by chance, Cormack appeared to be the only one in the university handling such isotopes. Working a few hours per week during six months in Groot Schurr Hospital he had a chance to see diagnostic and medical X-ray procedures.

In particular, one of the important problems for doctors was to control the amount of radiation delivered to a patient using such a procedure. Again, from the memories of Cormack [Co80a], the practices of that time were rather crude, so there was a motivation for an improvement. To control better the delivered radiation dose one should have at least known the attenuation values of tissues in regions that are crossed by X-rays. So the initial problem considered by Cormack was to reconstruct the attenuation map using X-rays.

By 1956, the exponential law of attenuation in homogeneous media (Beer's law) had been known almost for 60 years already. Having had it in mind and having noted that the tissues are characterized by their attenuation, Cormack quickly understood that the problem was actually mathematical.

[5]In this part of the exposition we mostly refer to his biographical notes [Co80], [Co80a] and to his seminal publications [Co63], [Co64] on computer assisted-tomography.

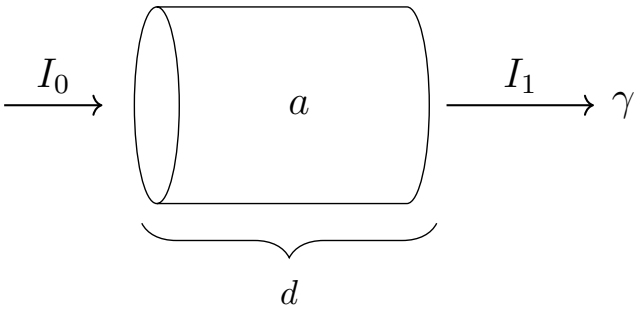

Figure 2.1 Beer's attenuation law

Beer's law of attenuation has the following form: if a ray of intensity I_0 is emitted in a region of length d with constant attenuation a, then the intensity of the ray on the exit I_1 is given by the formula (see Figure 2.1)

$$I_1 = I_0 e^{-d \cdot a}. \tag{2.6}$$

From (2.6) it is obvious that for heterogeneous media with attenuation $a = a(x)$, $x \in \mathbb{R}^2$, intensities I_0, I_1 will be related by the following formula:

$$I_1 = I_0 \exp\left(- \int_\gamma a(x)\, dx \right), \tag{2.7}$$

where element dx denotes the uniform Lebesgue measure along ray γ. Having obtained formula (2.7), Cormack reduced the problem of reconstruction of $a = a(x)$ to the following one:

reconstruct function $a = a(x)$ on $\mathbb{R}^2$ from its integrals Pa, where

$$Pa(\gamma) \stackrel{\text{def}}{=} \int_\gamma a(x)\, dx, \text{ where } \gamma \text{ is a ray on } \mathbb{R}^2; \tag{2.8}$$

moreover, it is assumed that a is supported in fixed open bounded domain D.

Though transitions from (2.6) to (2.8) may seem quite natural to the reader, it was not the case at the time of the events. In particular, in his notes on computer-assisted tomography [Co80], [Co80a], Cormack remarked that he even could not find formula (2.7) in any of the references he looked. Also, he consulted with mathematicians from Cape Town, United States and from United Kingdom to see if problem (2.8) was already solved.

Note that problem (2.8) was exactly the same as (2.3) considered by Radon in 1917! However, the motivation of A. Cormack was completely different to the one of Radon: map $a = a(x)$ was the attenuation coefficient of tissues, rays γ denoted trajectories of propagation of emitted gamma rays and, finally, "fixed domain" D was a slice section of a region in which the whole "scanning procedure" should have taken place. What a luck to find the same problem, but in a completely different domain!

Unfortunately or luckily for Cormack, he did not manage to find already existing mathematical results on this problem, so he started to work on a solution of (2.8) by himself. And it was quickly found and published in [Co63], [Co64]. Cormack's solution was different from the one of J. Radon, in particular, in his approach to the problem[6]. Basically, he decomposed function a into a series of radial and angle components and established their

[6]If one looks carefully at [Co63] one finds that the author at some moment obtained actually a version of formula of J. Radon (formula (26) in the original text) which gives exact reconstruction only for spherically symmetric functions. In particular, in [Ra17] it was used further to obtain the inversion formula for arbitrary functions, but this argument was missing in Cormack's work.

relationships with Pa from (2.8); for details, see [Co63]. In addition, for this publication Cormack, together with his colleagues, performed the first real tomographical experiment on a spherically symmetric phantom of wood and aluminum. The reconstruction results showed efficiency and accuracy of his method. In the next publication [Co64], Cormack modified some of his inversion formulas and also presented new numerical results for a more elaborate experiment on a non-spherically symmetric phantom. The results were again very promising, so some further attempts were made to interest hospital physicists in his method. Unfortunately, as Cormack remarked himself, his results generated very little interest until 1971, when a first commercial tomographical scanner appeared on the market. So how could it appear if not by the works of A. Cormack?

The reason for that was an outstanding and independent work of another person – British electrical engineer, Sir Godfrey Newbold Hounsfield[7].

After the World War II, during which Hounsfield served in British Royal Air Force as Radar Mechanic Instructor, also with the help of his connections from the military service, he got a grant to attend Faraday House Electrical Engineering College in London; see [Ho80], [Pi19]. After he had obtained there a diploma, he worked at Electronic and Musical Industries (EMI, Ltd.) in Middlesex where he was developing guided weapon systems and radars. Then, after a while he got interested in design of computers which were in their newborn state at those times. For example, among his achievements in EMI was the first British all-transistor computer – EMIDEC 1100.

The company trusted his creative capabilities and after a failure of one project for commercial reasons he was proposed to choose a new research project according to his own tastes. One can think, it looked surprising that a business company invested money into pure research.

According to its name, EMI was not only producing and selling the electronic equipment (such as television equipment, radars or computers), but was actually founded as a music recording company; see [EMI]. Among the musical stars who were recorded at EMI one could name: *Frank Sinatra*, *Nat King Cole*, *Peggy Lee*, *Adam Faith*, *Frankie Vaughan*, *Alma Cogan* and finally *The Beatles*. In 1963, the first single of The Beatles 'Love Me Do' was ranked only 17th in top UK charts, but the next 'Please, Please Me' became already second and this completely changed the world of music. The following period in music world was known as 'Beatlemania'[8] and in history there was no equivalent of such records success. Obviously, this success made EMI an ultra rich company so they had enough of money to invest in bold research projects. This was the case for one given away to Hounsfield; see [Pi19] for more details.

From the memories of G. Hounsfield [Ho80], around the period of work on 'Sergeant Pepper's Lonely Heart's Club Band' by The Beatles, just randomly he got the following idea:

> if the principle of radars are to be placed in the center of the region
> of interest and to scan the periphery, why not to try to invert this model?
> Basically, to reconstruct the interior part of an unknown object,
> for example, of a 3-D box using only exterior measurements. (2.9)

Developing this idea he decided to use X-rays and to consider the attenuation model in the same way as Cormack proposed in (2.8). Since Hounsfield was not aware of works

[7]Godfrey Hounsfield was knighted in 1981.

[8]From 1963, withing next eight years The Beatles recorded and released such albums as: 'Sgt. Peppers Lonely Hearts Club Band', 'Rubber Soul', 'Abbey Road' and 'The While Album'.

by Radon and Cormack, it was again a new independent rediscovery of Radon transforms! Hounsfield's solution of problem (2.8), published in 1971 in his patent [Ho71], was very simple and completely corresponded to the spirit of a talented engineer.

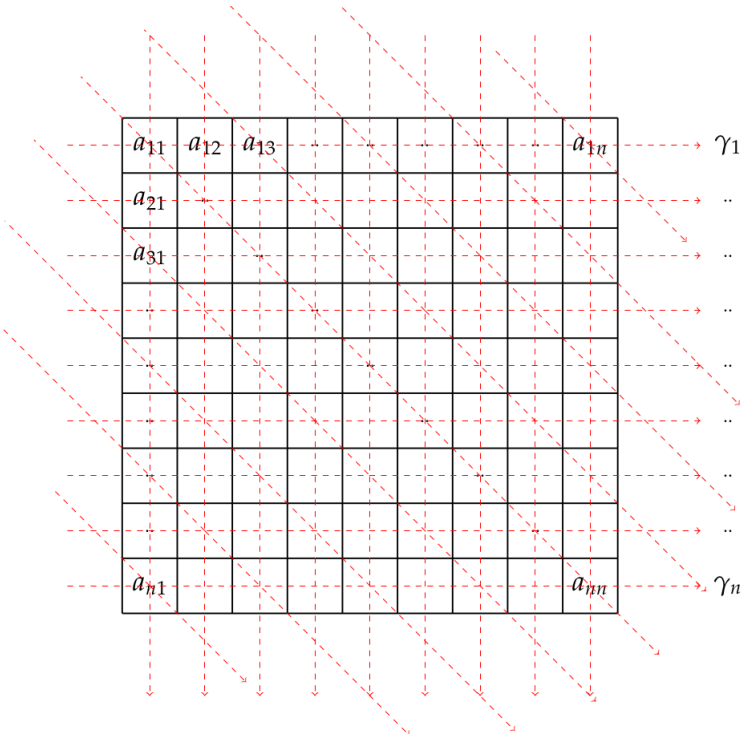

Figure 2.2 Hounsfield's idea to solve inverse problem (2.8)

Hounsfield understood that in practice only a plane image for attenuation $a = a(x)$ was needed. Because an image is just a two-dimensional array of pixels, then function a could be assumed locally constant within each pixel with corresponding values $\{a_{ij}\}_{i,j=1}^{n}$; see Figure 2.2. In this model the formula for Pa from (2.8) reduces to the following one:

$$Pa(\gamma) = \sum_{i,j=1}^{n} a_{ij} L_{ij}(\gamma), \tag{2.10}$$

where $L_{ij}(\gamma)$ are the lengths of intersections of ray γ with pixel cells; see Figure 2.2. Formula (2.10) can be seen as a linear equation on coefficients $\{a_{ij}\}_{i,j=1}^{n}$ which are unknown. So, taking enough of different rays for (2.10) one gets a solvable linear system of equations on $\{a_{ij}\}$. This simple and natural idea was practically realized by Hounsfield and, later, published as a patent. Interestingly, A. Cormack, in the introduction to his original paper [Co63], also considered equation (2.10), but he missed the argument that taking enough of different rays would be sufficient to compose a complete system of equations[9].

Tests of the method on brains of animals[10] showed that the method of G. Hounsfield was working and new clinical tests on humans were needed. In 1971 the first prototype, called the EMI brain scanner, was installed in Atkinson's Morley Hospital and the first patient

[9]In fact, G. Hounsfield took more rays in (2.10) than the number of coefficients $\{a_{ij}\}$. By doing so he obtained an overdetermined linear system of equations $Aa = Pa$, where A is a matrix of size $N \times n^2$, $N > n^2$. Such system was solved in the "least-squares sense" $A^T A = A^T Pa$, which corresponds to minimization ℓ_2-norm of the error $\varepsilon(a) = \|Aa - Pa\|_2^2$. This approach is quite natural to reduce the impact of errors in measurements.

[10]First experiments where performed on bullock's brains which G. Hounsfield was buying himself in a butcher shop in London; see [Pi19] and references therein.

was examined on October 1, 1971. The examination process was taking only 4.5 minutes for measurements and 20 seconds for reconstruction process. Produced images had resolution of 80 x 80 pixels and this was already an epoch changing result in radiology diagnostics. After a few presentations of these results on conferences (which finished by standing ovations [Pi19]), a great number of mathematicians, physicians and engineers joined the development of methods and machines for X-ray tomographic reconstructions. In two years resolution already reached 320 x 320 pixels and by now scanners have resolution approximately of 2048 x 2048 pixels.

Finally, in 1979 A. Cormack and G. Hounsfield were both awarded with a Nobel Prize for Physiology and Medicine and it is worth nothing to say that they met each other only at this ceremony; see also [Ag14]. Also, already by the time of Nobel Prize Award, the works of Radon and Cormack were conformed and now it is a general agreement to consider the work of Radon as the primary in tomographies based on inversions of Radon-type transforms.

1.3 Finalizing remarks

After the invention of computerized tomography the interest to Radon-type transforms was renewed. Though the first applications of the latter were in medicine, their success inspired to apply similar techniques in other applied fields. For example, Radon transforms and their generalizations are used now in medicine, optics, geophysics, astronomy, economics and in some others applied fields; see [Br56], [Na86], [De07], [Ku14], [HeSh90], [Ag+18].

In turn, new applications stimulated new studies of Radon-type transforms in mathematics; see, e.g., [Qu80], [Qu06], [Na86], [BQ87], [No02], [Il16], [RaSch18] and references therein. In particular, among examples of Radon-type transforms there are ones which are called *weighted Radon transforms* (or *generalized Radon transforms*[11]) which are also the central object for this work; see e.g., [Qu80], [Be84].

In the next section we define weighted Radon transforms precisely and give references to some already classical results.

2 Preliminaries for weighted Radon-type transforms

Definition 1. The *n-dimensional weighted Radon transform* $R_W^{d,n}$ is defined by

$$R_W^{d,n} f(P) = \int_P f(x) W(x,P)\, dx,\ P \in \mathcal{P}^{d,n},\ 1 \le n < d, \tag{2.11}$$

where $W(x,P)$ is the *the weight*, $f = f(x)$ is a *test-function* on $\mathbb{R}^d$,

$$\begin{aligned} &\mathcal{P}^{d,n} \text{ is the manifold of all oriented } n\text{-dimensional planes in } \mathbb{R}^d, \\ &\dim \mathcal{P}^{d,n} = (n+1)(d-n). \end{aligned} \tag{2.12}$$

In formula (2.11), element dx denotes the uniform Lebesgue measure on $P \in \mathcal{P}^{d,n}$. For f and W we assume that

$$f \text{ is continous and compactly supported on } \mathbb{R}^d, \tag{2.13}$$

$$W \text{ is real-valued, } W \ge c > 0,\ W \in L^\infty_{\mathrm{loc}}(Z), \tag{2.14}$$

[11] However, the term *generalized Radon transforms* is often used in more general context including non-abelian Radon transforms [No02a] and Radon transforms along curves on not necessarily flat manifolds [Ku06], [Ba05], [Ba09], [Pa+12], [Gu+16]. In our work we did not study this case, so we always use the term *weighted Radon transforms*.

where c is a constant, Z is a closed submanifold of $\mathbb{R}^d \times \mathcal{P}^{d,n}$ defined by

$$Z = \{(x, P) \in \mathbb{R}^d \times \mathcal{P}^{d,n} : \text{ point } x \text{ geometrically belongs to plane } P \text{ in } \mathbb{R}^d\}. \tag{2.15}$$

In the above definition we do not detail the structure of manifolds $\mathcal{P}^{d,n}$ and Z except two cases $n \in \{1,\, d-1\}$; for more details see, for example, [He99], [Fr89]. That is because we are mainly interested in studies of $R_W^{d,n}$ only for these two cases. For any n apart of $\{1,\, d-1\}$ we will specify $\mathcal{P}^{d,n}$ and Z, where it will be necessary.

Considering Definition 1 for $n = \{1, d-1\}$ we can rewrite it as follows.

Definition 2. Let f be a continuous function with compact support on $\mathbb{R}^d$, weight W be a function on $\mathbb{R}^d \times \mathbb{S}^{d-1}$ (i.e., $W = W(x, \theta)$) satisfying (2.14) with $\mathbb{R}^d \times \mathbb{S}^{d-1}$ in place of Z. Then, by *weighted Radon transform of f for weight W*, we denote the following function

$$R_W f(s, \theta) = \int\limits_{x\theta = s} f(x) W(x, \theta)\, dx,\ (s, \theta) \in \mathbb{R} \times \mathbb{S}^{d-1}, \tag{2.16}$$

where the integral above is taken with respect to the uniform Lebesgue measure on hyperplane $\{x \in \mathbb{R}^d : x\theta = s\}$.

Definition 3. Let f be a continuous function with compact support on $\mathbb{R}^d$, weight W be a function on $\mathbb{R}^d \times \mathbb{S}^{d-1}$ (i.e., $W = W(x, \theta)$) satisfying (2.14) with $\mathbb{R}^d \times \mathbb{S}^{d-1}$ in place of Z. Then, by *weighted ray transform of f for weight W*, we denote the following function

$$P_W f(x, \theta) = \int\limits_{-\infty}^{+\infty} f(x + t\theta) W(x + t\theta, \theta)\, dt,\ (x, \theta) \in T\mathbb{S}^{d-1}, \tag{2.17}$$

where $T\mathbb{S}^{d-1}$ is the tangent bundle of the unit sphere $\mathbb{S}^{d-1}$ and it is defined by

$$T\mathbb{S}^{d-1} = \{(x, \theta) \in \mathbb{R}^d \times \mathbb{S}^{d-1} : x\theta = 0\}. \tag{2.18}$$

In the definitions above the continuity of f is not essential, and for each particular case we will specify the regularity of test functions being considered.

Note that Definitions 2, 3 correspond to Definition 1 for $n = d-1$ and $n = 1$, respectively. Indeed, for $n = d-1$ the integrals in (2.11) are performed along oriented hyperplanes in $\mathbb{R}^d$, exactly as in (2.16). Manifolds $\mathcal{P}^{d,1}$ and Z of (2.12), (2.15), are isomorphic to $\mathbb{R} \times \mathbb{S}^{d-1}$, $\mathbb{R}^d \times \mathbb{S}^{d-1}$, respectively, where

$$\begin{aligned} &(s, \theta) \in \mathbb{R} \times \mathbb{S}^{d-1} \text{ corresponds to hyperplane} \{x \in \mathbb{R}^d : x\theta = s\}, \text{ where} \\ &\text{normal } \theta \in \mathbb{S}^{d-1} \text{ gives the orientation to the hyperplane;} \end{aligned} \tag{2.19}$$

$$(x, \theta) \in \mathbb{R}^d \times \mathbb{S}^{d-1} \text{ corresponds to } (x, (x\theta, \theta)) \in Z \text{ of (2.15) for } n = d-1. \tag{2.20}$$

For $n = 1$ the integrals in (2.11) are performed along rays (oriented straight lines) in $\mathbb{R}^d$ as in (2.17). Manifolds $\mathcal{P}^{d,1}$ and Z of (2.12), (2.15) are isomorphic to $T\mathbb{S}^{d-1}$, $\mathbb{R}^d \times \mathbb{S}^{d-1}$, respectively, where

$$\begin{aligned} &(x, \theta) \in T\mathbb{S}^{d-1} \text{ corresponds to ray } \gamma(x, \theta) = \{y \in \mathbb{R}^d : y = x + t\theta,\, t \in \mathbb{R}\}, \\ &\theta \in \mathbb{S}^{d-1} \text{ gives an orientation to the ray;} \end{aligned} \tag{2.21}$$

$$(x, \theta) \in \mathbb{R}^d \times \mathbb{S}^{d-1} \text{ corresponds to } (x, (x - (x\theta)\theta, \theta)) \in Z \text{ of (2.15) for } d = 1. \tag{2.22}$$

Note also that in dimension $d = 2$ transforms P_W and R_W are equivalent up to the following change of variables

$$\begin{aligned} &\mathbb{R} \times \mathbb{S}^1 \to T\mathbb{S}^1 : (s, \theta) \mapsto (s\theta, \theta^\perp), \\ &\theta = (\theta_1, \theta_2),\ \theta^\perp = (-\theta_2, \theta_1). \end{aligned} \tag{2.23}$$

Transforms P_W, R_W, and some of their generalizations arise in many domains of pure and applied mathematics. For example, they arise in studies of groups ([G+59], [G+62], [HC58a], [He65], [He99], [Il16]), harmonic analysis ([St82], [St91]), PDEs ([Be84], [Jo55]), integral geometry ([Sh12]), microlocal analysis ([Qu+14], [Qu+18]), they can be also of their own interest ([Qu80], [Fri+08], [Bo11], [Il19]) and, finally, they are widely used in computerized tomographies ([Qu83], [Na86], [Mi+87], [Ku14], [No02], [Qu06], [De07], [Ngu+09], [Ba09], [MiDeP11]). The above list of references is far from been complete and it should be seen also as containing the references therein.

In the next section we describe our motivation for this work and the related mathematical problems for P_W and R_W.

3 Problems and motivation

In this thesis we continue studies of weighted Radon-type transforms in applications to inverse problems. In particular, we study the following inverse problem

Problem 1. *Given W and $P_W f$, find f.*

As it was remarked in Section 2, for dimensions $d = 2, 3$, this problem arises in tomographies, in particular, in X-ray tomography, in SPECT and PET. Solving Problem 1 for weights arising in SPECT, was the initial motivation for this thesis. In the aforementioned tomographies Problem 1 arises usually for dimension $d = 2$, in slice-by-slice reconstruction approach; see also Subsection 4.1 for details. In this thesis we propose another approach for finding f from $P_W f$, which consists mainly in reduction of Problem 1 for $d = 2$ on many two-dimensional "slices" to an inverse problem for $R_{W'}$ for $d = 3$, where W' is another weight constructed from W. In other words, we also consider the following inverse problem

Problem 2. *Given W and R_W, find f.*

The aforementioned reduction is the principal argument of our results from Part I. In fact, it is well known that in dimension $d = 2$, Problem 1 for weights W arising in SPECT is perfectly solvable; see [No02], [Kun01] and Subsection 4.1. In particular, for operator P_W^{-1} there exists an exact analytic inversion formula [No02], which also admits very efficient numerical implementations [Kun01]. However, in SPECT, in practice, the measured data is not given by $P_W f(\gamma)$, $\gamma \in T\mathbb{S}^{d-1}$, but it is given by photon counts $N(\gamma)$, $\gamma \in T\mathbb{S}^{d-1}$, which are realizations of Poisson process on $T\mathbb{S}^{d-1}$ with intensities proportional to $P_W f(\gamma)$, $\gamma \in T\mathbb{S}^1$; see also Subsection 4.1. The presence of noise is a serious issue for stability of reconstructions in SPECT, because, actually, Problem 1 is initially *ill-posed* and, in fact, in presence of noise the explicit formula from [No02] becomes unstable in some regimes [GuNo05], [GuNo08], [GuNo12]. In view of the latter, our contributions of Part I of the thesis can be seen as an attempt to increase stability of reconstructions of f from $P_W f$ in SPECT. Having reformulated the original problem, we propose two new inversion methods for solving Problem 2, and we test them on synthetic and real data for SPECT.

The resume of these results is given in Subsection 4.1.

At the same time, Problems 1, 2 can be treated in a very general way, without assumptions on the special structure of weight W as it was for X-ray CT, PET or SPECT. In this case, the first arising question is if the above problems are solvable at all. On a mathematical level this reduces to the problem of injectivity and non-injectivity for P_W, R_W. Part II of this thesis is devoted to this question.

There exist many results on injectivity and non-injectivity for P_W and R_W, for example, [Ra17], [Co63], [BQ87], [Bo11], [LaBu73], [MaQu85], [Fi86], [No02], [No02a], [No14], [Qu83], [Ku92], [K+95] [Il16] and references therein. Our initial motivation was to continue studies of injectivity and non-injectivity for the latter transforms. In particular, we believe that we have succeeded in this, because we have found new interesting counterexamples to injectivities for P_W, R_W proceeding from the famous counterexample of Boman in [Bo93]. Our first result in this direction was obtained in Article 4, where we showed that $R_W^{d,2}$ (see definition (2.11)) may not be injective in dimensions $d \geq 3$ on $C_c^\infty(\mathbb{R}^d)$ for W satisfying (2.14) and also being continuous. This result was not so surprising in dimension $d = 3$, in view of the fact that the inverse problem for $R_W^{3,2}$ is non-overdetermined. On the other hand, for $d > 3$ the inverse problem for $R_W^{d,2}$ is strictly overdetermined, and in view of this fact our result was completely new and already surprising. Using our developments from this work, in Article 5 we constructed another example of non-injectivity for P_W on $C_c^\infty(\mathbb{R}^d)$ for $d \geq 2$, for weights satisfying (2.14) and being Hölder smooth (but not yet C^1-smooth). This result appeared to be very unexpected in view of many existing injectivity results for P_W for $d \geq 3$ for C^1-smooth weights, for example, [Fi86], [Il16]. In particular, intuitively it was unexpected because of the well-known *boundary stripping method* for proving injectivity of P_W in dimensions $d \geq 3$ for weights W satisfying (2.14).

To conclude our studies of injectivity and non-injectivity for P_W, R_W, in Article 3 we had constructed analogs of the counterexample of Boman for R_W for dimensions $d \geq 3$. Interestingly, to obtain these results, we had adapted the counterexample of J. Boman [Bo93] and our method of reduction of Problem 1 to Problem 2 from Article 1.

The aforementioned counterexamples to injectivity for P_W, R_W are valid in the framework of general weights W, which only satisfy (2.14). Such general considerations do not help directly to solve real inverse problems, but they help to understand better the limits of applicability of mathematical methods that are used in solving these problems. We see the results of Part II of the thesis exactly in this scope.

The resume of the aforementioned results on non-injectivity of P_W and R_W are given in Subsection 4.2.

4 Summary of our results

4.1 Summary of results from Part I

We begin the exposition by recalling frameworks of several conventional tomographies. Next, we explain the reduction of Problem 1 to Problem 2 in the framework of emission tomographies (Article 1), and we also present two new inversion methods for solving Problem 2 (Articles 1, 2). At the end, we give numerical examples of reconstructions for our methods.

Flavors of different tomographies

Tomography ($\tau o \mu o \sigma$ – slice and $\gamma \rho a \phi \omega$ - to write) can be seen as collection of techniques and methods for reconstruction of interior properties of objects from their exterior measurements.

One could also say that tomography is a part of a larger domain called *Imaging Sciences*, which is devoted to various forms of construction and analysis of images; see [BM04].

An important feature of tomographical techniques is that they are non-invasive, non-destructing. This makes them very appealing for many problems of medical imaging, technical diagnostics, quality control and of other domains. In this thesis we concentrate on medical applications of tomographies and in particular, on X-ray transmission tomography (or X-ray CT), positron and single-photon emission computed tomographies (PET and SPECT).

From a mathematical point of view the choice of this triple - X-ray CT, PET, and SPECT, is pleasant because the latter rely on the same mathematical object – *weighted ray transforms* P_W in three dimensions (see Definition 3), where W depends on type of tomography being used.

Next, we recall the frameworks of X-ray CT, PET and SPECT.

X-ray CT

For medical applications, the main goal in X-ray transmission tomography is to reconstruct the anatomical image in the given region of the human body.

In X-ray CT the reconstruction method is based on measuring losses of intensities of emitted X-rays passing the area of interest; see Figure 2.3. Because tissues of the body can be characterized by the strength of attenuation of X-rays, the problem reduces to finding attenuation coefficient $a = a(x)$, $x \in \mathbb{R}^3$.

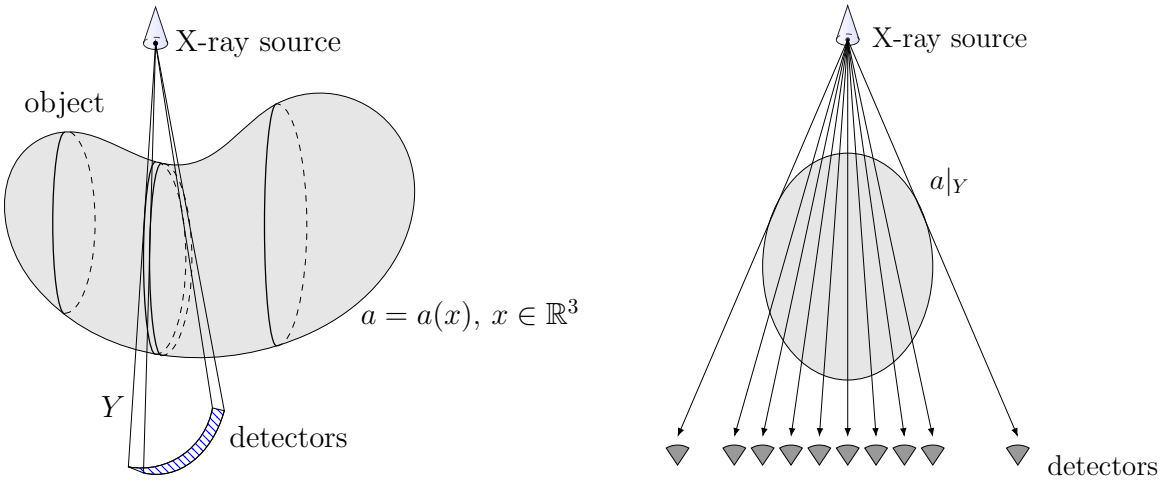

Figure 2.3 X-ray CT

Measuring the intensity losses for many rays and applying Beer's law of attenuation (see formula (2.7)), one can compute the classical ray transform Pa, which is given by the formula

$$Pa(x,\theta) = \int_{-\infty}^{+\infty} a(x+t\theta)\,dt,\ \gamma = \gamma(x,\theta) \in T\mathbb{S}^2, \tag{2.24}$$

where $a = a(x)$, $x \in \mathbb{R}^3$, is the attenuation coefficient to reconstruct. Therefore, on a mathematical level, the reconstruction problem is reduced to Problem 1 for $W \equiv 1$ in dimension $d = 3$.

Though the aim is to reconstruct attenuation a in three dimensions, for practical reasons it is often solved as a collection of Problems 1 for dimension $d = 2$, in so called *slice-by-slice reconstruction approach*. In this approach the support of unknown function a is sliced into a set of parallel planes, and reduction $a|_Y$ to each plane Y is reconstructed; see Figure 2.3.

For the reduced problem it is well-known that

$$Pa\big|_{T\mathbb{S}^1(Y)} \text{ uniquely determines } a\big|_Y, \tag{2.25}$$

where $T\mathbb{S}^1(Y)$ is the set of rays in Y. Moreover, the determination of $a\big|_Y$ can be implemented via the classical inversion formulas of Radon [Ra17]:

$$f(x) = \frac{1}{4\pi}\int\limits_{\mathbb{S}^1} \theta^\perp \nabla \tilde{q}_\theta(x\theta^\perp)\, d\theta,\ x \in \mathbb{R}^2, \tag{2.26}$$

$$\tilde{q}_\theta(s) = \frac{1}{\pi} p.v. \int\limits_{-\infty}^{+\infty} \frac{q_\theta(t)}{s-t}\, dt, \tag{2.27}$$

$$q_\theta(s) = Pf(s\theta^\perp, \theta),\ s \in \mathbb{R},\ \theta = (\theta_1, \theta_2) \in \mathbb{S}^1,\ \theta^\perp = (-\theta_2, \theta_1), \tag{2.28}$$

where Pa is given in (2.24).

From the above considerations it is obvious that the mathematical problem for X-ray CT is perfectly solvable. We also note that there are many other methods for reconstruction of a from Pa which mainly differ in the scheme of acquisition of ray data Pa. For example, modern scanners may not perform reconstructions slice-by-slice, but measure Pa on more complicated set of rays (for example, Katsevich's and Grangeat's methods) and perform reconstructions directly in 3D; for more details see [Gr91], [Na99], [Kat02], [Va+16].

In practice, apart of actual inversion of P there are many other important issues, for example: stability of reconstructions, dependence on finite data (sampling, incomplete data).

- Stability of reconstructions: transform P is a smoothing operator and for $d = 2$ acts, for example, from $H_0^s(\Omega)$ to $H_0^{s+1/2}([-1,1] \times \mathbb{S}^1)$, $s \geq 0$, where Ω is a unit ball in $\mathbb{R}^2$, H_0^s is the standard Sobolev space with zero-boundary condition. Because of this, the actual problem of inversion of P is *ill-posed* (to be rigorous, it is seen from the analysis of singular values of P), and it is a very important issue in applications; see also [La+86]. In a real procedure of X-ray CT the measured data are given by photon counts $N(\gamma)$ in a given time for each ray $\gamma \in T\mathbb{S}^1$. These photon counts $N(\gamma)$ can be modeled as Poisson process, [Wa08], with intensity equal to $CPa(\gamma)$, where C is a setup-dependent constant. Therefore, applying direct inverse formulas (for example, (2.26)-(2.28)) to noisy and raw data can cause artifacts and errors in reconstructed images. A way to stabilize reconstructions is to *regularize* the data, either by some data processing, [HoWe16], or by gaining a good statistic for the data or doing both.

- Methods of inversion of P: apart of inversion formulas (2.26)-(2.28) there are many other formulas and methods to find f from Pf (algebraic, iterative, statistical); see, for example, [Na99], [AdOk17]. The advantage of using exact inversion formulas is that many of them admit very efficient implementations in terms of speed which are called *filtered backprojection algorithms* (or shortly - FBP). On the other hand, these formulas always contain some operation which can be seen as unstable from the point of view of numerical methods – derivations or integrations with singular kernels. In view of this and that the measured data are always given on finite number of rays and it is corrupted with noise, numerical implementations require careful modification of the analytic formulas into their discrete analogs.

All the above questions have been studied for a long time and there is already a huge progress in all of the modalities of X-ray CT; see [Na86], [Ku14] and references therein. As we will see further, the corresponding mathematical and numerical parts of the inverse problems for PET and SPECT are far less simple.

PET

Positron emission tomography (PET) is a type of tomography used in nuclear medicine (also as X-ray CT and SPECT); [Na86], [To96], [Ku14]. On a medical level it mostly focuses on depicting physiological activity, metabolism or levels of chemical activities in a region of interest inside the body, whereas X-ray CT focuses on imaging of anatomy. To investigate the aforementioned activities, a patient gets an injection of a special medicament called *tracer*, which principal component is an isotope that has a short half-life. Then, using a special PET scanner the radiation emitted by the isotopes is measured and from this data the distribution of the isotopes, and hence, of the medicament is reconstructed. Finally, the image of the distribution is interpreted by specialists in order to provide a diagnosis.

On a physical level the emitted radiation is represented by gamma-photons, which are produced from the nuclear reactions inside the patient's body. In particular, due to the nuclear decay of the isotope, first, a positron is emitted and shortly after it is annihilated by a nearby electron. The product of the annihilation are two gamma-photons which travel in opposite directions; see Figure 2.4.

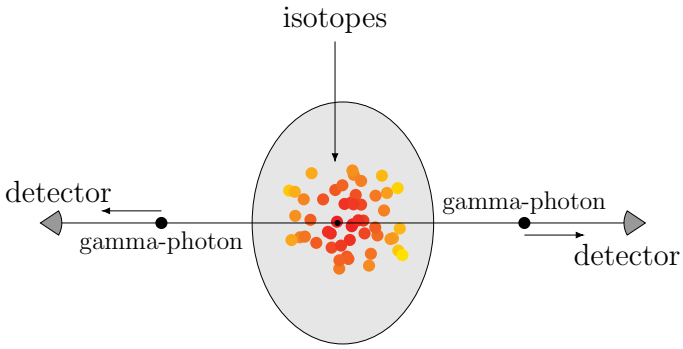

Figure 2.4 Measurements in PET

For each ray $\gamma \in T\mathbb{S}^2$, number of pairs of photons $N(\gamma)$ that have reached detectors along γ during a fixed period of time t constitutes the initial data (emission data) in PET.

On a mathematical level, the aforementioned photon counts $N(\gamma)$ are related to Radon-type transforms by the following formula:

$$N(\gamma) \sim \mathrm{Po}(CtP_{\omega_a} f(\gamma)),\ \gamma \in T\mathbb{S}^2, \tag{2.29}$$

where

$$\begin{aligned}
&\mathrm{Po}(\lambda) \text{ denotes the Poisson distribution with intensity } \lambda, \\
&C \text{ is a positive constant which depends on parameters of the setup,} && (2.30)\\
&t > 0 \text{ is the acquisition time per ray,} \\
&P_{\omega_a} \text{ is the weighted ray transform defined in (2.17) for } d = 3, && (2.31)\\
&f = f(x),\ x \in \mathbb{R}^3 \text{ is the density distribution of the isotope.} && (2.32)
\end{aligned}$$

Weight ω_a is given by the formula

$$\omega_a(x,\theta) = \exp\left(-Pa(x,\theta)\right),\ x \in \mathbb{R}^3,\ \theta \in \mathbb{S}^2, \tag{2.33}$$

where P is the classical ray transform defined in (2.17) for $W \equiv 1$, $a = a(x)$, $x \in \mathbb{R}^3$ is the attenuation map. In PET framework values for C, t and attenuation map $a = a(x)$, $x \in \mathbb{R}^3$ are assumed to be known *a priori*. In fact, attenuation map a is usually reconstructed using X-ray CT before the actual PET procedure. In addition, in the real PET procedure, photon

counts $N(\gamma)$ from (2.29) are often known only on a subset of $T\mathbb{S}^2$ which corresponds to slice-by-slice reconstruction framework[12] (see also the previous paragraph on X-ray CT).

From formulas (2.29)-(2.33) and their interpretations one may conclude the following:

1. The measured data $N(\gamma)$, $\gamma \in T\mathbb{S}^2$ are actually realizations of Poisson process with intensities proportional to $P_{\omega_a} f(\gamma), \gamma \in T\mathbb{S}^2$. From the point of view of Radon-type transforms, the data given by $P_{\omega_a} f$ corresponds to "ideal" denoised version of the real emission data. Indeed, from (2.29) and properties of Poisson distribution it follows that

$$\mathbb{E}N(\gamma) = CtP_{\omega_a} f(\gamma),\ \gamma \in T\mathbb{S}^2. \tag{2.34}$$

   Therefore, solving Problem 1 for PET, where $W = w_a$ defined in (2.33), corresponds to reconstruction of f from the "ideal" data given by $P_{\omega_a} f$.

2. From (2.33) it follows that $\omega_a(x, \theta)$ is constant for $x \in \gamma(x, \theta) \in T\mathbb{S}^2$ for fixed $\theta \in \mathbb{S}^2$. This makes the inversion of P_{ω_a} trivial. Indeed, from Definition 3 and formula (2.33) it follows that

$$P_{\omega_a} f(x, \theta) = \exp\left(-Pa(x, \theta)\right) Pf(x, \theta),\ (x, \theta) \in T\mathbb{S}^2, \tag{2.35}$$

   where P – is the classical ray transform in $\mathbb{R}^3$, a is the attenuation map. Then, the reconstruction of f from $P_{\omega_a} f$ and a can be implemented via the following formula:

$$f(x) = P^{-1}(\exp(Pa) P_{w_a} f)(x),\ x \in \mathbb{R}^3, \tag{2.36}$$

   where P^{-1} is the inversion of the classical ray transform.

From the above considerations one can see that Problem 1 for PET in 3D is easily solvable via formula (2.36). In addition, from (2.36) it follows that all techniques which are applicable for inversion of P can be applied in PET. On the other hand, analogously to X-ray CT, one of the major issues in PET is the stability of reconstructions. Indeed, from (2.29) it follows that Problem 1 for PET is much more ill-posed than the on for X-ray CT. In particular, it is seen already from (2.36), which informally can be interpreted as follows: ill-posedeness of inversion of P_{ω_a} is equal to the ill-posedeness of inversion of P times the exponential factor $\exp(-Pa)$, where $a \geq 0$ is the attenuation map. Therefore, strong attenuation increases the instability in reconstructions in PET; for more details see [Na86], [Ku14]. At the same time, in practice the emission data contains very strong Poisson noise which affects much stronger the stability of reconstructions than the ill-posedeness caused by attenuation. In presence of strong Poisson noise the statistical methods based on *maximum likelyhood approach* are used; see, for example, [Ka93], [V-Sl+15].

Despite the aforementioned issues, there is a very big progress in technological modalities of PET and by now it is a standard tool for diagnostics in medicine.

SPECT

Single-photon emission tomography (SPECT) also belongs to the domain of nuclear medicine and its main purposes are very similar to the ones of PET.

On a medical level, the main application of SPECT is the analysis of the bloodstream in the brain. Analogously to PET, in SPECT procedure a tracer integrated with an isotope is injected into the bloodstream and is diffused in the body. In fact, the tracer is chemically

[12]In fact, there exist PET scanners which produce the 4-dimensional emission data [To96]. This, in particular, is motivated by reduction of impact of strong noise in the measured data.

designed so that it concentrates mainly in the brain. Due to radioactive decay of the isotopes gamma-photons are emitted in different directions and being registered by detectors of the special SPECT scanner. Measuring this radiation for many different directions one can reconstruct the distribution of the tracer in the brain. The distribution can be used, for example, to detect areas in the brain with reduced blood flow or being injured.

On a physical level, the main difference between PET and SPECT is that in SPECT due to a nuclear decay of the isotope only one gamma-photon per reaction is emitted; see Figure 2.5.

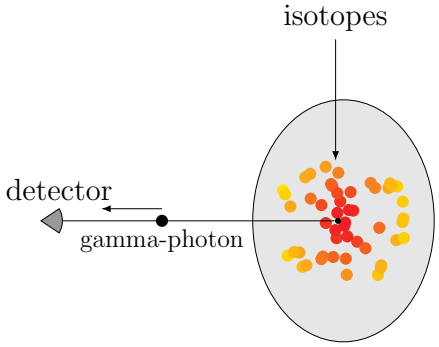

Figure 2.5 Measurements in SPECT

At the same time, the measured data are again given by photon counts $N(\gamma)$, $\gamma \in T\mathbb{S}^2$ and an analog of formula (2.29) holds. In particular, in SPECT the intensity of Poisson process in (2.29) is proportional to $P_{W_a} f$, where $f = f(x)$, $x \in \mathbb{R}^3$ is the density distribution of the tracer and weight W_a is given by the formulas:

$$W_a(x,\theta) = \exp(-Da(x,\theta)), \tag{2.37}$$

$$Da(x,\theta) = \int_0^{+\infty} a(x+t\theta)\,dt,\ x \in \mathbb{R}^3,\ \theta \in \mathbb{S}^2, \tag{2.38}$$

where $a = a(x)$, $x \in \mathbb{R}^3$ is the attenuation map.

Transform P_W for weight W_a of (2.37), (2.38) is also known as *the attenuated X-ray transform*. There is a long-story of studying this transform; see, for example, [TM80], [Ma84], [Fi86], [Sh93], [Na86], [Ar+98] and references therein. In particular, in the above publications the results were mainly on injectivity of P_{W_a} (local, and then global) and also on methods of inversions based on iterative schemes. Not a long time ago there was a big progress by Novikov, who derived exact analytic inversion formulas for $P_{W_a}^{-1}$; [No02]. The big difference of these formulas compared to the previous results and, in particular, to results from [Ar+98] is that Novikov's formulas had structure of Radon-type inversion formulas [Ra17]; see also discussion in [Fi03]. The new formulas were, in particular, very important for applications, because their structure allowed to implement the reconstructions in terms of the very efficient backprojection algorithm [Kun01].

In particular, the inversion of P_{W_a} could be given by the following formulas ([No02]):

$$f(x) = \frac{1}{4\pi} \int\limits_{\mathbb{S}^1} \theta^\perp \nabla_x (\exp[-Da(x,-\theta)] \tilde{g}_\theta(\theta^\perp x))\, d\theta, \tag{2.39}$$

$$\begin{aligned} \tilde{g}_\theta(s) = &\exp(A_\theta(s)) \cos(B_\theta(s)) H(\exp(A_\theta) \cos(B_\theta) g_\theta)(s) + \\ &\exp(A_\theta(s)) \sin(B_\theta(s)) H(\exp(A_\theta) \sin(B_\theta) g_\theta)(s), \end{aligned} \tag{2.40}$$

$$A_\theta(s) = \frac{1}{2} Pa(s\theta^\perp, \theta),\ B_\theta(s) = HA_\theta(s), g_\theta(s) = P_{W_a} f(s\theta^\perp, \theta), \tag{2.41}$$

$$Hu(s) = \frac{1}{\pi} p.v. \int\limits_{-\infty}^{+\infty} \frac{u(t)}{s-t}\, dt, \tag{2.42}$$

$$x \in \mathbb{R}^2, \theta^\perp = (-\theta_2, \theta_1) \text{ for } \theta = (\theta_1, \theta_2) \in \mathbb{S}^1,\ s \in \mathbb{R}.$$

An important property of (2.39)-(2.42) is that for non-attenuated case (i.e., $a = 0$), when P_{W_a} reduces to classical ray transform P, the formulas reduce to classical inversion formulas (2.26)-(2.28) for P^{-1}. In addition, a simpler form of (2.39)-(2.42) can be found, for example, in [Na01].

From the above discussion one can see that Problem 1 for SPECT is perfectly solvable. However, as it was for PET, exact inversion formulas were not yet a complete solution to the real problem. Though formulas (2.39)-(2.42) have been tested on synthetic and real emission data [Kun01], [Gu+02], it appeared that these formulas can be unstable against strong Poisson noise in emission data [GuNo12]. By now, the methods which are mostly used in SPECT are statistical ones; see, for example, [CrDeP07].

To conclude, there is still very active research on different modalities of SPECT; see also [BJ11], [Br00], [Ku14]. In particular, a lot of efforts are concentrated on development of stable methods of reconstructions also including new technological approaches [Ngu+09].

Inversions of weighted Radon-type transforms in tomographies

From previous paragraphs one could see that the reconstruction problems in tomographies were reduced either to Problem 1 or to Problem 2. Actually, the first step to resolve the latter ones is to see, if they are solvable in general.

On a mathematical level, this reduces to the question of injectivity and non-injectivity of P_W, R_W on certain functional spaces for weights W satisfying (2.14). In particular, in tomographies, like X-ray CT, PET and SPECT the question for injectivity of P_W, R_W is trivially resolved by the exact analytic inversion formulas – classical Radon inversion formulas (2.26)-(2.28) for X-ray CT and PET and Novikov's formulas (2.39)-(2.42) for SPECT.

For a general non-constant weight W, the situation with inversions of P_W, R_W is very different from the previous cases. First, it looks like there is no general analytic inversion formula for P_W, R_W, except of some particular cases when W has very specific symmetries [Ra17], [TM80], [No02], [Bo04], [Gi10], [No11], [GN16]. For some weights W satisfying (2.14) there are even counterexamples to injectivity for P_W, R_W for $d \geq 2$; see Subsection 4.2 for more details.

The first example of tomography where transforms P_W with non-trivial weights W are used is SPECT. Though in this case there exists an analytic inversion formula for P_W^{-1} for $d = 2$ (formulas (2.39)-(2.42)), it is not used yet in tomographical applications. More precisely, in case of noiseless data in SPECT (when $P_W f$ are known exactly) Novikov's formula gives perfect reconstructions in any models of attenuation [Kun01], [Na01]. But in case of strong Poisson noise in the emission data, it becomes numerically unstable and produces artifacts. There were already some attempts to apply regularization filters to

emission data [GuNo05], [GuNo08], [GuNo12], but the question of efficient stabilization of the formula is still open[13].

In our approach to the inverse problem in SPECT we decided to concentrate on approximate inversion methods which have better stability against the noise than exact analytic formulas. For slice-by-slice reconstructions such methods are Chang's approximate inversion formula [Ch78], [No11], and iterative inversion algorithm of Kunyansky [Ku92], [GuNo14].

Chang's formula. The Chang's approximate inversion formula (see [Ch78]) is defined by:

$$f_{appr}(x) \stackrel{\text{def}}{=} \frac{1}{4\pi w_0(x)} \int\limits_{\mathbb{S}^1} h'(x\theta^{\perp}, \theta)\, d\theta,\ x \in \mathbb{R}^2, \tag{2.43}$$

$$\begin{aligned} &h'(s,\theta) = \frac{d}{ds} h(s,\theta), \\ &h(s,\theta) = \frac{1}{\pi} p.v. \int\limits_{-\infty}^{+\infty} \frac{P_W f(t\theta^{\perp}, \theta)}{s-t}\, dt,\ s \in \mathbb{R},\ \theta \in \mathbb{S}^1,\ x \in \mathbb{R}^2, \end{aligned} \tag{2.44}$$

where $P_W f$ for $d = 2$ is defined in (2.17) and w_0 is defined by the formula

$$w_0(x) \stackrel{\text{def}}{=} \frac{1}{2\pi} \int\limits_{\mathbb{S}^1} W(x,\theta)\, d\theta,\ w_0(x) \neq 0 \text{ for all } x \in \mathbb{R}^2. \tag{2.45}$$

Note that formulas (2.43)-(2.44) are essentially Radon inversion formulas (2.26)-(2.28) applied to P_W with additional weighting factor w_0.

Though the proposed formula gives only approximate inversion of P_W, it appeared to be very effective in SPECT [Mu+87], and it was also used as a starting point for more complicated iterative schemes; see, for example, [Ku92].

Very naively, Chang's formula can be seen as a method for finding f approximately from $P_W f$, when $W \approx w_0$. Indeed, for $W(x,\theta) \equiv w_0(x)$ we have that

$$P_W f = P_{w_0} f = P(w_0 f) \Rightarrow f = \frac{P^{-1} P_W f}{w_0}, \tag{2.46}$$

where P^{-1} is the inverse of the classical Radon transform for $d = 2$. It was realized only not a long time ago in [No11], that effectiveness of Chang's formula is due to a weaker assumption on W than $W \approx w_0$.

Theorem 1 (Novikov, 2011)**.** *Let assumptions of* (2.14) *for* $d = 2$ *hold and let* W *be additionally continuous on* $\mathbb{R}^2 \times \mathbb{S}^1$*. Let* f_{appr} *be given by* (2.43)-(2.45)*. Then*

$$f_{appr} = f \textit{ (in the sense of distributions) on } \mathbb{R}^2 \textit{ for all } f \in C_c(\mathbb{R}^2) \tag{2.47}$$

if and only if

$$w_0(x) \equiv \frac{1}{2}(W(x,\theta) + W(x,-\theta)),\ x \in \mathbb{R}^2,\ \theta \in \mathbb{S}^1, \tag{2.48}$$

where $C_c(\mathbb{R}^2)$ *denotes the space of continuous compactly supported functions on* $\mathbb{R}^2$*.*

[13]Possibly, it will be resolved in future with more technological advances in construction of scanners. Nowadays, in measurements in SPECT almost all of the emitted photons are lost due to the collimation effect. A new possible approach to overcome this problem is the development of *Compton gamma-cameras*; see [Ngu+09] and references therein.

An easy way to understand Theorem 1 is to look at condition (2.48) in terms of expansions of W in spherical harmonics on $\mathbb{S}^1$. Let

$$W(x,\theta)=\sum_{k\in\mathbb{Z}} w_k(x)Y_k(\theta),\ x\in\mathbb{R}^2,\ \theta\in\mathbb{S}^1, \tag{2.49}$$

$$w_k(x)=\frac{1}{2\pi}\int\limits_{\mathbb{S}^1} W(x,\theta)Y_{-k}(\theta)\,d\theta,\ k\in\mathbb{Z}, \tag{2.50}$$

$$Y_k(\theta(\varphi))=(\theta_1(\varphi)+i\theta_2(\varphi))^k=e^{ik\varphi},\ \theta(\varphi)=(\cos\varphi,\sin\varphi)\in\mathbb{S}^1,\ \varphi\in[0,2\pi). \tag{2.51}$$

From (2.49)-(2.51) it is easy to see that condition (2.48) is equivalent to the following one

$$w_{2k}\equiv 0 \text{ on } \mathbb{R}^2,\ \text{for } k\in\mathbb{Z}\backslash\{0\}. \tag{2.52}$$

An important feature of (2.52) is that it contains no conditions on w_k for k odd. Therefore, for W such that it misses a lot of terms w_k in (2.49) for k even and has whatever terms w_k's for k odd, the formula of Chang will give almost perfect reconstructions! This explains the efficiency of formulas (2.43)-(2.45) in SPECT even though they are only approximate. At the same time, it is well-known that in case of strong attenuation in SPECT Chang's formula produces artifacts; see Figure 2.6. In this case more complicated reconstruction methods should be used, for example, a method of Kunyansky which we discuss in the next paragraph.

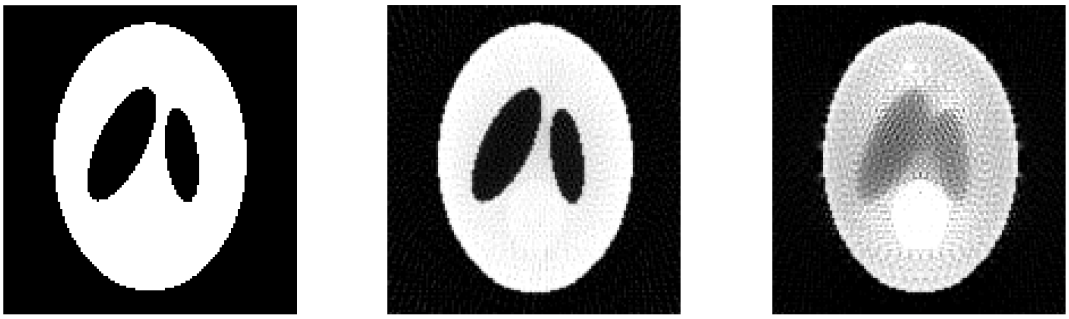

(a) test-function f (b) f_{appr}, weak attenuation (c) f_{appr}, strong attenuation

Figure 2.6 Reconstructions in SPECT using Chang's formula; for the attenuation map $a=a(x)$, $x\in\mathbb{R}^2$ (see formulas (2.37), (2.38)) we used 3D Shepp-Logan phantom [Ga+08]; weak and strong attenuation models in (b), (c) differed only in a constant multiplier for function $a=a(x)$, $x\in\mathbb{R}^2$.

Method of Kunyansky. An improvement of Chang's method is an iterative algorithm of Kunyansky [Ku92], [No14], [GuNo14][14]. The main idea of the method is to consider more even terms w_{2k} in expansion (2.49) than it was in Chang's formula. In this case, the inversion of R_W is not given by an analytic formula but as a solution of a certain integral equation.

We briefly explain the method following the notation from [GuNo14], because it will be similar to notations of our results from Article 2. In derivations below, at first, we do not bother with regularity assumptions or conditions on convergences of series but explain only the main concept. Then we present theorems that support our derivations. We also recall

[14]In particular, in [GuNo14], [No14] authors relax the assumptions on W under which the iterative algorithm from [Ku92] converges.

that for $d = 2$ transforms P_W, R_W are equivalent (see formula (2.23)) and we will use notations for R_W instead of P_W.

Let

$$D \text{ be a fixed open bounded domain in } \mathbb{R}^2, \tag{2.53}$$

$$f \in L^\infty(\mathbb{R}^2), \operatorname{supp} f \subset D. \tag{2.54}$$

Consider A_W defined by

$$A_W f \stackrel{\text{def}}{=} R^{-1} R_W f, \tag{2.55}$$

where R^{-1} is the inverse of the classical Radon transform for $d = 2$ (see formulas (2.26)-(2.28)). It was shown both in [Ku92] and [GuNo14] that

$$A_W f = R^{-1} R_{W_{sym}} f, \tag{2.56}$$

$$R_{W_{sym}} f(s,\theta) = \frac{1}{2}(R_W f(s,\theta) + R_W f(-s,-\theta)),\ (s,\theta) \in \mathbb{R} \times \mathbb{S}^1, \tag{2.57}$$

where W_{sym} is defined by the formula

$$W_{sym}(x,\theta) \stackrel{\text{def}}{=} \frac{1}{2}(W(x,\theta) + W(x,-\theta)),\ x \in \mathbb{R}^2,\ \theta \in \mathbb{S}^1. \tag{2.58}$$

Expanding W_{sym} of (2.58) in a series of spherical harmonics on $\mathbb{S}^1$ we have that

$$W_{sym}(x,\theta) = \sum_{l \in \mathbb{Z}} w_{2l}(x) Y_{2l}(\theta),\ x \in \mathbb{R}^2,\ \theta \in \mathbb{S}^1, \tag{2.59}$$

where w_{2k} are defined in (2.50), Y_{2k} are defined in (2.51).

Remark 1. Note that sufficiency in Theorem 1 follows directly from (2.48) and (2.55)-(2.59).

From (2.16), (2.59) it follows that

$$R_{W_{sym}} f(s,\theta) = R(w_0 f)(s,\theta) + \sum_{\mathbb{Z}\setminus\{0\}} Y_{2k}(\theta) R(w_{2k} f)(s,\theta),\ (s,\theta) \in \mathbb{R} \times \mathbb{S}^1. \tag{2.60}$$

Applying R^{-1} to both sides of (2.60) and using formula (2.56) we obtain the following identity

$$(I + Q_{W,D,\infty})(w_0 f) = R^{-1} R_W f, \tag{2.61}$$

where I is the identity operator, $Q_{W,D,\infty}$ is an integral operator defined by the formula

$$Q_{W,D,\infty} u \stackrel{\text{def}}{=} R^{-1}\left(\sum_{k \in \mathbb{Z}\setminus\{0\}} Y_{2k}(\theta) \int\limits_{x\theta = s} \frac{w_{2k}(x)}{w_0(x)} \chi_D(x) u(x)\, dx\right), \tag{2.62}$$

where $\chi_D = \chi_D(x)$ is the characteristic function of domain D.

The main idea of Kunyansky's method is to consider identity (2.61) as an integral equation on f, where $R^{-1} R_W f$ in the right hand-side is known. Then, if operator $I + Q_{W,D,\infty}$ from (2.61) is invertible, f can be found from $R_W f$ by the following formula:

$$f = (w_0)^{-1}(I + Q_{W,D,\infty})^{-1} R^{-1} R_W f. \tag{2.63}$$

Now, in order to give rigorous sense to formulas (2.58)-(2.63), one has to introduce functional spaces on which the aforementioned integral operators are well-defined. The following results are composed from [Ku92], [GuNo14].

Theorem 2 (Kunyansky 1992, Guillement-Novikov 2014)**.** *Let D, f be of* (2.53), (2.54), *$W \in C(\mathbb{R}^2 \times \mathbb{S}^1) \cap L^\infty(\mathbb{R}^2 \times \mathbb{S}^1)$, w_0, w_{2k}, $k \in \mathbb{Z}$ be defined by* (2.49)-(2.51) *and $w_0(x) \neq 0$ for all $x \in \mathbb{R}^2$. Assume also that*

$$\sum_{k \in \mathbb{Z} \setminus \{0\}} \left\| \frac{w_{2k}}{w_0} \right\|_{L^2(D)} < +\infty. \tag{2.64}$$

Then $R^{-1} R_W f \in L^2(\mathbb{R}^2)$. Moreover, if

$$\sigma_{W,D,\infty} \stackrel{\text{def}}{=} \sum_{k \in \mathbb{Z} \setminus \{0\}} \sup_{x \in D} \left| \frac{w_{2k}}{w_0} \right| < +\infty, \tag{2.65}$$

then operator $Q_{W,D,\infty}$ of (2.62) *is a linear bounded operator on $L^2(\mathbb{R}^2)$ and the following bound holds*

$$\|Q_{W,D,\infty}\|_{L^2(\mathbb{R}^2) \to L^2(\mathbb{R}^2)} \leq \sigma_{W,D,\infty}. \tag{2.66}$$

Moreover, operator $Q_{W,D,\infty}$ of (2.62) admits a simpler form.

Lemma 1 (Kunyansky 1992, Guillement-Novikov 2014)**.** *Assume that assumptions of Theorem 2 hold and, in addition, condition* (2.65) *is satisfied. Then, operator $Q_{W,D,\infty}$ of* (2.62) *can be rewritten in the following form:*

$$Q_{W,D,\infty} u = \sum_{k \in \mathbb{Z} \setminus \{0\}} d_{2k} * \frac{w_{2k}}{w_0} \chi_D u,\ u \in L^2(\mathbb{R}^2), \tag{2.67}$$

where $*$ – denotes the convolution in $\mathbb{R}^2$ and functions d_{2k} are defined by

$$d_{2k}(x(r,\varphi)) \stackrel{\text{def}}{=} (-1)^k \frac{|k|}{\pi} \frac{e^{2ki\varphi}}{r^2},\ x = (r\cos\varphi, r\sin\varphi),\ r > 0,\ \varphi \in [0, 2\pi). \tag{2.68}$$

In addition, for d_{2k} of (2.68) *the following property holds:*

$$F[d_{2k}](\xi(\rho,\psi)) = e^{2ki\psi},\ \xi = (\rho\cos\psi, \rho\sin\psi),\ \rho > 0,\ \psi \in [0, 2\pi), \tag{2.69}$$

where $F[\cdot]$ is the two-dimensional Fourier transform.

Theorem 2 and Lemma 1 are the core of the iterative method of Kunyansky. After having precised $Q_{W,D,\infty}$ as a linear continuous operator in $L^2(\mathbb{R}^2)$ one can investigate integral equation (2.61) for solvability.

(1) Assume that

$$\sigma_{W,D,\infty} < 1, \tag{2.70}$$

where $\sigma_{W,D,\infty}$ is defined in (2.65). Then, from (2.66) of Theorem 2 it follows that operator $I + Q_{W,D,\infty}$ is continuously invertible in $L^2(\mathbb{R}^2)$. Moreover, in this case operator $(I + Q_{W,D,\infty})^{-1}$ is given by Neumann series:

$$(I + Q_{W,D,\infty})^{-1} = \sum_{k=0}^{\infty} (-Q_{W,D,\infty})^k, \tag{2.71}$$

where $Q_{W,D}$ is given by (2.62) or by (2.67). Note that assumption (2.70) and formulas (2.63), (2.71) can be used to build the following iterative scheme:

$$\begin{cases} u^{(k+1)} = R^{-1} R_W f - Q_{W,D,\infty} u^{(k)},\ k \geq 1, \\ u^{(0)} = R^{-1} R_W f, \end{cases},\ u^{(k)} \xrightarrow{L^2(\mathbb{R}^2)} w_0 f. \tag{2.72}$$

Therefore, f can be well approximated by $w_0^{-1} u^{(N)}$ for N large enough. In practice, only a few iterations of scheme (2.72) are needed, because assumption (2.70) implies that convergence in (2.72) has geometric speed.

(2) Let assumption (2.70) be not satisfied. That is

$$\sigma_{W,D,\infty} \geq 1, \tag{2.73}$$

where $\sigma_{W,D,\infty}$ is defined in (2.65). Then, operator $I + Q_{W,D,\infty}$ is not necessarily continuously invertible, and even if it would be, it would not be possible to use Neumann series for $(I + Q_{W,D,\infty})^{-1}$ as in the previous case. However, an approximate inversion of R_W may be defined in the following manner.

Let W_m, $m \geq 0$ be a cutoff of W (see formula (2.49)) which is defined by the formula:

$$W_m(x,\theta) \stackrel{\text{def}}{=} \sum_{k=-2m}^{2m} w_k(x) Y_k(\theta),\ x \in \mathbb{R}^2,\ \theta \in \mathbb{S}^1. \tag{2.74}$$

Then, there are direct analogs of formulas (2.55)-(2.63), of Theorem 2 and of Lemma 1 for W_m in place of W. In particular, one can define an operator $Q_{W,D,m}$ on $L^2(\mathbb{R}^2)$ such that

$$Q_{W,D,m} u = \sum_{k=-m,\, k\neq 0}^{m} d_{2k} * \frac{w_{2k}}{w_0} \chi_D u,\ u \in L^2(\mathbb{R}^2), \tag{2.75}$$

$$\|Q_{W,D,m}\|_{L^2(\mathbb{R}^2)\to L^2(\mathbb{R}^2)} \leq \sigma_{W,D,m}, \tag{2.76}$$

where d_{2k} are the functions of (2.68), (2.69), w_{2k} are the functions of (2.50) and $\sigma_{W,D,m}$ is defined by

$$\sigma_{W,D,m} \stackrel{\text{def}}{=} \sum_{k=-m,\, k\neq 0}^{m} \sup_{x\in D} \left| \frac{w_{2k}}{w_0} \right|,\ \sigma_{W,D,0} = 0. \tag{2.77}$$

One calls f_m, $m \geq 0$ by *m-th approximation of* f ($f_m \approx f$), if it is a solution of the following integral equation:

$$(I + Q_{W,D,m})(w_0 f_m) = R^{-1} R_W f, \tag{2.78}$$

where operator $Q_{W,D,m}$ is defined in (2.75). Note that this equation is completely analogous to (2.61) and has the same right hand-side $R^{-1}R_W f$ which is assumed to be known.

The point of cutoff (2.74) is to choose $m \in \mathbb{N} \cup \{0\}$ to ensure the solvability of equation (2.78) by the method of successive approximations:

$$\begin{array}{l} \text{find largest } m \geq 0, \text{ such that} \\ \text{condition } \sigma_{W,D,m} < 1 \text{ is effectively fulfilled.} \end{array} \tag{2.79}$$

From (2.77) one can see that it is always possible find m such that (2.79) will be satisfied. In particular, for $m = 0$ operator $Q_{W,D,m}$ equals zero and equation (2.79) becomes trivial:

$$w_0 f_0 = R^{-1} R_W f \Rightarrow f_0 = \frac{R^{-1} R_W}{w_0}. \tag{2.80}$$

One can notice here that formula for f_0 in (2.80) is exactly the Chang's formula from (2.43)-(2.44). Choosing m such that condition (2.79) is fulfilled, one can again use the Neumann series for $(I + Q_{W,D,m})^{-1}$ to construct an iterative scheme for finding f_m:

$$\left\{ \begin{array}{l} u_m^{(k+1)} = R^{-1} R_W f - Q_{W,D,m} u_m^{(k)},\ k \geq 1, \\ u_m^{(0)} = R^{-1} R_W f, \end{array} \right. ,\ u_m^{(k)} \xrightarrow{L^2(\mathbb{R}^2)} w_0 f_m. \tag{2.81}$$

In this case approximation f_m can be given by $u_m^{(N)}/w_0$ for N large enough. As in the previous case, choice of m according to (2.79) implies that only a few iteration steps are needed.

The above considerations explain the iterative method by Kunyansky and, in particular, the method can be seen as a direct extension of original Chang's formula. From Figure 2.7 one can see that f_1 gives better approximation (c) to the original test-function (a) than the Chang's method (b).

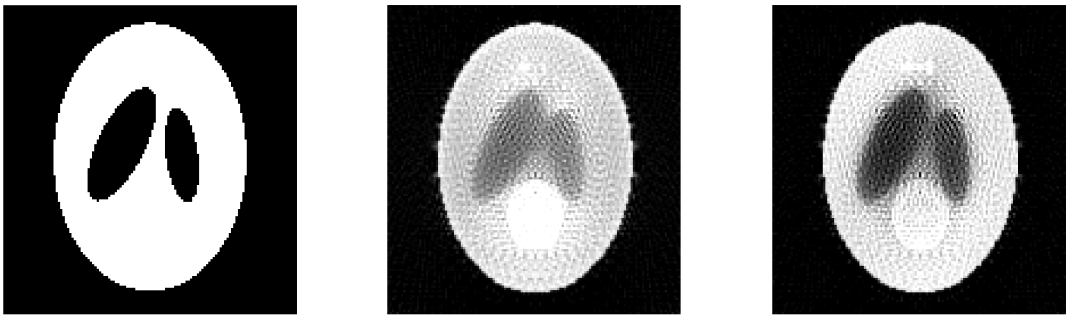

(a) test-function f (b) f_{appr}, Chang's method (c) f_1, method of Kunyansky

Figure 2.7 Reconstructions in SPECT using Chang's formula and Kunyansky method for $m = 1$; for the attenuation model $a = a(x)$, $x \in \mathbb{R}^2$ (see formulas (2.37), (2.38)) we used 3D Shepp-Logan phantom [Ga+08] with parameters for strong attenuation; see also Figure 2.6

Apart of Kunyansky's method for inversion of R_W for general weights W, there are other iterative methods, for example, the method of Beylkin [Be84]. In the method of Beylkin, reconstruction of f from W and $R_W f$ is also reduced to solving an integral equation on f. However, the integral equation in [Be84] is very different from (2.61). More precisely, in Beylkin's method the integral equation is of Fredholm type, whereas in (2.61) it is not because of singularities in kernels in expressions (2.67), (2.68) for operators $Q_{W,D,\infty}$, $Q_{W,D,m}$. The approach of constructing a Fredholm-type integral equation on f from W, $R_W f$ arises from the theory of elliptic pseudo-differential operators, and consists mainly in constructing *a parametrix* for an elliptic operator associated to R_W. Such approach[15] allows, for example, to perform "local" reconstructions from $R_W f$, that is reconstruct f having a sufficiently small support; see [Be84], [AG07].

An important feature of Kunyansky's method that it is quite robust against noise in measured data; see [GuNo14]. Also, note that Chang's formula and method of Kunyansky are applicable for any weights W satisfying (2.14) and corresponding regularity assumptions (2.64), (2.70), (2.79). These two features were important for us to introduce new inversion methods for different tomographies.

Resume of Article 1. In this article we consider Problem 1 for $d = 3$, where

transforms $P_W f$ are known for all rays
which are parallel to some fixed two-dimensional plane $\Sigma_\eta = \{x \in \mathbb{R}^3 : x\eta = 0\}$. (2.82)

[15]Constructing a parametrix for an elliptic pseudodifferential operator associated to R_W allows, for example, to reconstruct singularities of f from $R_W f$. Reconstruction of singularities of f from R_Wf is also known as *pseudo-local tomography* and by author's opinion it is the most beautiful example of applications of pseudo-differential calculus in imaging; see [Qu93], [Fa+01].

This setting corresponds to slice-by-slice reconstructions approach used in tomographies like X-ray CT, PET or SPECT; see Figure 2.8.

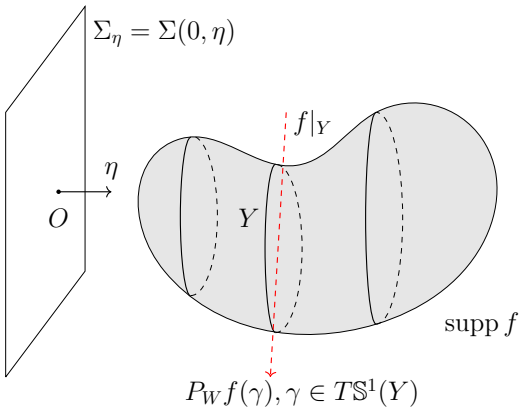

Figure 2.8 Slice-by-slice reconstructions

Instead of solving the inverse problem slice-by-slice, we propose another approach based on the following simple geometrical construction.

Let $\Sigma = \Sigma(s, \theta)$ be an arbitrary two-dimensional plane which is not parallel to Σ_η. Note that plane Σ can be "sliced" in a set of parallel rays which are parallel to Σ_η; see Figure 2.9.

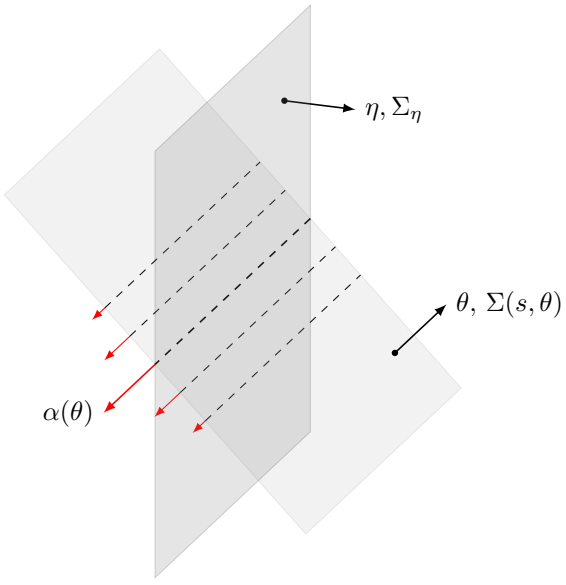

Figure 2.9

Moreover, direction $\alpha \in \mathbb{S}^2$ of rays which slice Σ is defined uniquely from $\eta, \theta \in \mathbb{S}^2$:

$$\alpha = \alpha(\theta) = \frac{[\eta, \theta]}{|[\eta, \theta]|} \in \mathbb{S}^2, \tag{2.83}$$

where $[\cdot, \cdot]$ denotes the standard vector product in $\mathbb{R}^3$. The point is that the following formulas hold:

$$\begin{aligned} &R_w f(s, \theta) = \int_{-\infty}^{+\infty} P_W f(s\theta + \tau[\theta, \alpha],\, \alpha)\, d\tau,\ (s, \theta) \in \mathbb{R} \times \mathbb{S}^2, \\ &w(x, \theta) = W(x, \alpha(\theta)),\ [\eta, \theta] \neq 0,\ x \in \mathbb{R}^3. \end{aligned} \tag{2.84}$$

where R_w is the standard weighted Radon transform for weight w along planes in $\mathbb{R}^3$, $\alpha(\theta)$ is given in (2.83).

Due to formulas of (2.84) the tomographical data modeled by $P_W f$ can be reduced to data modeled by $R_w f$. The intuition for such reduction is to reduce the impact of noise on reconstructions, for example, in emission tomographies. Indeed, in slice-by-slice reconstructions for each two-dimensional plane Y reduction $f|_Y$ is reconstructed from $P_W f|_{T\mathbb{S}^1(Y)}$ and the rest of the data is completely ignored (see Figure 2.8), whereas reduction of (2.84) contains a powerful integral which can be interpreted as a regularization of noise. As we will see further, by applying appropriate inversion methods to $R_w f$ one gets more stable reconstructions than by their analogs in slice-by-slice approach.

In view of the above discussion, we propose the following scheme for finding f from $P_W f$:

$$\begin{aligned} &\text{(i) Using (2.84) reduce the data given by weight } W \text{ and } P_W f \text{ on rays which are} \\ &\quad \text{parallel to } \Sigma_\eta \text{ to } w \text{ and } R_w f \text{ on all planes, except planes parallel to } \Sigma_\eta. \\ &\text{(ii) Apply an inversion method for } R_w \text{ for } d = 3 \text{ to find } f \text{ from } R_w f. \end{aligned} \tag{2.85}$$

Remark 2. Interestingly, formulas of (2.84) for $W \equiv 1$ are trivial and can be seen as a particular case of Fubini's Theorem: an integral $Rf(s,\theta)$ over a plane $\Sigma(s,\theta)$ can be seen as an integral of ray integrals $Pf(\cdot, \alpha(\theta))$ along rays which "slice" this plane. Nevertheless, for non-constant weights they were no such formulas until our result of Article 1.

After having introduced a method to reduce Problem 1 to Problem 2 for $d = 3$, it is necessary to have a method for solving Problem 2. As we were motivated by tomographical applications, we were also interested in approximate but efficient methods. A straightforward method to propose is an analog of Chang's approximate inversion formulas for $d \geq 3$.

In view of (2.43)-(2.45), we define the following approximate inversion formulas for R_W for $d \geq 2$:

$$f_{appr}(x) = \begin{cases} \dfrac{(-1)^{(d-2)/2}}{2(2\pi)^{d-1} w_0(x)} \displaystyle\int_{\mathbb{S}^{d-1}} \mathbb{H}\left[R_W f\right]^{(d-1)}(x\theta, \theta)\, d\theta, \ d \text{ is even}, \\ \dfrac{(-1)^{(d-1)/2}}{2(2\pi)^{d-1} w_0(x)} \displaystyle\int_{\mathbb{S}^{d-1}} \left[R_W f\right]^{(d-1)}(x\theta, \theta)\, d\theta, \ d \text{ is odd}, \end{cases} \tag{2.86}$$

where

$$w_0(x) \stackrel{\text{def}}{=} \frac{1}{\text{Vol}(\mathbb{S}^{d-1})} \int_{\mathbb{S}^{d-1}} W(x,\theta)\, d\theta, \ w_0(x) \neq 0, \ x \in \mathbb{R}^d, \tag{2.87}$$

$$\begin{aligned} &\left[R_W f\right]^{(d-1)}(s,\theta) = \left(\frac{d}{ds}\right)^{(d-1)} R_W f(s,\theta), \\ &\mathbb{H}g(s) \stackrel{\text{def}}{=} \frac{1}{\pi} p.v. \int_{\mathbb{R}} \frac{g(t)}{s-t} dt, \ s \in \mathbb{R}, \ \theta \in \mathbb{S}^{d-1}. \end{aligned} \tag{2.88}$$

In addition, we assume that formulas (2.86)-(2.88) are defined only for W satisfying (2.14).

Remark 3. In generic notation for weighted Radon transforms and their inversions, formula (2.86) has the following form:

$$f_{appr}(x) = \frac{R^{-1} R_W f(x)}{w_0(x)}, \ x \in \mathbb{R}^d, \tag{2.89}$$

where R^{-1} is the inverse of the classical Radon transform, $w_0(x)$, $x \in \mathbb{R}^d$ is defined in (2.87). From (2.46), (2.89) it is clear that formulas (2.86)-(2.88) are direct extensions Chang's formula to $d \geq 3$.

In addition, we extended Theorem 1 to higher dimensions $d \geq 3$, and in combination with it we had obtained the following result

Theorem 3. *Let W satisfy* (2.14) *and be also continuous on $\mathbb{R}^d \times \mathbb{S}^{d-1}$, $d \geq 2$. Let f_{appr} be defined by* (2.86)-(2.88) *in terms of $R_W f$ and w_0. Then*

$$f_{appr} = f \text{ (in the sense of distributions) on } \mathbb{R}^d \text{ for all } f \in C_c(\mathbb{R}^d) \tag{2.90}$$

if and only if

$$w_0(x) \equiv \frac{1}{2}\left(W(x,\theta) + W(x,-\theta)\right),\ x \in \mathbb{R}^d,\ \theta \in \mathbb{S}^{d-1}, \tag{2.91}$$

where $C_c(\mathbb{R}^d)$ denotes the space of continuous compactly supported functions on $\mathbb{R}^d$.

Remark 4. Note that weight w arising in (2.84) is not continuous, in general. The discontinuity of w is related to non-uniqueness of "slicing" for planes parallel to Σ_η. On the other hand, the set of discontinuity of w is of measure zero in $\mathbb{R} \times \mathbb{S}^2$ which makes Theorem 3 still applicable for w from (2.84).

The result of Theorem 3 supports the intuition that analogs (2.86)-(2.88) of Chang's formula from (2.43), (2.44) could be efficient for tomographical applications. This intuition was also supported by our numerical experiments which are presented further.

Finally, from the mathematical point of view Theorem 3 could be also interesting as an extension of Theorem 1 to odd dimensions, since it is known that inversions of Radon transforms are very different for even and odd dimensions; see [Na86].

The details of construction of (2.84) and proof of Theorem 3 are presented in Chapter 3.

Though with Chang's approximate inversion formulas for $d \geq 3$ one could test the proposed new inversion method for P_W, these formulas were still too simple and heuristic to conclude our studies. Next, in Article 2 we develop further our new inversion method by extending the Kunyansky's algorithm to $d \geq 3$.

Resume of Article 2. In this article we continue to develop the results of Article 1 and of articles [Ku92], [No14], [GuNo14]. In particular, we propose an extension of the iterative algorithm of Kunyansky from $d = 2$ to $d \geq 3$. For dimension $d = 3$ our extension is of importance for tomographical applications in view of the new reconstruction method from Article 1.

We consider Problem 2 and we assume that

$$W \in C(\mathbb{R}^3 \times \mathbb{S}^2) \cap L^\infty(\mathbb{R}^3 \times \mathbb{S}^2), \tag{2.92}$$

$$w_{0,0}(x) \stackrel{\text{def}}{=} \frac{1}{4\pi} \int\limits_{\mathbb{S}^2} W(x,\theta)\, d\theta,\ w_{0,0}(x) \neq 0,\ x \in \mathbb{R}^3, \tag{2.93}$$

$$f \in L^\infty(\mathbb{R}^3),\ \operatorname{supp} f \subset D, \tag{2.94}$$

where W, f are complex-valued, $d\theta$ is an element of uniform measure on $\mathbb{S}^2$, D is an open bounded domain (which is fixed *a priori*).

In a similar way as [Ku92], [GuNo14], we reduce the problem of inversion of R_W for $d = 3$, to solving a certain linear integral equation. In particular, we show that if the even part

of W in θ (i.e., $\frac{1}{2}(W(x,\theta)+W(x,-\theta))$) is close to $w_{0,0}$, then the integral equation can be solved by the method of successive approximations. On the other hand, if the aforementioned approximation does not hold, we define a series of approximations $f_m \approx f$, $m \in \mathbb{N}\cup\{0\}$, where m is chosen depending on W. This corresponds to (2.70), (2.73) for the original two-dimensional algorithm of Kunyansky.

Below we explain the extension of Kunyansky's algorithm to $d=3$. Details of our extensions to $d>3$ can be found in Chapter 4.

In a similar way with two-dimensional developments (2.56)-(2.81), we consider the following expansions:

$$W(x,\theta(\gamma,\varphi)) = \sum_{k=0}^{\infty}\sum_{n=-k}^{k} w_{k,n}(x)Y_k^n(\gamma,\varphi), \tag{2.95}$$

$$W_m(x,\theta(\gamma,\varphi)) \stackrel{\text{def}}{=} \sum_{k=0}^{m}\sum_{n=-k}^{k} w_{2k,n}(x)Y_{2k}^n(\gamma,\varphi),\ x\in\mathbb{R}^3,\ m\in\mathbb{N}\cup\{0\}, \tag{2.96}$$

$$Y_k^n(\gamma,\varphi) \stackrel{\text{def}}{=} p_k^{|n|}(\cos(\gamma))e^{in\varphi},\ k\in\mathbb{N}\cup\{0\},\ n=-k,\dots k, \tag{2.97}$$

$$\theta(\gamma,\varphi) = (\sin\gamma\cos\phi, \sin\gamma\sin\varphi, \cos\gamma)\in\mathbb{S}^2,\ \gamma\in[0,\pi],\ \varphi\in[0,2\pi], \tag{2.98}$$

where $p_k^n(x)$, $x\in[-1,1]$, are associated semi-normalized Legendre polynomials (see [SW16]). In particular, functions Y_k^n of (2.97) constitute the basis of spherical harmonics in $L^2(\mathbb{S}^2)$ with parametrization of (2.98). Coefficients $w_{k,n}$ of (2.95) are given by the formulas:

$$\begin{aligned} w_{k,n} &= c(k,n)\int_0^{2\pi} e^{-in\varphi}\,d\varphi\int_0^{\pi} W(x,\theta(\gamma,\phi))p_k^{|n|}(\cos\gamma)\sin\gamma\,d\gamma,\\ c(k,n) &= \frac{2k+1}{8\pi},\ k\in\mathbb{N}\cup\{0\},\ n=-k,\dots k. \end{aligned} \tag{2.99}$$

In view of the two-dimensional developments (2.55)-(2.81) we define the following objects:

$$Q_{W,D,\infty}u(x) \stackrel{\text{def}}{=} R^{-1}(R_{W,D,\infty}u)(x),\ x\in\mathbb{R}^3, \tag{2.100}$$

$$Q_{W,D,m}u(x) \stackrel{\text{def}}{=} R^{-1}(R_{W,D,m}u)(x),\ m\in\mathbb{N},\ Q_{W,D,m}u(x)=0 \text{ for } m=0, \tag{2.101}$$

$$\sigma_{W,D,\infty} \stackrel{\text{def}}{=} \sum_{k=1}^{\infty}\sum_{n=-2k}^{2k}\sup_{x\in D}\left|\frac{w_{2k,n}(x)}{w_{0,0}(x)}\right|, \tag{2.102}$$

$$\sigma_{W,D,m} \stackrel{\text{def}}{=} \sum_{k=1}^{m}\sum_{n=-2k}^{2k}\sup_{x\in D}\left|\frac{w_{2k,n}(x)}{w_{0,0}(x)}\right|,\ \text{for } m\in\mathbb{N}, \tag{2.103}$$

where R^{-1} is the classical inversion of Radon transforms for $d=3$ (see [Ra17], [Na86]), coefficients $w_{0,0}, w_{2k,n}$ are defined in (2.93), (2.99) and

$$R_{W,D,\infty}u(s,\theta(\gamma,\varphi)) \stackrel{\text{def}}{=} \sum_{k=1}^{\infty}\sum_{n=-2k}^{2k} Y_{2k}^n(\gamma,\varphi)R(\chi_D u)(s,\theta(\gamma,\varphi)), \tag{2.104}$$

$$R_{W,D,m}u(s,\theta(\gamma,\varphi)) \stackrel{\text{def}}{=} \sum_{k=1}^{m}\sum_{n=-2k}^{2k} Y_{2k}^n(\gamma,\varphi)R(\chi_D u)(s,\theta(\gamma,\varphi)), \tag{2.105}$$

$$x\in\mathbb{R}^3,\ s\in\mathbb{R},\ \theta(\gamma,\varphi)\in\mathbb{S}^2,$$

where Y_k^n are defined in (2.97), R is the classical Radon transform for $d = 3$, $\chi_D = \chi_D(x)$ is the characteristic function of domain D of (2.94), u is a test-function on $\mathbb{R}^3$.

Note that formulas (2.100)-(2.105) are direct analogs of (2.62), (2.65), (2.75), (2.77) of Kunyansky's method for $d = 2$. The only difference is that the expansions of W, W_m, new operators $Q_{W,D,\infty}$, $Q_{W,D,m}$ and of coefficients $w_{2k,n}$ are rewritten in terms of spherical harmonics Y_k^n on $\mathbb{S}^2$. Note also that in formulas (2.100)-(2.105) among terms $w_{k,n}$, Y_k^n only ones with even indices k are present. This is analogous to (2.55), (2.56) and, in particular, because $R^{-1}R_W f = R^{-1}R_{W_{sym}} f$, where W_{sym} is the even part of W in θ (i.e., $W_{sym}(x,\theta) = \frac{1}{2}(W(x,\theta) + W(x,-\theta))$).

Next, we show that $Q_{W,D,\infty}$, $Q_{W,D,m}$ are linear bounded operators in $L^2(\mathbb{R}^2)$.

Lemma 2. *Let operators $Q_{W,D,\infty}$, $Q_{W,D,m}$ be defined by* (2.100), (2.101), *respectively, and u be a test function on $\mathbb{R}^3$. Then*

$$Q_{W,D,\infty}u = \sum_{k=1}^{\infty}\sum_{n=-2k}^{2k} d_{2k,n} * \frac{w_{2k,n}}{w_{0,0}}\chi_D u, \tag{2.106}$$

$$Q_{W,D,m}u = \sum_{k=1}^{m}\sum_{n=-2k}^{2k} d_{2k,n} * \frac{w_{2k,n}}{w_{0,0}}\chi_D u, \tag{2.107}$$

where coefficients $w_{k,n}$ are defined in (2.99), *$*$ denotes the convolution in $\mathbb{R}^3$, $d_{2k,n}$ are defined by the formula:*

$$d_{2k,n}(x(r,\gamma,\varphi)) = (-1)^k \frac{2^{1/2}\Gamma(\frac{3}{2}+k)}{\pi\Gamma(k)}\frac{Y_{2k}^n(\gamma,\varphi)}{r^3},\ r > 0, \tag{2.108}$$

where $\Gamma(\cdot)$ is a Gamma-function, $x(r,\gamma,\varphi)$ is defined by the formula

$$x(r,\gamma,\phi) = (r\sin\gamma\cos\varphi, r\sin\gamma\sin\varphi, r\cos\gamma) \in \mathbb{R}^3,\ \gamma \in [0,\pi],\ \varphi \in [0,2\pi],\ r \geq 0. \tag{2.109}$$

In addition, for $d_{2k,n}$ of (2.108) *the following property holds:*

$$F[d_{2k,n}](\xi) = Y_{2k,n}\left(\frac{\xi}{|\xi|}\right),\ \xi \in \mathbb{R}^3\backslash\{0\}, \tag{2.110}$$

where $F[\cdot]$ is the Fourier transform in $\mathbb{R}^3$.

Lemma 3. *Operators $Q_{W,D,\infty}$, $Q_{W,D,m}$ defined in* (2.106), (2.107), *are linear bounded operators in $L^2(\mathbb{R}^2)$ and the following estimates hold:*

$$\|Q_{W,D,\infty}\|_{L^2(\mathbb{R}^2)\to L^2(\mathbb{R}^2)} \leq \sigma_{W,D,\infty}, \tag{2.111}$$

$$\|Q_{W,D,m}\|_{L^2(\mathbb{R}^2)\to L^2(\mathbb{R}^2)} \leq \sigma_{W,D,m},\ m \in \mathbb{N}\cup\{0\}, \tag{2.112}$$

where $\sigma_{W,D,\infty}$, $\sigma_{W,D,m}$ are defined in (2.102), (2.103).

In a similar way with the original Kunyansky's method, we reduce the inversion problem for R_W to solving a linear integral equation. In particular, this equation is obtained by applying R^{-1} to $R_W f$ and by expressing operator $R^{-1}R_W$ in terms of $Q_{W,D,\infty}$.

Lemma 4. *Let*

$$\sum_{k=1}^{\infty}\sum_{n=-2k}^{2k}\left|\left|\frac{w_{2k,n}}{w_{0,0}}\right|\right|_{L^2(D)} < +\infty, \tag{2.113}$$

where $w_{k,n}$ are defined in (2.99). *Then*

$$R^{-1}R_W f \in L^2(\mathbb{R}^3). \tag{2.114}$$

In addition, the following formula holds:

$$R^{-1}R_W f = w_{0,0}f + \sum_{k=1}^{\infty}\sum_{n=-2k}^{2k} d_{2k,n} * w_{2k,n}f = (I + Q_{W,D,\infty})(w_{0,0}f), \tag{2.115}$$

where f satisfies (2.94), *R^{-1} is the inversion of the classical Radon transform and $Q_{W,D,\infty}$ is given by* (2.100).

In view of the aforementioned method of Kunyansky and of results of Lemmas 2-4 we propose the following method of reconstruction of f from $R_W f$:

(1) Let

$$\sigma_{W,D,\infty} < 1. \tag{2.116}$$

Inequality (2.116) and estimate (2.111) imply that $I+Q_{W,D,\infty}$ is continuously invertible and the following identity holds (in the sense of operator norm in $L^2(\mathbb{R}^3)$):

$$(I + Q_{W,D,\infty})^{-1} = \sum_{j=0}^{\infty}(-Q_{W,D,\infty})^j. \tag{2.117}$$

Theorem 4. *Let conditions* (2.92)-(2.94), (2.116) *be fulfilled. Then R_W is injective and the following exact inversion formula holds:*

$$f = w_{0,0}^{-1}(I + Q_{W,D,\infty})^{-1}R^{-1}R_W f. \tag{2.118}$$

where $w_{0,0}$ is defined in (2.93), *R^{-1} is the inversion of the classical Radon transform, operator $(I + Q_{W,D,\infty})^{-1}$ is given in* (2.117).

Formula (2.118) can be seen as an integral equation for $w_{0,0}f$ and under assumption (2.116) it can be solved by the method of successive approximations:

$$\begin{cases} u^{(k+1)} = R^{-1}R_W f - Q_{W,D,\infty}u^{(k)},\ k \geq 1, \\ u^{(0)} = R^{-1}R_W f, \end{cases}, \ u^{(k)} \xrightarrow{L^2(\mathbb{R}^2)} w_{0,0}f. \tag{2.119}$$

Choosing N big enough in (2.119) one finds f as $u^{(N)}/w_{0,0}$. In practice, only a few iterations of the aforementioned scheme are needed, because under assumption (2.116) $u^{(k)}$ converges to $w_{0,0}f$ with geometric speed.

In practice, assumption (2.116) is not always fulfilled [GuNo14], so we propose a series of approximate inversions $f_m \approx f$, $m \in \mathbb{N} \cup \{0\}$.

(2) Let

$$\begin{aligned} &\sigma_{W,D,m} < 1, \text{ for some } m \in \mathbb{N} \cup \{0\}, \\ &\sigma_{W,D,\infty} < +\infty, \end{aligned} \tag{2.120}$$

where $\sigma_{W,D,m}, \sigma_{W,D,\infty}$ are defined in (2.102), (2.103), respectively.

Assumption of (2.120) and upper bound (2.112) in Lemma 3 imply that $I + Q_{W,D,m}$ is continuously invertible and the following identity holds (in the sense of the operator norm in $L^2(\mathbb{R}^3)$):

$$(I + Q_{W,D,m})^{-1} = \sum_{j=0}^{\infty}(-Q_{W,D,m})^j, \tag{2.121}$$

where I is the identity operator in $L^2(\mathbb{R}^3)$.

Theorem 5. *Let conditions* (2.92)-(2.94), (2.120) *be fulfilled. Then*

$$f \approx f_m \stackrel{\text{def}}{=} (w_{0,0})^{-1}(I + Q_{W,D,m})^{-1}R^{-1}R_W f, \tag{2.122}$$

$$f = f_m - (w_{0,0})^{-1}(I + Q_{W,D,m})^{-1}R^{-1}R_{\delta W_m} f, \tag{2.123}$$

$$\|f - f_m\|_{L^2(D)} \leq \frac{\|f\|_\infty}{c(1 - \sigma_{W,D,m})} \sum_{k=m+1}^{\infty} \sum_{n=-2k}^{2k} \|w_{2k,n}\|_{L^2(D)} < +\infty, \tag{2.124}$$

where

$$c = \min_{x \in D} |w_{0,0}(x)|,\ c > 0, \tag{2.125}$$

$$\delta W_m(x, \theta(\gamma, \varphi)) \stackrel{\text{def}}{=} W(x, \theta(\gamma, \varphi)) - \sum_{k=0}^{2m+1} \sum_{n=-k}^{k} w_{k,n}(x) Y_k^n(\gamma, \varphi), \tag{2.126}$$

$$x \in \mathbb{R}^3,\ \gamma \in [0, \pi],\ \varphi \in [0, 2\pi],\ m \in \mathbb{N} \cup \{0\}, \tag{2.127}$$

$w_{0,0}$ *is defined in* (2.93), $\theta(\gamma, \phi)$ *is defined in* (2.98), Y_k^n *are defined in* (2.97), *operator* $(I + Q_{W,D,m})^{-1}$ *is defined in* (2.121).

Remark 5. Formula (2.122) can be considered as the following linear integral equation on $w_{0,0} f_m$:

$$w_{0,0} f_m + Q_{W,D,m}(w_{0,0} f_m) = R^{-1} R_W f. \tag{2.128}$$

Inequalities of (2.120) and identity (2.121) imply that equation (2.128) is solvable by the method of successive approximations:

$$\begin{cases} u_m^{(k+1)} = R^{-1}R_W f - Q_{W,D,m} u_m^{(k)},\ k \geq 1, \\ u_m^{(0)} = R^{-1}R_W f, \end{cases},\ u_m^{(k)} \xrightarrow{L^2(\mathbb{R}^2)} w_{0,0} f. \tag{2.129}$$

In fact, condition $\sigma_{W,D,\infty} < +\infty$ can be relaxed to the following one:

$$\sum_{k=1}^{\infty} \sum_{n=-2k}^{2k} \left\| \frac{w_{2k,n}}{w_{0,0}} \right\|_{L^2(D)} < +\infty, \tag{2.130}$$

where $w_{k,n}$ are defined in (2.99).

Formula (2.122) is an extension of two-dimensional Chang's type formula from [Ch78], [No11], [GuNo14] and also an extension of Chang-type formula from Article 1, where this formula was given for $m = 0$.

Because $m \geq 0$ can be chosen, such that inequality is satisfied (2.120), we propose the following approximate reconstruction of f from R_W:

$$\begin{aligned} &(i) \quad \text{find maximal } m \text{ such that (2.120) is still efficiently fulfilled,} \\ &(ii) \quad \text{approximately reconstruct } f \text{ by } f_m \text{ using (2.122).} \end{aligned} \tag{2.131}$$

Remark 6. For practical applications it is obvious that it is never possible to consider an infinite number of summands in (2.106), even if inequality (2.116) is satisfied. Therefore, approach of (2.131) is used always. Numerical implementation of method of (2.131) is straightforward by formulas (2.95)-(2.98), (2.103), (2.120)-(2.122). In addition, implementation of operators $Q_{W,D,m}$ are very simple due formulas (2.106), (2.107) and property (2.110)

of $d_{2k,n}$. In view of these formulas, the operators $Q_{W,D,\infty}$, $Q_{W,D,m}$ can be rewritten in the following form:

$$\begin{aligned} Q_{W,D,\infty}u &= \mathcal{F}_{\xi}^{-1}\left(\sum_{k=1}^{\infty}\sum_{n=-2k}^{2k} Y_{2k}^{n}\left(\frac{\xi}{|\xi|}\right)\mathcal{F}_x\left(\frac{w_{2k,n}}{w_{0,0}}\chi_D u\right)(\xi)\right), \\ Q_{W,D,m}u &= \mathcal{F}_{\xi}^{-1}\left(\sum_{k=1}^{m}\sum_{n=-2k}^{2k} Y_{2k}^{n}\left(\frac{\xi}{|\xi|}\right)\mathcal{F}_x\left(\frac{w_{2k,n}}{w_{0,0}}\chi_D u\right)(\xi)\right), \end{aligned} \tag{2.132}$$

where $u \in L^2(\mathbb{R}^3)$, $\mathcal{F}_{\xi}^{-1}$, $\mathcal{F}_x$ are the inverse and direct Fourier transforms in variables ξ, $x \in \mathbb{R}^3$, respectively. Formulas of (2.132) are much easier to implement numerically than (2.106), (2.106), because the first ones are only the compositions of Fourier transforms and pointwise multiplications by spherical harmonics Y_{2k}^n. The details of our implementations and comments can be found in the next paragraph.

To conclude the exposition of results of Article 2, we also mention that formulas and methods of (2.92)-(2.132) admit straightforward extensions to $d > 3$. The details of such extensions are given in Chapter 4.

Next, we test numerically the Chang-type formula in three dimensions and also the Kunyansky-type method of (2.131).

Numerical experiment

Here we present numerical tests of our inversion methods from Articles 1, 2. All our tests were performed in the framework of SPECT in 3D, where the data were modeled by $P_W f$ in the framework of slice-by-slice reconstructions. More precisely, our numerical experiment consisted of the following steps:

1. For given attenuation model $a = a(x)$ and distribution phantom $f = f(x)$, $x \in \mathbb{R}^3$, simulate ray data $P_{W_a} f(\gamma)$, $\gamma \in \Gamma$, where W_a is given by (2.37), (2.38), Γ is a discrete grid in $T\mathbb{S}^2$ which corresponds to acquisitions in slice-by-slice reconstructions.

2. Using developments from Article 1 (formulas (2.83)-(2.84)), reduce the emission data $P_{W_a}(\gamma)$, $\gamma \in \Gamma$ to the data given by $R_W f(s,\theta)$, $(s,\theta) \in \Pi$, where Π is discrete grid in $\mathbb{R} \times \mathbb{S}^2$, weight W is constructed from W_a using formulas of (2.84).

3. Apply our inversion methods from Articles 1, 2 (i.e., analogs of Chang's formula and of the iterative algorithm of Kunyansky for $d = 3$) to reconstruct f from $R_W f(s,\theta)$, $(s,\theta) \in \Pi$.

For the experiment on synthetic data, our choice for attenuation models, nucleotide distributions and grids Γ, Π is described below in detail. The purpose of the experiment on synthetic data is to show that, indeed, the reduction from Article 1 brings more stability to reconstructions, independently of which method was used – either Chang-type formula or more advanced Kunyansky-type iterative method.

Together with experiments on synthetic data, we also applied our inversion methods on real data obtained from the *Service Hospitalier Frédéric Joliot, CEA (Orsay).* More precisely, the real-experiment was performed on a monkey who was subjected to a standard SPECT procedure. The details of this experiment are described further in the text. In the experiment on real data, because the real distribution of the nucleotide was not known, it was not possible measure quantitatively the quality of reconstructions. The goal of this experiment was to demonstrate that our method is applicable, in principle, in realistic SPECT procedures.

The contents of this subsection are organized as follows. First, we describe the experiment on synthetic data. We describe the models for attenuation maps, nucleotide distributions and the process of simulation of emission data (geometry of acquisitions of $P_{W_a} f$, modelization of noise). Then, we present reconstructions of the nucleotide distributions using Chang-type formula and the Kunyansky-type iterative method in 3D. We compare visually and numerically the quality of our reconstructions against two-dimensional methods based on Chang inversion formula and Kunyansky iterative algorithm. Second, we present the results of reconstructions for the real experiment on the monkey. In this case we present only images of reconstructions for our three-dimensional method based on Chang-type formula. Finally, we comment our implementations and provide a link to them.

Attenuation phantoms

In our experiments for the attenuation model we used the extension of the famous of Shepp-Logan phantom to 3D ([Ga+08], [SL74]); see Figure 2.10. This phantom imitates the human head and is standard for testing reconstruction algorithms for tomographies.

(a) $i_z = 40$ (b) $i_z = 64$ (c) $i_z = 80$

Figure 2.10 Attenuation maps: Cross-sections of the Shepp-Logan phantom by planes $z = const$

The model consists of one large ellipsoid which represents the brain and of several smaller ellipsoids which represent its features. The outer ellipsoidal layer with axes of length 13.8cm, 18cm, and 18.4cm corresponds to bone of the cranium; the standard attenuation of the bone material is equal to 0.17cm^{-1}. The attenuation within smaller inner ellipsoid representing the brain material and is equal to 0.15cm^{-1}. Smaller spheres (dark gray spheres on Figure 2.10) represent inclusions in the brain and have attenuation of 0.10cm^{-1}. The model also includes cavities which are given by two ellipsoidal regions near the center of the phantom (see the ellipsoids in black color, Figure 2.10 (b), (c)). In these regions the attenuation was set to zero.

The quantitative feature which describes the strength of the attenuation is the optical length of attenuation along some selected paths (the optical length along a path is an integral of the attenuation coefficient along this path). In the given model the optical lengths along X, Y, Z axis are equal to 2.44, 3.89 and 4.81, respectively. From practical point of view, such values correspond to strong attenuation.

To investigate the efficiency of our reconstructions methods for different attenuation regimes we used two models. The first one, which is referred by a_1 or *"strong attenuation"*, is the Shepp-Logan phantom with parameters described above. The second model, which is referred by a_2 or *"weak attenuation"*, corresponds to the same phantom as the first one but the attenuation values were multiplied by a factor of 1/10 (i.e., $a_2 = 10^{-1} a_1$). Hence, the optical lengths along X, Y, Z axis for the second attenuation model a_2 are equal to 0.244,

0.389 and 0.481, respectively. From the practical point of view, this corresponds to the case of very weak attenuation.

Before to proceed, we note that all our images in this subsection will be presented in a linear grayscale, where darker colors correspond to smaller values (black color corresponds to zero).

Phantoms for nucleotide distributions

We used two models for nucleotide distributions. The first one, further denoted by f_1 or *Phantom 1*, is described by a characteristic function of the inner ellipsoid of the Shepp-Logan phantom from the previous paragraph, see Figure 2.11 (a).

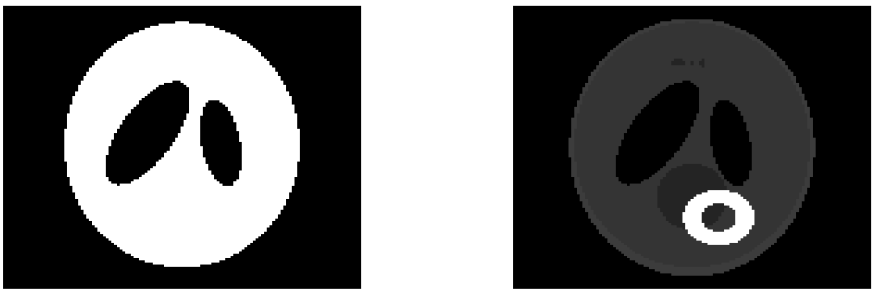

(a) Phantom 1, f_1 (b) Phantom 2, f_2

Figure 2.11 Nucleotide distributions

The purpose of Phantom 1 is to test the ability to reconstruct spatially uniform and slowly varying distributions of the nucleotide.

At the same time it is important to test the algorithms when activity distribution has highly non-uniform distribution in space. For these reasons we use phantom f_2 or *Phantom 2*, which is described by a spherical layer placed almost in the center of the attenuation phantom; see Figure 2.11 (b) (the background model in gray is placed only for visualization of position of f_2 with respect to the attenuation model). The outer radius of the spherical layer is 4cm and the radius of the inner one is equal to 2cm. In particular, Phantom 2 is used to simulate the classical setting in SPECT: reconstruct the distribution of a nucleotide which tends to concentrate in the brain of a patient.

Finally, note that on Figure 2.11 only slices of Phantoms 1, 2 are presented, whereas the latter are complete three-dimensional objects.

Simulation of noiseless data

We recall, that in SPECT the emission data is modeled by $P_{W_a} f(\gamma)$ on rays which γ correspond the slice-by-slice reconstructions framework; see also Figure 2.8.

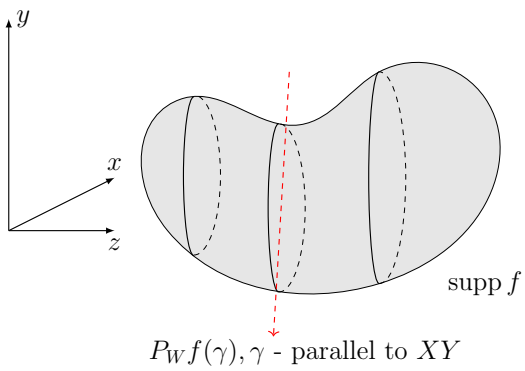

Figure 2.12

More precisely, it means that

$P_{W_a} f(\gamma)$ are given for all rays γ which are parallel to XY plane; see Figure 2.12, (2.133)

where

1. test functions $f = f(x)$, $x \in \mathbb{R}^3$, are given by f_1, f_2.
2. weight W_a is given by formulas (2.37), (2.38), where a is given by a_1, a_2.

Activity phantoms f_1, f_2 and attenuation maps a_1, a_2 are given by their values on Cartesian grid of the unit cube $[-1,1]^3$ and it is assumed that these functions are supported in the centered ball of radius $R = 1.0$.

In particular, grid Cartesian grid Ω_N on $[-1,1]^3$ was defined as follows

$$\begin{aligned} &\Omega_N = \{(x_i, y_j, z_k) : x_i = -R + i\Delta x,\ y_j = -R + j\Delta y,\ z_k = -R + k\Delta z\}, \\ &\Delta x = \Delta y = \Delta z = 2R/(N-1),\ i,\ j,\ k \in \{0, \dots N-1\}, \end{aligned} \tag{2.134}$$

where N is the number points in the grid in one direction. In all our computations we took $N = 129$ which corresponds to the standard resolution in SPECT. For evaluations of $P_{W_a} f$ for weights W_a given by (2.37) on such discrete grids we assumed that functions f_1, f_2 and a_1, a_2 were piecewise linear and continuous between the grid points.

To make a discretized version of (2.133) we used grid Γ in the set of rays which corresponded to the framework of slice-by-slice reconstructions, where in each plane $z = const$ the emission data $P_{W_a} f$ was modelized for parallel-beam geometry; [Na86]. According to this configuration grid Γ consists of a grid of rays withing each plane parallel to XY (i.e., $z = const$) and of a grid along Z-coordinate in range $[-1,1]$. More precisely, grid Γ was defined as follows:

$$\begin{aligned} &\Gamma = \{\gamma = \gamma(z_i, s_j, \varphi_k) : z_i = -R + i\Delta z,\ s_j = -R + j\Delta s,\ \varphi_k = k\Delta\varphi\}, \\ &i = 0, \dots n_z - 1,\ j = 0, \dots n_s - 1,\ k = 0, \dots n_\varphi - 1, \\ &\Delta z = 2R/(n_z - 1),\ \Delta s = 2R/(n_s - 1),\ \Delta\varphi = 2\pi/n_\varphi, \end{aligned} \tag{2.135}$$

where $\gamma(z, s, \varphi)$ was given by the formulas

$$\begin{aligned} &\text{ray } \gamma = \gamma(z, s, \varphi) \text{ for } (z, s, \varphi) \in [-1,1] \times [-1,1] \times [0, 2\pi] \text{ is defined as} \\ &\gamma(z, s, \varphi) = \{(x_1, x_2, x_3) : x_1 = s\cos(\varphi) - t\sin(\varphi),\ x_2 = s\sin(\varphi) + t\cos(\varphi),\ x_3 = z,\ t \in \mathbb{R}\}. \end{aligned} \tag{2.136}$$

For our experiments we used $n_z = n_s = 129$. The number of projections n_φ was chosen equals to 128. Note, that this number is less than in [Kun01] ($n_\varphi = 400$), where the value

for n_φ was chosen according to Shannon-Nyquist type sampling condition for ray transforms (see Chapter 3 in [Na86]). Our choice for $n_\varphi = 128$ was motivated by the experiment on real data in which we had only this number of directions in each slicing plane.

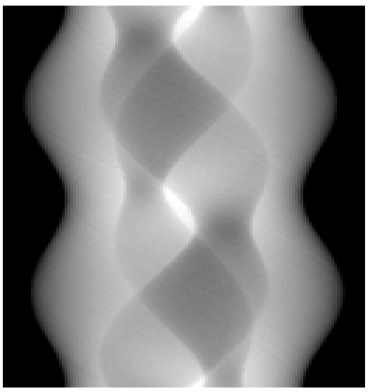

(a) $P_{W_a} f_1$, weak attenuation

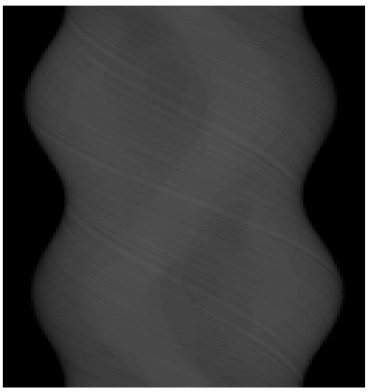

(b) $P_{W_a} f_1$, weak attenuation

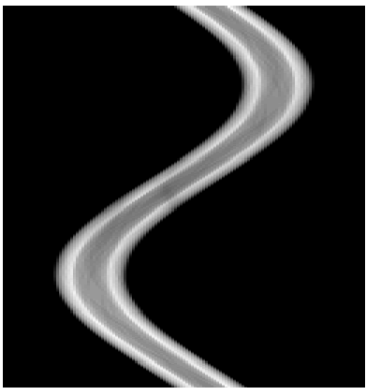

(a) $P_{W_a} f_2$, weak attenuation

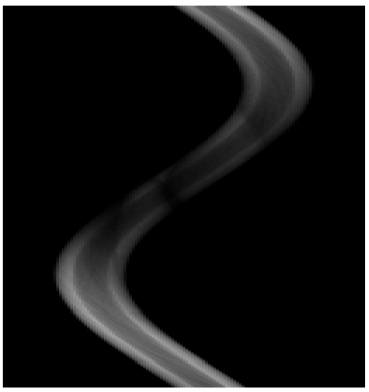

(b) $P_{W_a} f_2$, strong attenuation

Figure 2.14 Ray data $P_{W_a} f$ in plane $z = 0$

In Figure 2.14 we give examples for values of weighted ray transforms $P_{W_a} f(z, s, \varphi)$ in slice $z = 0$ (such images are also called *sinograms*); horizontal and vertical axis correspond to variables $(s, \varphi) \in [-1, 1] \times [0, 2\pi)$, respectively. One can see already from here that along some directions strong attenuation may cause significant decrease or complete loss of the signal.

Testing any reconstruction algorithm on emission data given by $P_{W_a} f$ without noise can be seen only as a first step. Strong Poisson noise in the emission data is the major mathematical and practical issue in SPECT and PET. Therefore any algorithm for SPECT and PET must be tested on stability against noise. To perform such tests we modelized the Poisson noise from emission data $P_{W_a} f(\gamma)$, $\gamma \in \Gamma$.

In the next paragraph, we explain how we modelized noise in ray data $P_{W_a} f(\gamma)$, $\gamma \in \Gamma$.

Modelling of the noise in emission data

The real measurements in SPECT consist of the number of registered photons $N(\gamma)$ that have reached a detector along ray $\gamma \in \Gamma$, where Γ is the grid from (2.135). With good

approximation $N(\gamma)$ has Poisson distribution with intensity $\lambda(\gamma)$ which is given by the formula

$$\lambda(\gamma) = CtP_{W_a}f(\gamma),\ \gamma \in \Gamma,\ C > 0,\ t > 0, \tag{2.137}$$

where C is a setup-dependent constant, t is the time of exposure per projection, $P_{W_a}f$ weighted ray transform defined by (2.37), (2.38).

Using formula (2.137) and considerations from the previous paragraph, we modelized noise in emission data in the following manner.

First, for given attenuation and activity phantoms (attenuation models a_1, a_2, activity phantoms f_1, f_2) we computed the noiseless data given by $P_{W_a}f(\gamma)$, $\gamma \in \Gamma$. Then we chose a normalization constant $C = C_n$ such that

$$C_n \max_{\gamma\in\Gamma} P_{W_a}f(\gamma) = n, \tag{2.138}$$

where n is a constant corresponding to the maximal number of photons registered along rays in Γ if the time of exposures was $t = 1$ for all rays. In our experiments we used two different values for n: $n_1 = 50$ and $n_2 = 500$ which corresponded to strong and weak noise levels, respectively (see also Remarks 7, 8 below).

Next, according to (2.137), we defined intensities $\lambda(\gamma)$, $\gamma \in \Gamma$, for Poisson process by the formula

$$\lambda(\gamma) = C_nP_{W_a}f(\gamma), \tag{2.139}$$

where C_n is a constant of (2.138). Finally, for each $\gamma \in \Gamma$ we generated independently $N(\gamma) \sim \mathrm{Po}(\lambda(\gamma))$, where $\mathrm{Po}(\lambda)$ denotes Poisson distribution with intensity λ.

Remark 7. In real experiments, setup-dependent constant C and exposure time t from (2.137), are known. In view of this fact, for the experiment on synthetic data it is fine to assume that C_n is also known and it can be used to preprocess the data. More precisely, using C_n and knowing $N(\gamma)$, $\gamma \in \Gamma$, the true values for weighted ray transforms $P_{W_a}f(\gamma)$ may be approximated as follows:

$$P_{W_a}f(\gamma) \approx \frac{N(\gamma)}{C_n},\ \gamma \in \Gamma. \tag{2.140}$$

Here, we recall that, in the experiment, after having modelized noise for the emission data, we cannot longer assume that $P_{W_a}f$ are known. In particular, approximation (2.140) is based on the following property of Poisson distribution:

$$\text{Let } N(\gamma) \sim \mathrm{Po}\left(C_nP_{W_a}f(\gamma)\right),\ \text{then } \mathbb{E}\left(\frac{N(\gamma)}{C_n}\right) = P_{W_a}f(\gamma),\ \gamma \in \Gamma, \tag{2.141}$$

where $\mathrm{Po}(\lambda)$ denotes the Poisson distribution, $\mathbb{E}$ - denotes the mathematical expectation.

Remark 8. The choice of constant n in (2.138) allows to control the noise level in generated emission data. More precisely, choosing intensities $\lambda(\gamma)$ as in (2.139) we have that

$$\mathrm{Var}\left(\frac{N(\gamma)}{C_n}\right) = \frac{P_{W_a}f(\gamma)}{C_n} = \frac{P_{W_a}f(\gamma)\max\limits_{\gamma\in\Gamma} P_{W_a}f(\gamma)}{n},\ \gamma \in \Gamma, \tag{2.142}$$

where $\mathrm{Var}(\cdot)$ denotes the variance. Identity (2.142) is based on the following property of Poisson distribution: $\xi \sim \mathrm{Po}(\lambda)$, $\mathrm{Var}(\xi) = \lambda$. From (2.139)-(2.142) is follows that that bigger n correspond to better approximations in (2.140). In particular, our choice $n_1 = 50$ corresponds to the case of strong noise and is actually close to the setting of our experiment on real data; see [GuNo08]. Finally, from (2.137), (2.138) one can see that choosing bigger n can be interpreted as having longer acquisition time t, which is not always possible due to practical limitations in SPECT.

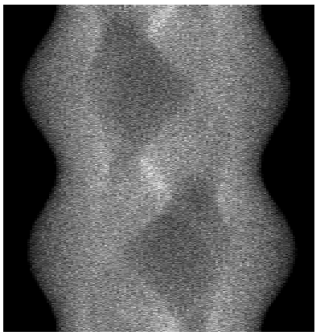

(a) $P_{W_a} f_1$, weak attenuation

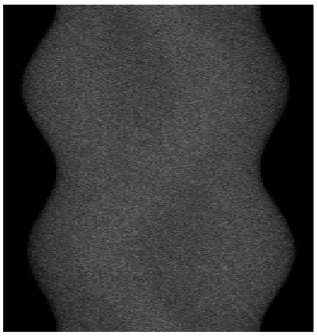

(b) $P_{W_a} f_1$, strong attenuation

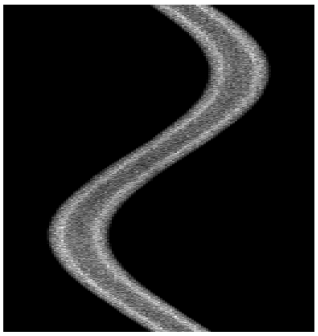

(a) $P_{W_a} f_2$, weak attenuation

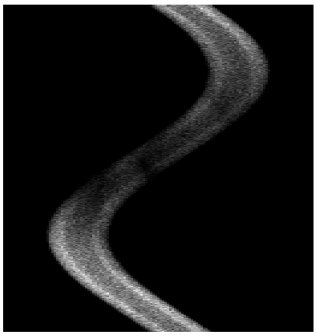

(b) $P_{W_a} f_2$, strong attenuation

Figure 2.16 Modelling of strong noise $n = n_1 = 50$

In Figure 2.16 the modelling of noisy data $N(\gamma), \gamma \in \Gamma$ for rays in plane $z = 0$ is given.

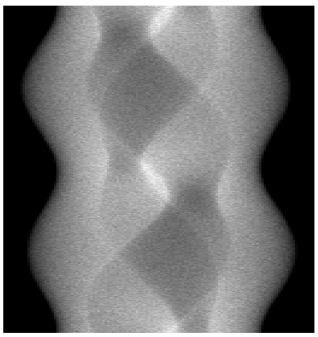

(a) $P_{W_a} f_1$, weak attenuation

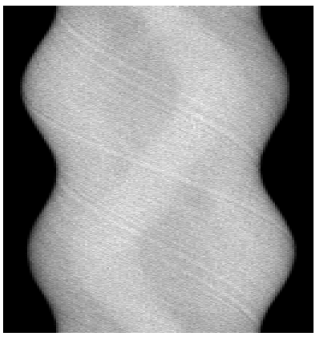

(b) $P_{W_a} f_1$, strong attenuation

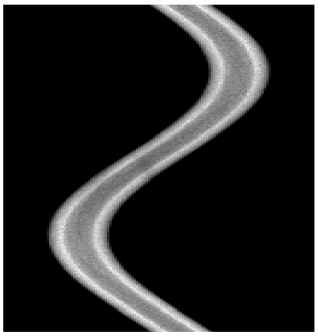

(a) $P_{W_a} f_2$, weak attenuation

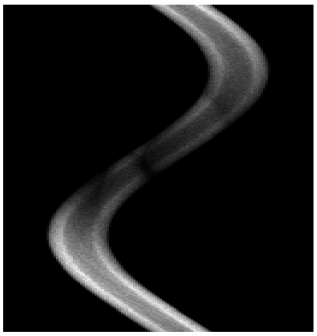

(b) $P_{W_a} f_2$, strong attenuation

Figure 2.18 Modelisation of weak noise $n = n_2 = 500$

Note that for the case of weak noise ($n_2 = 500$), the images almost do not differ from the denoised originals in Figure 2.14. This was explained in Remark 8 that noise level decreases with increase of number of registered photons (i.e., with increase of n).

Reduction of data along rays to data along planes

Our method of inversion from Articles 1, 2 is based on reduction of emission data given by $P_{W_a} f$ to data given by weighted Radon transforms $R_W f$ along planes in 3D. More precisely, the reduction is described by formulas (2.83), (2.84), from which one can see that new data are given by $R_W f$ on all two-dimensional planes, except those which are parallel to XY; see also Figure 2.12.

For our computations we used the following grid in the set of oriented planes

$$\Pi = \{(s_i, \theta(\varphi_j, \psi_k)) : s_i - \text{ grid on } [-1,1],\ \theta(\varphi_j, \psi_k) - \text{grid on } \mathbb{S}^2\}, \tag{2.143}$$

where

$$\begin{aligned} &s_i = -R + i\Delta s,\ i = 0, \dots n_s - 1,\ \Delta s = 2R/(n_s - 1), \\ &\varphi_j = j\Delta\varphi,\ j = 0, \dots n_\varphi - 1,\ \Delta\varphi = 2\pi/n_\varphi, \\ &\psi_k = \arccos(t_k),\ k = 0, \dots, n_\psi - 1, \\ &\{t_k\}_{k=0}^{n_\psi - 1} - \text{ points for Gauss-Legendre quadrature rule on } [-1,1] \end{aligned} \tag{2.144}$$

and $\theta(\varphi, \psi) = (\sin(\psi)\cos(\varphi), \sin(\psi)\sin(\varphi), \cos(\psi)) \in \mathbb{S}^2$. In particular, in all our numerical experiments we used $n_s = 129$, $n_\varphi = 128$, $n_\psi = 128$.

To reduce $P_{W_a} f(\gamma)$, $\gamma \in \Gamma$ to $R_W f(s, \theta)$, $(s, \theta) \in \Pi$, we rewrite (2.84) as follows:

$$\begin{aligned} &R_W f(s, \theta(\varphi, \psi)) = \int\limits_{-\sqrt{1-s^2}}^{\sqrt{1-s^2}} P_{W_a} f(\gamma(z(s, \varphi, \psi, \tau), \varphi,\ \sigma(s, \varphi, \psi, \tau))\, d\tau, \\ &\gamma = \gamma(z, \sigma, \varphi) \text{ is given in (2.136) for } z \in [-1,1],\ \sigma \in [-1,1],\ \varphi \in [0, 2\pi), \\ &z(s, \varphi, \psi, \tau) = s\cos(\psi) + \tau\sin(\psi), \\ &\sigma(s, \varphi, \psi, \tau) = s\sin(\psi) - \tau\cos(\psi), \end{aligned} \tag{2.145}$$

where W is given by the formula

$$W(x, \theta(\varphi, \psi)) = W_a\left(x, \theta\left(\varphi + \frac{\pi}{2}, \frac{\pi}{2}\right)\right) \text{ for } W_a(x, \theta) \text{ from (2.37), (2.38).} \tag{2.146}$$

Parameter τ in (2.145) plays the role of parametrization of rays $\gamma(z, \sigma, \varphi)$ which "fiber" oriented plane $(s, \theta(\varphi, \psi))$ and satisfy the assumption in (2.133). Also, to obtain (2.145), (2.146) from (2.83) , (2.84), we used the fact that $\eta = (0, 0, 1)$ and f is supported in the centered unit ball.

Finally, in order to reduce initial data $P_{W_a} f(\gamma)$, $\gamma \in \Gamma$ to $R_W f(s, \theta)$, $(s, \theta) \in \Pi$ we use straightforward discretizations of (2.145), (2.146). In particular, in (2.145) to compute $P_{W_a} f(\gamma)$ for rays $\gamma(z, \sigma, \varphi)$ that are not in grid Γ we used quadratic interpolation in variable z and spline interpolation in variable σ (interpolation in φ was not needed since angles $\{\varphi_j\}_{j=0}^{n_\varphi - 1}$ in grids Γ and Π were the same). We would like to note here that mathematically such interpolations are not correct, because rigorously one has to do interpolation in the image of P_{W_a}. Such interpolation is complicated in view of the fact, that the image of attenuated Radon transform is described by infinite number of integral identities (Paley-Wiener Theorem for Radon transforms; see [G+03], [Na86]), which seems hard to use them in applications. In fact, such high orders of interpolations were used because of artifacts for piecewise linear interpolations. This could be explained by the property that P_W, in general, is a smoothing operator (see [Na86] for the case of $W \equiv 1$). Therefore, the image of operator P_{W_a} contains smoother functions and higher orders of interpolations must be used.

Now, having all the description above about the simulation of our data, we present the reconstructions, where attenuations were a_1, a_2 and nucleotide distributions were f_1, f_2.

Reconstructions using Chang-type formulas in 2D and 3D

Noiseless case

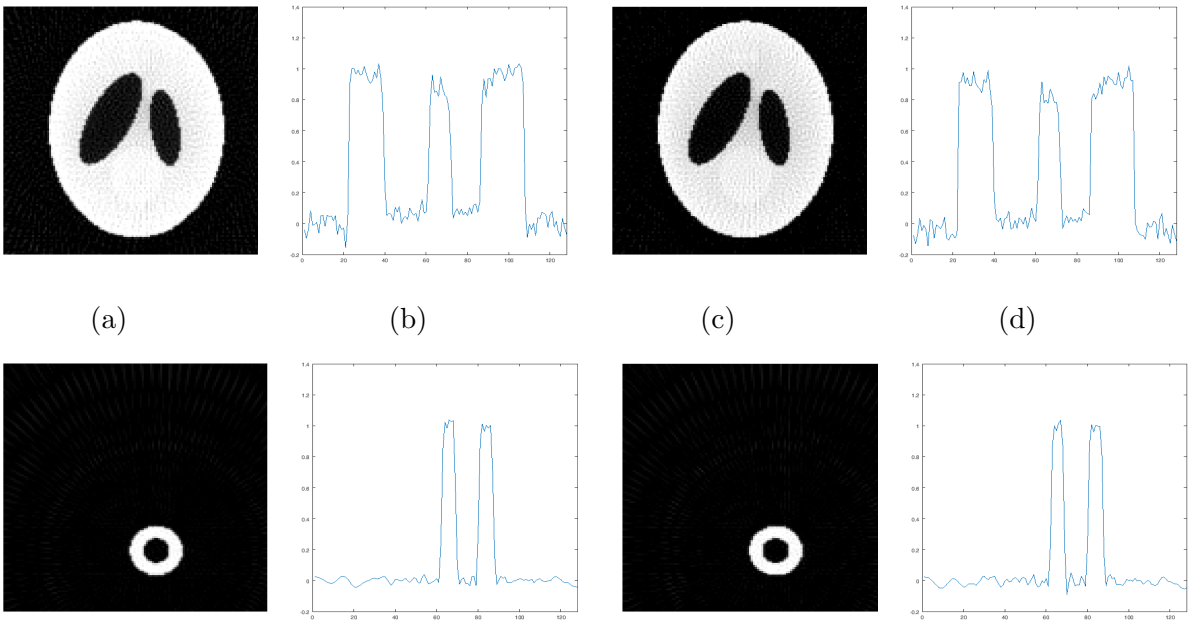

(a) (b) (c) (d)

(e) (f) (g) (h)

Figure 2.19 : weak attenuation, no noise; reconstructions of f_1, f_2 using Chang-type formulas in 3D (a), (e) and in 2D (c), (g); (b), (d), (f), (h) – sections along X-axis

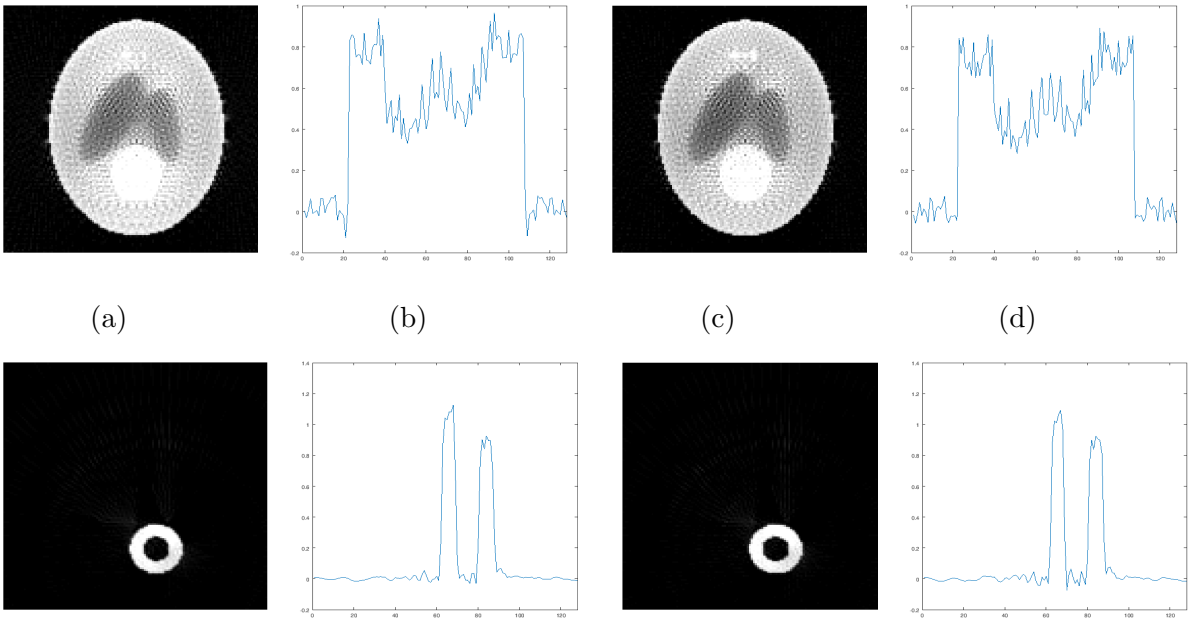

(a) (b) (c) (d)

(e) (f) (g) (h)

Figure 2.20 : strong attenuation, no noise; reconstructions of f_1, f_2 using Chang-type formulas in 3D (a), (e) and in 2D (c), (g); (b), (d), (f), (h) – sections along X-axis

Case with noise

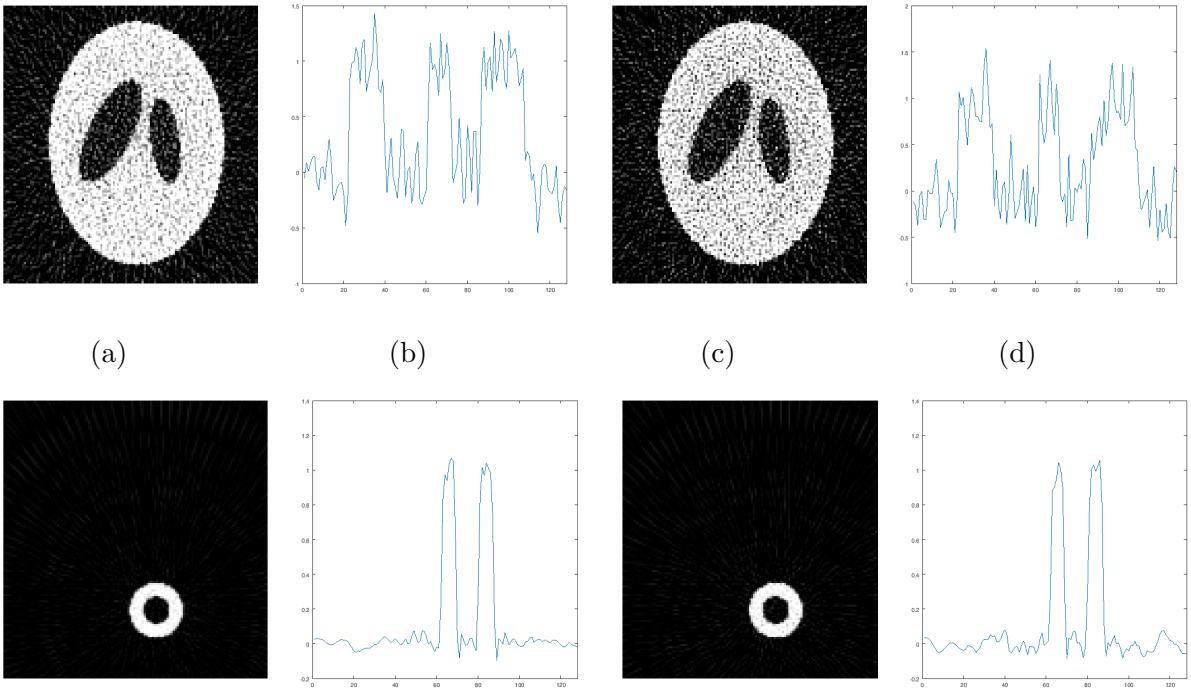

(a) (b) (c) (d)

(e) (f) (g) (h)

Figure 2.21 : weak attenuation, weak noise ($n_2 = 500$); reconstructions of f_1, f_2 using Chang-type formulas in 3D (a), (e) and in 2D (c), (g); (b), (d), (f), (h) – sections along X-axis

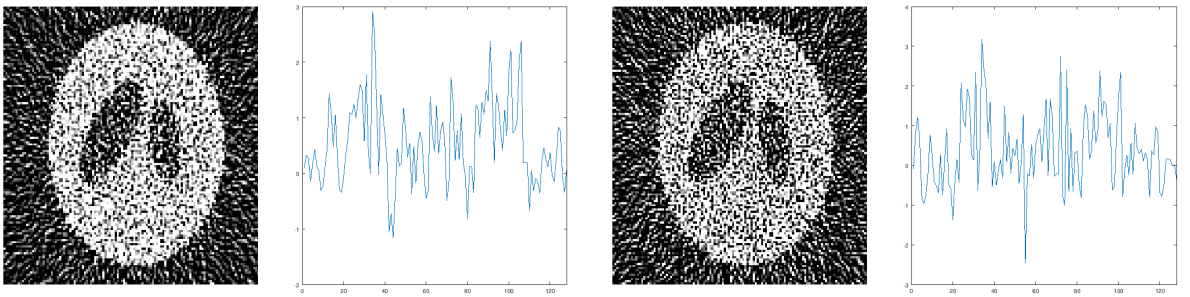

(a) (b) (c) (d)

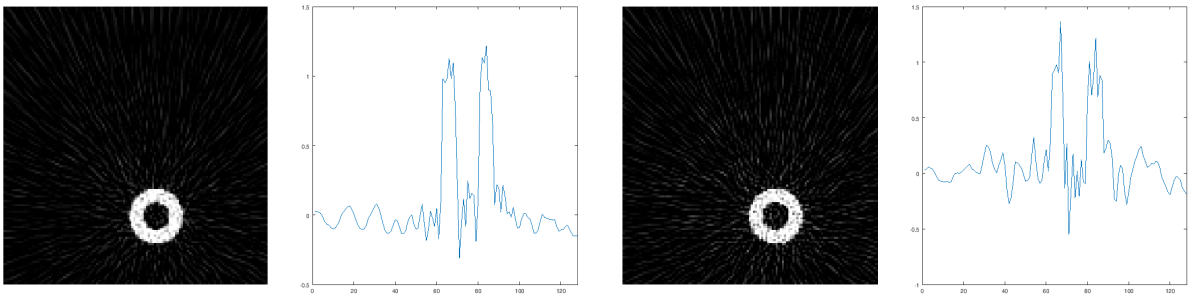

(e) (f) (g) (h)

Figure 2.22 : weak attenuation, strong noise ($n_1 = 50$); reconstructions of f_1, f_2 using Chang-type formulas in 3D (a), (e) and in 2D (c), (g); (b), (d), (f), (h)-sections along X-axis

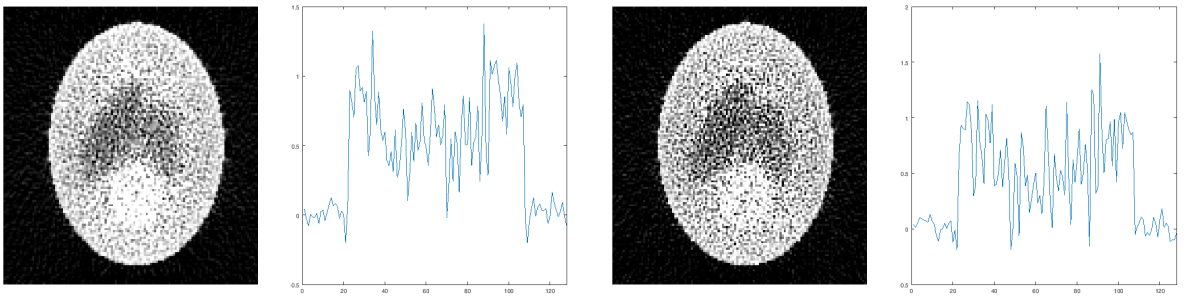

(a) (b) (c) (d)

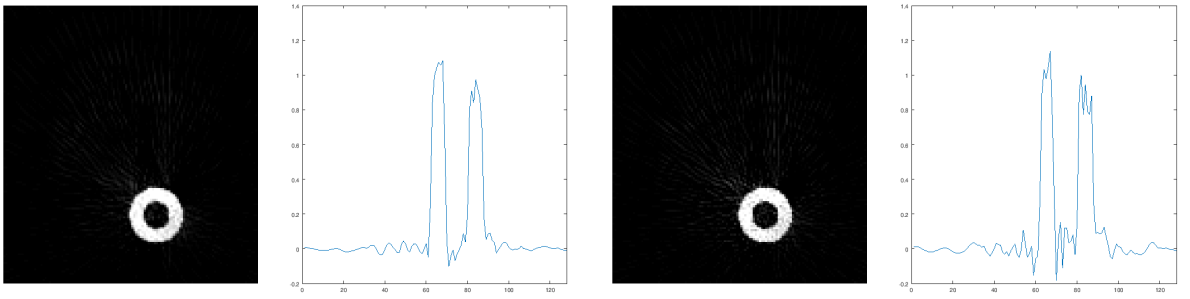

(e) (f) (g) (h)

Figure 2.23 : strong attenuation, weak noise ($n_2 = 500$); reconstructions of f_1, f_2 using Chang-type formulas in 3D (a), (e) and in 2D (c), (g); (b), (d), (f), (h) – sections along X-axis

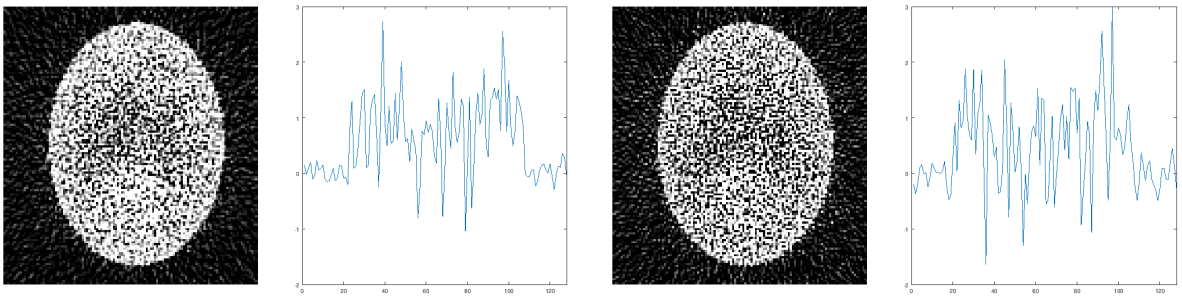

(a) (b) (c) (d)

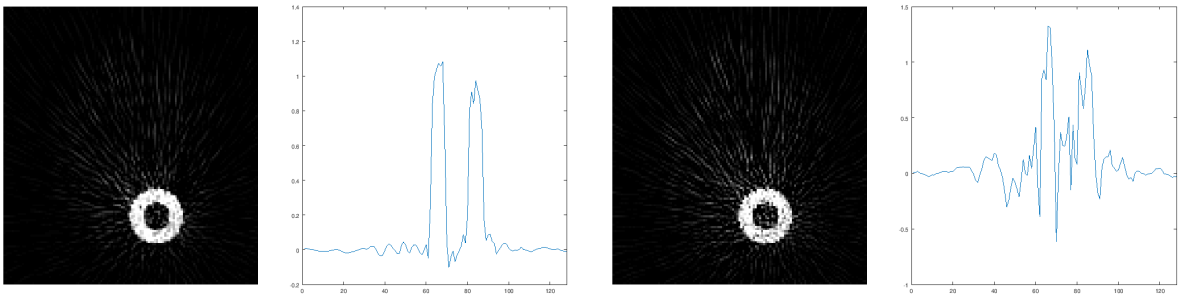

(e) (f) (g) (h)

Figure 2.24 : strong attenuation, strong noise ($n_1 = 50$); reconstructions of f_1, f_2 using Chang-type formulas in 3D (a), (e) and in 2D (c), (g); (b), (d), (f), (h) – sections along X-axis

For our reconstructions we used formulas (2.86)-(2.88) for $d = 2, 3$ from Article 1. Note that in Figure 2.20 there is almost no difference between reconstructions using two-dimensional or three-dimensional Chang-type formulas. At the same time, in Figures 2.21-2.24 reconstructions obtained using Chang-type formula for $d = 3$ look already less noisy than their analogs for $d = 2$. This supports the intuition that our reduction from Article 1 works as a regularization of noise.

To measure the effect of noise, we computed the relative squared distance between images corresponding to reconstructions with noise and their denoised versions.

Let

$$\begin{aligned} &\tilde{f}_i^{a_j},\ i = 1, 2,\ j = 1, 2,\ \text{be the reconstructions of } f_1, f_2 \text{ for} \\ &\text{strong and weak attenuation levels } a_1, a_2 \text{ without noise and} \\ &\text{reduced to plane } z = 0 \text{ (see Figures 2.19, 2.20).} \end{aligned} \tag{2.147}$$

Reconstructions from the data with noise will be denoted as follows:

$$\begin{aligned} &\tilde{f}_i^{a_j,\, n_k},\ i = 1, 2,\ j = 1, 2,\ k = 1, 2,\ \text{be the reconstructions of } f_1, f_2 \text{ for strong} \\ &\text{and weak attenuation levels } a_1, a_2 \text{ for noise levels } n_1, n_2, \text{ respectivley, and} \\ &\text{reduced to plane } z = 0 \text{ (see Figures 2.27-2.30).} \end{aligned} \tag{2.148}$$

Then, the error of reconstructions $\varepsilon_{f_i,a_j,n_k}$ is defined by the formula

$$\varepsilon_{f_i,a_j,n_k} = \frac{\|\tilde{f}_i^{a_j,n_k} - \tilde{f}_i^{a_j}\|_2}{\|\tilde{f}_i^{a_j}\|_2},\ i = 1, 2,\ j = 1, 2,\ k = 1, 2, \tag{2.149}$$

where $\|\cdot\|_2$ denotes the Frobenius norm of two-dimensional images seen as matrices of size $N \times N$, where N is the number of pixels in single direction. The reason to compute errors

using formula (2.149) is that Chang-type formulas provide only approximate reconstructions. To measure the effect of noise one must compare approximate reconstructions from noisy data only with approximate reconstructions from the data without noise.

For our reconstructions by Chang-type formulas we had the following errors:

Method / Error	$\varepsilon_{f_1,a_1,n_1}$	$\varepsilon_{f_1,a_2,n_1}$	$\varepsilon_{f_1,a_1,n_2}$	$\varepsilon_{f_1,a_2,n_2}$	$\varepsilon_{f_2,a_1,n_1}$	$\varepsilon_{f_2,a_2,n_1}$	$\varepsilon_{f_2,a_1,n_2}$	$\varepsilon_{f_2,a_2,n_2}$
2D-method	1.193	1.340	0.377	0.434	0.644	0.625	0.211	0.202
3D-method	0.779	0.942	0.251	0.299	0.438	0.432	0.137	0.135

Table 2.1 Relative errors in reconstructions using Chang-type formulas

From Table 2.1 one could see that our three-dimensional method using Chang-type formula outperforms its two-dimensional analog for all cases of activity phantoms, attenuations and noise levels. Moreover, the gain of stability in reconstructions is already visible from Figures 2.21-2.24.

Iterative inversions

For iterative reconstructions we used the Kunyansky-type iterative algorithm from Article 2 in dimension $d = 3$ and the original two-dimensional algorithm from [Ku92]. In particular, we used schemes of (2.79), (2.131) for approximate inversions for $m = 1$. Our choice for $m = 1$ was motivated by convergence conditions (2.79), (2.120) in two and three dimensions, respectively. More precisely, for weak attenuation a_2, Chang-type formulas were giving already almost-perfect reconstructions of f_1, f_2 (modulo the noise) (see Figure 2.19 (a), (c), (e), (g)), however, for strong attenuation a_1 Chang-type formulas were producing strong artifacts (see Figure 2.20 (a), (c), (e), (g)). For strong attenuation a_1, condition (2.120) was barely satisfied ($\sigma_{W,D,1} = 0.89$ for $d = 3$ and 0.52 for $d = 2$) therefore, to be able to compare two-dimensional and three-dimensional algorithms we kept $m = 1$. Finally, for weak attenuation a_2, conditions (2.79), (2.120) were efficiently satisfied ($\sigma_{W,D,1} = 0.17$ for $d = 3$ and 0.11 for $d = 2$). So the choice $m = 1$ was, indeed, due to the case of strong attenuation.

Noiseless case

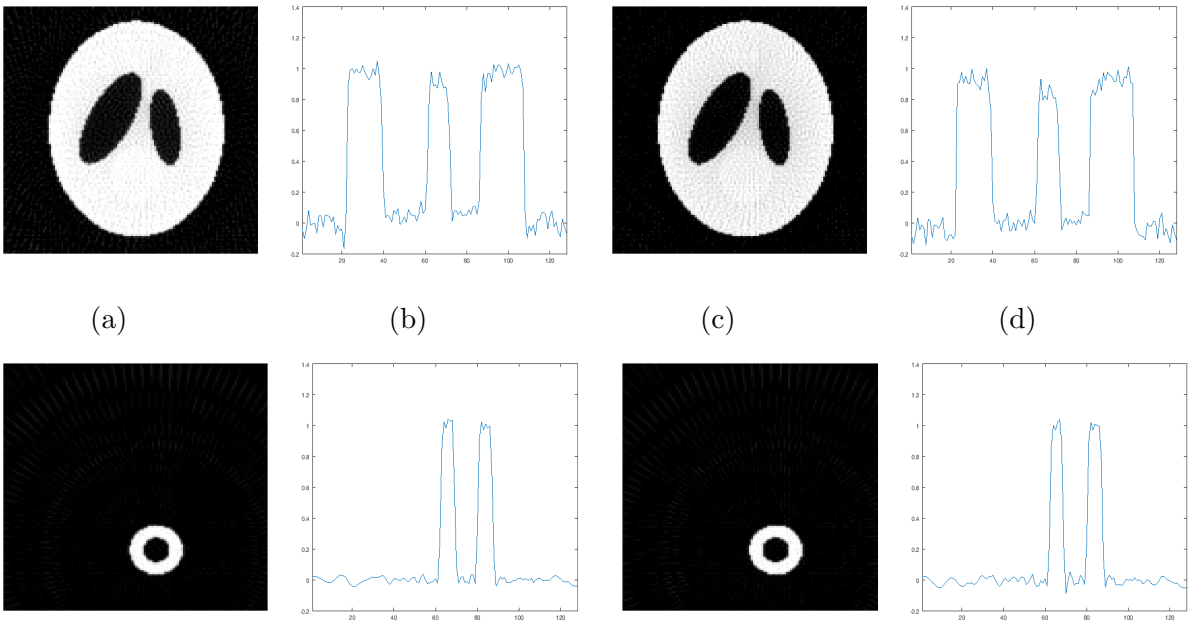

(a) (b) (c) (d)

(e) (f) (g) (h)

Figure 2.25 : weak attenuation a_2, no noise; reconstructions of f_1, f_2 using iterative Kunyansky-type algorithms in 3D (a), (e) and in 2D (c), (g); (b), (d), (f), (h) – sections along X-axis

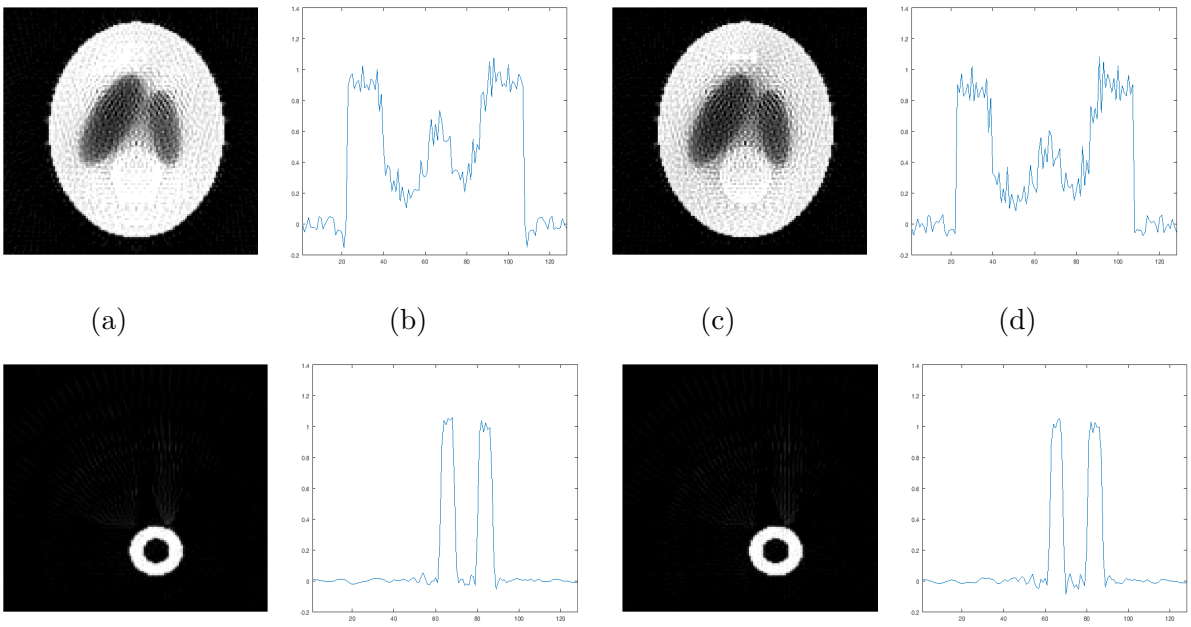

(a) (b) (c) (d)

(e) (f) (g) (h)

Figure 2.26 : strong attenuation a_1, no noise; reconstructions of f_1, f_2 using iterative Kunyansky-type algorithms in 3D (a), (e) and in 2D (c), (g); (b), (d), (f), (h) – sections along X-axis

Case with noise

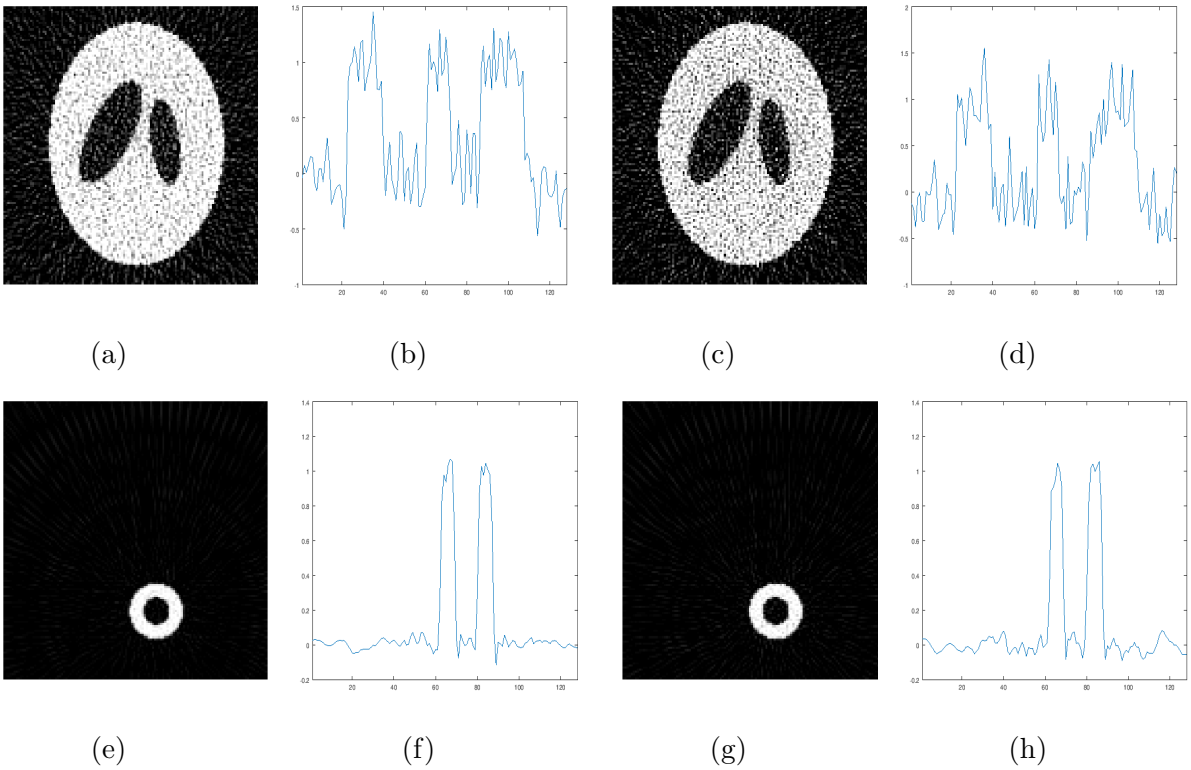

(a) (b) (c) (d)

(e) (f) (g) (h)

Figure 2.27 : weak attenuation a_2, weak noise ($n_2 = 500$); reconstructions of f_1, f_2 using Kunyansky-type iterative algorithms in 3D (a), (e) and in 2D (c), (g); (b), (d), (f), (h) – sections along X-axis

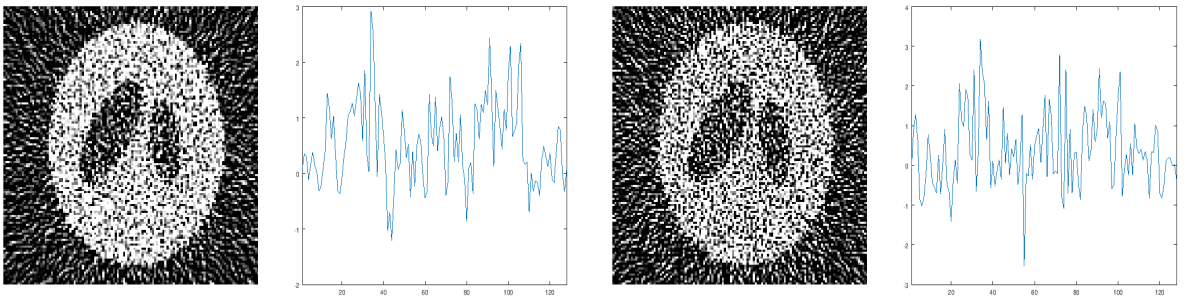

(a) (b) (c) (d)

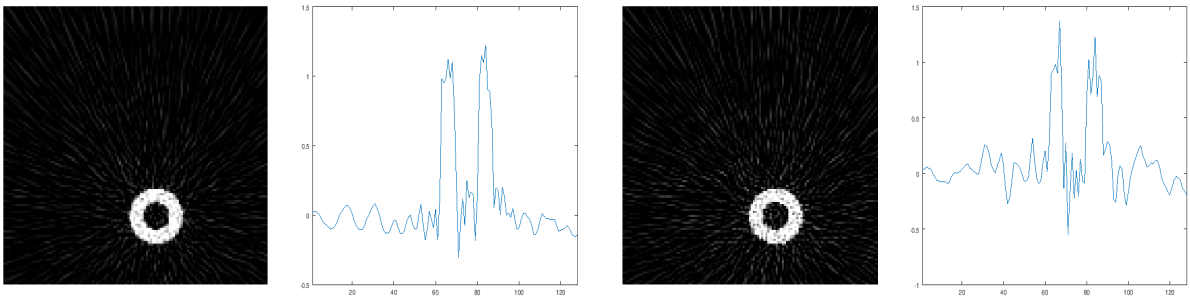

(e) (f) (g) (h)

Figure 2.28 : weak attenuation a_2, strong noise ($n_1 = 50$); reconstructions of f_1, f_2 using Kunyansky-type algorithms in 3D (a), (e) and in 2D (c), (g); (b), (d), (f), (h) – sections along X-axis

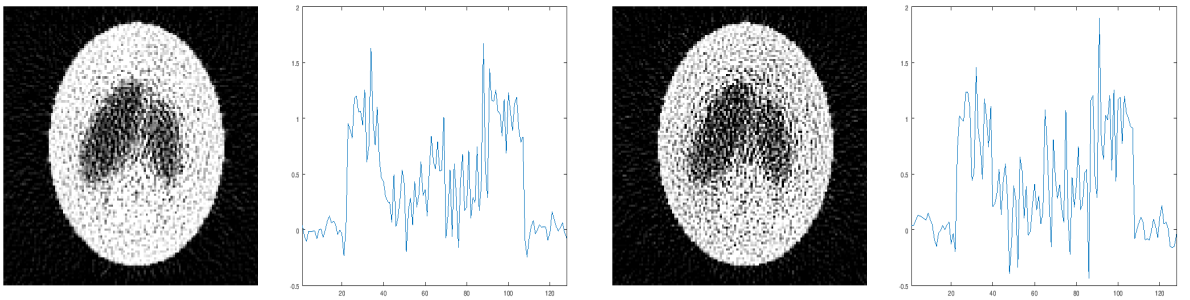

(a) (b) (c) (d)

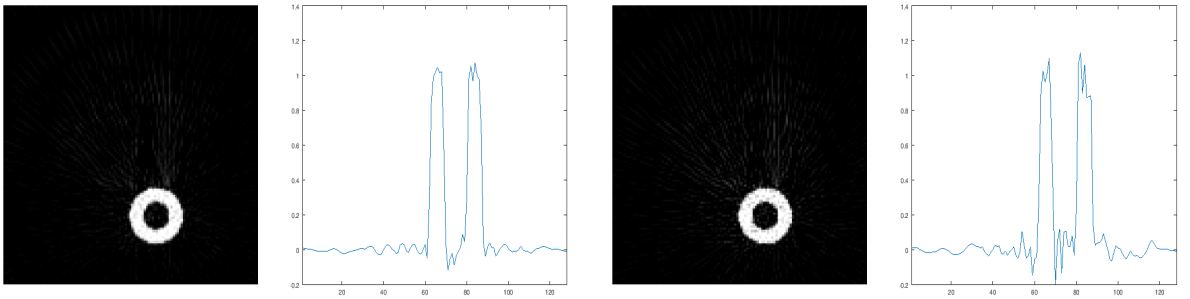

(e) (f) (g) (h)

Figure 2.29 : strong attenuation a_1, weak noise ($n_2 = 500$); reconstructions of f_1, f_2 using Kunyansky-type algorithms in 3D (a), (e) and in 2D (c), (g); (b), (d), (f), (h) – sections along X-axis

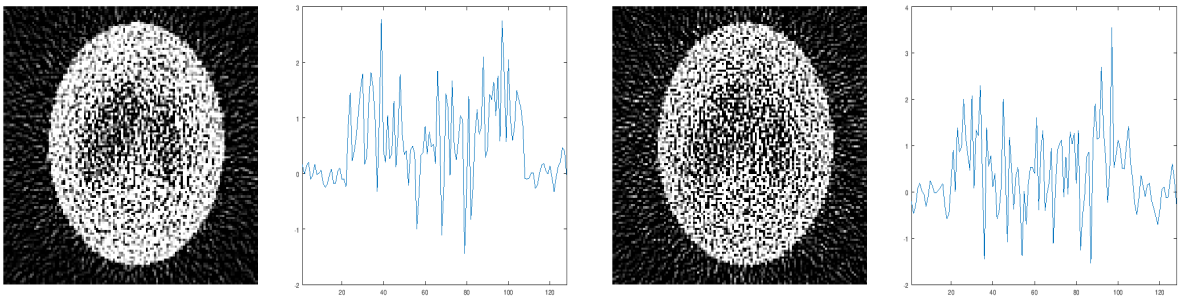

(a) (b) (c) (d)

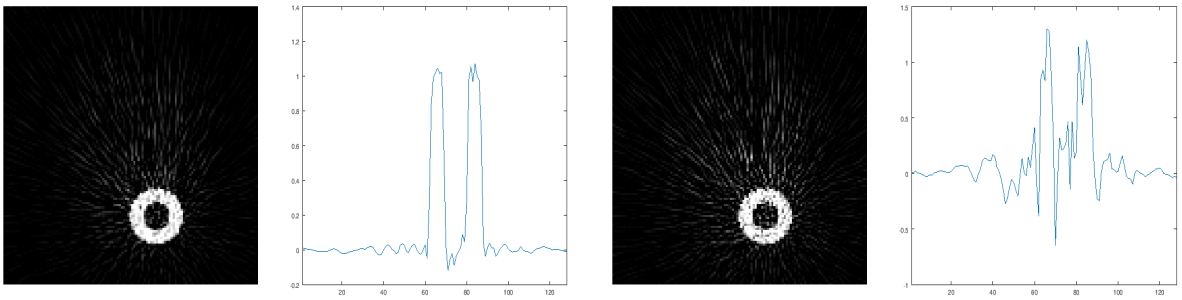

(e) (f) (g) (h)

Figure 2.30 : strong attenuation a_1, strong noise ($n_1 = 50$); reconstructions of f_1, f_2 using Kunyansky-type algorithms in 3D (a), (e) and in 2D (c), (g); (b), (d), (f), (h) – sections along X-axis

In addition, analogously to the experiment for Chang-type formulas, we also computed the relative errors for two-dimensional and three-dimensional reconstructions.

Let

$$\hat{f}_i^{a_j},\ i = 1, 2,\ j = 1, 2,\ \text{be the reconstructions of } f_1, f_2 \text{ for strong and weak attenuation levels } a_1, a_2 \text{ without noise and reduced to plane } z = 0 \text{ (see Figures 2.25, 2.26).} \tag{2.150}$$

The above functions may be considered as "ideal reconstructions" for the used iterative methods. Reconstructions in presence of noise are defined as follows:

$$\hat{f}_i^{a_j, n_k},\ i = 1, 2,\ j = 1, 2,\ k = 1, 2,\ \text{denote the reconstructions of } f_1, f_2 \text{ for strong and weak attenuation levels } a_1, a_2 \text{ for noise levels } n_1, n_2, \text{ respectivley, and reduced to plane } z = 0 \text{ (see Figures 2.27-2.30).} \tag{2.151}$$

The error $\varepsilon_{f_i, a_j, n_k}$ of reconstructions was defined by the formula

$$\varepsilon_{f_i, a_j, n_k} = \frac{\|\hat{f}_i^{a_j, n_k} - \hat{f}_i^{a_j}\|_2}{\|\hat{f}_i^{a_j}\|_2},\ i = 1, 2,\ j = 1, 2,\ k = 1, 2, \tag{2.152}$$

where $\|\cdot\|_2$ denotes the Frobenius norm of two-dimensional images seen as matrices of size $N \times N$, where N is the number of pixels in single direction.

For our iterative reconstructions we had the following errors:

Method / Error	$\varepsilon_{f_1,a_1,n_1}$	$\varepsilon_{f_1,a_2,n_1}$	$\varepsilon_{f_1,a_1,n_2}$	$\varepsilon_{f_1,a_2,n_2}$	$\varepsilon_{f_2,a_1,n_1}$	$\varepsilon_{f_2,a_2,n_1}$	$\varepsilon_{f_2,a_1,n_2}$	$\varepsilon_{f_2,a_2,n_2}$
2D-method	1.279	1.415	0.437	0.438	0.714	0.634	0.254	0.205
3D-method	0.847	0.952	0.316	0.303	0.494	0.439	0.187	0.138

Table 2.2 Relative errors in reconstructions using iterative algorithms

From Table 2.2 one could see that our three-dimensional iterative method outperforms the two-dimensional one for all cases of activity phantoms, attenuation models and noise levels. Moreover, the gain of stability in reconstructions is already visible from Figures 2.27-2.30.

Experiment on real data

In this experiment we wanted show that, in principle, our approach of reduction of Problem 1 for $d = 2$ in slice-by-slice reconstructions framework to Problem 2 for $d = 3$ can be used in real SPECT applications.

A SPECT procedure was performed on a monkey. The data for this experiment was provided by *Service Hospitalier Frédéric Joliot, CEA (Orsay)*. The provided data consisted of two files: first one contained the three-dimensional attenuation map of monkey's head and the second contained emission data in terms of photon counts $N(\gamma)$ along rays γ, $\gamma \in \Gamma$, where Γ was given by (2.135) for $n_z = n_s = n_\varphi = 128$. The provided attenuation map $a = a(x)$, $x \in \mathbb{R}^3$ was given in a form of a volumetric image of $128 \times 128 \times 128$ pixels.

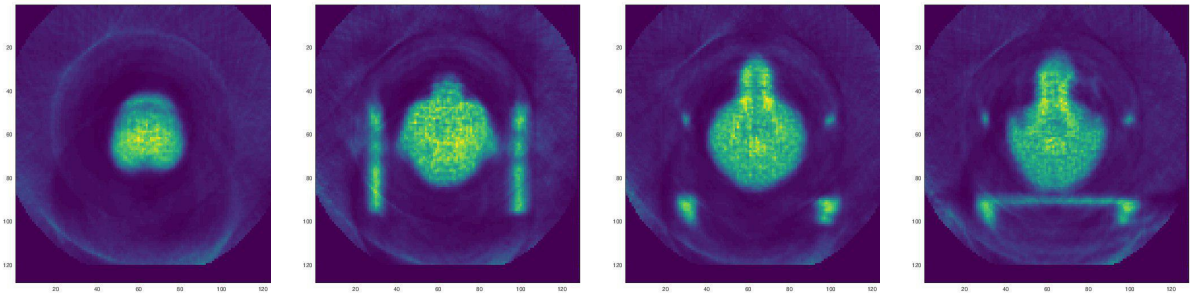

(a) $i_z = 45$ (b) $i_z = 60$ (c) $i_z = 70$ (d) $i_z = 80$

Figure 2.31 : Attenuation map of monkey's head. Subfigures (a), (b), (c), (d) represent the attenuation map reduced to sequence of planes $z = const$. Green region in the center of image (a) corresponds to brain material, vertical and horizontal lines on images (b), (d) correspond to plates which were used to fix the head of the monkey.

Unfortunately, in the given data the units for the attenuation map were not provided, which is crucial due to non-linear dependence of transform P_{W_a} on the attenuation. To overcome this lack of information we multiplied the attenuation map by a constant so that the brain material in Figure 2.31 (a) corresponded to attenuation of water 0.15cm^{-1}. Also, constant C from (2.137) was not provided, which made possible to reconstruct the nucleotide distribution only up to a multiplicative constant[16]. The time of acquisition per projection was 14 seconds and the radius of rotation of detectors was 261mm. The total number of registered photons was approximately $4.6 \cdot 10^6$ and the maximal number of registered photons per one projection was 60.

[16]For medical reasons it is still sufficient, because in SPECT only a relative distribution of the tracer is important.

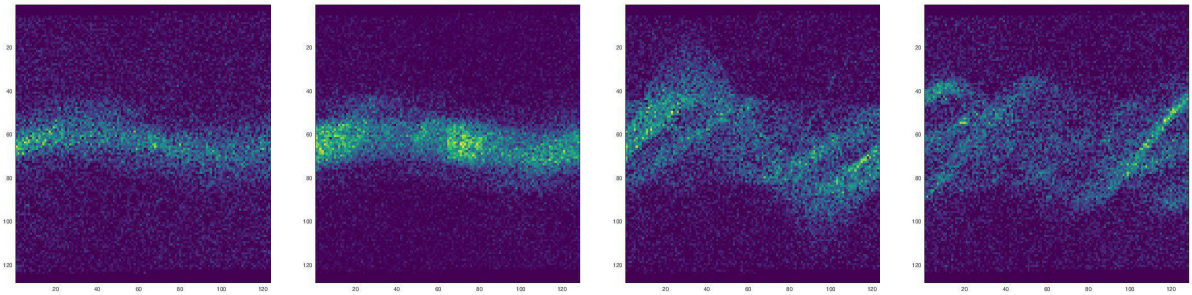

(a) $i_z = 42$ (b) $i_z = 53$ (c) $i_z = 63$ (d) $i_z = 95$

Figure 2.32 : Emission data in the experiment on a monkey. Subfigures (a)-(d) show the photon counts $N(\gamma)$, where rays γ belong to different slicing planes $z = const$. In each plane $z = const$ rays are parametrized by (s, φ), $s \in [-1, 1]$, $\varphi \in [0, 2\pi]$ (see formula (2.136)). Horizontal axis on (a)-(d) corresponds to variable φ, vertical axis corresponds to variable s.

Applying the reduction method and Chang-type formula for $d = 3$ from Artice I, we obtained approximate reconstructions of the nucleotide distribution in the brain of the monkey.

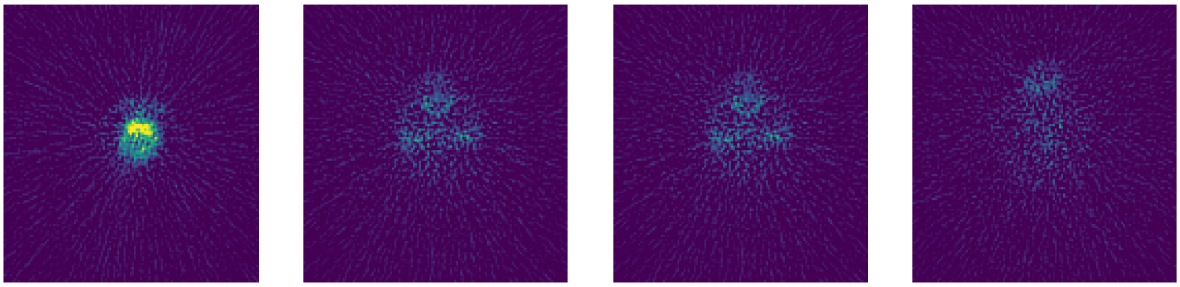

(a) $i_z = 45$ (b) $i_z = 60$ (c) $i_z = 70$ (d) $i_z = 89$

Figure 2.33 : Reconstruction of the nucleotide distribution in different slicing planes $z = const$. Note that slicing plane $i_z = 45$ (a) corresponds to the region of monkey's brain.

Finally, on Figure 2.33(a) one can see high concentration of nucleotide. This area geometrically corresponded to position of the monkey's brain (see also Figure 2.31). In addition, for the tracer in SPECT it is known a priory that it tends to concentrate in brain, so this result supports our proposition that our methods from Articles 1, 2, in principle, can be applied to real problems.

A few words on our numerical implementations

From formulas (2.83), (2.84), (2.86), (2.89) from Resume of Article 1 and formulas (2.120)-(2.128) from Resume of Article 2 one could see that there were only two crucial steps for our numerical implementations:

1. Numerical realization of formulas (2.83), (2.84) for reduction of $P_{W_a} f$ to $R_w f$. This question was already commented in (2.145). We used quadratic and spline interpolations in z, s, respectively, to sample $P_{W_a} f$ for missing rays. By doing so we definitely were obtaining the data which did not belong to the image of operator P_W. To our knowledge, efficient interpolation of data even for Pf, where P is the classical ray transform, is still an open question.

2. Inversion of the classical Radon transform R for $d = 3$. The reconstruction methods from Articles 1, 2 (Chang-type formula, Kunyansky-type iterative method) are based on the inversion of the classical Radon transform R^{-1} in dimension $d = 3$. There exist a lot of open-access libraries for efficient computations of R^{-1} for $d = 2$ (for example, in MATLAB/Octave, C, Python), but for $d = 3$ we did not find any accessible libraries. For our purposes we implemented our own numerical version of R^{-1} using the Fourier transform and the Slice Projection Theorem (see [Na86]) and also a very nice NFFT library for MATLAB/Octave developed in TU Chemnitz [K+09].

The details of our implementations can be found at GitHub repository: github.com/fedor-goncharov/Weighted-ray-Radon-transforms-in-3D.

4.2 Summary of results from Part II

If in Part I we were considering Problems 1, 2 from the point of view of applications in tomographies, in Part II we considered these problems in full generality. The first question to be posed in this case, is if the aforementioned inverse problems are solvable at all. On mathematical level this reduces to study the injectivity and non-injectivity properties of transforms P_W, R_W. Part II of this thesis is devoted to this question.

From the point of view of injectivity and non-injectivity the inverse problems for P_W and R_W (Problems 1, 2, respectively) are very different. Problem 1 is non-overdetermined for dimension $d = 2$ and is overdetermined for $d \geq 3$. Indeed, function $P_W f$ depends on $2d - 2$ variables (as a function on $T\mathbb{S}^{d-1}$) whereas f depends on d variables (as a function on $\mathbb{R}^d$) and the following formula holds

$$2d - 2 = d \text{ only for } d = 2 \text{ and } 2d - 2 > d \text{ for } d \geq 3. \tag{2.153}$$

At the same time, Problem 2 is non-overdetermined in all dimensions $d \geq 2$. This is due to the fact that $R_W f$ is a function of d variables (as a function on $\mathbb{R} \times \mathbb{S}^{d-1}$, see (2.16)), the same as for function f. The overdeterminancy of Problem 1 for $d \geq 3$ gives intuition that weighted ray transforms should be injective under reasonably mild assumptions on W and on the class of test-functions. This intuition was also supported by many positive results, for example, in [Fi86], [Il16].

Theorem 6 (Finch, 1986, Ilmavirta, 2016). *Let $W \in C^{1+\varepsilon}(\mathbb{R}^d \times \mathbb{S}^{d-1})$, $d \geq 3$, where ε is an arbitrary positive number. Then P_W is injective on $L^p_c(\mathbb{R}^d)$, $p > 2$ ($L^p_c(\mathbb{R}^d)$ – p-integrable compactly supported functions on $\mathbb{R}^d$).*

In particular, the injectivity of P_W for $d \geq 3$ is based on the fact that P_W is locally injective for $d = 2$, when W satisfies (2.14) and is at least of regularity $C^{1+\varepsilon}$ for arbitrary $\varepsilon > 0$; see [LaBu73], [MaQu85], [LaBu73], [Il16].

Theorem 7 (Lavrent'ev, et. al., 1973, Markoe, Quinto, 1985, Ilmavirta, 2016a). *Suppose that $W \in C^{1+\varepsilon}(\mathbb{R}^2 \times \mathbb{S}^1)$ for arbitrary $\varepsilon > 0$ and*

$$W \geq c > 0, \ \|W\|_{C^{1+\varepsilon}(\mathbb{R}^2 \times \mathbb{S}^1)} \leq N, \tag{2.154}$$

for some constants c, N. Then, for any $p > 2$, there exists $\delta = \delta(\varepsilon, c, N, p) > 0$ such that P_W is injective on $L^p(B(x, \delta))$ for any $x \in \mathbb{R}^2$, where

$$\begin{aligned} &L^p(B(x,\delta)) = \{f \in L^p(\mathbb{R}^2) : \operatorname{supp} f \subset \bar{B}(x,\delta)\}, \\ &\bar{B}(x,\delta) = \{x' \in \mathbb{R}^2 : |x - x'| \leq \delta\}. \end{aligned} \tag{2.155}$$

The aforementioned publications for Theorem 7 differ, in particular, in regularity assumptions on W, going from C^∞ in [LaBu73], down to $C^{1+\varepsilon}$ in [Il16].

Note that the result of Theorem 7 directly implies the result of Theorem 6. The proof of Theorem 6 is so short and simple, so we present it here:

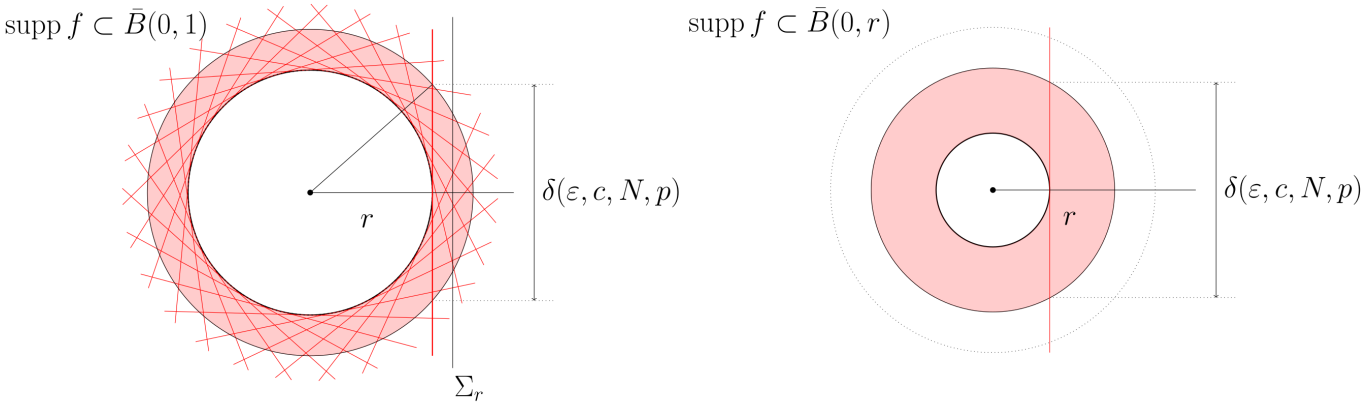

Figure 2.34 Boundary stripping method

Proof. Let $d \geq 3$ and suppose that $f \in \ker P_W$, $f \neq 0$, $f \in \operatorname{supp} \bar{B}(0,1)$. Any two-plane Σ_r whose distance from the origin is $r > 0$ meets $\bar{B}(0,1)$ in a plane subset Ω_r whose diameter is bounded by $d(r) \leq 2\sqrt{1-r^2} > 0$. Choosing r such that $d(r) \leq \delta$ for δ from Theorem 7 we have that $f \equiv 0$ in $\bar{B}(0,1) \backslash B(0,r)$. Iterating this argument for ball $\bar{B}(0,r)$ and further we have that $f \equiv 0$ on $\mathbb{R}^d$. □

The above method of proving injectivity of P_W for $d \geq 3$ is known as *boundary stripping method* (see also Figure 2.34) and it is widely used as a main tool in many publications, for example, in [Fi86], [Il16]. Note also that the argument of overdeterminancy of the inverse problem for P_W for $d \geq 3$ is crucial here. In the case of R_W, when the inverse problem is non-overdetermined, the situation is completely different.

From Theorem 7 we know that R_W is *locally injective* for $d = 2$ (in dimension $d = 2$ transforms P_W and R_W are equivalent up to change of variables). That is, having assumption (2.14) on W satisfied with some "additional regularity" R_W is injective on test-functions with sufficiently small support. But what happens if we assume bigger support of test-functions, or equivalently, is there *a global injectivity* of R_W for $d \geq 2$ and for W satisfying (2.14), maybe with some additional regularity assumptions?

The first answer to this question could be given by the famous result of J. Boman [Bo93]:

Theorem 8 (J. Boman, 1993)**.** *There exist a function $f \in C_c^\infty(\mathbb{R}^2)$, $f \neq 0$ and W satisfying (2.14) for $d = 2$ and also infinitely smooth, such that*

$$R_W f \equiv 0 \text{ on } \mathbb{R} \times \mathbb{S}^1. \tag{2.156}$$

In particular, this result shows the importance of the overdeterminancy on the injectivity properties for inverse problems for P_W, R_W. It is also interesting that R_W for weight W constructed in [Bo93], is not globally injective on $C_c^\infty(\mathbb{R}^2)$ but is still locally-injective because of Theorem 7. The difference between local and global injectivities for R_W can be intuitively explained using a perturbation argument for R_W. Informally, for weights W satisfying (2.14) and "smooth enough", the action of R_W on test-functions with "small" support can be approximated by action of classical Radon transform R (R_W for $W \equiv 1$) plus some

integral operator K_W with a small norm on functions with small support (for, example, integral operators with regular kernel functions). An example of using such argument with rigorous quantifications of all above steps can be found, for example, in [MaQu85].

Interestingly, for weights W which have "symmetries", transform R_W can be injective even under reasonably mild regularity assumptions. A particular example are *rotation invariant* weights W which also arise in PET; see [Qu83].

Definition 4 (Quinto, 1983)**.** Weight $W = W(x, \theta)$ is called rotation invariant if it can be written in the following form:

$$W(x, \theta) = U(|x - (x\theta)\theta|, x\theta),\ x \in \mathbb{R}^d,\ \theta \in \mathbb{S}^{d-1}, \tag{2.157}$$

where U is some strictly positive, continuous function on $\mathbb{R}^2$ such that

$$U(r, s) = U(-r, s) = U(r, -s) \text{ for all } (r, s) \in \mathbb{R}^2. \tag{2.158}$$

Note also that symmetries (2.157), (2.158) can be also written as

$$W(x, \theta) = \tilde{U}(|x|, x\theta),\ x \in \mathbb{R}^d,\ \theta \in \mathbb{S}^{d-1}, \tag{2.159}$$

$$\tilde{U}(r, s) = \tilde{U}(-r, s) = \tilde{U}(r, -s),\ (r, s) \in \mathbb{R}^2, \tag{2.160}$$

where $\tilde{U}$ is continuous and strictly positive on $\mathbb{R}^2$.

For weighted Radon transforms R_W with rotation invariant weights the following injectivity result holds

Theorem 9 (Quinto, 1983)**.** *Let W satisfy* (2.14)*, $W \in C^\infty(\mathbb{R}^d \times \mathbb{S}^{d-1})$, $d \geq 2$, and be rotation invariant. Then, $R_W : L^2_c(\mathbb{R}^d) \to L^2(\mathbb{R} \times \mathbb{S}^{d-1})$ is injective.*

Remark 9. In fact, in the above theorem assumption $W \in C^\infty(\mathbb{R}^d \times \mathbb{S}^{d-1})$ could be replaced by $W \in C^1(\mathbb{R}^d \times \mathbb{S}^{d-1})$ in dimensions $d = 2$, 3; see [Qu83].

Though the inverse problem for R_W for rotation invariant weights is non-overdetermined, the symmetry of W compensates the lack of smoothness. In particular, the weight W in the counterexample of J. Boman was not rotation-invariant.

Concluding the exposition of known injectivity results for R_W for $d \geq 2$, we present the following theorem

Theorem 10 (Boman, Quinto, 1987)**.** *Assume that $(s_0, \theta_0) \in \mathbb{R} \times \mathbb{S}^{d-1}$ and $f \in \mathcal{E}'(\mathbb{R}^d)$ (distributions on $\mathbb{R}^d$ with compact support). Let $W(x, \theta)$ satisfy* (2.14)*, be real-analytic function on $\mathbb{R}^d \times \mathbb{S}^{d-1}$ and even in θ, i.e., $W(x, \theta) = W(x, -\theta)$. Let V be an open neighborhood of θ_0. Finally, assume that $R_W f(s, \theta) = 0$ for $s > s_0$ and $\theta \in V$. Then $f = 0$ on the half-space $x\theta_0 > s_0$.*

Corollary 10.1. *Let f be a continuous function with compact support on $\mathbb{R}^d$ and W satisfy conditions of the above theorem. If $R_W f(s, \theta) \equiv 0$ on $\mathbb{R} \times \mathbb{S}^{d-1}$, then $f \equiv 0$.*

Interestingly, together with Boman's counterexample the above results uncover another phase transition of injectivity of R_W. Though C^∞-regularity was not enough for injectivity for general weights, analyticity of W spreads injectivity for R_W on compactly supported test-functions. The proof of Theorem 10 is based on theory of analytic elliptic pseudodifferential operators and of analytic wave front sets [BQ87]. Similar considerations could be performed for smooth non-analytic weights, but then, it is well-known that a general elliptic

pseudodifferential operator may have a smooth compactly supported function in its kernel.

Now, having in hand all of the above classical results we can pass to our contributions from Part II of the thesis. In particular, our contributions consist of three counterexamples to the above injectivity theorems, when assumptions on weights slightly relaxed. First, we start by a counterexample from Article 3 (Chapter 5), which we see as the simplest one. Next, we proceed with our results from Articles 4, 5 (Chapters 6, 7), where the constructed counterexamples are more interesting and unexpected.

Resume of Article 3. Let

$$(e_1, \dots e_d) \text{ be a canonical basis in } \mathbb{R}^d, \tag{2.161}$$

$$\Theta(v_1, v_2) = \{\theta \in \mathbb{S}^{d-1} : \theta \perp v_1,\, \theta \perp v_2\} \simeq \mathbb{S}^{d-3},\, v_1, v_2 \in \mathbb{R}^d,\, v_1 \perp v_2, \tag{2.162}$$

where $\perp$ denotes the orthogonality between two vectors in $\mathbb{R}^d$.

Theorem 11. *For $d \geq 3$, there are W and f, such that*

$$R_W f \equiv 0 \text{ on } \mathbb{R} \times \mathbb{S}^{d-1}, \tag{2.163}$$

$$W \text{ satisfies (2.14)},\, f \in C_c^\infty(\mathbb{R}^d),\, f \neq 0. \tag{2.164}$$

In addition

$$W \text{ is } C^\infty\text{– smooth on } \mathbb{R}^d \times (\mathbb{S}^{d-1} \backslash \Theta(e_1, e_2)), \tag{2.165}$$

where e_1, e_2 and $\Theta(e_1, e_2)$ are defined in (2.161), (2.162).

This result can be seen as an attempt to construct an example of non-injectivity of R_W in higher dimensions $d \geq 3$, with similar properties of W as in Theorem 8 of J. Boman. We recall that the inverse problem for R_W is non-overdetermined, so it could be expected that Theorem 8 admits direct analogs in higher dimensions.

In Theorem 11, from (2.162), (2.165) one can see that W is infinitely smooth only almost everywhere on $\mathbb{R}^d \times \mathbb{S}^{d-1}$, whereas in the example of Boman the weight was of class C^∞ on the whole space. In fact, on set $\mathbb{R}^d \times \Theta(e_1, e_2)$ from (2.165) which is of measure zero, the weight in our example has a discontinuity of the second type. Such discontinuity is a particular property of our construction, and we believe that an another example of non-injectivity of R_W with everywhere smooth W could be constructed.

Resume of Article 4.

Theorem 12. *There exist a non-zero spherically symmetric function $f \in C_c^\infty(\mathbb{R}^3)$ with support in a closed unit ball, and weight W satisfying (2.14) and also being rotation invariant (see Definition 4), such that*

$$R_W f \equiv 0 \text{ on } \mathbb{R} \times \mathbb{S}^2. \tag{2.166}$$

This result is already an improvement of Theorem 11 for $d = 3$, where the weight was satisfying (2.14) but was not yet continuous at some points. Note also that R_W is injective on $L_c^2(\mathbb{R}^3)$ if W satisfies (2.14) and is, at least, C^1-smooth (by Theorem 9 for $d = 3$). The above theorem makes the regularity assumption on W to be crucial for this injectivity result. It is important to note that the construction of W and f was developed in a large extent adopting the Boman's counterexample from Theorem 8.

Though in Theorem 12 the weight is not infinitely smooth, as in the example of Boman, the rotation invariance of W is the principle advantage of our construction.

The rotation invariance of W and spherical symmetry of f allow to extend Theorem 12 in the way as follows.

Consider $\tilde{U}$ and $\tilde{f}$ such that

$$W(x,\theta)=\tilde{U}(|x|,|x\theta|),\ f(x)=\tilde{f}(|x|),\ x\in\mathbb{R}^3,\ \theta\in\mathbb{S}^2, \tag{2.167}$$

where W and f are the functions from Theorem 12. Here we used that W is rotation invariant (see formulas (2.159), (2.160)) and f is spherically symmetric.

Corollary 12.1. *Let W and f be defined as*

$$W(x,P)=\tilde{U}(|x|,\operatorname{dist}(P,\{0\})),\ P\in\mathcal{P}^{d,2},\ x\in P, \tag{2.168}$$

$$f(x)=\tilde{f}(|x|),\ x\in\mathbb{R}^d, \tag{2.169}$$

where P is a two-dimensional oriented plane in $\mathbb{R}^d$, i.e., $P\in\mathcal{P}^{d,2}$, $\operatorname{dist}(P,\{0\})$ denotes distance from the origin $\{0\}\in\mathbb{R}^d$ to plane P, $\tilde{U}$ and $\tilde{f}$ are the functions from (2.167)*, $d>3$. Then,*

$$R_W^{d,2}f\equiv 0 \text{ on } \mathcal{P}^{d,2}. \tag{2.170}$$

In addition, the weight W is continuous strictly positive and rotation invariant, f is infinitely smooth compactly supported on $\mathbb{R}^d$ and $f\not\equiv 0$.

In this case, the obtained counterexample is much more interesting, because the inverse problem for $R_W^{d,2}$, $d>3$, is already overdetermined. Indeed,

$$\dim\mathcal{P}^{d,2}=3d-6>\dim\mathbb{R}^d=d \text{ for } d>3. \tag{2.171}$$

This injectivity example gave us the intuition that a similar development could be performed for P_W for $d\geq 3$. In particular, we could expect P_W for $d\geq 3$ to be not injective if the regularity assumption for W is reduced from $C^{1+\varepsilon}$ down to, say, continuity.

Resume of Article 5. Adopting and developing considerations from Article 5 and from [Bo93] we had obtained the following result.

Let

$$\Omega=\mathbb{R}^d\times\mathbb{S}^{d-1}, \tag{2.172}$$

$$\Omega(\Lambda)=\{(x,\theta)\in\mathbb{R}^d\times\mathbb{S}^{d-1}:|x-(x\theta)\theta|\in\Lambda\},\ \Lambda\subset[0,+\infty). \tag{2.173}$$

In view of (2.15), (2.22) set $\Omega(\Lambda)$ from (2.173) can be interpreted as points on rays in $\mathbb{R}^d$, where the value of distance between a ray and the origin $\{0\}\in\mathbb{R}^d$ belongs to $\Lambda\subset[0,+\infty)$.

Theorem 13. *There exists a weight W satisfying* (2.14) *and a non-zero function $f\in C_c^\infty(\mathbb{R}^d)$, $d\geq 2$, such that*

$$P_Wf\equiv 0 \text{ on } T\mathbb{S}^{d-1}, \tag{2.174}$$

where P_W is defined in (2.17)*. In addition, W is rotation invariant, i.e., satisfies* (2.157)*,* (2.158)*, and f is spherically symmetric with support in a closed unit ball. Moreover,*

$$W\in C^\infty(\Omega\backslash\Omega(\{1\})), \tag{2.175}$$

$$W\in C^\alpha(\mathbb{R}^d\times\mathbb{S}^{d-1}) \text{ for } \alpha\in(0,\alpha_0),\ \alpha_0=1/16, \tag{2.176}$$

$$W\geq 1/2 \text{ on } \Omega \text{ and } W\equiv 1 \text{ on } \Omega([1,+\infty)), \tag{2.177}$$

$$W(x,\theta)\equiv 1 \text{ for } |x|\geq R>1,\ \theta\in\mathbb{S}^{d-1}, \tag{2.178}$$

where $\Omega,\Omega(\{1\}),\Omega([1,+\infty))$ are defined by (2.172)*,* (2.173)*, R is a constant.*

This result is very surprising for several reasons. First, this is already a counterexample to Theorem 9 when the regularity assumption on W is slightly relaxed from C^1 in dimensions $d = 2, 3$, and from C^2 for $d > 3$ down to C^α, $\alpha \in (0, 1/16)$. Apart from this, the constructed example of non-injectivity for P_W for $d \geq 3$ is remarkable because the inverse problem for P_W is overdetermined (see (2.153)) and is injective for $W \in C^{1+\varepsilon}$, $\varepsilon > 0$, by Theorem 6. Moreover, because the global injectivity of P_W for $d \geq 3$ is consequence of local-injectivity for $d = 2$ (by Theorem 7 and the boundary stripping method), we automatically obtain a counterexample to local-injectivity.

Corollary 13.1. *For any $\alpha \in (0, 1/16)$ there is $N > 0$ such that for any $\delta > 0$ there are W_δ, f_δ satisfying*

$$W_\delta \geq 1/2,\ W_\delta \in C^\alpha(\mathbb{R}^2 \times \mathbb{S}^1),\ \|W_\delta\|_{C^\alpha(\mathbb{R}^2\times\mathbb{S}^1)} \leq N, \tag{2.179}$$

$$f_\delta \in C^\infty(\mathbb{R}^2),\ f_\delta \neq 0,\ \operatorname{supp} f_\delta \subset \bar{B}(0, \delta), \tag{2.180}$$

$$P_{W_\delta} f_\delta \equiv 0 \text{ on } T\mathbb{S}^1. \tag{2.181}$$

The best way to understand Corollary 13.1 is to rexplain Theorem 7. According to this theorem, P_W for $d = 2$ is injective on functions with sufficiently small support, provided that W is at least C^1-smooth. Moreover, the "smallness" of the support depends on "smoothness" of the weight; see definition for δ in Theorem 7. The above corollary states exactly that local-injectivity for P_W for $d = 2$ can be violated if W is a little bit less smooth than C^1![17]

Another interesting corollary of Theorem 13 is related to property (2.178). In particular, we used this property and the compact support of f to construct new weights W such that P_W will act on functions supported on disjoint balls in the same way as in Theorem 13.

Theorem 14. *For any $n \in \mathbb{N} \cup \{\infty\}$ there exists a weight W_n satisfying* (2.14) *such that*

$$\dim \ker P_{W_n} \geq n \text{ on } C_c^\infty(\mathbb{R}^d),\ d \geq 2, \tag{2.182}$$

where P_W is defined in (2.17)*. Moreover,*

$$W_n \in C^\infty(\mathbb{R}^2 \times \mathbb{S}^1) \text{ for } d = 2, \tag{2.183}$$

$$W_n \text{ is infinitely smooth almost everywhere on } \mathbb{R}^d \times \mathbb{S}^{d-1}, \tag{2.184}$$

$$W_n \in C^\alpha(\mathbb{R}^d \times \mathbb{S}^{d-1}),\ \alpha \in (0, 1/16) \text{ for } d \geq 3, \tag{2.185}$$

$$W_n(x, \theta) \equiv 1 \text{ for } |x| \geq R > 1,\ \theta \in \mathbb{S}^{d-1} \text{ for } n \in \mathbb{N},\ d \geq 2, \tag{2.186}$$

where R is a constant.

To our knowledge, examples of W satisfying (2.14) such that $\dim \ker P_W \geq n$ for arbitrary $n \in \mathbb{N} \cup \infty$ were not given in literature before our work even for $n = 1$ in dimension $d \geq 3$ and even for $n = 2$ in dimension $d = 2$.

Finalizing the exposition of our contributions from Part II, we would like to note that all of the results of Articles 3-5 were obtained by developing, in particular, considerations of Boman from [Bo93]. It appeared that his original counterexample had some degree of freedom in choosing how to start the construction process. First, we observed this degree of freedom in Article 4 and managed to develop it in further in Article 5. In particular, the title for Part II of the thesis "A breakdown of injectivity for weighted Radon transforms" is devoted to our results from Article 5. The details of our proofs and constructions are presented in Chapters 5-7.

[17] Apart of direct geometric interpretation given for Corollary 13.1, it is very interesting to understand this result in terms of PDEs. It is well-known that P_W for W satisfying (2.14) is related to elliptic pseudodifferential operators, for which it is expected to have some form of *unique continuation property*: basically, if $Pu = 0$, where P is elliptic operator and u vanishes in too big set, then $u \equiv 0$ everywhere. A study of this remark could be a topic for future research.

5 Conclusions

The main results of the present work can be summarized as follows:

1. We present new approach of solving inverse problems for weighted ray transforms which is based on the reduction to inverse problems for weighted Radon transforms.

2. We apply the aforementioned approach to inverse problems in tomographies. In particular, we show that the tomographical data modeled by weighted ray transforms and acquired in slice-by-slice reconstruction approach can be reduced to the new data modeled by weighted Radon transforms (for another weight) over planes in three-dimensions. Such reduction is of particular importance for tomographies, because it can strongly reduce the impact of noise on reconstructions.

3. We present two new inversion methods for weighted Radon transforms in multidimensions: one method is an extension of Chang's approximate inversion formula and the other one is an extension of Kunyansky's iterative algorithm.

4. Using the aforementioned approach based on reduction of the inverse problems in tomographies we present numerical tests of our new reconstruction methods. In particular, we test our reconstruction methods in the framework of single-photon emission computed tomography (SPECT). Our tests include experiments on synthetic and real data. For the case of synthetic data, i.e., when a comparison between reconstructions by different methods is possible, our new approach appears to be numerically more stable against noise than the conventional reconstruction methods used in slice-by-slice reconstruction approach. By the numerical test on real data we show that our approach is also applicable in real SPECT procedures.

5. We continue studies of injectivity and non-injectivity of weighted ray and Radon transforms for arbitrary strictly positive weights. In particular, we establish a series of new results on non-injectivity of the latter.

6. We construct an example of non-injectivity for weighted Radon transforms in multidimensions with strictly positive weight which is also infinitely smooth almost everywhere. This result can be seen as an attempt to extend the famous counterexample to injectivity by Boman (1993) to higher dimensions $d \geq 3$.

7. We construct an example of non-injectivity for weighted Radon transforms along two-dimension planes in $\mathbb{R}^d$, $d \geq 3$, such that the weight is continuous, rotation invariant and strictly positive. This result is already very unexpected for two reasons:

   (i). By Quinto (1983) it was proved that weighted Radon transforms R_W for positive rotation invariant weights are injective if W is C^∞-smooth (C^1 in dimensions $d = 2, 3$). Our result shows that smoothness assumption was crucial for this injectivity result.

   (ii). The inverse problem for weighted Radon transforms along two-dimensional planes in $\mathbb{R}^d$ is overdetermined for $d > 3$. Though there were no results on injectivity and non-injectivity in a such setting, usually the overdeterminancy leads to injectivity of Radon-type transforms.

8. We construct a counterexample to injectivity for weighted ray transforms in dimensions $d \geq 2$, where the weight is positive, rotation invariant and Hölder smooth. This result is very surprising in view of many known injectivity results for weighted ray transforms

when W is at least C^1-smooth. From this result it follows that the smoothness of the weight is crucial for these injectivity results, even if the corresponding inverse problems are overdetermined. Informally, such phenomenon we called by "breakdown of injectivity" for weighted ray transforms.

One can propose, in particular, the following possible developments of the subjects studied in the thesis:

1. The formulas for the reduction of the inverse problem for weighted ray transforms to the inverse problem for weighted Radon transforms from Article 1 yet do not give a complete mathematical answer why the reconstructions become more stable numerically. The effect of noise regularization could be studied in more detail.

2. Possibly, the counterexample from Article 3 could be adapted to construct a new counterexample to injectivity for weighted Radon transforms in multidimensions. In particular, in the new example it would be important to construct a weight which is strictly positive and infinitely smooth everywhere. This would complete the extension of counterexample of J. Boman (1993) to dimensions $d \geq 3$.

3. It is very interesting to find an interpretation of the counterexample to injectivity from Article 5 in terms of PDE's and the theory of elliptic pseudo-differential operators. In particular, to operators P_W, R_W it is possible to associate some pseudo-differential operators which will appear to be elliptic under the assumption that weight W is positive. The injectivity of the aforementioned weighted Radon-type transforms is closely related to properties of these elliptic operators. In particular, a compactly supported function in the kernel of an elliptic differential operator means the violation of the well-known unique continuation property for this class of operators. One example of such violation is especially interesting, constructed by Pliś [Pl63]. In particular, from the example of Pliś it follows that there is a breakdown of unique continuation property for elliptic operators if the coefficients in the operator are Hölder smooth or less.

Bibliography

[AdOk17] J. Adler, O. Öktem, Solving ill-posed inverse problems using iterative deep neural networks. *Inverse Problems*, 33(12): 124007, 2017

[Ag14] A. D. Agaltsov, Imaging and integral geometry. *Essay, Lomonosov Moscow State University, (unpublished)*, 2014.

[Ag15] A. D. Agaltsov, A characterization theorem for a generalized Radon transform arising in a model of mathematical economics. *Functional Analysis and Its Applications*, 49(3): 201-204, 2015.

[Ag+18] A. D. Agaltsov, E. G. Molchanov, A. A. Shananin, Inverse Problems in Models of Resource Distribution. *The Journal of Geometric Analysis*, 28(1): 726-765, 2018.

[AG07] S. Alinhac, P. Gérard. Pseudo-differential operators and the Nash-Moser theorem. *American Mathematical Soc.*, Vol.82, 2007.

[Ar+98] E.V. Arbuzov, A. L. Bukhgeim, S. G. Kazantsev. Two-dimensional tomography problems and the theory of A-analytic functions. *Siberian Advances in Mathematics* 8(4): 1-20, 1998.

[Ba05] G. Bal, Ray transforms in hyperbolic geometry. *Journal de mathématiques pures et appliquées*, 84(10): 1362-1392, 2005.

[Ba09] G. Bal, Inverse transport theory and applications, *Inverse Problems*, 25(5), 053001, 2009.

[BJ11] G. Bal, A. Jollivet, Combined source and attenuation reconstructions in SPECT. Tomography and Inverse Transport Theory, Contemp. Math, 559, 13-27, 2011.

[BM04] H. H. Barrett, K. K. Myers, Foundation of Imaging Science, *Wiley Interscience*, New York, 2004.

[Be84] G. Beylkin, The inversion problem and applications of the generalized Radon transform. *Communications on pure and applied mathematics*, 37(5): 579-599, 1984.

[Br56] R. N. Bracewell, Strip integration in radio astronomy. *Australian Journal of Physics*, 9(2): 198-217, 1956.

[Bo06] H. Bockwinkel, On the propagation of light in a biaxial crystal about a midpoint of oscillation. *Verh. Konink Acad. V. Wet. Wissen. Natur.*, 14: 636, 1906.

[BQ87] J. Boman, E. T. Quinto, Support theorems for real-analytic Radon transforms. *Stockholm Universitet*, Matematika Institutionen, 1987.

[Bo93] J. Boman, An example of non-uniqueness for a generalized Radon transform. *Journal d'Analyse Mathématique*, 61(1): 395-401, 1993.

[Bo04] J. Boman, J.-O. Strömberg. Novikov's inversion formula for the attenuated Radon transform—a new approach. *The Journal of Geometric Analysis* 14(2), 2004.

[Bo11] J. Boman, Local non-injectivity for weighted Radon transforms. *Contemp. Math* 559: 39-47, 2011.

[Br00] A. V. Bronnikov, Reconstruction of attenuation map using discrete consistency conditions. *IEEE Transactions on medical imaging* 19(5): 451-462, 2000.

[Ch78] L.-T. Chang, A method for attenuation correction in radionuclide computed tomography. *IEEE Transactions on Nuclear Science*, 25(1): 638-643, 1978.

[Co63] A. M. Cormack, Representation of a function by its line integrals, with some radiological applications, *Journal of applied physics*, 34(9): 2722-2727, 1963.

[Co64] A. M. Cormack, Representation of a function by its line integrals, with some radiological applications. II, *Journal of applied physics*, 35(10): 2908-2913, 1963.

[Co80] Allan M. Cormack – Biographical. NobelPrize.org. NobelMedia AB 2019.

[Co80a] A. M. Cormack, Recollections of my work with computer assisted tomography. *Molecular and cellular biochemistry*, 32(2): 57-61, 1980.

[CrDeP07] F. Crepaldi, A, R. De Pierro, Activity and attenuation reconstruction for positron emission tomography using emission data only via maximum likelihood and iterative data refinement. *IEEE Transactions on Nuclear Science*, 54(1): 100-106, 2007.

[Da10] S. Dann, On the Minkowski-Funk transform. arXiv preprint: 1003.5565, 2010.

[De07] S. R. Deans, The Radon transform and some of its applications, Courier Corporation, 2007.

[EMI] History of EMI, Ltd. http://www.emimusci.com/about/history/

[Fa+01] A. Faridani, K. A. Buglione, P. Huabsomboon, O. D. Iancu, J. McGrath, Introduction to local tomography. Contemporary Mathematics 278: 29-48, 2001.

[Fi86] D. Finch, Uniqueness for attenuated X-ray transform in the physical range. *Inverse Problems*, 2(2), 1986.

[Fi03] D. V. Finch, The attenuated X-ray transform: recent developments. *Inverse Problems and Applications*, (edited by G. Uhlmann), 47-66, 2003.

[Fr89] K. Fritz, Inversion of k-plane Transforms and Applications in Computer Tomographies. *SIAM Review*, 31(2): 273-298, 1989

[Fri+08] B. Frigyik, P. Stefanov, G. Uhlmann, The X-ray transform for a generic family of curves and weights, *Journal of Geometric Analysis*, 18(1), 2008.

[Fu13] P. Funk, Uber Flächen mit lauter geschlossenen geodätischen Linien. *Mathematische Annalen, Band 74*, 1913.

[Fu13a] P. Funk, Nachruf auf Prof. Johann Radon. *Mathematische Nachrichten*, 62: 191-199, 1913.

[Ga+08] H. M. Gach, C. Tanase, F. Boada. 2D & 3D Shepp-Logan phantom standards for MRI. *19th International Conference on Systems Engineering*, pp. 521-526, 2008.

[G+03] I. M. Gelfand, S. Gindikin, M. Graev, Selected topics in integral geometry. *American Mathematical Soc.*, Vol. 220, 2003

[G+59] I. M Gelfand, M. I. Graev. Geometry of homogeneous spaces, representations of groups in homogeneous spaces and related questions of integral geometry. *Trudy Moskov. Mat. Obshch.*, 8:321–390, 1959.

[G+69] I. M. Gelfand, M. I. Graev, Z. Y. Shapiro. Differential forms and integral geometry. *Functional Anal. and Appl.*, 3:24–40, 1969.

[G+62] I. M. Gelfand, M. I. Graev, N. J. Vilenkin. Obobshchennye funktsii, Vyp. 5. Integralnaya geometriya i svyazannye s nei voprosy teorii predstavlenii, *Gosudarstv. Izdat. Fiz.-Mat. Lit.*, 1962.

[Gi10] S. Gindikin, A remark on the weighted Radon transform on the plane. *Inverse Problems & Imaging* 4(4): 649-653, 2010.

[Go17] F. O. Goncharov, An iterative inversion of weighted Radon transforms along hyperplanes. *Inverse Problems*, 33(12): 124005, 2017.

[GN16] F. O. Goncharov, R. G. Novikov, An analog of Chang inversion formula for weighted Radon transforms in multidimensions. *Eurasian Journal of Mathematical and Computer Applications*, 4(2): 23-32, 2016.

[GoNo17] F. O. Goncharov, R. G. Novikov, An example of non-uniqueness for Radon transforms with continuous positive rotation invariant weights. *The Journal of Geometric Analysis*, 28(4), 2017.

[GoNo17a] F. O. Goncharov, R. G. Novikov, A breakdown of injectivity for weighted ray transforms in multidimensions. *arXiv preprint*, arXiv: 1711.060163 (to appear in Arkiv för Matematik), 2019.

[GoNo18] F. O. Goncharov, R. G. Novikov, An example of non-uniqueness for weighted Radon transforms along hyperplanes in multidimensions. *Inverse Problems*, 34 054001, 2018.

[Gr91] P. Grangeat, Mathematical framework of cone beam 3D reconstruction via the first derivative of the Radon transform. *Mathematical methods in tomography*, pp. 66-97, 1991.

[Gu+02] J.-P. Guillement, F. Jauberteau, L. Kunyansky, R. G. Novikov, R. Trebossen. On single-photon emission computed tomography imaging based on an exact formula for the nonuniform attenuation correction. *Inverse Problems*, 18(6): L11, 2002.

[GuNo08] J.-P. Guillement, R. G. Novikov, On Wiener type filters in SPECT. *Inverse Problems*, 24(2), 2008

[GuNo05] J.-P. Guillement, R. G. Novikov, On the data dependent filtration techniques in single-photon emission computed tomography. *hal archives*, hal-00009611, 2005.

[GuNo12] J.-P. Guillement, R. G. Novikov, Optimized analytic reconstruction for SPECT. *Journal of Invers and Ill-Posed Problems*, 20(4): 489-500, 2012.

[GuNo14] J-P. Guillement, R. G. Novikov, Inversion of weighted Radon transforms via finite Fourier series weight approximations. *Inverse Problems in Science and Engineering*, 22(5): 787-802, 2014.

[Gu+16] C. Guillarmou, G. P. Paternain, M. Salo, G. Gunther Uhlmann. The X-ray transform for connections in negative curvature. *Communications in Mathematical Physics*, 343(1): 83-127, 2016.

[He99] S. Helgason, The Radon transform. Vol.2. Boston: Birkhäuser, 1999.

[HeSh90] G. M. Henkin, A. A. Shananin, Bernstein theorems and Radon transform. Application to the theory of production functions. *AMS: Translation of mathematical monographs*, 81: 189-223, 1990.

[HC58] Harish-Chandra, Spherical functions on a semi-simple Lie group I. *American Journal of Mathematics*, 80:241–310, 1958.

[HC58a] Harish-Chandra, Spherical functions on a semi-simple Lie group II. *American Journal of Mathematics*, 80: 553–613, 1958.

[He65] S. Helgason. Radon-Fourier transforms on symmetric spaces and related group representations. *Bull. Amer. Math. Soc.*, 71: 757–763, 1965.

[He65a] S. Helgason, The Radon transform on Euclidean spaces, compact two-point homogeneous spaces and Grassman manifolds. *Acta Math.*, 113:153–180, 1965.

[He66] S. Helgason. A duality in integral geometry on symmetric spaces. *In Proc. U.S.-Japan Seminar in Differential Geometry, Kyoto*, 1965.

[He70] S. Helgason. A duality for symmetric spaces, with applications to group representations. *Advances in Math.*, 5:1–154, 1970.

[HoWe16] T. Hohage, F. Werner, Inverse problems with Poisson data: statistical regularization theory. Applications and algorithms. *Inverse Problems*, 32(9), 093001, 2016.

[Ho71] G. Hounsfield, Method and Apparatus for measuring X- or gamma-radiation absorption or transmission at plural angles and analyzing the data. *United States Patent US3778614A, Assigned to EMI Limited*, 1971.

[Ho80] G. Hounsfield, Godfrey N. Hounsfield – Biographical. *NobelPrize.org. NobelMedia AB 2019. Mon. 11 Mar*, 2019.

[Il16] J. Ilmavirta, On Radon transforms on compact Lie groups. *Proceedings of the American Mathematical Society*, 144(2): 681-691, 2016.

[Il19] J. Ilmavirta, J. Rassalo, Geodesic ray transform with matrix weights for piecewise constant functions *arXiv preprint*, arXiv:1901.030525, 2019.

[Jo55] F. John, Plane Waves and Spherical Means Applied to Partial Differential Equations. Dover Publications, 1955.

[Il16] J. Ilmavirta, Coherent quantum tomography. *SIAM Journal on Mathematical Analysis*, 48(5): 3039-3064, 2016.

[Kat02] A. Katsevich, Theoretically exact filtered backprojection-type inversion algorithm for spiral CT. *SIAM Journal on Applied Mathematics*, 62(6): 2012-2026, 2002.

[Ka93] L. Kaufman, Maximum likelihood, least squares, and penalized least squares for PET. *IEEE Transactions on Medical Imaging*, 12(2): 200-214, 1993.

[Ka18] S. Kazantsev, Funk-Minkowski transform and spherical convolution of Hilbert type and reconstructing functions on the sphere. *arXiv preprint* arxiv:1806.06672, 2018.

[K+09] J. Keiner, S. Kunis, D. Potts, Using NFFT 3 - a software library for various nonequispaced fast Fourier transforms. *ACM Trans. Math. Software*, 36, Article 19, 1-30, 2009.

[Ku06] P. Kuchement, Generalized transforms of Radon-type and their applications. *Proceedings of Symposia in Applied Mathematics*, 2006.

[Ku14] P. Kuchement, The Radon transform and medical imaging, *SIAM*, Vol. 85., 2014.

[K+95] Kuchment, P., Lancaster, K., Mogilevskaya L., On local tomography. *Inverse Problems*, 11(3): 571-589, 1995.

[Ku92] Kunyansky, L., Generalized and attenuated Radon transforms: restorative approach to the numerical inversion. *Inverse Problems*, 8(5): 809-819, 1992.

[Kun01] L. Kunyansky, A new SPECT reconstruction algorithm based on Novikov explicit inversion formula. *Inverse Problems*, 17(2), 2001.

[LaBu73] M. M. Lavrent'ev, A. L. Bukhgeim, A class of operator equations of the first kind. *Functional Analysis and Its Applications*, 7(4): 290-298, 1973.

[La+86] M. Lavrent'ev, V. G. Romanov, S. P. Shishatski, Ill-posed problems of mathematical physics. *American Mathematical Society*, Vol. 64, 1986.

[Ma27] Ph. Mader, Über die Darstellung von Punktfunktionen im n-dimensionalen euklidischen Raum durch Ebenenintegrale. *Math. Zeit*, 26: 646-652, 1927.

[Ma84] A. Markoe, Fourier inversion of the attenuated X-ray transform. *SIAM Journal on Mathematical Analysis*, 15(4): 718-722, 1984.

[MaQu85] A. Markoe, E. T. Quinto, An elementary proof of local invertibility for generalized and attenuated Radon transforms. *SIAM Journal on Mathematical Analysis*, 16(5): 1114-1119, 1985.

[Mi+87] D. Miller, M. Oristaglio, G. Beylkin, A new slant on seismic imaging: Migration and integral geometry. *Geophysics*, 52(7): 943-964, 1987.

[Mi04] H. Minkowski, About bodies of constant width, *Mathematics Sbornik*, 25: 505-508, 1904.

[MiDeP11] E. Miqueles, A. R. De Pierro, Iterative reconstruction in X-ray fluorescence tomography based on Radon transform. *IEEE Transactions on medical imaging*, 30(2): 438-450, 2011.

[Mu+87] K. Murase, H. Itoh, H. Mogami, M. Ishine, M. Kawamura, A. Lio, K. Hamamoto, A comparative study of attenuation correction algorithms in single photon emission computed tomography (SPECT). *European Journal on Nuclear Medicine*, 13: 55-62, 1987.

[Na86] F. Natterer, The mathematics of computerized tomography, *SIAM*, Vol. 32, 1986.

[Na99] F. Natterer, Mathematical methods in tomography, *Acta Numerica* 8: 107-141, 1999.

[Na01] F. Natterer, Inversion of the attenuated Radon transform. *Inverse problems*, 17(1), 2001.

[Ngu+09] M. K. Nguyen, T.T. Truong, D. Driol, H. Zaidi, On a novel approach to Compton scattered emission imaging. IEEE Transactions on Nuclear Science, 56(3): 1430-1437, 2009.

[No11] R. G. Novikov, Weighted Radon transforms for which Chang's approximate inversion formula is exact. *Russian Mathematical Surveys* 66(2), 2011.

[No14] R. G. Novikov, Weighted Radon transforms and first order differential systems on the plane. *Moscow Mathematical Journal*, 14(4): 807–823, 2014.

[No02a] Novikov, R.G., On determination of a gauge field on $\mathbb{R}^d$ from its non-abelian Radon transform along oriented straight lines. *Journal of the Institute of Mathematics of Jussieu*, 1(4), 559-629., 2002.

[Pa+12] G. P. Paternain, M. Salo, G. Uhlmann, The attenuated ray transform for connections and Higgs fields. *Geometric and functional analysis*, 22(5): 1460-1489, 2012.

[No02] R. G. Novikov, An inversion formula for the attenuated X-ray transform. Arkiv für Mathematik, 40(1): 145-167, 2002.

[Pi19] J. Pietzsch, With a Little Help from My Friends. *NobelPrize.org. Nobel Media AB 2019. Fri. 8 Mar*, 2019.

[Pl63] A. Pliś, On non-uniqueness in Cauchy problem for an elliptic second order differential equation. *Bull. Acad. Polon. Sci. Sér. Sci. Math. Astronom. Phys 11*, 1963.

[Ra17] J. Radon, Über die Bestimmung von Funktionen durch ihre Integralwerte längs gewisser Mannigfaltigkeiten. *Ber. Saechs Akad. Wiss. Leipzig, Math-Phys*, 69:262–267, 1917.

[RaSch18] R. Ramlau, O. Scherzer, The first 100 years of Radon transform, *Inverse Problems*, 34 090201, 2018.

[Sh93] V. A. Sharafutdinov, Uniqueness theorems for the exponential X-ray transform. *Journal of Inverse and Ill-Posed Problems*, 1(4): 355-372, 1993

[Sh12] V. A. Sharafutdinov, Integral geometry of tensor fields, *Walter de Gruyter*, Vol. 1, 2012.

[SL74] L. Shepp, B. Logan, The Fourier reconstruction of a head section. *IEEE Transactions on nuclear science*, 21(3): 21-43, 1974.

[SW16] E. M. Stein, G. Weiss. Introduction to Fourier analysis on Euclidean spaces (PMS-32), Princeton University Press, 2016.

[St82] R. S. Strichartz, Radon inversion–variations on a theme. *The American Mathematical Monthly*, 89(6): 377-423, 1982.

[St91] R. S. Strichartz, L^p harmonic analysis and Radon transforms on the Heisenberg group. *Journal of functional Analysis*, 96(2): 350-406, 1991.

[TiAr77] A. N. Tikhonov, V. Ya. Arsenin, Methods of solving ill-posed problems, *Nauka*, Moscow, 1974.

[To96] P. Toft, The Radon Transform: Theory and Implementation. PhD Thesis, Technical University of Denmark, 1996.

[TM80] O. Tretiak, C. Metz. The exponential Radon transform. *SIAM Journal on Applied Mathematics*, 39(2): 341-354, 1980.

[Qu80] E. T. Quinto, The dependence of the generalized Radon transforms on defining measures. *Transactions on the American Mathematical Society*, 257(2): 331-346, 1980.

[Qu83] E. T. Quinto, The invertibility of rotation invariant Radon transforms. *Journal of Mathematical Analysis and Applications*, 91(2): 510-522, 1983.

[Qu93] E. T. Quinto, Singularities of the X-ray transform and limited data tomography in $\mathbb{R}^2$ and $\mathbb{R}^3$. *SIAM Journal on Mathematical Analysis*, 24(5): 1215-1225, 1993.

[Qu06] E. T. Quinto, An introduction to X-ray tomography and Radon transforms. *Proceedings of symposia in Applied Mathematics, Vol. 63*, 2006.

[Qu+14] E. T. Quinto, G. Ambartsoumian, R. Felea, V. Krishnan, C. Nolan, Microlocal Analysis and Imaging, a short note in "The mathematics of the planet Earth". Chapter 7, pages 8-11, Springer, Berlin, New York, 2014.

[Qu+18] E. T. Quinto, C. Grathwohl, P. Kunstmann, A. Rieder, Microlocal Analysis of imaging operators for effective common offset seismic reconstruction. *Inverse Problems*, 34(11), 2018.

[V-Sl+15] K. Van Slambrouck, S. Stute, C. Comtat, M. Sibomana, F.H. van Velden, R. Boellaard, J. Nuyts, Bias reduction for low-statistics PET: maximum likelihood reconstruction with a modified Poisson distribution. *IEEE Transactions on medical imaging*, 34(1): 126-136, 2015.

[Va+16] M. Vassholz, B. Koberstein-Schwarz, A. Ruhlandt, M. Krenkel, T. Salditt, New X-ray tomography method based on the 3D Radon transform compatible with anisotropic sources. *Physical review letters*, 116(8): 088101, 2016.

[Wa08] J. Wang, H. Lu, Z. Liang, D. Eremina, G. Zhang, S. Wang, J. Chen, J. Manzione, An experimental study on the noise properties of X-ray CT sinogram data in Radon space, *Physics in Medicine & Biology*, 53(12): 3327, 2008.

Part I

Inversions of weighted Radon transforms in 3D

Article 1. An analog of Chang inversion formula for weighted Radon transforms in multidimensions

F. O. Goncharov, R. G. Novikov

In this work we study weighted Radon transforms in multidimensions. We introduce an analog of Chang approximate inversion formula for such transforms and describe all weights for which this formula is exact. In addition, we indicate possible tomographical applications of inversion methods for weighted Radon transforms in 3D.

1 Introduction

We consider the weighted Radon transforms R_W defined by the formula

$$R_W f(s,\theta) \stackrel{\text{def}}{=} \int\limits_{x\theta=s} W(x,\theta) f(x) dx, \tag{3.1}$$
$$(s,\theta) \in \mathbb{R}\times\mathbb{S}^{n-1},\ x\in\mathbb{R}^n,\ n\geq 2,$$

where $W = W(x,\theta)$ is the weight, $f = f(x)$ is a test function; see e.g. [BQ87]. Such transforms arise in many domains of pure and applied mathematics; see e.g. [De07], [DuBi84], [GGV14], [Gr91], [Ku92], [Na86]. In the present work we assume that

$$\begin{aligned} &W \text{ is complex – valued,}\\ &W\in C(\mathbb{R}^n\times\mathbb{S}^{n-1})\cap L^\infty(\mathbb{R}^n\times\mathbb{S}^{n-1}),\\ &w_0(x) \stackrel{\text{def}}{=} \frac{1}{\text{vol}(\mathbb{S}^{n-1})}\int\limits_{\mathbb{S}^{n-1}} W(x,\theta)\,d\theta \neq 0,\ x\in\mathbb{R}^n, \end{aligned} \tag{3.2}$$

where $d\theta$ is the element of standard measure on $\mathbb{S}^{n-1}$, $|\mathbb{S}^{n-1}|$ is the standard measure of $\mathbb{S}^{n-1}$.

If $W\equiv 1$, then $R = R_W$ is the classical Radon transform in $\mathbb{R}^n$; see for example [GGV14], [He11], [Lu96], [Ra17]. Explicit inversion formulas for R were given for the first time in [Ra17].

In dimension $n = 2$, the transforms R_W are also known as weighted ray transforms on the plane; see e.g. [Ku92], [Na86]. For several important cases of W satisfying (3.2) for $d = 2$, explicit (and exact) inversion formulas for R_W were obtained in [BS04], [Gi10], [No02b], [No11], [TM80].

On the other hand, it seems that no explicit inversion formulas for R_W were given yet in the literature under assumptions (3.2) for $n\geq 3$, if $W\neq w_0$.

In the present work we introduce an analog of Chang approximate (but explicit) inversion formula for R_W under assumptions (3.2), for $n \geq 3$, and describe all W for which this formula is exact. These results are presented in Section 2.

In addition, we indicate possible tomographical applications of inversion methods for R_W in dimension $n = 3$. These considerations are presented in Section 3.

2 Chang-type formulas in multidimensions

We consider the following approximate inversion formulas for R_W under assumptions (3.2) in dimension $n \geq 2$:

$$f_{appr}(x) \stackrel{\text{def}}{=} \frac{(-1)^{(n-2)/2}}{2(2\pi)^{n-1} w_0(x)} \int\limits_{\mathbb{S}^{n-1}} \mathbb{H}\left[R_W f\right]^{(n-1)}(x\theta, \theta) d\theta, \tag{3.3}$$

$x \in \mathbb{R}^n$, n is even,

$$f_{appr}(x) \stackrel{\text{def}}{=} \frac{(-1)^{(n-1)/2}}{2(2\pi)^{n-1} w_0(x)} \int\limits_{\mathbb{S}^{n-1}} \left[R_W f\right]^{(n-1)}(x\theta, \theta) d\theta, \tag{3.4}$$

$x \in \mathbb{R}^n$, n is odd,

$$\left[R_W f\right]^{(n-1)}(s, \theta) = \frac{d^{n-1}}{ds^{n-1}} R_W f(s, \theta), s \in \mathbb{R}, \theta \in \mathbb{S}^{n-1}, \tag{3.5}$$

$$\mathbb{H}\phi(s) \stackrel{\text{def}}{=} \frac{1}{\pi} p.v. \int\limits_{\mathbb{R}} \frac{\phi(t)}{s-t} dt, \; s \in \mathbb{R}. \tag{3.6}$$

For $W \equiv 1$ formulas (3.3), (3.4) are exact, i.e. $f_{appr} = f$, and are known as the classical Radon inversion formulas, going back to [Ra17].

As a corollary of the classical Radon inversion formulas and definition (3.1), formulas (3.3), (3.4) for $W \equiv w_0$ are also exact.

Formula (3.3) for $n = 2$ is known as Chang approximate inversion formula for weighted Radon transforms on the plane. This explicit but approximate inversion formula was suggested for the first time in [Ch78] for the case when

$$W(x, \theta) = \exp\left(-Da(x, \theta^{\perp})\right), \tag{3.7}$$

$$Da(x, \theta^{\perp}) = \int\limits_0^{+\infty} a(x + t\theta^{\perp}) dt, \tag{3.8}$$

where a is a non-negative sufficiently regular function on $\mathbb{R}^2$ with compact support, and $\theta = (\theta_1, \theta_2) \in \mathbb{S}^{n-1}$, $\theta^{\perp} = (\theta_2, -\theta_1)$. We recall that R_W for W given by (3.7), (3.8) is known as attenuated Radon transform on the plane and arises, in particular, in the single photon emission tomography (SPECT). In this case an explicit and simultaneously exact inversion formula for R_W was obtained for the first time in [No02b].

We emphasize that formulas (3.3), (3.4) are approximate, in general. In addition, the following result holds:

Theorem 1. *Let W satisfy (3.2). Let f_{appr} be defined by (3.3), (3.4) in terms of $R_W f$ and w_0, $n \geq 2$. Then $f_{appr} = f$ (in the sense of distributions) on $\mathbb{R}^n$ for all $f \in C_0(\mathbb{R}^n)$ if and only if*

$$W(x, \theta) - w_0(x) \equiv w_0(x) - W(x, -\theta), \; x \in \mathbb{R}^n, \; \theta \in \mathbb{S}^{n-1}. \tag{3.9}$$

Here $C_0(\mathbb{R}^n)$ denotes the space of all continous compactly supported functions on $\mathbb{R}^n$.

The result of Theorem 1 for $n = 2$ was obtained for the first time in [No11]. Theorem 1 in the general case is proved in Section 4.

If W satisfy (3.2), $f \in C_0(\mathbb{R}^n)$, but the the symmetry condition (3.9) does not hold, i.e.

$$w_0(x) \neq \frac{1}{2}\left(W(x,\theta) + W(x,-\theta)\right), \text{ for some } x \in \mathbb{R}^n,\ \theta \in \mathbb{S}^{n-1},$$

then (3.3), (3.4) can be considered as approximate formulas for finding f from $R_W f$.

3 Weighted Radon transforms in 3D in tomographies

In several tomographies the measured data are modeled by weighted ray transforms $P_w f$ defined by the formula

$$P_w f(x,\alpha) = \int\limits_{\mathbb{R}} w(x+\alpha t,\alpha) f(x+\alpha t)\, dt,\ (x,\alpha) \in T\mathbb{S}^2, \tag{3.10}$$
$$T\mathbb{S}^2 = \{(x,\alpha) \in \mathbb{R}^3 \times \mathbb{S}^2 : x\alpha = 0\},$$

where f is an object function defined on $\mathbb{R}^3$, w is the weight function defined on $\mathbb{R}^3 \times \mathbb{S}^2$, and $T\mathbb{S}^2$ can be considered as the set of all rays (oriented straight lines) in $\mathbb{R}^3$. In particular, in the case of the single-photon emission computed tomography (SPECT) the weight w is given by formulas (3.7), (3.8), where $\theta^\perp = \alpha \in \mathbb{S}^2$, $x \in \mathbb{R}^3$.

In practical tomographical considerations $P_w f(x,\alpha)$ usually arises for rays (x,α) parallel to some fixed plane

$$\Sigma_\eta = \{x \in \mathbb{R}^3 : x\eta = 0\},\ \eta \in \mathbb{S}^2, \tag{3.11}$$

i.e., for $\alpha\eta = 0$.

The point is that the following formulas hold:

$$R_W f(s,\theta) = \int\limits_{\mathbb{R}} P_w f(s\theta + \tau[\theta,\alpha],\alpha) d\tau,\ s \in \mathbb{R},\ \theta \in \mathbb{S}^2, \tag{3.12}$$
$$W(x,\theta) = w(x,\alpha),\ \alpha = \alpha(\eta,\theta) = \frac{[\eta,\theta]}{|[\eta,\theta]|},\ [\eta,\theta] \neq 0,\ x \in \mathbb{R}^3,$$

where $[\cdot,\cdot]$ stands for the standart vector product in $\mathbb{R}^3$.

Due to formula (3.12) the measured tomographical data modeled by $P_w f$ can be reduced to averaged data modeled by $R_W f$. In particular, this reduction drastically reduces the level of random noise in the initial data.

Therefore, formula (3.4) for $n = 3$ and other possible methods for finding f from $R_W f$ in 3D may be important for tomographies, where measured data are modeled by $P_w f$ of (3.10).

Remark 1. The weight W arising in (3.12) is not continuous, in general. However, the result of Theorem 1 remains valid for this W, at least, under the assumptions that w is bounded and continuous on $\mathbb{R}^3 \times \mathbb{S}^2$, and $w_0(x) \neq 0$, $x \in \mathbb{R}^3$, where w_0 is defined in (3.2).

4 Proof of Theorem 1

For W satisfying (3.2) we also consider its symmetrization defined by

$$W_s(x,\theta) \stackrel{\text{def}}{=} \frac{1}{2}\left(W(x,\theta) + W(x,-\theta)\right),\ x \in \mathbb{R}^n,\ \theta \in \mathbb{S}^{n-1}. \tag{3.13}$$

Using definitions (3.1), (3.13) we obtain

$$R_{W_s}f(s,\theta) = \frac{1}{2}\left(R_W f(s,\theta) + R_W f(-s,-\theta)\right). \tag{3.14}$$

In addition, if W satisfies (3.9), then

$$W_s(x,\theta) = w_0(x),\ x \in \mathbb{R}^n,\ \theta \in \mathbb{S}^{n-1}. \tag{3.15}$$

4.1 Proof of sufficiency

The sufficiency of symmetry (3.9) follows from formulas (3.3), (3.4) for the exact case with $W \equiv w_0$, the identities

$$f_{appr}(x) = \frac{(-1)^{(n-2)/2}}{2(2\pi)^{n-1}w_0(x)} \int\limits_{\mathbb{S}^{n-1}} \mathbb{H}\left[R_{W_s}f\right]^{(n-1)}(x\theta,\theta)d\theta, \tag{3.16}$$

for even n,

$$f_{appr}(x) = \frac{(-1)^{(n-1)/2}}{2(2\pi)^{n-1}w_0(x)} \int\limits_{\mathbb{S}^{n-1}} \left[R_{W_s}f\right]^{(n-1)}(x\theta,\theta)d\theta, \tag{3.17}$$

for odd n,

and from the identities (3.14), (3.15).

In turn, (3.16) follows from the identities

$$\begin{aligned}
&\int\limits_{\mathbb{S}^{n-1}} \mathbb{H}\left[R_W f\right]^{(n-1)}(x\theta,\theta)d\theta \\
&= \frac{1}{2}\int\limits_{\mathbb{S}^{n-1}} \left(\mathbb{H}\left[R_W f\right]^{(n-1)}(x\theta,\theta) + \mathbb{H}\left[R_W f\right]^{(n-1)}(-x\theta,-\theta)\right)d\theta \\
&= \int\limits_{\mathbb{S}^{n-1}} \mathbb{H}\left[R_{W_s}f\right]^{(n-1)}(x\theta,\theta)d\theta.
\end{aligned} \tag{3.18}$$

In addition, the second of the identities of (3.18) follows from the identities:

$$\begin{aligned}
\mathbb{H}\left[R_{W_s}f\right]^{(n-1)}(s,\theta) &= \frac{1}{2\pi}p.v.\int\limits_{\mathbb{R}} \frac{1}{s-t}\times \\
&\times \frac{d^{n-1}}{dt^{n-1}}\Big[R_W f(t,\theta) + R_W f(-t,-\theta)\Big]dt \\
&= \frac{1}{2}\mathbb{H}\Big[R_W f\Big]^{(n-1)}(s,\theta) + \frac{(-1)^{n-1}}{2\pi}p.v.\int\limits_{\mathbb{R}} \frac{\left[R_W f\right]^{(n-1)}(-t,-\theta)}{s-t}dt;
\end{aligned} \tag{3.19}$$

$$\begin{aligned}
\frac{(-1)^{n-1}}{\pi}p.v.\int\limits_{\mathbb{R}} \frac{\left[R_W f\right]^{(n-1)}(-t,-\theta)}{s-t}dt &= -\frac{(-1)^{n-1}}{\pi}p.v.\int\limits_{\mathbb{R}} \frac{\left[R_W f\right]^{(n-1)}(t,-\theta)}{-s-t}dt \\
&= (-1)^n\mathbb{H}\left[R_W f\right]^{(n-1)}(-s,-\theta) = \mathbb{H}\left[R_W f\right]^{(n-1)}(-s,-\theta).
\end{aligned} \tag{3.20}$$

This concludes the proof of sufficiency for n even.

Finally, (3.17) follows from the identities

$$\int\limits_{\mathbb{S}^{n-1}} [R_W f]^{(n-1)}(x\theta,\theta)d\theta$$
$$= \frac{1}{2}\int\limits_{\mathbb{S}^{n-1}} \Big([R_W f]^{(n-1)}(x\theta,\theta) + [R_W f]^{(n-1)}(-x\theta,-\theta)\Big)\, d\theta, \tag{3.21}$$

$$\begin{aligned}[R_{W_s} f]^{(n-1)}(t,\theta) &= \frac{1}{2}\frac{d^{n-1}}{dt^{n-1}}\Big[[R_W f](t,\theta) + [R_W f](-t,-\theta)\Big] \\ &= \frac{1}{2}\Big[[R_W f]^{(n-1)}(t,\theta) + (-1)^{n-1}[R_W f]^{(n-1)}(-t,-\theta)\Big] \\ &= \frac{1}{2}\Big[[R_W f]^{(n-1)}(t,\theta) + [R_W f]^{(n-1)}(-t,-\theta)\Big]. \end{aligned} \tag{3.22}$$

This concludes the proof of sufficiency for odd n.

4.2 Proof of necessity

Using that $f_{appr} = f$ for all $f \in C_0(\mathbb{R}^n)$ and using formulas (3.3), (3.4) for the exact case $W \equiv w_0$, we obtain

$$\int\limits_{\mathbb{S}^{n-1}} \Big(\mathbb{H}\,[R_W f]^{(n-1)}(x\theta,\theta) - \mathbb{H}\,[R_{w_0} f]^{(n-1)}(x\theta,\theta)\Big)\, d\theta = 0 \tag{3.23}$$

on $\mathbb{R}^n$ for even n,

$$\int\limits_{\mathbb{S}^{n-1}} [R_W f - R_{w_0} f]^{(n-1)}(x\theta,\theta)d\theta = 0 \tag{3.24}$$

on $\mathbb{R}^n$ for odd n,

for all $f \in C_0(\mathbb{R}^n)$.

Identities (3.18), (3.21), (3.22), (3.23), (3.24) imply the identities

$$\int\limits_{\mathbb{S}^{n-1}} \Big(\mathbb{H}\,[R_{W_s} f]^{(n-1)}(x\theta,\theta) - \mathbb{H}\,[R_{w_0} f]^{(n-1)}(x\theta,\theta)\Big)\, d\theta = 0 \tag{3.25}$$

on $\mathbb{R}^n$ for even n,

$$\int\limits_{\mathbb{S}^{n-1}} [R_{W_s} f - R_{w_0} f]^{(n-1)}(x\theta,\theta)d\theta = 0 \tag{3.26}$$

on $\mathbb{R}^n$ for odd n,

for all $f \in C_0(\mathbb{R}^n)$.

The necessity of symmetry (3.9) follows from the identities (3.25), (3.26) and the following lemmas:

Lemma 1. *Let* (3.25), (3.26) *be valid for fixed* $f \in C_0(\mathbb{R}^n)$ *and* W *satisfying* (3.2), $n \geq 2$. *Then*

$$R_{W_s} f = R_{w_0} f. \tag{3.27}$$

Lemma 2. *Let* (3.27) *be valid for all* $f \in C_0(\mathbb{R}^n)$ *and fixed* W *satisfying* (3.2), $n \geq 2$. *Then*

$$W_s = w_0. \tag{3.28}$$

Lemmas 1 and 2 are proved in Sections 5 and 6.

5 Proof of Lemma 1

We will use the following formulas

$$\int\limits_{\mathbb{R}^n} e^{i\xi x} \int\limits_{\mathbb{S}^{n-1}} g(x\theta,\theta)\, d\theta\, dx$$
$$= \frac{\sqrt{2\pi}}{|\xi|^{n-1}} \left(\hat{g}\left(|\xi|, \frac{\xi}{|\xi|} \right) + \hat{g}\left(-|\xi|, -\frac{\xi}{|\xi|} \right) \right), \tag{3.29}$$
$$\int\limits_{\mathbb{R}^n} e^{i\xi x} \int\limits_{\mathbb{S}^{n-1}} g^{(n-1)}(x\theta,\theta)\, d\theta\, dx = \int\limits_{\mathbb{R}^n} e^{i\xi x} \int\limits_{\mathbb{S}^{n-1}} (\theta\nabla_x)^{n-1} g(x\theta,\theta)\, d\theta\, dx$$
$$= (-i)^{n-1}\sqrt{2\pi} \left(\hat{g}\left(|\xi|, \frac{\xi}{|\xi|} \right) + (-1)^{n-1} \hat{g}\left(-|\xi|, -\frac{\xi}{|\xi|} \right) \right), \tag{3.30}$$
$$\hat{g}(\tau,\theta) = \frac{1}{\sqrt{2\pi}} \int\limits_{\mathbb{R}} e^{i\tau s} g(s,\theta) ds,\ \tau \in \mathbb{R},\ \theta \in \mathbb{S}^{n-1}, \tag{3.31}$$

where $g \in C(\mathbb{S}^{n-1}, L^2(\mathbb{R}))$, $\xi \in \mathbb{R}^n$. The validity of formulas (3.29), (3.30) (in the sense of distributions) follows from Theorem 1.4 of [Na86].

5.1 The case of odd n

Using identity (3.14) we get

$$g(s,\theta) = g(-s,-\theta),\ \text{for all } s \in \mathbb{R},\ \theta \in \mathbb{S}^{n-1}, \tag{3.32}$$

where

$$g(s,\theta) = \left[R_{W_s} f(s,\theta) - R_{w_0} f(s,\theta) \right]. \tag{3.33}$$

From (3.32), we obtain the same symmetry for the Fourier transform $\hat{g}(\cdot,\theta)$ of $g(\cdot,\theta)$:

$$\begin{aligned} \hat{g}(t,\theta) &= \frac{1}{\sqrt{2\pi}} \int\limits_{\mathbb{R}} g(s,\theta) e^{its} ds \\ &= \frac{1}{\sqrt{2\pi}} \int\limits_{\mathbb{R}} g(-s,-\theta) e^{i(-s)(-t)} ds \\ &= \frac{1}{\sqrt{2\pi}} \int\limits_{\mathbb{R}} g(s,-\theta) e^{-its} ds = \hat{g}(-t,-\theta), t \in \mathbb{R},\ \theta \in \mathbb{S}^{n-1}. \end{aligned} \tag{3.34}$$

For odd n, from identities (3.26), (3.30) it follows that

$$\hat{g}\left(|p|, \frac{p}{|p|} \right) + \hat{g}\left(-|p|, -\frac{p}{|p|} \right) = 0 \text{ in } L^2_{loc}(\mathbb{R}^n). \tag{3.35}$$

Using (3.34), (3.35) we obtain

$$\begin{cases} \hat{g}\left(|p|, \frac{p}{|p|} \right) = 0, \\ \hat{g}\left(-|p|, -\frac{p}{|p|} \right) = 0 \end{cases} \Leftrightarrow \hat{g} = 0 \Leftrightarrow g = 0. \tag{3.36}$$

Formula (3.27) for odd n follows from (3.33), (3.36).

5.2 The case of even n

We consider

$$g(s,\theta) = \mathbb{H}\left[R_{W_s}f - R_{w_0}f\right](s,\theta),\ s\in\mathbb{R},\ \theta\in\mathbb{S}^{n-1}, \tag{3.37}$$

arising in (3.25). Using the identity

$$\begin{aligned}\mathbb{H}\left[R_{W_s}f - R_{w_0}f\right](-s,-\theta) &= \frac{1}{\pi}p.v.\int\limits_{\mathbb{R}}\frac{R_{W_s}f(t,-\theta)-R_{w_0}f(t,-\theta)}{-s-t}dt \qquad (3.38)\\ &= \frac{1}{\pi}p.v.\int\limits_{\mathbb{R}}\frac{R_{W_s}f(-t,-\theta)-R_{w_0}f(-t,-\theta)}{-s+t}dt\\ &= -\frac{1}{\pi}p.v.\int\limits_{\mathbb{R}}\frac{R_{W_s}f(t,\theta)-R_{w_0}f(t,\theta)}{s-t}dt = -\mathbb{H}\left[R_{W_s}f - R_{w_0}\right](s,\theta),\end{aligned}$$

we obtain

$$g(s,\theta) = -g(-s,-\theta),\ \text{for all } s\in\mathbb{R},\ \theta\in\mathbb{S}^{n-1}. \tag{3.39}$$

From (3.39), similarly with (3.34), we obtain the same symmetry for the Fourier transform $\hat{g}(\cdot,\theta)$ of $g(\cdot,\theta)$:

$$\hat{g}(t,\theta) = -\hat{g}(-t,-\theta),\ t\in\mathbb{R},\theta\in\mathbb{S}^{n-1}. \tag{3.40}$$

For n even, from the property of the Hilbert transform

$$\mathbb{H}\left[\phi^{(k)}\right] = \left(\mathbb{H}\left[\phi\right]\right)^{(k)},\ \phi\in C_0^k(\mathbb{R}),$$

where this identity holds in the sense of distributions if $\phi\in C_0(\mathbb{R})$, and identities (3.25), (3.30) it follows that

$$\hat{g}\left(|p|,\frac{p}{|p|}\right) - \hat{g}\left(-|p|,-\frac{p}{|p|}\right) = 0 \text{ in } L^2_{loc}(\mathbb{R}^n). \tag{3.41}$$

Using (3.40), (3.41) we again obtain (3.36) but already for even n. Due to (3.36), (3.37) we have

$$\mathbb{H}\left[R_{W_s}f - R_{w_0}f\right] = 0. \tag{3.42}$$

Formula (3.27) for even n follows from (3.42), invertibility of the Hilbert transform on L^p, $p>1$ and the fact that $R_W f\in C_0(\mathbb{R}\times\mathbb{S}^{n-1})$.

Lemma 1 is proved.

6 Proof of Lemma 2

Suppose that

$$W_s(y,\theta) - w_0(y) = z\neq 0 \tag{3.43}$$

for some $y\in\mathbb{R}^n$, $\theta\in\mathbb{S}^{n-1}$, $z\in\mathbb{C}$. Since W satisfies (3.2), then for any $\varepsilon>0$ there exists $\delta(\varepsilon)>0$ such that

$$\forall\, y' : |y'-y|<\delta \to |W_s(y',\theta) - w_0(y') - z| < \varepsilon, \tag{3.44}$$

for fixed y,θ.

Let $f\in C_0(\mathbb{R}^n)$, $f\geq 0$ and satisfies the conditions

$$f(y') \equiv 1,\ y'\in B_{\delta/2}(y), \tag{3.45}$$

$$supp\, f \subset B_\delta(y), \tag{3.46}$$

where $B_\delta(y)$ is the open ball with radius δ, centered at y, $\delta = \delta(\varepsilon)$, $0 < \varepsilon < |z|$. It suffices to show that

$$|R_{W_s} f(y\theta, \theta) - R_{w_0} f(y\theta, \theta)| > 0, \tag{3.47}$$

which contradicts the condition of the lemma.

The identity (3.47) follows from the formulas

$$\begin{aligned}
&|R_{W_s}(y\theta, \theta) - R_{w_0}(y\theta, \theta)| = \Big| \int\limits_{x\theta = y\theta} f(x)(W_s(x, \theta) - w_0(x))dx \Big| \\
&= \Big| \int\limits_{x\theta = y\theta} f(x)(W_s(x, \theta) - w_0(x) - z)dx + z \int\limits_{x\theta = y\theta} f(x)dx \Big| \\
&\geq |z| \int\limits_{x\theta = y\theta} f(x)dx - \int\limits_{x\theta = y\theta} f(x) \left| W_s(x, \theta) - w_0(x) - z \right| dx \\
&\geq (|z| - \varepsilon) \int\limits_{x\theta = y\theta} f(x)dx > 0, \text{ for } 0 < \varepsilon < |z|.
\end{aligned} \tag{3.48}$$

Lemma 2 is proved.

Bibliography

[BQ87] J. Boman and E. T. Quinto, *Support theorems for real-analytic Radon transforms*, Duke Mathematical J., 55(4), (1987), 943-948.

[BS04] J. Boman and J. Strömberg, Novikov's inversion formula for the attenuated Radon transform – a new approach, *The Journal of Geometric Analysis*, 14(2), (2004), 185–198.

[Ch78] L. Chang, A method for attenuation correction in radionuclide computed tomography, *IEEE Transactions on Nuclear Science*, 25(1), (1978), 638–643.

[De07] S. R. Deans, The Radon Transform and some of Its Applications, *Courier Corporation*, 2007.

[DuBi84] T. Durrani and D. Bisset, The Radon transform and its properties, *Geophysics*, 49(8), (1984), 1180–1187.

[GGV14] I. M. Gel'fand, M. I. Graev, and N. Ya. Vilenkin, Integral Geometry and Representation Theory, *Academic press,* Vol. 5, 2014.

[Gi10] S. Gindikin, A remark on the weighted Radon transform on the plane, *Inverse Problems and Imaging*, 4, (2010), 649–653.

[Gr91] P. Grangeat, Mathematical framework of cone beam 3D reconstruction via the first derivative of the Radon transform, *Mathematical methods in tomography, Springer*, (1991), 66-97.

[He11] S. Helgason, The Radon Transform on R^n, *Springer*, 2011.

[Ku92] L. A. Kunyansky, Generalized and attenuated Radon transforms: restorative approach to the numerical inversion, *Inverse Problems*, 8(5), (1992), 809-819.

[Lu96] D. Ludwig, The Radon transform on Euclidean space, *Communications on Pure and Applied Mathematics*, 19(1), (1996), 49–81.

[Na86] F. Natterer, The Mathematics of Computerized Tomography, Vol. 32, *SIAM*, 1986.

[No02b] R. G. Novikov, An inversion formula for the attenuated X-ray transformation, *Arkiv för matematik*, 40(1), (2002), 145–167.

[No11] R. G. Novikov, Weighted Radon transforms for which Chang's approximate inversion formula is exact, *Russian Mathematical Surveys*, 66(2), (2011), 442–443.

[Ra17] J. Radon, Über die Bestimmung von Funktionen durch ihre Integralwerte längs gewisser Mannigfaltigkeiten. *Ber. Saechs Akad. Wiss. Leipzig, Math-Phys*, 69:262–267, 1917.

[TM80] O. Tretiak and C. Metz, The exponential Radon transform, *SIAM Journal on Applied Mathematics*, 39(2), (1980), 341–354.

Article 2. An iterative inversion of weighted Radon transforms in multidimensions

F. O. Goncharov

We propose iterative inversion algorithms for weighted Radon transforms R_W along hyperplanes in $\mathbb{R}^3$. More precisely, expanding the weight $W = W(x,\theta), x \in \mathbb{R}^3, \theta \in \mathbb{S}^2$, into the series of spherical harmonics in θ and assuming that the zero order term $w_{0,0}(x) \neq 0, x \in \mathbb{R}^3$, we reduce the inversion of R_W to solving a linear integral equation. In addition, under the assumption that the even part of W in θ (i.e., $\frac{1}{2}(W(x,\theta) + W(x,-\theta))$) is close to $w_{0,0}$, the aforementioned linear integral equation can be solved by the method of successive approximations. Approximate inversions of R_W are also given. Our results can be considered as an extension to 3D of two-dimensional results of Kunyansky (1992), Novikov (2014), Guillement, Novikov (2014). In our studies we are motivated, in particular, by problems of emission tomographies in 3D. In addition, we generalize our results to the case of dimension $n > 3$.

1 Introduction

We consider the weighted Radon transforms R_W defined by the formula

$$R_W f(s,\theta) = \int\limits_{x\theta=s} W(x,\theta) f(x)\, dx,\ (s,\theta) \in \mathbb{R} \times \mathbb{S}^2,\ x \in \mathbb{R}^3, \tag{4.1}$$

where $W = W(x,\theta)$ is the weight, $f = f(x)$ is a test function.

In this work we assume that

$$W \in C(\mathbb{R}^3 \times \mathbb{S}^2) \cap L^\infty(\mathbb{R}^3 \times \mathbb{S}^2), \tag{4.2}$$

$$w_{0,0}(x) \stackrel{\text{def}}{=} \frac{1}{4\pi} \int\limits_{\mathbb{S}^2} W(x,\theta)\, d\theta,\ w_{0,0}(x) \neq 0,\ x \in \mathbb{R}^3, \tag{4.3}$$

$$f \in L^\infty(\mathbb{R}^3),\ \operatorname{supp} f \subset D, \tag{4.4}$$

where W and f are complex-valued, $d\theta$ is element of standard measure on $\mathbb{S}^2$, D is an open bounded domain (which is fixed apriori).

If $W \equiv 1$, then R_W is reduced to the classical Radon transform along hyperplanes in $\mathbb{R}^3$ introduced in [Ra17]; see also, e.g., [Na86], [De2016].

For known results on the aforementioned transforms R_W with non-constant W we refer to [Qu83], [Be84], [BQ87], [GN16]. In particular, in [Qu83] it was shown that R_W is injective

on $L_0^p(\mathbb{R}^3)$, $p \geq 2$ (L^p functions on $\mathbb{R}^3$ with compact support) if $W \in C^2$ and is real-valued, strictly positive and satisfies the strong symmetry assumption of rotation invariancy (see [Qu83] for details). On the other hand, in [BQ87] it was also proved that R_W is injective if W is real-analytic and strictly positive.

Besides, in [Be84] the inversion of R_W is reduced to solving a Fredholm type linear integral equation in the case of infinitely smooth strictly positive W with the symmetry $W(x,\theta) = W(x,-\theta)$.

In turn, [GN16] extends to the case of weighted Radon transforms along hyperplanes in multidimensions the two-dimensional Chang approximate inversion formula (see [Ch78]) and the related two-dimensional result of [No11]. In particular, [GN16] describes all W for which such Chang-type formulas are simultaneously explicit and exact in multidimensions.

We recall that inversion methods for R_W admit tomographical applications in the framework of the scheme described as follows (see [GN16]).

It is well-known that in many tomographies measured data are modeled by weighted ray transforms $P_w f$ defined by the formula

$$P_w f(x,\alpha) = \int\limits_{\mathbb{R}} w(x+\alpha t,\alpha) f(x+\alpha t)\, dt,\ (x,\alpha) \in T\mathbb{S}^2, \tag{4.5}$$
$$T\mathbb{S}^2 = \{(x,\alpha) \in \mathbb{R}^3 \times \mathbb{S}^2 : x\alpha = 0\},$$

where f is an object function defined on $\mathbb{R}^3$, w is the weight function defined on $\mathbb{R}^3 \times \mathbb{S}^2$, and $T\mathbb{S}^2$ can be considered as the set of all rays (oriented straight lines) in $\mathbb{R}^3$, see, e.g., [Ch78], [Na86], [Ku92], [GuN14].

In addition, in [GN16] (Section 3) it was shown that if $P_w f$ are given for all rays parallel to some fixed plane Σ in $\mathbb{R}^3$ then $R_W f$ with appropriate W can be obtained by the explcit formulas from $P_w f$ and w (in a similair way with the case $w \equiv 1$, $W \equiv 1$, see Chapter 2, formula (1.1) of [Na86] and also [Gr91], [De2016]). Therefore, reconstruction of f from data modeled by $P_w f$, defined by (4.5) and restricted to all rays parallel to Σ, can be reduced to reconstruction of f from $R_W f$, defined by (4.1). In [GN16] it was aslo indicated that the reduction from $P_w f$ to $R_W f$ with subsequent reconstruction of f from $R_W f$ and W can drastically reduce the impact of the random noise in the initial data modeled as $P_w f$. This result of [GN16] is recalled by formulas (4.73)-(4.75) of Subsection 3.4.

In the present work we continue studies of [GN16], on one hand, and of [Ku92], [No14], [GuN14], on the other hand. In particular, we extend to the case of weighted Radon transforms along hyperplanes in multidimensions the two-dimensional results of [Ku92], [No14], [GuN14]. In particular, under the assumptions (4.2), (4.3), expanding $W = W(x,\theta)$ into the series of spherical harmonics in θ we reduce the reconstruction of f to solving a linear integral equation (see Section 3). In particular, if the even part of W in θ (i.e., $\tilde{W}(x,\theta) = \frac{1}{2}(W(x,\theta) + W(x,-\theta))$) is close to $w_{0,0}$, then such linear integral equation can be solved by the method of successive approximations (see Subsections 3.1, 3.3 for details).

Note that our linear integral equation is very different from the aforementioned linear integral equation of [Be84] (in particular, in our conditions on $\tilde{W}$, ensuring the applicability of the method of successive approximations).

Note also that in [Ch78], [Ku92], [No14], [GuN14] the two-dimensional prototype of our inversion approach was developed in view of its numerical efficiency in problems of emission tomographies, including good stability to strong random noise in the emission data.

In more details our results can be sketched as follows.

We use the following expansion for W:

$$W(x,\theta(\gamma,\phi)) = \sum_{k=0}^{\infty}\sum_{n=-k}^{k} w_{k,n}(x)Y_k^n(\gamma,\phi),\ x\in\mathbb{R}^3, \tag{4.6}$$

$$Y_k^n(\gamma,\phi) \stackrel{\text{def}}{=} p_k^{|n|}(\cos\gamma)e^{in\phi},\ k\in\mathbb{N}\cup\{0\},\ n=\overline{-k,k}, \tag{4.7}$$

$$\theta(\gamma,\phi) = (\cos\gamma,\ \sin\gamma\cos\phi,\ \sin\gamma\sin\phi)\in\mathbb{S}^2\subset\mathbb{R}^3,\ \gamma\in[0,\pi],\ \phi\in[0,2\pi], \tag{4.8}$$

where $p_k^n(x)$, $x\in[-1,1]$, are the associated Legendre polynomials with Schmidt semi-normalization. Polynomials p_k^n are well-known in literature (see e.g. [SW16]) and are defined using the ordinary Legendre polynomials p_k by the formulas:

$$p_k^n(x) = (-1)^n\sqrt{\frac{2(k-n)!}{(k+n)!}}(1-x^2)^{n/2}\frac{d^n}{dx^n}(p_k(x)),\ n,k\in\mathbb{N}\cup\{0\}, \tag{4.9}$$

$$p_k(x) = \frac{1}{2^k k!}\frac{d^k}{dx^k}[(x^2-1)^k],\ x\in[-1,1], \tag{4.10}$$

see also [SW16], [ZT79] for other properties of the associated Legendre polynomials. In addition, coefficients $w_{k,n}$ in (4.6) are defined by the formulas:

$$w_{k,n}(x) = c(k,n)\int_0^{2\pi} d\phi\, e^{-in\phi}\int_0^{\pi} W(x,\theta(\gamma,\phi))p_k^{|n|}(\cos\gamma)\sin\gamma\, d\gamma, \tag{4.11}$$

$$c(k,n) = \frac{(2k+1)}{8\pi},\ k\in\mathbb{N}\cup\{0\},\ n=0,\pm1,\cdots,\pm k.$$

Under assumption (4.2), for each fixed x, series (4.6) converge in $L^2(\mathbb{S}^2)$; see e.g. [SW16] (Chapter 4), [Mo98] (Chapter 2), [ZT79].

We consider also

$$\sigma_{\widetilde{W},D,m} = \sum_{k=1}^{m}\sum_{n=-2k}^{2k}\sup_{x\in D}\left|\frac{w_{2k,n}(x)}{w_{0,0}(x)}\right| \text{ for } m\in\mathbb{N}, \tag{4.12}$$

$$\sigma_{\widetilde{W},D,m} = 0 \text{ for } m=0,$$

$$\sigma_{\widetilde{W},D,\infty} = \lim_{m\to\infty}\sigma_{W,D,m}, \tag{4.13}$$

$$W_N(x,\theta(\gamma,\phi)) = \sum_{k=0}^{N}\sum_{n=-k}^{k} w_{k,n}(x)Y_k^n(\gamma,\phi), \tag{4.14}$$

$$\widetilde{W}_N(x,\theta(\gamma,\phi)) = \sum_{k=0}^{[N/2]}\sum_{n=-2k}^{2k} w_{2k,n}(x)Y_{2k}^n(\gamma,\phi), \tag{4.15}$$

$$x\in\mathbb{R}^3,\ \gamma\in[0,\pi],\ \phi\in[0,2\pi],$$

where coefficients $w_{k,n}$ are defined in (4.11), $[N/2]$ denotes the integer part of $N/2$.

Our expansion (4.6) and the related formulas are motivated by their two-dimensional prototypes of [Ku92], [No14], [GuN14].

In the present article we obtained, in particular, the following results under assumptions (4.2), (4.3), (4.4):

1. If $\sigma_{\widetilde{W},D,\infty} < 1$, then R_W is injective and, in addition, the inversion of R_W is given via formulas (4.52), (4.53); see Subsection 3.1 for details.

2. If $\sigma_{\widetilde{W},D,\infty} \geq 1$, then f can be approximately reconstructed from $R_W f$ as $f \approx (R_{\widetilde{W}_N})^{-1} R_W f$, where $R_{\widetilde{W}_N}$ is defined according to (4.1) for $\widetilde{W}_N$ defined by (4.15) for $N = 2m$, where m is chosen as the largest while condition $\sigma_{W,D,m} < 1$ holds. More precisely, approximate inversion of $R_W f$ is given via the formulas (4.57), (4.58); see Subsection 3.2 for details.

   In addition, if $W = W_N$ defined by (4.14) and $\sigma_{\widetilde{W},D,m} < 1$, $m = [N/2]$, then R_{W_N} is injective and invertible by formula (4.67); see Subsection 3.3 for details.

In addition, in these results assumptions (4.2), (4.3) can be relaxed as follows:

$$W \in L^\infty(\mathbb{R}^3 \times \mathbb{S}^2), \tag{4.16}$$

$$w_{0,0} \geq c > 0 \text{ on } \mathbb{R}^3, \tag{4.17}$$

where $w_{0,0}$ is defined (4.3), c is some positive constant.

Prototypes of these results for the weighted Radon transforms in 2D were obtained in [Ku92], [No14], [GuN14].

The present work also continues studies of [GN16], where approximate inversion of R_W was realized as $(R_{W_N})^{-1}$ for $N = 0$ or by other words as an approximate Chang-type inversion formula. We recall that the original two-dimensional Chang formula ([Ch78]) is often used as an efficient first approximation in the framework of slice-by-slice reconstructions in the single photon emission computed tomography.

In Section 2 we give some notations and preliminary results.

The main results of the present work are presented in detail in Section 3.

In Section 4 we generalize results of Sections 2, 3 for the case of dimension $n > 3$.

Proofs of results of Sections 2, 3, 4 are presented in Sections 5, 6.

2 Some preliminary results

2.1 Some formulas for R and R^{-1}

We recall that for the classical Radon transform R (formula (4.1) for $W \equiv 1$) the following identity holds (see [Na86], Theorem 1.2, p.13):

$$R(f *_{\mathbb{R}^3} g) = Rf *_{\mathbb{R}} Rg, \tag{4.18}$$

where $*_{\mathbb{R}^3}, *_{\mathbb{R}}$ denote the 3D and 1D convolutions (respectively), f, g are test functions.

The classical Radon inversion formula is defined as follows (see, e.g., [Na86]):

$$R^{-1}q(x) = -\frac{1}{8\pi^2} \int\limits_{\mathbb{S}^2} q^{(2)}(x\theta, \theta) d\theta,\ x \in \mathbb{R}^3, \tag{4.19}$$

$$q^{(2)}(s, \theta) = \frac{d^2}{ds^2} q(s, \theta),\ (s, \theta) \in \mathbb{R} \times \mathbb{S}^2,$$

where q is a test function on $\mathbb{R} \times \mathbb{S}^2$.

In addition, from the Projection theorem (see [Na86], Theorem 1.1, p.11) it follows that:

$$R^{-1}q(x) \stackrel{\text{def}}{=} \int\limits_{\mathbb{R}} \frac{\rho^2}{2} d\rho \int\limits_{\mathbb{S}^2} \hat{q}(\rho, \omega) e^{2\pi i \rho (x\omega)} d\omega,\ x \in \mathbb{R}^3, \tag{4.20}$$

$$\hat{q}(s, \theta) \stackrel{\text{def}}{=} \int\limits_{\mathbb{R}} q(t, \theta) e^{-2\pi i t s}\, dt,\ (s, \theta) \in \mathbb{R} \times \mathbb{S}^2, \tag{4.21}$$

where $q(t,\theta)$ is a test function on $\mathbb{R}\times\mathbb{S}^2$.

For the case of $\hat{q}$ even (i.e., $\hat{q}(s,\theta)=\hat{q}(-s,-\theta)$, $(s,\theta)\in\mathbb{R}\times\mathbb{S}^2$, where $\hat{q}$ is defined in (4.21)), formulas (4.20), (4.21) can be rewritten as follows:

$$R^{-1}q=\mathcal{F}[\hat{q}]=\mathcal{F}^{-1}[\hat{q}], \tag{4.22}$$

where $\mathcal{F}[\cdot],\mathcal{F}^{-1}[\cdot]$ denote the Fourier transform and its inverse in 3D, respectively, and are defined by the following formulas (in spherical coordinates):

$$\mathcal{F}[q](\xi)\stackrel{\text{def}}{=}\int\limits_0^{+\infty}\rho^2 d\rho\int\limits_{\mathbb{S}^2}q(\rho,\omega)e^{-2\pi i\rho(\xi\omega)}d\omega, \tag{4.23}$$

$$\mathcal{F}^{-1}[q](\xi)\stackrel{\text{def}}{=}\int\limits_0^{+\infty}\rho^2 d\rho\int\limits_{\mathbb{S}^2}q(\rho,\omega)e^{2\pi i\rho(\xi\omega)}d\omega,\ \xi\in\mathbb{R}^3, \tag{4.24}$$

where $q(\rho,\omega)$ is a test-function on $[0,+\infty)\times\mathbb{S}^2$ (identified with $\mathbb{R}^3$).

2.2 Symmetrization of W

Let

$$A_W f=R^{-1}R_W f, \tag{4.25}$$

where R_W is defined in (4.1), f is a test function, satisfying assumptions of (4.4).

Let

$$\widetilde{W}(x,\theta)\stackrel{\text{def}}{=}\frac{1}{2}(W(x,\theta)+W(x,-\theta)),\ x\in\mathbb{R}^3,\theta\in\mathbb{S}^2. \tag{4.26}$$

The following formulas hold:

$$A_W f=R^{-1}R_{\widetilde{W}}f, \tag{4.27}$$

$$R_{\widetilde{W}}f(s,\theta)=\frac{1}{2}(R_W f(s,\theta)+R_W f(-s,-\theta)),\ (s,\theta)\in\mathbb{R}\times\mathbb{S}^2, \tag{4.28}$$

$$\widetilde{W}(x,\theta(\gamma,\phi))=\sum_{k=0}^{\infty}\sum_{n=-2k}^{2k}w_{2k,n}(x)Y_{2k}^n(\gamma,\phi), \tag{4.29}$$

$x\in\mathbb{R}^3$, $\gamma\in[0,\pi]$, $\phi\in[0,2\pi]$.

Identity (4.27) is proved in [GN16] in 3D, where $\widetilde{W}$ is denoted as W_{sym}.

Identity (4.29) follows from (4.6), (4.7), (4.26) and the following identities:

$$p_k^n(-x)=(-1)^{n+k}p_k^n(x),\ x\in[-1,1], \tag{4.30}$$

$$e^{in(\phi+\pi)}=(-1)^n e^{in\phi},\ k\in\mathbb{N}\cup\{0\},\ n=\overline{-k,k}. \tag{4.31}$$

Note also that $\widetilde{W}_N$ defined by (4.15) is the approximation of $\widetilde{W}$ defined by (4.26) and

$$\widetilde{W}_N(x,\cdot)\xrightarrow[N\to\infty]{L^2(\mathbb{S}^2)}\widetilde{W}(x,\cdot)\text{ for each fixed }x\in\mathbb{R}^3. \tag{4.32}$$

Using formulas (4.28)-(4.29) we reduce inversion of R_W to the inversion of $R_{\widetilde{W}}$ defined by (4.1) for $W=\widetilde{W}$.

In our work $A_W f$ (or, more precisely, $(w_{0,0})^{-1}A_W f$) is used as the *initial point* for our iterative inversion algorithms (see Section 3).

Note that the simmetrization $\widetilde{W}$ of W arises in (4.27).

In addition, prototypes of (4.25), (4.27), (4.29) for the two-dimensional case can be found in [Ku92], [No11].

2.3 Operators $Q_{\widetilde{W},D,m}$ and numbers $\sigma_{\widetilde{W},D,m}$

Let

$$c \stackrel{\text{def}}{=} \inf_{x\in D} |w_{0,0}(x)| > 0, \tag{4.33}$$

where the inequality follows from the continuity of W on $\overline{D}$ (closure of D) and assumption (4.3).

Let D be the domain of (4.4), and χ_D denote the characteristic function of D, i.e.

$$\chi_D \equiv 1 \text{ on } D,\ \chi_D \equiv 0 \text{ on } \mathbb{R}^3\backslash D. \tag{4.34}$$

Let

$$Q_{\widetilde{W},D,m}u(x) \stackrel{\text{def}}{=} R^{-1}(R_{\widetilde{W},D,m}u)(x),\ m \in \mathbb{N} \tag{4.35}$$

$$Q_{\widetilde{W},D,m}u(x) = 0 \text{ for } m = 0,$$

$$Q_{\widetilde{W},D,\infty}u(x) \stackrel{\text{def}}{=} R^{-1}(R_{\widetilde{W},D,\infty}u)(x), \tag{4.36}$$

where

$$R_{\widetilde{W},D,m}u(s,\theta(\gamma,\phi)) \stackrel{\text{def}}{=} \int\limits_{x\theta=s} \left(\sum_{k=1}^{m}\sum_{n=-2k}^{2k} \frac{w_{2k,n}(x)}{w_{0,0}(x)} Y_{2k}^n(\gamma,\phi)\right) \chi_D(x)u(x)\,dx, \tag{4.37}$$

$$R_{\widetilde{W},D,\infty}u(s,\theta(\gamma,\phi)) \stackrel{\text{def}}{=} \lim_{m\to\infty} R_{\widetilde{W},D,m}u(s,\theta(\gamma,\phi))$$

$$= \int\limits_{x\theta=s} \left(\sum_{k=1}^{\infty}\sum_{n=-2k}^{2k} \frac{w_{2k,n}(x)}{w_{0,0}(x)} Y_{2k}^n(\gamma,\phi)\right) \chi_D(x)u(x)\,dx, \tag{4.38}$$

$x \in \mathbb{R}^3,\ s \in \mathbb{R},\ \theta(\gamma,\phi) \in \mathbb{S}^2,$

where Y_k^n are defined in (4.7), R^{-1} is defined by (4.20) (or (4.19)), u is a test function, $w_{0,0}, w_{2k,n}$ are the Fourier-Laplace coefficients defined by (4.11) and $w_{2k,n}/w_{0,0}$, χ_D are considered as multiplication operators on $\mathbb{R}^3$. Note also that $R_{\widetilde{W},D,\infty}f = R_{\widetilde{W}}f$ under assumptions (4.2)-(4.4).

Let

$$d_{2k,n}(x) \stackrel{\text{def}}{=} R^{-1}(\delta(\cdot)Y_{2k}^n)(x),\ x \in \mathbb{R}^3,\ k \in \mathbb{N},\ n = \overline{-2k, 2k}, \tag{4.39}$$

where $\delta = \delta(s)$ denotes the 1D Dirac delta function. In (4.39) the action of R^{-1} on the generalized functions is defined by formula (4.20).

Lemma 1. *Let $d_{2k,n}$ be defined by* (4.39). *Then*

$$d_{2k,n}(x(r,\gamma,\phi)) = \frac{(-1)^k\Gamma(\frac{3}{2}+k)}{2\pi^{3/2}\Gamma(k)} \frac{Y_{2k}^n(\gamma,\phi)}{r^3}, r > 0, \tag{4.40}$$

where $\Gamma(\cdot)$ is the Gamma-function, $x(r,\gamma,\phi)$ is defined by the identity:

$$x(r,\gamma,\phi) = (r\cos\gamma, r\sin\gamma\cos\phi, r\sin\gamma\sin\phi) \in \mathbb{R}^3,\ \gamma \in [0,\pi],\ \phi \in [0,2\pi],\ r \geq 0. \tag{4.41}$$

In addition, the following inequality holds:

$$|\mathcal{F}[d_{2k,n}](\xi)| \leq 1,\ \xi \in \mathbb{R}^3, \tag{4.42}$$

where $\mathcal{F}[\cdot]$ is the Fourier transform, defined in (4.23).

The following lemma gives some useful expressions for operators $Q_{\widetilde{W},D,m}$, $Q_{\widetilde{W},D,\infty}$ defined in (4.35), (4.36).

Lemma 2. *Let operators $Q_{\widetilde{W},D,m}, Q_{\widetilde{W},D,\infty}$ be defined by (4.35), (4.36), respectively, and u be a test function satisfying (4.4). Then*

$$Q_{\widetilde{W},D,m}u = \sum_{k=1}^{m}\sum_{n=-2k}^{2k} d_{2k,n} *_{\mathbb{R}^3} \frac{w_{2k,n}}{w_{0,0}}u, \tag{4.43}$$

$$Q_{\widetilde{W},D,\infty}u = \sum_{k=1}^{\infty}\sum_{n=-2k}^{2k} d_{2k,n} *_{\mathbb{R}^3} \frac{w_{2k,n}}{w_{0,0}}u, \tag{4.44}$$

where coefficients $w_{k,n}$ are defined in (4.11), $d_{2k,n}$ is defined by (4.40) (or equivalently by (4.39)), $*_{\mathbb{R}^3}$ denotes the convolution in 3D.

Remark 1. Convolution terms in the right-hand side of (4.43), (4.44) are well defined functions in $L^2(\mathbb{R}^3)$. This follows from identity (4.40) and the Calderón-Zygmund theorem for convolution-type operators with singular kernels (see [Kn05], p.83, Theorem 3.26).

The following lemma shows that $Q_{\widetilde{W},D,m}$, $Q_{\widetilde{W},D,\infty}$ are well-defined operators in $L^2(\mathbb{R}^3)$.

Lemma 3. *Operator $Q_{\widetilde{W},D,m}$ defined by (4.43) (or equivalently by (4.35)) is a linear bounded operator in $L^2(\mathbb{R}^3)$ and the following estimate holds:*

$$\|Q_{\widetilde{W},D,m}\|_{L^2(\mathbb{R}^3)\to L^2(\mathbb{R}^3)} \le \sigma_{\widetilde{W},D,m}, \tag{4.45}$$

where $\sigma_{\widetilde{W},D,m}$ is defined by (4.12).

If $\sigma_{\widetilde{W},D,\infty} < +\infty$, where $\sigma_{\widetilde{W},D,\infty}$ is defined by (4.13), then $Q_{\widetilde{W},D,\infty}$, defined by (4.44) (or equivalently by (4.36)), is a linear bounded operator in $L^2(\mathbb{R}^3)$ and the following estimate holds:

$$\|Q_{\widetilde{W},D,\infty}\|_{L^2(\mathbb{R}^3)\to L^2(\mathbb{R}^3)} \le \sigma_{\widetilde{W},D,\infty}. \tag{4.46}$$

Lemma 4. *Let*

$$\sum_{k=1}^{\infty}\sum_{n=-2k}^{2k} \left|\left|\frac{w_{2k,n}}{w_{0,0}}\right|\right|_{L^2(D)} < +\infty, \tag{4.47}$$

where $w_{k,n}$ are defined in (4.11). Then

$$R^{-1}R_W f \in L^2(\mathbb{R}^3). \tag{4.48}$$

In addition, the following formula holds:

$$R^{-1}R_W f = w_{0,0}f + \sum_{k=1}^{\infty}\sum_{n=-2k}^{2k} d_{2k,n} *_{\mathbb{R}^3} w_{2k,n}f = (I + Q_{\widetilde{W},D,\infty})(w_{0,0}f), \tag{4.49}$$

where f satisfies (4.4), operator R^{-1} is defined by (4.20) and $Q_{\tilde{W},D,\infty}$ is given by (4.44).

In particular, if $W = W_N$, $N \in \mathbb{N}\cup\{0\}$ then the following analog of (4.49) holds:

$$R^{-1}R_W f = w_{0,0}f + \sum_{k=1}^{m}\sum_{n=-2k}^{2k} d_{2k,n} *_{\mathbb{R}^3} w_{2k,n}f = (I + Q_{\widetilde{W},D,m})(w_{0,0}f),\ m = [N/2], \tag{4.50}$$

where $Q_{\widetilde{W},D,m}$ is given by (4.43).

3 Main results

3.1 Case of $\sigma_{\widetilde{W},D,\infty} < 1$

Let

$$\sigma_{\widetilde{W},D,\infty} < 1, \tag{4.51}$$

where $\sigma_{\widetilde{W},D,\infty}$ is defined by (4.13).

Inequality (4.51) and upper bound (4.46) in Lemma 3 imply that operator $I + Q_{\widetilde{W},D,\infty}$ is continuosly invertible in $L^2(\mathbb{R}^3)$ and the following identity holds (in the sense of the operator norm in $L^2(\mathbb{R}^3)$):

$$(I + Q_{\widetilde{W},D,\infty})^{-1} = I + \sum_{j=1}^{\infty} (-Q_{\widetilde{W},D,\infty})^j, \tag{4.52}$$

where I is the identity operator in $L^2(\mathbb{R}^3)$.

Theorem 1. *Let conditions* (4.2)-(4.4), (4.51) *be fulfilled. Then* R_W, *defined by* (4.1), *is injective and the following exact inversion formula holds:*

$$f = (w_{0,0})^{-1} (I + Q_{\widetilde{W},D,\infty})^{-1} R^{-1} R_W f, \tag{4.53}$$

where $w_{0,0}$ *is defined in* (4.3), R^{-1} *is defined in* (4.19), *operator* $(I + Q_{\widetilde{W},D,\infty})^{-1}$ *is given in* (4.52).

Remark 2. Formula (4.53) can be considered as the following linear integral equation for the $w_{0,0} f$:

$$w_{0,0} f + Q_{\widetilde{W},D,\infty}(w_{0,0} f) = R^{-1} R_W f. \tag{4.54}$$

Inequality (4.51) and identity (4.52) imply that equation (4.54) can be solved by the method of successive approximations.

One can see that, under conditions (4.2)-(4.4) and (4.51), Theorem 1 gives an exact inversion of R_W. However, condition (4.51) is not always fulfilled in practice; see [GuN14] for related numerical analysis in 2D. If condition (4.51) is not fulfilled, then, approximating W by finite Fourier series, in a similar way with [Ch78], [Ku92], [No14], [GuN14] we suggest approximate inversion of R_W; see Subsections 3.2, 3.3.

3.2 Case of $1 \leq \sigma_{\widetilde{W},D,\infty} < +\infty$

Let

$$\sigma_{\widetilde{W},D,m} < 1, \text{ for some } m \in \mathbb{N} \cup \{0\}, \tag{4.55}$$

$$\sigma_{\widetilde{W},D,\infty} < +\infty, \tag{4.56}$$

where $\sigma_{\widetilde{W},D,m}$ is defined by (4.12), $\sigma_{\widetilde{W},D,\infty}$ is defined by (4.13).

Inequality (4.55) and upper bound (4.45) in Lemma 3 imply that $I + Q_{\widetilde{W},D,m}$ is continuously invertible in $L^2(\mathbb{R}^3)$ and the following identity holds (in the sense of the operator norm in $L^2(\mathbb{R}^3)$):

$$(I + Q_{\widetilde{W},D,m})^{-1} = I + \sum_{j=1}^{\infty} (-Q_{\widetilde{W},D,m})^j, \tag{4.57}$$

where I is the identity operator in $L^2(\mathbb{R}^3)$.

Theorem 2. *Let conditions* (4.2)-(4.4), (4.55), (4.56) *be fulfilled. Then*

$$f \approx f_m \stackrel{\text{def}}{=} (w_{0,0})^{-1}(I + Q_{\widetilde{W},D,m})^{-1}R^{-1}R_W f, \tag{4.58}$$

$$f = f_m - (w_{0,0})^{-1}(I + Q_{\widetilde{W},D,m})^{-1}R^{-1}R_{\delta W_m} f, \tag{4.59}$$

$$\|f - f_m\|_{L^2(D)} \leq \frac{\|f\|_\infty}{c(1 - \sigma_{\widetilde{W},D,m})} \sum_{k=m+1}^{\infty} \sum_{n=-2k}^{2k} \|w_{2k,n}\|_{L^2(D)} < +\infty, \tag{4.60}$$

where

$$\delta W_m(x, \theta(\gamma,\phi)) \stackrel{\text{def}}{=} W(x, \theta(\gamma,\phi)) - \sum_{k=0}^{2m+1} \sum_{n=-k}^{k} w_{k,n}(x) Y_k^n(\gamma,\phi), \tag{4.61}$$

$$x \in \mathbb{R}^3,\ \gamma \in [0,\pi],\ \phi \in [0, 2\pi],\ m \in \mathbb{N} \cup \{0\}, \tag{4.62}$$

$w_{0,0}$ *is defined in* (4.3), $\theta(\gamma,\phi)$ *is defined in* (4.8), Y_k^n *are defined in* (4.7), $(I + Q_{\widetilde{W},D,m})^{-1}$ *is given in* (4.57), *constant* c *is defined in* (4.33).

Remark 3. Formula (4.58) can be considered as the following linear integral equation for $w_{0,0}f$:

$$w_{0,0}f + Q_{\widetilde{W},D,m}(w_{0,0}f) = R^{-1}R_W f. \tag{4.63}$$

Inequality (4.55) and identity (4.57) imply that equation (4.63) is solvable by the method of successive approximations.

Note also that condition (4.56) can be relaxed to the following one:

$$\sum_{k=1}^{\infty} \sum_{n=-2k}^{2k} \left|\left| \frac{w_{2k,n}}{w_{0,0}} \right|\right|_{L^2(D)} < +\infty, \tag{4.64}$$

where $w_{2k,n}$ are defined in (4.11).

Formula (4.58) is an extension to 3D of the Chang-type two-dimensional inversion formulas in [Ch78], [No14], [GuN14]. In addition, formula (4.58) is an extension of approximate inversion formula in [GN16], where this formula was given for $m = 0$.

If (4.55) is fulfilled for some $m \geq 1$, then f_m is a refinement of the Chang-type approximation f_0 and, more generally, f_j is a refinement of f_i for $0 \leq i < j \leq m$. In addition, $f_j = f_i$ if $w_{2k,n} \equiv 0$ for $i < k \leq j$, $n = \overline{-2k, 2k}$. Thus, we propose the following approximate reconstruction of f from $R_W f$:

(i) find maximal m such that (4.55) is still efficiently fulfilled,

(ii) approximately reconstruct f by f_m using (4.58).

3.3 Exact inversion for finite Fourier series weights

Let

$$W = W_N,\ N \in \mathbb{N} \cup \{0\}, \tag{4.65}$$

where W_N is defined by (4.14).

Suppose that

$$\sigma_{\widetilde{W},D,m} < 1 \text{ for } m = [N/2], \tag{4.66}$$

where $\sigma_{\widetilde{W},D,m}$ is defined by (4.12).

Theorem 3. *Let conditions* (4.2)-(4.4), (4.65), (4.66) *be fulfilled. Then* R_W *defined by* (4.1) *is injective and the following exact inversion formula holds:*

$$f = (w_{0,0})^{-1}(I + Q_{\widetilde{W},D,m})^{-1}R^{-1}R_W f, \tag{4.67}$$

where $w_{0,0}$ *is defined in* (4.2), $(I + Q_{\widetilde{W},D,m})^{-1}$ *is given in* (4.57), R^{-1} *is defined by* (4.19).

Remark 4. Formula (4.67) can be considered as the following linear integral equation for $w_{0,0}f$:

$$w_{0,0}f + Q_{\widetilde{W},D,m}(w_{0,0}f) = R^{-1}R_W f. \tag{4.68}$$

Identity (4.66) imply that (4.68) can be solved by the method of successive approximations.

Remark 5. Note that Theorems 1, 2, 3 remain valid under assumptions (4.16), (4.17) in place of (4.2), (4.3). This follows from the fact that in the proofs in Sections 5, 6 it is required only existence of integral transforms, given by operators R_W, R^{-1}, $\mathcal{F}[\cdot]$, $\mathcal{F}^{-1}[\cdot]$, $Q_{\widetilde{W},D,\infty}$, $Q_{\widetilde{W},D,m}$ and their compositions (see Subsections 2.1, 2.3) and of uniform upper bound on $(w_{0,0})^{-1}$.

3.4 Additional comments

The class of weights for which the results of Subsections 3.1, 3.2, 3.3 can be applied is rather large.
For example, condition (4.51) is satisfied for the weights W of the following form:

$$W(x,\theta) = c + w(x,\theta),\ (x,\theta) \in \mathbb{R}^3 \times \mathbb{S}^2, \tag{4.69}$$

where

$$\begin{aligned} &c > 0 \text{ - is some constant,} \\ &w \in C^3(\mathbb{R}^3 \times \mathbb{S}^2),\ \|w\|_{C^3(D\times\mathbb{S}^2)} \le L(c,D), \end{aligned} \tag{4.70}$$

where L is some positive constant depending only on c of (4.69) and on domain D of (4.4).

On the other hand, all weights W which admit the finite Fourier series expansions (i.e., $W = W_N$ of (4.14) for some $N \in \mathbb{N} \cup \{0\}$) are dense in the spaces $L^2(D \times \mathbb{S}^2)$ and also in $C(D \times \mathbb{S}^2)$ (square integrable and continuous weights on $\mathbb{R}^3 \times \mathbb{S}^2$, repsectively, which are restricted to $D \times \mathbb{S}^2$). In addition, for such $W \in C(\mathbb{R}^3 \times \mathbb{S}^2)$ the sense of each of conditions (4.51), (4.55), (4.56), (4.64), (4.66) is especially clear. Moreover, condition (4.56) is always satisfied if $W \in C^3(\mathbb{R}^3 \times \mathbb{S}^2)$ by the definition (4.14) of W_N. In addition, even if (4.55) is not satisfied for the whole W_N, one can consider such cutoff W_m of the Fourier expansion of W_N so that (4.55) holds and, therefore, results of Subsection 3.2 can be applied.

In fact, the most common example of W arises in the framework of the singular photon emission computed tomography (SPECT), where the initial data is modeled by $P_w f$ of (4.5) and w is given by the formulas (see [Na86]):

$$w(x,\theta) = \exp\big(-Da(x,\theta)\big), \tag{4.71}$$

$$Da(x,\theta) = \int_0^\infty a(x+t\theta)\,dt,\ (x,\theta) \in \mathbb{R}^3 \times \mathbb{S}^2, \tag{4.72}$$

where a (attenuation) is a real-valued non-negative sufficiently regular function on $\mathbb{R}^3$ with sufficient decay at infinity.

The weight W and the related $R_W f$ are given by the formulas (see [GN16]):

$$R_W f(s,\theta) = \int\limits_{\mathbb{R}} P_w f(s\theta + \tau[\theta,\alpha(\theta)],\, \alpha(\theta))\, d\tau,\ (s,\theta) \in \mathbb{R}\times\mathbb{S}^2, \tag{4.73}$$

$$W(x,\theta) = w(x,\alpha(\theta)),\ w \text{ - is given by (4.71)},\ (x,\theta)\in\mathbb{R}^3\times\mathbb{S}^2, \tag{4.74}$$

$$\alpha(\theta) = \begin{cases} \dfrac{[\eta,\theta]}{|[\eta,\theta]|},\ \text{if } \theta \neq \pm\eta, \\ \text{any vector } \alpha\in\mathbb{S}^2,\ \text{such that } \alpha\perp\theta,\ \text{if } \theta = \pm\eta, \end{cases}, \tag{4.75}$$

where η is some fixed vector from $\mathbb{S}^2$, $[\cdot,\cdot]$ denotes the standard vector product in $\mathbb{R}^3$, $\perp$ denotes the orthogonality of vectors. Note that such W has two discontinuities at $\theta = \pm\eta$, however, it belongs to $L^\infty(R^3\times\mathbb{S}^2)$ so decomposition (4.6) and the subsequent results of Section 3 are still valid.

Finally, we recall also that in many cases even zero order approximation $W \approx W_0 = w_{0,0}$ can be practically efficient, in particular, in view of results presented in [Ch78], [Gr91], [No11], [GN16]. Therefore, we expect that our inversion algorithms which are based on the higher order Fourier approximations of W are even more efficient for reconstructions in the framework of different tomographies.

4 Generalization to multidimensions

Definition (4.1) and assumptions (4.2)-(4.4) are naturally extended as follows to the case of dimension $n > 3$:

$$R_W f(s,\theta) = \int\limits_{x\theta=s} W(x,\theta) f(x)\, dx,\ (s,\theta)\in\mathbb{R}\times\mathbb{S}^{n-1},\ x\in\mathbb{R}^n, \tag{4.76}$$

$$W \in L^\infty(\mathbb{R}^n\times\mathbb{S}^{n-1}), \tag{4.77}$$

$$w_{0,0}(x) \stackrel{\text{def}}{=} \frac{1}{\text{vol}(\mathbb{S}^{n-1})} \int\limits_{\mathbb{S}^{n-1}} W(x,\theta)\, d\theta,\ w_{0,0} \geq c > 0, \tag{4.78}$$

$$f\in L^\infty(\mathbb{R}^n),\ \text{supp}\, f \subset D, \tag{4.79}$$

where $\text{vol}(\mathbb{S}^{n-1})$ denotes the standard Euclidean volume of $\mathbb{S}^{n-1}$, c is some positive constant, D is an open bounded domain in $\mathbb{R}^n$.

For the weight W we consider the Fourier-Laplace expansion:

$$W(x,\theta) = \sum_{k=0}^{\infty} \sum_{i=0}^{a_{k,n}-1} w_{k,i}(x) Y_k^i(\theta),\ x\in\mathbb{R}^n,\ \theta\in\mathbb{S}^{n-1}, \tag{4.80}$$

where

$$w_{k,i}(x) = \|Y_k^i\|^{-2}_{L^2(\mathbb{S}^{n-1})} \int\limits_{\mathbb{S}^{n-1}} W(x,\theta)\overline{Y_k^i(\theta)}\, d\theta, \tag{4.81}$$

$$a_{k,n+1} = \frac{(n+k)!}{k!n!} - \frac{(n+k-2)!}{(k-2)!n!},\ n,k\geq 2;\ a_{0,n}=1,\ a_{1,n}=n, \tag{4.82}$$

where $\{Y_k^i \,|\, k = \overline{0,\infty}, i = \overline{0, a_{k,n}-1}\}$ is the Fourier-Laplace basis of harmonics on $\mathbb{S}^{n-1}$, $\overline{Y_k^i}$ denotes the complex conjugate of Y_k^i ; see [SW16], [Mo98]. In the present work we choose the basis Y_k^i as in [Hi87] without normalizing constants ${}_nc_L^l$ (i.e., $\{Y_k^i\}$ are the products of

the Legendre polynomials with one complex exponent and without any additional constants).

In dimension $n > 3$, formulas (4.12), (4.13), (4.35), (4.36), are rewritten as follows:

$$\sigma_{\widetilde{W},D,m} \stackrel{\text{def}}{=} \sum_{k=1}^{m} \sum_{i=0}^{a_{2k,n}-1} \sup_{x\in D} \left| \frac{w_{2k,i}(x)}{w_{0,0}(x)} \right|, \tag{4.83}$$

$$\sigma_{\widetilde{W},D,\infty} \stackrel{\text{def}}{=} \lim_{m\to+\infty} \sigma_{\widetilde{W},D,m} \tag{4.84}$$

$$Q_{\widetilde{W},D,m}u(x) \stackrel{\text{def}}{=} R^{-1}(R_{\widetilde{W},D,m}u)(x),\ m \in \mathbb{N} \tag{4.85}$$

$$Q_{\widetilde{W},D,m}u(x) = 0 \text{ for } m = 0,$$

$$Q_{\widetilde{W},D,\infty}u(x) \stackrel{\text{def}}{=} R^{-1}(R_{\widetilde{W},D,\infty}u)(x), \tag{4.86}$$

where

$$R_{\widetilde{W},D,m}u(s,\theta) \stackrel{\text{def}}{=} \int\limits_{x\theta=s} \left(\sum_{k=1}^{m} \sum_{i=0}^{a_{2k,n}-1} \frac{w_{2k,i}(x)}{w_{0,0}(x)} Y_{2k}^{i}(\theta) \right) \chi_D(x)u(x)\,dx, \tag{4.87}$$

$$R_{\widetilde{W},D,\infty}u(s,\theta) \stackrel{\text{def}}{=} \lim_{m\to\infty} R_{\widetilde{W},D,m}u(s,\theta), \tag{4.88}$$

$$x \in \mathbb{R}^n,\ s \in \mathbb{R},\ \theta \in \mathbb{S}^{n-1},$$

where R^{-1} is defined further in (4.89).

Under assumptions (4.77), (4.79) series of (4.80) converge in $L^2(\mathbb{S}^{n-1})$; see e.g. [SW16] (Chapter 4), [Mo98] (Chapter 2), [ZT79].

Formula (4.20) is extended as follows:

$$R^{-1}q(x) = \int\limits_{\mathbb{R}} \frac{|\rho|^{n-1}}{2}\,d\rho \int\limits_{\mathbb{S}^{n-1}} \hat{q}(\rho,\theta)e^{2\pi i\rho(x\theta)}d\theta,\ x \in \mathbb{R}^n, \tag{4.89}$$

where $q(s,\theta)$ is a test function on $\mathbb{R}\times\mathbb{S}^{n-1}$, $\hat{q}(s,\theta)$ is defined as in (4.21) (with $\mathbb{S}^{n-1}$ in place of $\mathbb{S}^2$).

The Fourier transforms, defined in (4.23), (4.24), are extended as follows:

$$\mathcal{F}[q](\xi) \stackrel{\text{def}}{=} \int\limits_{0}^{+\infty} \rho^{n-1}d\rho \int\limits_{\mathbb{S}^{n-1}} q(\rho,\omega)e^{-2\pi i\rho(\xi\omega)}d\omega, \tag{4.90}$$

$$\mathcal{F}^{-1}[q](\xi) \stackrel{\text{def}}{=} \int\limits_{0}^{+\infty} \rho^{n-1}d\rho \int\limits_{\mathbb{S}^{n-1}} q(\rho,\omega)e^{2\pi i\rho(\xi\omega)}d\omega,\ \xi \in \mathbb{R}^n, \tag{4.91}$$

where $q(\rho,\omega)$ is a test function on $[0,+\infty)\times\mathbb{S}^{n-1}$ (identified with $\mathbb{R}^n$).

In dimension $n > 3$, formulas (4.25)-(4.29) remain valid with Y_k^m defined in (4.7) replaced by general basis of spherical harmonics $\{Y_k^i\}$ on $\mathbb{S}^{n-1}$. In particular, the following multidimensional analog of formula (4.29) holds:

$$Y_k^i(-\theta) = (-1)^k Y_k^i(\theta),\ \theta \in \mathbb{S}^{n-1},\ k \in \mathbb{N}\cup\{0\},\ i = \overline{0, a_{k,n}-1}, \tag{4.92}$$

where $a_{k,n}$ is defined by (4.82). Identity (4.92) reflects the fact that $Y_k^i(\theta) = Y_k^i(\theta_1,\theta_2,\cdots,\theta_n)$, $\theta = (\theta_1,\theta_2,\cdots,\theta_n) \in \mathbb{S}^{n-1}$, $i = \overline{0, a_{k,n}-1}$ is a homogenous polynomial of degree k, see e.g. [SW16], [Mo98].

Formula (4.39) is now rewritten as follows:

$$d_{2k,i}(x) \stackrel{\text{def}}{=} R^{-1}(\delta(\cdot)Y_{2k}^i)(x),\ x \in \mathbb{R}^n,\ i = \overline{0, a_{k,n}-1}. \tag{4.93}$$

Results of Lemma 1 remain valid with formula (4.40) replaced by the following one:

$$d_{2k,i}(r,\theta) = c(k,n)\frac{(-1)^k Y_{2k}^i(\theta)}{r^n},\ r > 0,\ \theta \in \mathbb{S}^{n-1}, \tag{4.94}$$

where

$$c(k,n) = \frac{\sqrt{2}\pi^{(1-n)/2}\Gamma(k+\frac{1}{2})\Gamma(k+\frac{n}{2})}{\Gamma(k)\Gamma(k+\frac{n-1}{2})} \cdot \left(\frac{\Gamma(k+1)}{\Gamma(k+\frac{1}{2})}\right)^{n-2}, \tag{4.95}$$

$\Gamma(\cdot)$ is the Gamma function.

In addition, inequality (4.42) is rewritten as follows:

$$|\mathcal{F}[d_{2k,i}](\xi)| \leq 1,\ \xi \in \mathbb{R}^n, \tag{4.96}$$

where $\mathcal{F}[\cdot]$ is the Fourier transform defined in (4.90). The constant $c(k,n)$ in (4.95) is obtained using formulas (4.89), (4.93) and Theorems 1, 2 in [Go16].

The results of Lemma 2 remain valid in the case of dimension $n > 3$, with formulas (4.43), (4.44) rewritten as follows:

$$Q_{\widetilde{W},D,m}u = \sum_{k=1}^{m}\sum_{i=0}^{a_{k,n}-1} d_{2k,i} *_{\mathbb{R}^n} \frac{w_{2k,i}}{w_{0,0}}u, \tag{4.97}$$

$$Q_{\widetilde{W},D,\infty}u = \sum_{k=1}^{\infty}\sum_{i=0}^{a_{k,n}-1} d_{2k,i} *_{\mathbb{R}^n} \frac{w_{2k,i}}{w_{0,0}}u, \tag{4.98}$$

where coefficients $w_{2k,i}$, $w_{0,0}$ are defined in (4.81), $a_{k,n}$ is defined in (4.82), $d_{2k,i}$ is defined in (4.94), $*_{\mathbb{R}^n}$ denotes the convolution in $\mathbb{R}^n$.

The result of Lemma 3 remains valid with $\mathbb{R}^3$ replaced by $\mathbb{R}^n$, $n > 3$, where we use definitions (4.83), (4.85), (4.86).

Assumption (4.47) in Lemma 4 is rewritten now as follows:

$$\sum_{k=1}^{\infty}\sum_{i=0}^{a_{k,n}-1} \left|\left|\frac{w_{2k,i}}{w_{0,0}}\right|\right|_{L^2(D)} < +\infty. \tag{4.99}$$

Under assumption (4.99), property (4.48) of Lemma 4 remains valid in dimension $n > 3$. In particular, formula (4.49) is rewritten as follows:

$$R^{-1}R_W f = w_{0,0}f + \sum_{k=1}^{\infty}\sum_{i=0}^{a_{k,n}-1} d_{2k,i} *_{\mathbb{R}^n} w_{2k,i}f, \tag{4.100}$$

where R^{-1} is defined in (4.89), f is a test function satisfying (4.79), $d_{2k,i}$ is now defined in (4.94).

Using formulas and notations from (4.80)-(4.98) we obtain straightforward extensions of Theorems 1, 2, 3.

- The result of Theorem 1 remains valid in dimension $n > 3$, under assumptions (4.77)-(4.79) and under condition (4.51), where $w_{0,0}$ is defined in (4.78), R^{-1} is defined in (4.89), $\sigma_{\widetilde{W},D,\infty}$ is defined in (4.84), $Q_{\widetilde{W},D,\infty}$ is defined in (4.86).

- The result of Theorem 2 remains valid in dimension $n > 3$, under assumptions (4.77)-(4.79) and under conditions (4.55), (4.56), where $w_{0,0}$ is defined in (4.78), R^{-1} is defined in (4.89), $\sigma_{\widetilde{W},D,m}$ is defined in (4.83), $Q_{\widetilde{W},D,m}$ is defined in (4.85) and where formulas (4.59)-(4.61) are rewritten as follows:

$$\|f - f_m\|_{L^2(D)} \leq \frac{\|f\|_\infty}{c(1-\sigma_{\widetilde{W},D,m})} \sum_{k=m+1}^{\infty} \sum_{i=0}^{a_{k,n}-1} \|w_{2k,i}\|_{L^2(D)} < +\infty, \tag{4.101}$$

$$\delta W_m(x,\theta) \stackrel{\text{def}}{=} W(x,\theta) - \sum_{k=0}^{2m+1} \sum_{i=0}^{a_{k,n}-1} w_{k,i}(x) Y_k^i(\theta), \tag{4.102}$$

$x \in \mathbb{R}^n$, $\theta \in \mathbb{S}^{n-1}$.

- The result of Theorem 3 remains valid in dimension $n > 3$, under assumptions (4.77)-(4.79) and under conditions (4.65), (4.66), where $w_{0,0}$ is defined in (4.78), R^{-1} is defined in (4.89), $\sigma_{\widetilde{W},D,m}$ is defined in (4.83), $Q_{\widetilde{W},D,m}$ is defined in (4.85).

The related proofs are the straightforward extensions to the case of dimension $n > 3$ of proofs in Section 6 for $n = 3$.

5 Proofs of Lemma 1, 2, 3, 4

5.1 Proof of Lemma 1

We consider $x(r,\gamma,\phi)$ defined by (4.41) and $\omega(\gamma,\phi) = x(1,\gamma,\phi)$ (i.e., $\omega \in \mathbb{S}^2$).

Identity (4.41) implies the following expression for the scalar product $(x\omega)$ in spherical coordinates in $\mathbb{R}^3$:

$$(x\omega) = (x(r,\tilde\gamma,\tilde\phi),\omega(\gamma,\phi)) = r(\cos\gamma\cos\tilde\gamma + \sin\gamma\sin\tilde\gamma\cos(\phi-\tilde\phi)), \tag{4.103}$$

where $\gamma,\tilde\gamma \in [0,\pi]$, $\phi,\tilde\phi \in [0,2\pi]$, $r \geq 0$.

From formulas (4.7), (4.20), (4.39), (4.103) it follows that

$$\begin{aligned}
d_{2k,n}(x(r,\tilde\gamma,\tilde\phi)) &= \int_{\mathbb{R}} \frac{\rho^2}{2} d\rho \int_{\mathbb{S}^2} e^{2\pi i\rho(x\omega(\gamma,\phi))} Y_{2k}^n(\gamma,\phi)\, d\omega(\gamma,\phi) \\
&= \int_{\mathbb{R}} \frac{\rho^2}{2} d\rho \int_0^\pi \sin(\gamma)\, p_{2k}^{|n|}(\cos\gamma)\, d\gamma \int_0^{2\pi} e^{2\pi i\rho(x\omega(\gamma,\phi))+in\phi} d\phi \\
&= e^{in\tilde\phi} \int_{\mathbb{R}} \frac{\rho^2}{2} d\rho \int_0^\pi \sin(\gamma) p_{2k}^{|n|}(\cos\gamma) e^{2\pi i\rho r\cos\gamma\cos\tilde\gamma}\, d\gamma \int_0^{2\pi} e^{2\pi i\rho r\sin\gamma\sin\tilde\gamma\cos(\phi-\tilde\phi)+in(\phi-\tilde\phi)} d\phi \\
&= e^{in\tilde\phi} \int_{\mathbb{R}} \frac{\rho^2}{2} d\rho \int_0^\pi \sin(\gamma) p_{2k}^{|n|}(\cos\gamma) e^{2\pi i\rho r\cos\gamma\cos\tilde\gamma}\, d\gamma \int_0^{2\pi} e^{2\pi i\rho r\sin\gamma\sin\tilde\gamma\cos\phi+in\phi} d\phi \\
&= 2\pi e^{in(\tilde\phi+\pi/2)} \int_{\mathbb{R}} \frac{\rho^2}{2} d\rho \int_0^\pi \sin(\gamma) p_{2k}^{|n|}(\cos\gamma) e^{i\rho r\cos\gamma\cos\tilde\gamma} J_n(2\pi\rho r\sin\gamma\sin\tilde\gamma)\, d\gamma,
\end{aligned} \tag{4.104}$$

where J_n is the n-th standard Bessel function of the first kind; see e.g. [Te11]. In (4.104) we used the well known formula for the Bessel function J_n:

$$J_n(t) \stackrel{\text{def}}{=} \frac{1}{2\pi}\int\limits_{-\pi}^{\pi} e^{i(n\phi - t\sin\phi)}d\phi = \frac{e^{-in\pi/2}}{2\pi}\int\limits_{0}^{2\pi} e^{i(n\phi + t\cos\phi)}d\phi.$$

The integral in $d\gamma$ in the right-hand side of (4.104) was considered in [N+06], where the following exact analytic solution was given:

$$\int\limits_0^{\pi} \sin(\gamma) p_{2k}^{|n|}(\cos\gamma) e^{2\pi i \rho r \cos\gamma\cos\tilde{\gamma}} J_n(2\pi\rho r\sin\gamma\sin\tilde{\gamma})\, d\gamma = 2i^{2k-|n|} p_{2k}^{|n|}(\cos\tilde{\gamma}) j_{2k}(2\pi\rho r), \tag{4.105}$$

where j_{2k} is the standard spherical Bessel function of order $2k$; see e.g. [Te11].

From identities (4.104), (4.105) it follows that:

$$\begin{aligned} d_{2k,n}(x(r,\tilde{\gamma},\tilde{\phi})) &= 2\pi(-1)^k p_{2k}^{|n|}(\cos\tilde{\gamma}) e^{in\tilde{\phi}} \int\limits_{\mathbb{R}} \rho^2 j_{2k}(2\pi\rho r)\, d\rho \\ &= \frac{(-1)^k \Gamma(\frac{3}{2}+k)}{2\pi^{3/2}\Gamma(k)} \frac{p_{2k}^{|n|}(\cos\tilde{\gamma}) e^{in\tilde{\phi}}}{r^3},\ r>0. \end{aligned} \tag{4.106}$$

where $\Gamma(\cdot)$ is the Gamma function.

Defenition (4.7) and identity (4.106) imply formula (4.40).
Formulas (4.22), (4.30), (4.31), (4.39) imply that

$$d_{2k,n}(x(r,\tilde{\gamma},\tilde{\phi})) = \mathcal{F}^{-1}[Y_{2k}^n](x(r,\tilde{\gamma},\tilde{\phi})),\ r>0,\ \tilde{\gamma}\in[0,\pi],\ \tilde{\phi}\in[0,2\pi], \tag{4.107}$$

where $\mathcal{F}^{-1}[\cdot]$ is defined in (4.24).

From the invertibility of the Fourier transform defined in (4.23) and identity (4.107) the following identity holds:

$$\mathcal{F}[d_{2k,n}] = \mathcal{F}\mathcal{F}^{-1}[Y_{2k}^n] = Y_{2k}^n. \tag{4.108}$$

For Y_k^n defined in (4.7) the following inequality holds (see [Lo98]):

$$|Y_k^n(\gamma,\phi)| \le 1,\ \gamma\in[0,\pi],\ \phi\in[0,2\pi]. \tag{4.109}$$

Identities (4.107) and inequality (4.109) imply (4.42).

Note that $|\mathcal{F}[d_{2k,n}](\xi)|$, $\xi\in\mathbb{R}^3$, is uniformly bounded by 1 except only one point $\xi=0$, where direction $\xi/|\xi|\in\mathbb{S}^2$ is not defined. However, point $\xi=0$ is of Lebesgue measure zero and $\mathcal{F}[d_{2k,n}]$ can be defined with any value at the origin in $\mathbb{R}^3$.

Lemma 1 is proved.

5.2 Proof of Lemma 2

From identity (4.35) it follows that

$$\begin{aligned} Q_{\widetilde{W},D,m}u &= R^{-1}\left(\sum_{k=1}^{m}\sum_{n=-2k}^{2k} Y_{2k}^n R\left(\frac{w_{2k,n}}{w_{0,0}}\chi_D u\right)\right) \\ &= R^{-1}\left(\sum_{k=1}^{m}\sum_{n=-2k}^{2k} (\delta(\cdot)Y_{2k}^n) *_{\mathbb{R}} R\left(\frac{w_{2k,n}}{w_{0,0}}\chi_D u\right)\right) \\ &= R^{-1}\left(\sum_{k=1}^{m}\sum_{n=-2k}^{2k} R(d_{2k,n}) *_{\mathbb{R}} R\left(\frac{w_{2k,n}}{w_{0,0}}\chi_D u\right)\right) \end{aligned} \tag{4.110}$$

where $*_{\mathbb{R}}$ denotes the 1D convolution, $\delta = \delta(s)$ is the 1D Dirac delta function, $d_{2k,n}$ is defined by (4.39).

Identities (4.18), (4.110) imply (4.43).

For the operator $Q_{\widetilde{W},D,\infty}$ defined by (4.36) we proceed according to identity (4.110) with $m \to +\infty$. Identites (4.18), (4.110) and linearity of operator R^{-1} defined by (4.19) imply (4.44).

Lemma 2 is proved.

5.3 Proof of Lemma 3

From formula (4.43) and the fact that the Fourier transform defined in (4.23) does not change the L^2-norm we obtain:

$$\begin{aligned}\|Q_{\widetilde{W},D,m}u\|_{L^2(\mathbb{R}^3)} &\le \sum_{k=1}^{m}\sum_{n=-2k}^{2k}\left|\left|d_{2k,n} *_{\mathbb{R}^3} \frac{w_{2k,n}}{w_{0,0}}\chi_D u\right|\right|_{L^2(\mathbb{R}^3)} \\ &= \sum_{k=1}^{m}\sum_{n=-2k}^{2k}\left|\left|\mathcal{F}[d_{2k,n}]\mathcal{F}\left[\frac{w_{2k,n}}{w_{0,0}}\chi_D u\right]\right|\right|_{L^2(\mathbb{R}^3)}. \end{aligned} \tag{4.111}$$

From inequalities (4.42), (4.111) we obtain:

$$\begin{aligned}\|Q_{\widetilde{W},D,m}u\|_{L^2(\mathbb{R}^3)} &\le \sum_{k=1}^{m}\sum_{n=-2k}^{2k}\left|\left|\mathcal{F}\left(\frac{w_{2k,n}}{w_{0,0}}\chi_D u\right)\right|\right|_{L^2(\mathbb{R}^3)} \\ &= \sum_{k=1}^{m}\sum_{n=-2k}^{2k}\left|\left|\frac{w_{2k,n}}{w_{0,0}}\chi_D u\right|\right|_{L^2(\mathbb{R}^3)} \\ &\le \sigma_{\widetilde{W},D,m}\|u\|_{L^2(D)}, \end{aligned} \tag{4.112}$$

where $\sigma_{\widetilde{W},D,m}$ is defined by (4.12).

Inequality (4.112) implies (4.45).

Estimate (4.46) follows from definition (4.36), formula (4.44), linearity of operator R^{-1} defined by (4.19) and inequalities (4.111), (4.112) for $m \to +\infty$.

Lemma 3 is proved.

5.4 Proof of Lemma 4

From formulas (4.1), (4.6) it follows that

$$R_W f(s,\theta(\gamma,\phi)) = \sum_{k=0}^{\infty}\sum_{n=-k}^{k} Y_k^n(\gamma,\phi) R(w_{k,n}f)(s,\theta(\gamma,\phi)), \tag{4.113}$$

$$s \in \mathbb{R},\ \gamma \in [0,\pi],\ \phi \in [0,2\pi], \tag{4.114}$$

where $\theta(\gamma,\phi)$ is defined in (4.8), $Y_k^n(\gamma,\phi)$ are defined by (4.7), $w_{k,n}$ are defined in (4.11).

Formula (4.49) follows from formulas (4.25), (4.27), (4.29), (4.36) and formula (4.44) in Lemma 2, where test function u is replaced by $w_{0,0}u$.

From inequality (4.42), formulas (4.18), (4.49) and the fact that the Fourier tranfsform

defined in (4.23) does not change the L^2-norm we obtain:

$$\begin{aligned}\|R^{-1}R_W f\|_{L^2(\mathbb{R}^3)} &\le \|w_{0,0}f\|_{L^2(\mathbb{R}^3)} + \sum_{k=1}^{\infty}\sum_{n=-2k}^{2k} \|d_{2k,n} *_{\mathbb{R}^3} w_{2k,n}f\|_{L^2(\mathbb{R}^3)} \\ &= \|w_{0,0}f\|_{L^2(\mathbb{R}^3)} + \sum_{k=1}^{\infty}\sum_{n=-2k}^{2k} \|\mathcal{F}[d_{2k,n}]\mathcal{F}[w_{2k,n}f]\|_{L^2(\mathbb{R}^3)} \qquad (4.115) \\ &\le \|w_{0,0}f\|_{L^2(\mathbb{R}^3)} + \|f\|_{\infty}\sum_{k=1}^{\infty}\sum_{n=-2k}^{2k} \|w_{2k,n}\|_{L^2(D)},\end{aligned}$$

where $\|\cdot\|_{\infty}$ denotes the L^{∞}-norm, $\mathcal{F}[\cdot]$ is defined in (4.23).

From assumption (4.47) and formula (4.33) it follows that

$$\sum_{k=1}^{\infty}\sum_{n=-2k}^{2k} \|w_{2k,n}\|_{L^2(D)} < +\infty. \qquad (4.116)$$

Assumptions (4.2)-(4.4) and inequalities (4.115), (4.116) imply that

$$\|R^{-1}R_W f\|_{L^2(\mathbb{R}^3)} \le \|w_{0,0}f\|_{L^2(\mathbb{R}^3)} + \|f\|_{\infty}\sum_{k=1}^{\infty}\sum_{n=-2k}^{2k} \|w_{2k,n}\|_{L^2(D)} < +\infty. \qquad (4.117)$$

Lemma 2 is proved.

6 Proofs of Theorems 1, 2, 3

6.1 Proof of Theorem 1

By assumption (4.51) property (4.48) and identity (4.49) of Lemma 4 hold.

Formulas (4.48), (4.49), (4.51), (4.52) imply formula (4.53).

The injectivity of R_W follows from formula (4.53).

Theorem 1 is proved.

6.2 Proof of Theorem 3

By assumption (4.66) property (4.48) and identity (4.50) of Lemma 4 hold.

Formulas (4.48), (4.50), (4.57), (4.66) imply formula (4.67).

The injectivity of R_W follows from formula (4.67).

Theorem 3 is proved.

6.3 Proof of Theorem 2

By assumption (4.56) inequality (4.47) holds. Hence, formulas (4.48), (4.49) (in Lemma 4) hold.

Assumptions (4.2)-(4.4), (4.55) and inequality (4.45) from Lemma 3 imply that $f_m \in L^2(\mathbb{R}^3)$, where f_m is defined in (4.58).

We split expansion (4.6) of weight W defined by (4.2) in the following way:

$$W(x,\theta) = W_{N+1}(x,\theta) + \delta W_m(x,\theta),\ \theta \in \mathbb{S}^2,\ x \in \mathbb{R}^3,\ m = [N/2], \qquad (4.118)$$

where W_{N+1} is defined by (4.14), $[N/2]$ denotes the integer part of $N/2$, δW_m is defined by (4.61).

From (4.2)-(4.4) and from (4.118) it follows that

$$R_W f = R_{W_{N+1}} f + R_{\delta W_m} f, \tag{4.119}$$

where $R_W f, R_{W_{N+1}} f, R_{\delta W_m} f$ are defined by (4.1) for the case of weights $W, W_{N+1}, \delta W_m$ defined in (4.2), (4.11), (4.61), respectively.

Identity (4.119) implies that

$$R^{-1} R_W f = R^{-1} R_{W_N} f + R^{-1} R_{\delta W_m} f, \tag{4.120}$$

where R^{-1} is defined by (4.19). By assumption (4.56) inequality (4.47) holds for the cases of weights W, W_N, δW_m, respectively. Therefore, Lemma 4 holds for weights W, W_N, δW_m and, in particular, from (4.48) we have that:

$$R^{-1} R_{W_N} f \in L^2(\mathbb{R}^3),\ R^{-1} R_{\delta W_m} f \in L^2(\mathbb{R}^3). \tag{4.121}$$

By assumption (4.55) Theorem 3 holds for $W = W_N$, $N = 2m$. Therefore, from formula (4.67) we obtain:

$$f = (w_{0,0})^{-1} (I + Q_{\widetilde{W},D,m})^{-1} R^{-1} R_{W_N} f, \tag{4.122}$$

where operator $Q_{\widetilde{W},D,m}$ is defined in (4.35) for m arising in (4.55).

From (4.58), (4.120), (4.121), (4.122) it follows that:

$$\begin{aligned} f_m &= (w_{0,0})^{-1} (I + Q_{\widetilde{W},D,m})^{-1} R^{-1} R_W f \\ &= (w_{0,0})^{-1} (I + Q_{\widetilde{W},D,m})^{-1} R^{-1} R_{W_N} f \\ &+ (w_{0,0})^{-1} (I + Q_{\widetilde{W},D,m})^{-1} R^{-1} R_{\delta W_m} f \\ &= f + (w_{0,0})^{-1} (I + Q_{\widetilde{W},D,m})^{-1} R^{-1} R_{\delta W_m} f. \end{aligned} \tag{4.123}$$

Formula (4.59) directly follows from (4.123).

Inequality (4.55) and identities (4.57), (4.59) imply the following inequality:

$$\|f - f_m\|_{L^2(\mathbb{R}^3)} \le \frac{1}{c} \|(I + Q_{\widetilde{W},D,m})^{-1}\|_{L^2(\mathbb{R}^3) \to L^2(\mathbb{R}^3)} \cdot \|R^{-1} R_{\delta W_m} f\|_{L^2(\mathbb{R}^3)}, \tag{4.124}$$

where c is defined in (4.33), $Q_{\widetilde{W},D,m}$ is defined by (4.35) for m in (4.55).

From (4.45) of Lemma 3 and from identity (4.57) it follows that:

$$\|(I + Q_{\widetilde{W},D,m})^{-1}\|_{L^2(\mathbb{R}^3) \to L^2(\mathbb{R}^3)} \le 1 + \sum_{j=1}^{\infty} \|Q_{\widetilde{W},D,m}\|^j_{L^2(\mathbb{R}^3) \to L^2(\mathbb{R}^3)} \le \frac{1}{1 - \sigma_{\widetilde{W},D,m}}. \tag{4.125}$$

From formulas (4.49), (4.61) and according to (4.115) it follows that

$$\|R^{-1} R_{\delta W_m} f\|_{L^2(\mathbb{R}^3)} \le \|f\|_{\infty} \sum_{k=m+1}^{\infty} \sum_{n=-2k}^{2k} \|w_{2k,n}\|_{L^2(D)}, \tag{4.126}$$

where R^{-1} is defined by (4.19), $w_{2k,n}$ are defined by (4.11).

Putting the estimates (4.125), (4.126) in the right-hand side of (4.124) we obtain (4.60).

Theorem 2 is proved.

7 Acknowledgments

The present work was fulfilled in the framework of research conducted under the direction of Prof. R.G. Novikov. The author is also grateful to the referees for remarks that have helped to improve the presentation. This work is partially supported by the PRC n° 1545 CNRS/RFBR: Équations quasi-linéares, problèmes inverses et leurs applications.

Bibliography

[BQ87] J. Boman, E. T. Quinto. Support theorems for real-analytic Radon transforms. *Duke Mathematical J.*, 55(4):943-948, 1987.

[Be84] G. Beylkin. The inversion problem and applications of the generalized Radon transform. *Communications on pure and applied mathematics*, 37(5):579-599, 1984.

[Ch78] L. Chang. A method for attenuation correction in radionuclide computed tomography. *IEEE Transactions on Nuclear Science*, 25(1):638–643, 1978.

[De2016] A. Denisiuk. *Inversion of the x-ray transform for complexes of lines in* $\mathbb{R}^n$. Inverse Problems, 32(2), 2016.

[GN16] F. O. Goncharov, R. G. Novikov. An analog of Chang inversion formula for weighted Radon transforms in multidimensions. *Eurasian Journal of Mathematical and Computer Applications*, 4(2):23-32, 2016.

[Go16] F. O. Goncharov, Integrals of spherical harmonics with Fourier exponents in multidimensions. *Eurasian Journal of Mathematical and Computer Applications*, 4(4), 2016.

[Gr91] P. Grangeat. Mathematical framework of cone beam 3D reconstruction via the first derivative of the Radon transform. In *Mathematical methods in tomography*, p. 66–97, 1991.

[GuN14] J.-P. Guillement, R. G. Novikov. Inversion of weighted Radon transforms via finite Fourier series weight approximations. *Inverse Problems in Science and Engineering*, 22(5):787–802, 2014.

[Hi87] A. Higuchi. Symmetric tensor spherical harmonics on the n-sphere and their application to the de Sitter group SO(N, 1). *Journal of mathematical physics*, 28(7):1553–1566, 1987.

[Kn05] A. W. Knapp. *Advanced real analysis*. Springer, 2005.

[Ku92] L. A. Kunyansky. Generalized and attenuated Radon transforms: restorative approach to the numerical inversion. *Inverse Problems*, 8(5):809, 1992.

[Lo98] G. Lohöfer. Inequalities for the Associated Legendre functions. *Journal of Approximation Theory*, 95:178-193, 1998.

[Mo98] M. Morimoto. *Analytic functionals on the sphere*. American Mathematical Society, 1998.

[Na86] F. Natterer. *The mathematics of computerized tomography.*, vol. 32. SIAM, 1986.

[N+06] A. A. Neves, L.A. Padilha, A. F., E. Rodriguez, C. Cruz, L. Barbosa, C. Cesar. Analytical results for a Bessel function times Legendre polynomials class integrals. *Journal of Physics A: Mathematical and General*, 39(18):293, 2006.

[No11] R. G. Novikov. Weighted Radon transforms for which Chang's approximate inversion formula is exact. *Russian Mathematical Surveys*, 66(2):442–443, 2011.

[No14] R. G. Novikov. Weighted Radon transforms and first order differential systems on the plane. *Moscow mathematical journal*, 14(4):807–823, 2014.

[Qu83] E. Quinto. The invertibility of rotation invariant Radon transforms. *Journal of Mathematical Analysis and Applications*, 91(2):510–522, 1983.

[Ra17] J. Radon. Uber die Bestimmung von Funktionen durch ihre Integralwerte längs gewisser Mannigfaltigkeiten. *Ber. Saechs Akad. Wiss. Leipzig, Math-Phys*, 69:262–267, 1917.

[SW16] E. M. Stein, G. Weiss. *Introduction to Fourier analysis on Euclidean spaces (PMS-32)*, vol. 32. Princeton University Press, 2016.

[Te11] N. M. Temme. *Special functions: An introduction to the classical functions of mathematical physics*. John Wiley & Sons, 2011.

[ZT79] S. B. Zhizhiashvili, L. V. Topuriya. Fourier-Laplace series on a sphere. *Journal of Soviet Mathematics*, 12(6):682–714, 1979.

Part II

A breakdown of injectivity for weighted ray and Radon transforms

Article 3. A counterexample to injectivity for weighted Radon transforms

F. O. Goncharov, R. G. Novikov

We consider the weighted Radon transforms R_W along hyperplanes in $\mathbb{R}^d$, $d \geq 3$, with strictly positive weights $W = W(x, \theta)$, $x \in \mathbb{R}^d$, $\theta \in \mathbb{S}^{d-1}$. We construct an example of such a transform with non-trivial kernel in the space of infinitely smooth compactly supported functions. In addition, the related weight W is infinitely smooth almost everywhere and is bounded. Our construction is based on the famous example of non-uniqueness of J. Boman (1993) for the weighted Radon transforms in $\mathbb{R}^2$ and on a recent result of F. Goncharov and R. Novikov (2016).

1 Introduction

We consider the weighted Radon transforms R_W, defined by the formulas:

$$R_W f(s, \theta) = \int\limits_{x\theta=s} W(x, \theta) f(x)\, dx,\ (s, \theta) \in \mathbb{R} \times \mathbb{S}^{d-1},\ x \in \mathbb{R}^d,\ d \geq 2, \tag{5.1}$$

where $W = W(x, \theta)$ is the weight, $f = f(x)$ is a test function on $\mathbb{R}^d$.

We assume that W is real valued, bounded and strictly positive, i.e.:

$$W = \overline{W} \geq c > 0,\ W \in L^\infty(\mathbb{R}^d \times \mathbb{S}^{d-1}), \tag{5.2}$$

where $\overline{W}$ denotes the complex conjugate of W, c is a constant.

If $W \equiv 1$, then R_W is reduced to the classical Radon transform R along hyperplanes in $\mathbb{R}^d$. This transform is invertible by the classical Radon inversion formulas; see [Ra17].

If W is strictly positive, $W \in C^\infty(\mathbb{R}^d \times \mathbb{S}^{d-1})$ and $f \in C_0^\infty(\mathbb{R}^d)$, then in [Be84] the inversion of R_W is reduced to solving a Fredholm type linear integral equation. Besides, in [BQ87] it was proved that R_W is injective (for example, in $L_0^2(\mathbb{R}^d)$) if W is real-analytic and strictly positive. In addition, an example of R_W in $\mathbb{R}^2$ with infinitely smooth strictly positive W and with non-trivial kernel $\mathrm{Ker} R_W$ in $C_0^\infty(\mathbb{R}^2)$ was constructed in [Bo93]. Here C_0^∞, L_0^2 denote the spaces of functions from C^∞, L^2 with compact support, respectively.

In connection with the most recent progress in inversion methods for weighted Radon transforms R_W, see [Go17].

We recall also that inversion methods for R_W in $\mathbb{R}^3$ admit applications in the framework of emission tomographies (see [GN16]).

In the present work we construct an example of R_W in $\mathbb{R}^d$, $d \geq 3$, with non-trivial kernel $\mathrm{Ker} R_W$ in $C_0^\infty(\mathbb{R}^d)$. The related W satisfies (5.2). In addition, our weight W is infinitely smooth almost everywhere on $\mathbb{R}^d \times \mathbb{S}^{d-1}$.

In our construction we proceed from results of [Bo93] and [GN16].

In Section 2, in particular, we recall the result of [GN16].

In Section 3 we recall the result of [Bo93].

In Section 4 we obtain the main result of the present work.

2 Relations between the Radon and the ray transforms

We consider also the weighted ray transforms P_w in $\mathbb{R}^d$, defined by the formulas:

$$P_w f(x,\theta) = \int\limits_{\mathbb{R}} w(x+t\theta,\theta) f(x+t\theta)\, dt,\ (x,\theta) \in T\mathbb{S}^{d-1}, \tag{5.3}$$

$$T\mathbb{S}^{d-1} = \{(x,\theta) \in \mathbb{R}^d \times \mathbb{S}^{d-1} : x\theta = 0\},\ d \geq 2, \tag{5.4}$$

where $w = w(x,\theta)$ is the weight, $f = f(x)$ is a test-function on $\mathbb{R}^d$.

We assume that w is real valued, bounded and strictly positive, i.e.:

$$w = \overline{w} \geq c > 0,\ w \in L^\infty(\mathbb{R}^d \times \mathbb{S}^{d-1}). \tag{5.5}$$

We recall that $T\mathbb{S}^{d-1}$ can be interpreted as the set of all oriented rays in $\mathbb{R}^d$. In particular, if $\gamma = (x,\theta) \in T\mathbb{S}^{d-1}$, then

$$\gamma = \{y \in \mathbb{R}^d : y = x + t\theta,\ t \in \mathbb{R}\}, \tag{5.6}$$

where θ gives the orientation of γ.

We recall that for $d = 2$, transforms P_w and R_W are equivalent up to the following change of variables:

$$R_W f(s,\theta) = P_w f(s\theta, \theta^\perp),\ s \in \mathbb{R},\ \theta \in \mathbb{S}^1, \tag{5.7}$$

$$\begin{aligned} &W(x,\theta) = w(x,\theta^\perp),\ x \in \mathbb{R}^2,\ \theta \in \mathbb{S}^1, \\ &\theta^\perp = (-\sin\phi, \cos\phi) \text{ for } \theta = (\cos\phi, \sin\phi),\ \phi \in [0, 2\pi), \end{aligned} \tag{5.8}$$

where f is a test-function on $\mathbb{R}^2$.

For $d = 3$, the transforms R_W and P_w are related by the following formulas (see [GN16]):

$$R_W f(s,\theta) = \int\limits_{\mathbb{R}} P_w f(s\theta + \tau[\theta, \alpha(\theta)],\ \alpha(\theta))\, d\tau,\ (s,\theta) \in \mathbb{R} \times \mathbb{S}^2, \tag{5.9}$$

$$W(x,\theta) = w(x, \alpha(\theta)),\ x \in \mathbb{R}^3,\ \theta \in \mathbb{S}^2, \tag{5.10}$$

$$\alpha(\theta) = \begin{cases} \dfrac{[\eta,\theta]}{|[\eta,\theta]|},\ \text{if } \theta \neq \pm\eta, \\ \text{any vector } e \in \mathbb{S}^2,\ \text{such that } e \perp \theta,\ \text{if } \theta = \pm\eta, \end{cases} \tag{5.11}$$

where η is some fixed vector from $\mathbb{S}^2$, $[\cdot,\cdot]$ denotes the standard vector product in $\mathbb{R}^3$, $\perp$ denotes the orthogonality of vectors. Actually, formula (5.9) gives an expression for $R_W f$ on $\mathbb{R} \times \mathbb{S}^2$ in terms of $P_w f$ restricted to the rays $\gamma = \gamma(x,\theta)$, such that $\theta \perp \eta$, where W and w are related by (5.10).

Below we present analogs of (5.9)-(5.10) for $d > 3$.

Let

$$\Sigma(s,\theta) = \{x \in \mathbb{R}^d : x\theta = s\},\ s \in \mathbb{R},\ \theta \in \mathbb{S}^{d-1}, \tag{5.12}$$

$$\Xi(v_1,\dots,v_k) = \mathrm{Span}\{v_1,\dots,v_k\}, v_i \in \mathbb{R}^d,\ i = \overline{1,k}, 1 \le k \le d, \tag{5.13}$$

$$\Theta(v_1,v_2) = \{\theta \in \mathbb{S}^{d-1} : \theta \perp v_1, \theta \perp v_2\} \simeq \mathbb{S}^{d-3},\ v_1, v_2 \in \mathbb{R}^d,\ v_1 \perp v_2, \tag{5.14}$$

$(e_1, e_2, e_3, \dots, e_d)$ - be some fixed orthonormal, positively oriented basis in $\mathbb{R}^d$. (5.15)

If $(e_1,\dots,e_d)$ is not specified otherwise, it is assumed that $(e_1,\dots,e_d)$ is the standard basis in $\mathbb{R}^d$.

For $d > 3$, the transforms R_W and P_w are related by the following formulas:

$$R_W f(s,\theta) = \int\limits_{\mathbb{R}^{d-2}} P_w f(s\theta + \sum_{i=1}^{d-2} \tau_i \beta_i(\theta), \alpha(\theta))\, d\tau_1 \dots d\tau_{d-2},\ (s,\theta) \in \mathbb{R} \times \mathbb{S}^{d-1}, \tag{5.16}$$

$$W(x,\theta) = w(x, \alpha(\theta)),\ x \in \mathbb{R}^d,\ \theta \in \mathbb{S}^{d-1}, \tag{5.17}$$

where $\alpha(\theta)$, $\beta_i(\theta)$, $i = \overline{1, d-2}$, are defined as follows:

$$\alpha(\theta) = \begin{cases} \text{direction of one-dimensional intersection } \Sigma(s,\theta) \cap \Xi(e_1,e_2), \text{ where} \\ \text{the orientation of } \alpha(\theta) \text{ is chosen such that } \det(\alpha(\theta), \theta, e_3, \dots, e_d) > 0, \text{ if } \theta \notin \Theta(e_1,e_2), \\ \text{any vector } e \in \mathbb{S}^{d-1} \cap \Xi(e_1,e_2), \text{ if } \theta \in \Theta(e_1,e_2), \end{cases} \tag{5.18}$$

$(\alpha(\theta), \beta_1(\theta), \dots, \beta_{d-2}(\theta))$ is an orthonormal basis on $\Sigma(s,\theta)$, (5.19)

and $\Sigma(s,\theta)$, $\Theta(e_1,e_2)$ are given by (5.12), (5.14), respectively. Here, due to the condition $\theta \notin \Theta(e_1,e_2)$:

$$\dim(\Sigma(s,\theta) \cap \Xi(e_1,e_2)) = 1. \tag{5.20}$$

Formula (5.20) is proved in Section 5.

Note that formulas (5.16)-(5.20) are also valid for $d = 3$. In this case these formulas are reduced to (5.9)-(5.11), where $e_3 = -\eta$.

Note that, formula (5.16) gives an expression for $R_W f$ on $\mathbb{R} \times \mathbb{S}^{d-1}$ in terms of $P_w f$ restricted to the rays $\gamma = (x,\alpha)$, such that $\alpha \in \mathbb{S}^{d-1} \cap \Xi(e_1,e_2)$.

Remark 1: In (5.18) one can also write:

$$\alpha(\theta) = (-1)^{d-1} \star (\theta \wedge e_3 \wedge \dots \wedge e_d), \text{ if } \theta \notin \Theta(e_1,e_2), \tag{5.21}$$

where $\star$-denotes the Hodge star, $\wedge$ - is the exterior product in $\Lambda^*\mathbb{R}^d$ (exterior algebra on $\mathbb{R}^d$).

Note that the value of the integral in the right hand-side of (5.16) does not depend on the particular choice of $(\beta_1(\theta),\dots,\beta_{d-2}(\theta))$ of (5.19).

Note also that, due to (5.10), (5.11), (5.17), (5.18), the weight W is defined everywhere on $\mathbb{R}^d \times \mathbb{S}^{d-1}$, $d \ge 3$. In addition, this W has the same smoothness as w in x on $\mathbb{R}^d$ and in θ on $\mathbb{S}^{d-1} \backslash \Theta(e_1,e_2)$, where $\Theta(e_1,e_2)$ is defined in (5.14) and has zero Lebesgue measure on $\mathbb{S}^{d-1}$.

3 Boman's example

For $d = 2$, in [Bo93] there were constructed a weight W and a function f, such that:

$$R_W f \equiv 0 \text{ on } \mathbb{R} \times \mathbb{S}^1, \tag{5.22}$$

$$1/2 \le W \le 1, W \in C^\infty(\mathbb{R}^2 \times \mathbb{S}^1), \tag{5.23}$$

$$f \in C_0^\infty(\mathbb{R}^2),\ f \not\equiv 0,\ \mathrm{supp}\, f \subset \overline{B^2} = \{x \in \mathbb{R}^2 : |x| \le 1\}. \tag{5.24}$$

In addition, as a corollary of (5.7), (5.8), (5.22)-(5.24), we have that

$$P_{w_0} f_0 \equiv 0 \text{ on } T\mathbb{S}^1, \tag{5.25}$$
$$1/2 \le w_0 \le 1,\ w_0 \in C^\infty(\mathbb{R}^2 \times \mathbb{S}^1), \tag{5.26}$$
$$f_0 \in C_0^\infty(\mathbb{R}^2),\ f_0 \not\equiv 0,\ \operatorname{supp} f \subset \overline{B^2} = \{x \in \mathbb{R}^2 : |x| \le 1\}, \tag{5.27}$$

where

$$w_0(x,\theta) = W(x, -\theta^\perp),\ x \in \mathbb{R}^2,\ \theta \in \mathbb{S}^1, \tag{5.28}$$
$$f_0 \equiv f. \tag{5.29}$$

4 Main results

Let

$$B^d = \{x \in \mathbb{R}^d : |x| < 1\}, \tag{5.30}$$
$$\overline{B^d} = \{x \in \mathbb{R}^d : |x| \le 1\}, \tag{5.31}$$
$$(e_1, \dots, e_d) \text{ - be the canonical basis in } \mathbb{R}^d. \tag{5.32}$$

Theorem 1. *There are W and f, such that*

$$R_W f \equiv 0 \text{ on } \mathbb{R} \times \mathbb{S}^{d-1}, \tag{5.33}$$
$$W \text{ satisfies (5.2)},\ f \in C_0^\infty(\mathbb{R}^d),\ f \not\equiv 0, \tag{5.34}$$

where R_W is defined by (5.1). *In addition,*

$$1/2 \le W \le 1,\ W \text{ is } C^\infty\text{-smooth on } \mathbb{R}^d \times (\mathbb{S}^{d-1} \backslash \Theta(e_1, e_2)), \tag{5.35}$$

where $\Theta(e_1, e_2)$ is defined by (5.14). *Moreover, weight W and function f are given by formulas* (5.17), (5.37)-(5.39) *in terms of the J. Boman's weight w_0 and function f_0 of* (5.28), (5.29).

Remark 2: According to (5.17), (5.18), $W(x,\theta)$ for $\theta \in \Theta(e_1, e_2)$ can be specified as follows:

$$W(x,\theta) = W(x_1, \dots, x_d, \theta) \stackrel{\text{def}}{=} w_0(x_1, x_2, e_1),\ \theta \in \Theta(e_1, e_2),\ x \in \mathbb{R}^d. \tag{5.36}$$

Proof of Theorem 1. We define

$$w(x,\alpha) = w(x_1, \dots, x_d, \alpha) \stackrel{\text{def}}{=} w_0(x_1, x_2, \alpha_1, \alpha_2), \tag{5.37}$$
$$f(x) = f(x_1, \dots, x_d) \stackrel{\text{def}}{=} \psi(x_3, \dots, x_d) f_0(x_1, x_2), \tag{5.38}$$
$$\text{for } x = (x_1, \dots, x_d) \in \mathbb{R}^d,\ \alpha = (\alpha_1, \alpha_2, 0, \dots, 0) \in \mathbb{S}^{d-1} \cap \Xi(e_1, e_2) \simeq \mathbb{S}^1,$$

where

$$\psi \in C_0^\infty(\mathbb{R}^{d-2}),\ \operatorname{supp} \psi = \overline{B^{d-2}} \text{ and } \psi(x) > 0 \text{ for } x \in B^{d-2}. \tag{5.39}$$

From (5.3), (5.25), (5.37)-(5.39) it follows that:

$$\begin{aligned} P_w f(x,\alpha) &= \int\limits_{\mathbb{R}} w(x_1 + t\alpha_1, x_2 + t\alpha_2, x_3, \dots, x_d, \alpha) f(x_1 + t\alpha_1, x_2 + t\alpha_2, x_3, \dots, x_d)\, dt \\ &= \psi(x_3, \dots, x_d) \int\limits_{\mathbb{R}} w_0(x_1 + t\alpha_1, x_2 + t\alpha_2, \alpha_1, \alpha_2) f_0(x_1 + t\alpha_1, x_2 + t\alpha_2)\, dt \\ &= \psi(x_3, \dots, x_d) P_{w_0} f_0(x_1, x_2, \alpha_1, \alpha_2) = 0 \\ &\text{for any } \alpha = (\alpha_1, \alpha_2, 0, \dots, 0) \in \Xi(e_1, e_2) \cap \mathbb{S}^{d-1} \simeq \mathbb{S}^1. \end{aligned} \tag{5.40}$$

Properties (5.33)-(5.35) follow from (5.17)-(5.19), (5.21), (5.23), (5.24), (5.36), (5.37).

Theorem 1 is proved. □

5 Proof of formula (5.20)

Note that

$$\dim(\Xi(e_1, e_2)) + \dim(\Sigma(s, \theta)) = d + 1 > d, \tag{5.41}$$

which implies that the intersection $\Sigma(s, \theta) \cap \Xi(e_1, e_2)$ is one of the following:

1. The intersection is the one dimensional line $l = l(s, \theta)$:

$$l(s, \theta) = \{x \in \mathbb{R}^d : x = x_0(s, \theta) + \alpha(\theta)t,\, t \in \mathbb{R}\},\, \alpha(\theta) \in \mathbb{S}^2, \tag{5.42}$$

   where $x_0(s, \theta)$ is an arbitrary point of $\Sigma(s, \theta) \cap \Xi(e_1, e_2)$, the orientation of $\alpha(\theta)$ is chosen such that:

$$\det(\alpha(\theta),\, \theta,\, e_3, \ldots, e_d) > 0. \tag{5.43}$$

   Condition (5.43) fixes uniquely the direction of $\alpha(\theta)$ of (5.42).

   Formulas (5.12), (5.13), (5.14) imply that (5.43) can hold if and only if $\theta \notin \Theta(e_1, e_2)$.

2. The intersection is the two-dimensional plane $\Xi(e_1, e_2)$. Formulas (5.12), (5.13) imply that it is the case if and only if

$$s = 0,\, \theta \perp e_1,\, \theta \perp e_2. \tag{5.44}$$

3. The intersection is an empty set. Formulas (5.12), (5.13) imply that it is the case if and only if

$$s \neq 0,\, \theta \perp e_1,\, \theta \perp e_2. \tag{5.45}$$

Note that

$$\text{cases 2 and 3 occur if and only if } \theta \perp e_1,\, \theta \perp e_2,\ \text{i.e., } \theta \in \Theta(e_1, e_2). \tag{5.46}$$

This completes the proof of formula (5.20).

6 Acknowledgments

This work is partially supported by the PRC n° 1545 CNRS/RFBR: Équations quasi-linéares, problèmes inverses et leurs applications.

Bibliography

[Be84] G. Beylkin. The inversion problem and applications of the generalized Radon transform. *Communications on pure and applied mathematics*, 37(5): 579-599, 1984.

[BQ87] J. Boman, E. Quinto. Support theorems for real-analytic Radon transforms. *Duke Mathematical Journal*, 55(4): 943-948, 1987.

[Bo93] J. Boman. An example of non-uniqueness for a generalized Radon transform. *Journal d'Analyse Mathematique*, 61(1): 395–401, 1993.

[GN16] F. O. Goncharov, R. G. Novikov. An analog of Chang inversion formula for weighted Radon transforms in multidimensions. *Eurasian Journal of Mathematical and Computer Applications*, 4(2): 23-32, 2016.

[Go17] F. O. Goncharov. An iterative inversion of weighted Radon transforms along hyperplanes, *Inverse Problems*, **33** 124 005, 2017.

[MQ85] A. Markoe, E. Quinto. An elementary proof of local invertibility for generalized and attenuated Radon transforms. *SIAM Journal on Mathematical Analysis*, 16(5): 1114–1119, 1985.

[Ra17] J. Radon, Über die Bestimmung von Funktionen durch ihre Integralwerte längs gewisser Mannigfaltigkeiten. *Ber. Saechs Akad. Wiss. Leipzig, Math-Phys*, 69: 262–267, 1917.

Article 4. An example of non-uniqueness for Radon transforms with positive continuous rotation invariant weights

F.O. Goncharov, R. G. Novikov

We consider weighted Radon transforms R_W along hyperplanes in $\mathbb{R}^3$ with strictly positive weights W. We construct an example of such a transform with non-trivial kernel $\mathrm{Ker} R_W$ in the space of infinitely smooth compactly supported functions and with continuous weight. Moreover, in this example the weight W is rotation invariant. In particular, by this result we continue studies of Quinto (1983), Markoe, Quinto (1985), Boman (1993) and Goncharov, Novikov (2017). We also extend our example to the case of weighted Radon transforms along two-dimensional planes in $\mathbb{R}^d$, $d \geq 3$.

1 Introduction

We consider weighted Radon transforms R_W in $\mathbb{R}^d$ defined by

$$R_W f(s,\theta) = \int\limits_{x\theta=s} W(x,\theta) f(x)\, dx, \tag{6.1}$$
$$s \in \mathbb{R},\ \theta \in \mathbb{S}^{d-1},\ x \in \mathbb{R}^d,\ d \geq 2,$$

where $W = W(x,\theta)$ is the weight, $f = f(x)$ is a test function on $\mathbb{R}^d$.

We assume that

$$W = \overline{W} \geq c > 0,\ W \in L^\infty(\mathbb{R}^d \times \mathbb{S}^{d-1}), \tag{6.2}$$

where $\overline{W}$ denotes the complex conjugate of W, c is a constant.

Note that

$$R_W f(s,\theta) = R_W f(P) = \int\limits_P W(x,P) f(x)\, dx, \tag{6.3}$$

where

$$W(x,P) = W(x,\theta) \text{ for } x \in P,\ \theta \perp P, \tag{6.4}$$
$$P = P_{(s,\theta)} = \{x \in \mathbb{R}^d : x\theta = s\},\ s \in \mathbb{R},\ \theta \in \mathbb{S}^{d-1}. \tag{6.5}$$

That is the transforms R_W are weighted Radon transforms along oriented hyperplanes P in $\mathbb{R}^d$.

The transforms R_W arise in various domains of pure and applied mathematics; see, e.g., [Be84], [Be85], [BQ87], [Bo93], [Fi86], [LB73], [GN16], [Go17], [GN17], [Ku92], [Na01], [No14], [Qu83], [Qu83Err] and references therein.

In particular, studies on the transforms R_W under assumptions (6.2) were recently continued in [GN16], [Go17], [GN17] for $d \geq 3$.

Note that the works [GN16], [Go17] extend to the case of R_W, $d \geq 3$, the two-dimensional injectivity and reconstruction results of [Ku92], [No11], [No14], [GuN14].

On the other hand, under assumptions (6.2), the work [GN17] gives an example of R_W, $d \geq 3$, with non-trivial kernel in $C_0^\infty(\mathbb{R}^d)$ (infinitely smooth functions with compact support). This example was constructed in [GN17] proceeding from the example of non-uniqueness of [Bo93] for R_W in $\mathbb{R}^2$ and a recent result of [GN16].

In the two-dimensional example of non-uniqueness of [Bo93] the weight W satisfies (6.2), for $d = 2$, and is infinitely smooth everywhere. In the multidimensional example of non-uniqueness of [GN17] the weight W satisfies (6.2), for $d \geq 3$, is infinitely smooth almost everywhere but is not yet continuous at some points.

In the present work we construct an example of R_W, for $d = 3$, with non-trivial kernel in $C_0^\infty(\mathbb{R}^3)$, where W satisfies (6.2) and is continuous everywhere. Moreover, in this example W is rotation invariant and $R_W f \equiv 0$ for some non-zero spherically symmetric $f \in C_0^\infty(\mathbb{R}^3)$; see Theorem 1 of Section 3.

The rotation invariancy of the latter example is its principal advantage in comparison with the aforementioned examples of [Bo93] and [GN17].

By our rotation invariant example of non-uniqueness we also continue studies of [MQ85], where a rotation invariant example of non-uniqueness for R_W was constructed for $d = 2$. In the example of [MQ85] the weight W is bounded, positive and rotation invariant but is not yet continuous and strictly positive. The continuity and strict positivity of W is the principal advantage of the example of the present work in comparison with the example of [MQ85].

In a similar way with [Qu83], we say that W is rotation invariant if and only if

$$\begin{aligned} &W(x,P) \text{ is independent of the orientation of } P, \\ &W(x,P) = W(Ax,AP) \text{ for } x \in P,\ P \in \mathcal{P}, A \in O(d), \end{aligned} \tag{6.6}$$

where $\mathcal{P}$ denotes the manifold of all oriented planes in $\mathbb{R}^d$, $O(d)$ denotes the group of orthogonal transformations of $\mathbb{R}^d$.

Note also that property (6.6) can be rewritten in the form (6.16), (6.17) or (6.18), (6.19); see Section 2.

On the other hand, we recall that weighted Radon transforms R_W in $\mathbb{R}^d$ with rotation invariant, strictly positive and smooth weights W satisfying properties (6.6) are injective on $L_0^2(\mathbb{R}^d)$ (square integrable functions on $\mathbb{R}^d$ with compact support); see [Qu83]. Here the smoothness of W can be specified, at least, as C^1 for $d = 2$ and $d = 3$. In view of this result of [Qu83], the rotation invariant example of non-uniqueness of R_W constructed in the present work with strictly positive and, at least, continuous weight W is surprising.

In the present work we also extend our rotation invariant example of non-uniqueness for R_W in $\mathbb{R}^3$ to the case of weighted Radon transforms $R_W^{d,2}$ along two-dimensional planes in $\mathbb{R}^d$, $d > 3$; see Corollary 1.1 of Section 4. In this case $R_W^{d,2} f$ is defined on $\mathcal{P}^{d,2}$ (manifold of all oriented two-dimensional planes in $\mathbb{R}^d$) and is overdetermined already. That is

$$\dim \mathcal{P}^{d,2} = 3d - 6 > \dim \mathbb{R}^d = d \text{ for } d > 3. \tag{6.7}$$

Nevertheless, $R_W^{d,2} f \equiv 0$ on $\mathcal{P}^{d,2}$ in our result.

We expect that the results of the present work admit generalizations to the weighted Radon transforms $R_W^{d,n}$ along n-dimensional planes in $\mathbb{R}^d$ for arbitrary d and n such that $1 \le n < d$, $d \ge 2$. For $n = 1$ such results are already obtained in [GN17].

Note also that the construction of the present work was developed in a large extent in the process of adopting the Boman's construction of the aforementioned work [Bo93].

In Section 2 we give some preliminaries.

Our main results are formulated in detail in Sections 3 and 4.

Proofs are given in Sections 5-8.

2 Some preliminaries

Notations for $d = 3$. Let

$$B = \{x \in \mathbb{R}^3 : |x| < 1\}, \overline{B} = \{x \in \mathbb{R}^3 : |x| \le 1\}, \tag{6.8}$$

$$\mathcal{P} = \mathbb{R} \times \mathbb{S}^2, \tag{6.9}$$

$$\mathcal{P}_0(\delta) = \{(s, \theta) \in \mathcal{P} : |s| > \delta\}, \tag{6.10}$$

$$\mathcal{P}_1(\delta) = \mathcal{P} \backslash \mathcal{P}_0(\delta) = \{(s, \theta) \in \mathcal{P} : |s| \le \delta\},\ \delta > 0, \tag{6.11}$$

$$\mathcal{P}(\Lambda) = \{(s, \theta) \in \mathcal{P} : s \in \Lambda\},\ \Lambda \subset \mathbb{R}, \tag{6.12}$$

$$\Omega(\Lambda) = \{(x, \theta) \in \mathbb{R}^3 \times \mathbb{S}^2 : x\theta \in \Lambda\},\ \Lambda \subset \mathbb{R}, \tag{6.13}$$

$$\mathcal{J}_{s,\varepsilon} = \mathcal{J}_{|s|,\varepsilon} = (-|s| - \varepsilon, -|s| + \varepsilon) \cup (|s| - \varepsilon, |s| + \varepsilon) \subset \mathbb{R},\ s \in \mathbb{R},\ \varepsilon > 0. \tag{6.14}$$

Note that $\mathcal{P}_0(\delta), \mathcal{P}_1(\delta)$ of (6.10), (6.11) are particular cases of $P(\Lambda)$ of formula (6.12).

In addition, we interpret $\mathcal{P}$ as the set of all oriented planes in $\mathbb{R}^3$. If $P = (s, \theta) \in \mathcal{P}$, then

$$P = P_{(s,\theta)} = \{x \in \mathbb{R}^3 : x\theta = s\} \text{ (modulo orientation)} \tag{6.15}$$

and θ gives the orientation of P (in the sense that ordered tuple (e_1, e_2, θ) is positively oriented in $\mathbb{R}^3$ with any orthonormal positively oriented basis e_1, e_2 on P).

The set $\mathcal{P}_0(\delta)$ in (6.10) is considered as the set of all oriented planes in $\mathbb{R}^3$ which are positioned at distance greater than δ from the origin.

The set $\mathcal{P}_1(\delta)$ in (6.11) is considered as the set of all oriented planes in $\mathbb{R}^3$ which are located at distance less or equal than δ.

Rotation invariancy for $d = 3$. Using formulas (6.4), (6.5), for positive and continuous W property (6.6) can be rewritten in the following equivalent form:

$$W(x, \theta) = U(|x - (x\theta)\theta|, x\theta),\ x \in \mathbb{R}^d,\ \theta \in \mathbb{S}^{d-1}, \tag{6.16}$$

for some positive and continuous U such that

$$U(r, s) = U(-r, s) = U(r, -s),\ r \in \mathbb{R},\ s \in \mathbb{R}. \tag{6.17}$$

In addition, symmetries (6.16), (6.17) of W can be also written as

$$W(x, \theta) = \tilde{U}(|x|, x\theta),\ x \in \mathbb{R}^3,\ \theta \in \mathbb{S}^2, \tag{6.18}$$

$$\tilde{U}(r, s) = \tilde{U}(r, -s),\ \tilde{U}(r, s) = \tilde{U}(-r, s),\ r \in \mathbb{R},\ s \in \mathbb{R}, \tag{6.19}$$

where $\tilde{U}$ is positive and continuous on $\mathbb{R} \times \mathbb{R}$. Using the formula $|x|^2 = |x\theta|^2 + |x - (x\theta)\theta|^2$, $\theta \in \mathbb{S}^2$, one can see that symmetries (6.16), (6.17) and symmetries (6.18), (6.19) of W are equivalent.

Additional notations. For a function f on $\mathbb{R}^d$ we denote its restriction to a subset Σ by $f|_\Sigma$.

By C_0, C_0^∞ we denote continuous compactly supported and infinitely smooth compactly supported functions, respectively.

Partition of unity. We recall the following classical result (see Theorem 5.6 in [MD92]): *Let $\mathcal{M}$ be a C^∞-manifold, which is Hausdorff and satisfies second countability axiom (i.e. has countable base). Let also $\{U_i\}_{i=1}^\infty$ be the open locally-finite cover of $\mathcal{M}$.*

Then there exists a C^∞-smooth locally-finite partition of unity $\{\psi_i\}_{i=1}^\infty$ on $\mathcal{M}$, such that

$$\operatorname{supp}\psi_i \subset U_i. \tag{6.20}$$

In particular, any open interval $(a,b) \subset \mathbb{R}$ and $\mathcal{P} \simeq \mathbb{R}\times\mathbb{S}^2$ satisfy conditions of the aforementioned statement. It will be used in Subsection 3.4.

3 Main results for $d = 3$

Theorem 1. *There exist a non-zero spherically symmetric function $f \in C_0^\infty(\mathbb{R}^3)$ with support in $\overline{B}$, and W satisfying* (6.2), (6.16), (6.17) *such that*

$$R_W f \equiv 0, \tag{6.21}$$

where R_W is defined in (6.1).

The construction of f and W proving Theorem 1 is presented below in Subsections 3.1-3.4 and commented in Remarks 1-6. This construction adopts considerations of [Bo93]. In particular, we construct f, first, and then W.

3.1 Construction of f

The function f is constructed as follows:

$$f = \sum_{k=1}^{\infty} \frac{f_k}{k!}, \tag{6.22}$$

$$f_k(x) = f_k(|x|) = \Phi(2^k(1-|x|))\cos(8^k|x|^2), x\in\mathbb{R}^3,\ k = 1,2,\dots, \tag{6.23}$$

for arbitrary $\Phi \in C^\infty(\mathbb{R})$ such that

$$\operatorname{supp}\Phi = [4/5, 6/5], \tag{6.24}$$

$$0 < \Phi(t) \le 1 \text{ for } t \in (4/5, 6/5), \tag{6.25}$$

$$\Phi(t) = 1 \text{ for } t \in [9/10, 11/10]. \tag{6.26}$$

Properties (6.24), (6.25) imply that functions f_k in (6.23) have disjoint supports and series (6.22) converges for every fixed $x \in \mathbb{R}^3$.

Lemma 1. *Let f be defined by* (6.22)-(6.26). *Then f is spherically symmetric, $f \in C_0^\infty(\mathbb{R}^3)$ and* $\operatorname{supp} f \subseteq \overline{B}$. *In addition, if $P \in \mathcal{P}$, $P \cap B \neq \emptyset$, then $f|_P \not\equiv 0$ and $f|_P$ has non-constant sign.*

Lemma 1 is proved in Section 5.

Remark 1. Formulas (6.22)-(6.26) for f are similar to the formulas for f in [Bo93] in $\mathbb{R}^2$. However, the important difference is that in formula (6.23) the factor $\cos(8^k|x|^2)$ depends only on $|x|$, whereas in [Bo93] the corresponding factor is $\cos(3^k\phi)$ and it depends only on the angle ϕ in the polar coordinates in $\mathbb{R}^2$. In a similar way with [Bo93], we use the property that the restriction of the function $\cos(8^k|x|^2)$ to an arbitrary plane P intersecting the open ball oscillates sufficiently fast (with change of the sign) for large k.

3.2 Construction of W

In our example W is of the following form:

$$\begin{aligned} W(x,\theta) &= \sum_{i=0}^{N} \xi_i(|x\theta|)W_i(x,\theta) \\ &= \xi_0(|x\theta|)W_0(x,\theta) + \sum_{i=1}^{N} \xi_i(|x\theta|)W_i(x,\theta),\ x \in \mathbb{R}^3,\ \theta \in \mathbb{S}^2, \end{aligned} \tag{6.27}$$

where

$$\{\xi_i(s),\ s \in \mathbb{R}\}_{i=0}^{N} \text{ is a } C^\infty\text{-smooth partition of unity on } \mathbb{R}, \tag{6.28}$$

$$\xi_i(s) = \xi_i(-s),\ s \in \mathbb{R},\ i = 0,\dots,N, \tag{6.29}$$

$$\begin{aligned} &W_i(x,\theta) \text{ are bounded continuous strictly positive and} \\ &\text{rotation invariant (according to (6.16), (6.17)) on } \operatorname{supp}\xi_i(|x\theta|),\ i = 0,\dots,N, \text{ respectively.} \end{aligned} \tag{6.30}$$

From (6.27)-(6.30) it follows that W of (6.27) satisfies the conditions (6.2), (6.16), (6.17). The weight W_0 is constructed in Subsection 3.3 and has the following properties:

$$W_0 \text{ is bounded, continuous and rotation invariant on } \{(x,\theta) : |x\theta| > 1/2\}, \tag{6.31}$$

there exists $\delta_0 \in (1/2, 1)$ such that:

$$W_0(x,\theta) \geq 1/2 \text{ if } |x\theta| > \delta_0, \tag{6.32}$$

$$W_0(x,\theta) = 1 \quad \text{if } |x\theta| \geq 1,$$

$$R_{W_0}f(s,\theta) = 0 \text{ for } |s| > 1/2,\ \theta \in \mathbb{S}^2, \tag{6.33}$$

where R_{W_0} is defined according to (6.1) for $W = W_0$, f is given by (6.22), (6.23).

In addition,

$$\operatorname{supp}\xi_0 \subset (-\infty, -\delta_0) \cup (\delta_0, +\infty), \tag{6.34}$$

$$\xi_0(s) = 1 \text{ for } |s| \geq 1, \tag{6.35}$$

where δ_0 is the number of (6.32).

In particular, from (6.28), (6.32), (6.34) it follows that

$$W_0(x,\theta)\xi_0(|x\theta|) > 0 \text{ if } \xi_0(|x\theta|) > 0. \tag{6.36}$$

Remark 2. The result of (6.31)-(6.33) can be considered as a counterexample to the Cormack-Helgason support theorem (see Theorem 3.1 in [Na01]) in the framework of the theory of weighted Radon transforms under assumptions (6.2) and even under assumptions (6.2), (6.16), (6.17).

In addition,

$$\xi_i(|x\theta|)W_i(x,\theta) \text{ are bounded, continuous and rotation invariant on } \mathbb{R}^3 \times \mathbb{S}^2, \tag{6.37}$$

$$W_i(x,\theta) \geq 1/2 \text{ if } \xi_i(|x\theta|) \neq 0, \tag{6.38}$$

$$R_{W_i} f(s,\theta) = 0 \text{ if } \xi_i(|s|) \neq 0, \tag{6.39}$$

$$i = 1, \ldots, N,\ x \in \mathbb{R}^3,\ \theta \in \mathbb{S}^2,\ s \in \mathbb{R}. \tag{6.40}$$

Weights $W_1, \ldots, W_N$ of (6.27) and $\{\xi_i\}_{i=0}^N$ are constructed in Subsection 3.4.

Result of Theorem 1 follows from Lemma 1 and formulas (6.27)-(6.33), (6.36)-(6.40).

We point out that the construction of W_0 of (6.27) is substantially different from the construction of $W_1, \ldots, W_N$. In particular, the weight W_0 is defined on the planes $P \in \mathcal{P}$ which can be close to the boundary ∂B of B which results in restrictions on the smoothness of W_0.

Remark 3. The construction of W summarized above in formulas (6.27)-(6.40) arises from a choice of W such that

$$R_W f \equiv 0 \text{ on } \mathcal{P} \text{ for } f \text{ defined in Subsection 3.1}, \tag{6.41}$$

under the condition that W is strictly positive, sufficiently regular and rotation invariant (see formulas (6.2), (6.16), (6.17)). In addition, the weights W_i, $i = 0, \ldots, N$, in (6.27) are chosen such that

$$R_{W_i} f = 0 \text{ on } \Omega_i,\ i = 0, \ldots, N, \tag{6.42}$$

under the condition that $W_i = W_i(x, P)$ are strictly positive, sufficiently regular and rotation invariant for $x \in P$, $P \in \Omega_i$, $i = 0, \ldots, N$, where

$$\{\Omega_i\}_{i=0}^N \text{ is an open cover of } \mathcal{P} \text{ and } \Omega_0 = \mathcal{P}_0(\delta_0), \tag{6.43}$$

where $\mathcal{P}$, $\mathcal{P}_0$ are defined in (6.9), (6.10), δ_0 is the number of (6.32). This is similar to the construction in [Bo93] with the important difference that in the present work f is spherically symmetric and W, W_i, $i = 0, \ldots, N$, are rotation invariant. In the present work we have also that

$$\Omega_i = \mathcal{P}(\Lambda_i) \text{ for some open } \Lambda_i \subset \mathbb{R},\ i = 0, \ldots, N, \tag{6.44}$$

where $P(\Lambda)$ is defined in (6.12). In addition, the functions ξ_i, $i = 0, \ldots, N$, in (6.27) can be interpreted as a partition of unity on $\mathcal{P}$ subordinated to the open cover $\{\Omega_i\}_{i=0}^N$.

3.3 Construction of W_0

Let

$$\{\psi_k\}_{k=1}^\infty \text{ be a } C^\infty \text{ partition of unity on } (1/2, 1), \text{ such that } \operatorname{supp} \psi_k \subset (1-2^{-k+1}, 1-2^{-k-1}),\ k \in \mathbb{N}. \tag{6.45}$$

Note that

$$1 - 2^{-(k-2)-1} < 1 - 2^{-k}(6/5),\ k \geq 3. \tag{6.46}$$

Therefore,

$$s_0, t_0 \in \mathbb{R}, s_0 \in \operatorname{supp} \psi_{k-2},\ t_0 \in \operatorname{supp} \Phi(2^k(1-t)) \Rightarrow s_0 < t_0,\ k \geq 3. \tag{6.47}$$

The weight W_0 is defined by the following formulas

$$W_0(x,\theta) = \begin{cases} 1 - G(x,\theta) \sum\limits_{k=3}^{\infty} k! f_k(x) \dfrac{\psi_{k-2}(|x\theta|)}{H_k(x,\theta)}, \ 1/2 < |x\theta| < 1, \\ 1, \ |x\theta| \geq 1 \end{cases}, \tag{6.48}$$

$$G(x,\theta) = \int\limits_{y\theta = x\theta} f(y)\, dy, \ H_k(x,\theta) = \int\limits_{y\theta = x\theta} f_k^2(y)\, dy, \tag{6.49}$$

$$x \in \mathbb{R}^3, \ \theta \in \mathbb{S}^2,$$

where f_k are defined in (6.23).

Formula (6.48) implies that W_0 is defined on $\mathcal{P}_0(1/2) \subset \mathcal{P}$. Due to (6.23) and (6.47), in (6.49) we have that $H_k(x,\theta) \neq 0$ if $\psi_{k-2}(|x\theta|) \neq 0$.

Also, due to the partition of unity $\{\psi_k\}_{k=1}^{\infty}$, for any fixed $(x,\theta) \in \mathbb{R}^3 \times \mathbb{S}^2$, $1/2 < |x\theta| < 1$, the series in the right hand-side of (6.48) has only a finite number of non-zero terms (in fact, no more than two) and, hence, W_0 is well-defined.

By the spherical symmetry of f, functions G, H_k in (6.48) are of the type (6.18), (6.19). Therefore, W_0 is rotation invariant (in the sense (6.16), (6.17) or (6.18), (6.19)).

Actually, formula (6.33) follows from (6.22)-(6.24), (6.48), (6.49) (see Subsection 5.2 for details).

Using the construction of W_0 and the assumption that $|x\theta| > 1/2$ (implying that $\mathrm{sign}(x\theta)$ is locally constant) one can see that W_0 is C^∞ on its domain of definition, possibly, except points with $|x\theta| = 1$.

Lemma 2. *Let W_0 be defined by* (6.48), (6.49). *Then the following estimate holds:*

$$|1 - W_0(x,\theta)| \leq C_0 \rho(|x\theta|) \left(\log_2 \frac{1}{\rho(|x\theta|)} \right)^4, \tag{6.50}$$

$$W_0(x,\theta) \to 1 \ \textit{as} \ |x\theta| \to 1, \tag{6.51}$$

$$x \in \mathbb{R}^3, \ \theta \in \mathbb{S}^2, \ 1/2 < |x\theta| < 1.$$

where $\rho = \rho(s) = 1 - s$, $s \in (1/2, 1)$, C_0 is a positive constant depending on Φ.

Lemma 2 is proved in Section 6.

Note that Lemma 2 implies strict positivity of W_0 on $(x,\theta) \in \mathbb{R}^3 \times \mathbb{S}^2 : |x\theta|$ is close to 1. This allows to choose $\delta_0 \in (1/2, 1)$ for (6.32) to be satisfied.

This completes the proof of (6.32) and the description of W_0 and δ_0.

Remark 4. Formulas (6.48), (6.49) given above for the weight W_0 are considered for the planes from $\mathcal{P}_0(\delta_0)$ (mentioned in Remark 3) and, in particular, for planes close to the tangent planes to ∂B. This is similar to the related formulas in [Bo93] with the important difference that f, f_k are spherically symmetric in the present work and, as a corollary, W_0 is rotation invariant. Also, in a similar way with [Bo93], in the present work we show that $G(x,\theta)$ tends to zero sufficiently fast as $|x\theta| \to 1$. This is a very essential point for Lemma 2 and for continuity of W_0.

3.4 Construction of $W_1, \ldots, W_N$ and $\xi_0, \ldots, \xi_N$

Lemma 3. *Let $f \in C_0(\mathbb{R}^3)$ be spherically symmetric, $P_{(s_0,\theta_0)} \in \mathcal{P}$, $f|_{P_{(s_0,\theta_0)}} \not\equiv 0$ and $f|_{P_{(s_0,\theta_0)}}$ changes the sign. Then:*

(i) there exist $\varepsilon > 0$ and weight $W_{f,s_0,\varepsilon}$ such that

$$R_{W_{f,s_0,\varepsilon}} f(s,\theta) = 0 \text{ for } s \in \mathcal{J}_{s_0,\varepsilon},\ \theta \in \mathbb{S}^2, \tag{6.52}$$

where $\mathcal{J}_{s,\varepsilon}$ is defined in (6.14)*, $W_{f,s_0,\varepsilon}$ is defined on the open set $\Omega(\mathcal{J}_{s_0,\varepsilon})$, defined by* (6.13)*;*

(ii) weight $W_{f,s_0,\varepsilon}$ is bounded, continuous, strictly positive and rotation invariant on $\Omega(\mathcal{J}_{s_0,\varepsilon})$.

Lemma 3 is proved in Section 7.

Remark 5. In Lemma 3 the construction of $W_{f,s_0,\varepsilon}$ arises from

1. finding strictly positive and regular weight $W_{f,s_0,\varepsilon}$ on the planes $P = P_{(s,\theta)}$ with fixed $\theta = \theta_0$, where $s \in \mathcal{J}_{s_0,\varepsilon}$ for some $\varepsilon > 0$, such that (6.52) holds for $\theta = \theta_0$ and under the condition that

$$W_{f,s_0,\varepsilon}(x,P) = W_{f,s_0,\varepsilon}(|x - x_P|, P),\ x \in P = (s,\theta_0),\ s \in \mathcal{J}_{s_0,\varepsilon}, \tag{6.53}$$

   where x_P is the closest point on the plane P to the origin in $\mathbb{R}^3$;

2. extending $W_{f,s_0,\varepsilon}$ to all planes $P_{(s,\theta)}$, $s \in \mathcal{J}_{s_0,\varepsilon}$, $\theta \in \mathbb{S}^2$, via formula (6.6).

Let f be the function of (6.22), (6.23). Then, using Lemmas 1, 3 one can see that

$$\begin{aligned} &\forall \delta \in (0,1) \text{ there exist } \{J_i = \mathcal{J}_{s_i,\varepsilon_i}, W_i = W_{f,s_i,\varepsilon_i}\}_{i=1}^N \\ &\text{such that } J_i,\ i = 1,\dots,N, \text{ is an open cover of } [-\delta,\delta] \\ &\text{and } W_i \text{ satisfy (i) and (ii) (of Lemma 3) on } \Omega(J_i). \end{aligned} \tag{6.54}$$

Actually, we consider (6.54) for the case of $\delta = \delta_0$ of (6.32).
Note that in this case $\{\mathcal{P}(J_i)\}_{i=1}^N$ for J_i of (6.54) is an open cover of $\mathcal{P}_1(\delta_0)$.
To the set $\mathcal{P}_0(\delta_0)$ we associate the open set

$$J_0 = (-\infty, \delta_0) \cup (\delta_0, +\infty) \subset \mathbb{R}. \tag{6.55}$$

Therefore, the collection of intervals $\{J_i,\ i = 0,\dots,N\}$ is an open cover of $\mathbb{R}$.

We construct the partition of unity $\{\xi_i\}_{i=0}^N$ on $\mathbb{R}$ as follows:

$$\xi_i(s) = \xi_i(|s|) = \frac{1}{2}(\tilde{\xi}_i(s) + \tilde{\xi}_i(-s)),\ s \in \mathbb{R}, \tag{6.56}$$

$$\operatorname{supp} \xi_i \subset J_i,\ i = 0,\dots,N, \tag{6.57}$$

where $\{\tilde{\xi}_i\}_{i=0}^N$ is a partition of unity for the open cover $\{J_i\}_{i=0}^N$ (see Section 2, Partition of unity, for $U_i = J_i$).

Properties (6.34), (6.57) follow from (6.20) for $\{\tilde{\xi}_i\}_{i=0}^N$ (with $U_i = J_i$), the symmetry of $J_i = \mathcal{J}_{s_i,\varepsilon_i}$, $i = 1,\dots,N$, choice of J_0 in (6.55) and from (6.56).

In addition, (6.35) follows from (6.55) and the construction of J_i, $i = 1,\dots,N$, from (6.54) (see the proof of Lemma 3 and properties (6.54) in Section 7 for details).

Properties (6.37)-(6.40) follow from (6.54) for $\delta = \delta_0$ and from (6.55)-(6.57).

Remark 6. We have that $J_i = \Lambda_i$, $i = 1,\dots,N$, where Λ_i are the intervals in formula (6.44) of Remark 3 and J_i are the intervals considered in (6.54), (6.55).

4 Extension to the case of $R_W^{d,2}$

We consider the weighted Radon transforms $R_W^{d,2}$ along two-dimensional planes in $\mathbb{R}^d$, defined by

$$R_W^{d,2} f(P) = \int\limits_P W(x,P) f(x)\, dx,\ P \in \mathcal{P}^{d,2},\ x \in P,\ d \geq 3, \tag{6.58}$$

where $W = W(x,P)$ is the weight, $f = f(x)$ is a test function on $\mathbb{R}^d$,

$$\mathcal{P}^{d,2} \text{ is the manifold of all oriented two-dimensional planes } P \text{ in } \mathbb{R}^d. \tag{6.59}$$

Note that the transform $R_W^{d,2}$ is reduced to R_W of (6.1) for $d = 3$.

We say that positive and continuous W in (6.58) is rotation invariant if and only if

$$W(x,P) = \tilde{U}(|x|, \operatorname{dist}(P,\{0\})), \tag{6.60}$$

$$\tilde{U}(r,s) = \tilde{U}(r,-s),\ \tilde{U}(r,s) = \tilde{U}(-r,s),\ r \in \mathbb{R},\ s \in \mathbb{R}, \tag{6.61}$$

where $\tilde{U}$ is some positive and continuous function on $\mathbb{R}\times\mathbb{R}$, $\operatorname{dist}(P,\{0\})$ denotes the distance from the origin $\{0\} \in \mathbb{R}^d$ to the plane P. Note that $W(x,P)$ is independent of the orientation of P in this case.

Consider $\tilde{U}$ and $\tilde{f}$ such that

$$W(x,\theta) = \tilde{U}(|x|,|x\theta|),\ f(x) = \tilde{f}(|x|),\ x \in \mathbb{R}^3,\ \theta \in \mathbb{S}^2, \tag{6.62}$$

for W and f of Theorem 1 of Section 3.

Theorem 1 implies the following corollary:

Corollary 1.1. *Let W and f be defined as*

$$W(x,P) = \tilde{U}(|x|, \operatorname{dist}(P,\{0\})),\ P \in \mathcal{P}^{d,2},\ x \in P, \tag{6.63}$$

$$f(x) = \tilde{f}(|x|),\ x \in \mathbb{R}^d, \tag{6.64}$$

where $\tilde{U}$, $\tilde{f}$ are the functions of (6.62) *and $d > 3$. Then*

$$R_W^{d,2} f \equiv 0 \text{ on } \mathcal{P}^{d,2}. \tag{6.65}$$

In addition, the weight W is continuous strictly positive and rotation invariant, f is infinitely smooth compactly supported on $\mathbb{R}^d$ and $f \not\equiv 0$.

Formula (6.65) is proved as follows:

$$R_W^{d,2}(P) = \int\limits_P \tilde{U}(|x|, \operatorname{dist}(P,\{0\}))\tilde{f}(|x|)\, dx = I \stackrel{\text{def}}{=} \int\limits_{P'} \tilde{U}(|x|,s)\tilde{f}(|x|)\, dx, \tag{6.66}$$

$$P' = \{se_3 + x_1e_1 + x_2e_2 : x = (x_1,x_2) \in \mathbb{R}^2\},\ s = \operatorname{dist}(P,\{0\}),$$

where $(e_1,\dots,e_d)$ is the standard basis in $\mathbb{R}^d$. In addition, $I = 0$ by Theorem 1.

Properties of W and f mentioned in Corollary 1.1 follow from definitions (6.63), (6.64) and properties of $\tilde{U}$ and $\tilde{f}$ (arising in Theorem 1).

5 Proofs of Lemma 1 and formula (6.33)

5.1 Proof of Lemma 1

The spherical symmetry of f follows from (6.22), (6.23).
The series in (6.22) converges uniformly with all derivatives of f_k. Therefore, $f \in C^\infty(\mathbb{R}^3)$. Due to (6.22), (6.23), (6.24), (6.25) we have that $\operatorname{supp} f_k \subset B$, $k \geq 1$. Therefore, $\operatorname{supp} f \subseteq \overline{B}$.

It remains to show that f restricted to any straight line l in $\mathbb{R}^3$ intersecting B changes the sign. This implies change of the sign for $f|_P$ for any plane P such that $P \cap B \neq \emptyset$.

We consider

$$D_k = \{x \in \mathbb{R}^3 : |x| \in (1 - 2^{-k}(6/5), 1 - 2^{-k}(4/5))\},\ k \geq 1, \tag{6.67}$$

$$l(x_0, \omega) = \{x \in \mathbb{R}^3 : x = x(t) = x_0 + \omega t,\ t \in \mathbb{R}\}, \omega \in \mathbb{S}^2,\ x_0 \in \mathbb{R}^3,\ x_0\omega = 0. \tag{6.68}$$

Note that $\operatorname{supp} f_k = \overline{D}_k \subset B$. Note also that the line $l(x_0, \omega)$ intersects B if and only if $|x_0| < 1$.

Assuming that

$$|x_0| < 1 - 2^{-k}(6/5), \tag{6.69}$$

we consider $D_k \cap l(x_0, \omega) = I_k^- \sqcup I_k^+$ (see Figure 1):

$$I_k^- = \{x(t) : t \in (-t_1, -t_0)\}, \tag{6.70}$$

$$I_k^+ = \{x(t) : t \in (t_0, t_1)\}, \tag{6.71}$$

$$t_0 := t_0(k),\ t_1 := t_1(k).$$

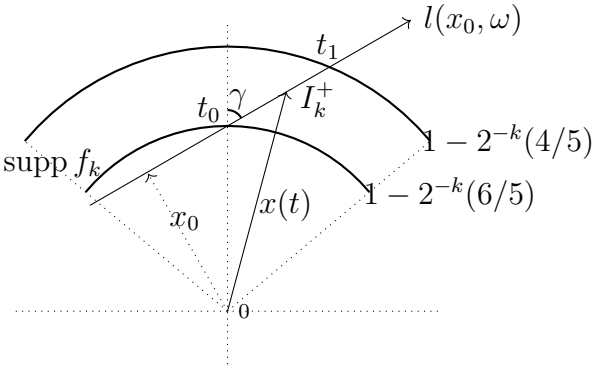

Figure 1.

One can see that assumption (6.69) holds for all $k \geq k_0(|x_0|) = -\ln\left(\frac{5}{6}(1 - |x_0|)\right)$.

By the Cosine theorem we have (see Figure 1):

$$\varphi(t) := |x(t)|^2 = (t - t_0)^2 + |x(t_0)|^2 - 2|x(t_0)|(t - t_0)\cos(\pi - \gamma) \text{ for } t \in [t_0, t_1]. \tag{6.72}$$

One can see also that

$$\gamma \in [0, \pi/2],\ \cos(\pi - \gamma) \leq 0. \tag{6.73}$$

Let

$$g_k(t) := \cos(8^k \varphi(t)),\ t \in [t_1, t_2], \tag{6.74}$$

where $\varphi(t)$ is defined in (6.72).

It is sufficient to show that g_k changes the sign on (t_0, t_1) for sufficiently large k.

Due to (6.22)-(6.25) this implies that f changes the sign on I_k^+.

From (6.72), (6.73) we obtain the inequality

$$\varphi'(t) = 2(t-t_0) - 2|x(t_0)|\cos(\pi-\gamma) \geq 0 \text{ for } t \in (t_0,t_1),\ \gamma \in [0,\pi/2], \tag{6.75}$$

which implies the phase in (6.74) is monotonously increasing on $t \in (t_0,t_1)$.

The full variation $V_{(t_0,t_1)}(\varphi)$ of the monotonous phase $\varphi(t)$ on (t_0,t_1) is given by the formula

$$V_{(t_0,t_1)}(\varphi) = (t_1-t_0)^2 - 2|x(t_0)|(t_1-t_0)\cos(\pi-\gamma). \tag{6.76}$$

From (6.73), (6.76) we obtain the following inequality

$$V_{(t_0,t_1)}(\varphi) \geq (t_1-t_0)^2. \tag{6.77}$$

From (6.74), (6.77) it follows that g_k changes the sign on $t \in (t_0,t_1)$, for example, if

$$8^k V_{(t_0,t_1)}(\varphi) \geq 2\pi \text{ or } (t_1-t_0) \geq \sqrt{2\pi}4^{-k}. \tag{6.78}$$

On the other hand, (t_1-t_0) is exactly the length of the segment I_k^+ (see Figure 1). Therefore,

$$(t_1-t_0) \geq (2/5)2^{-k}. \tag{6.79}$$

Inequality (6.79) implies that (6.78) holds for $k \geq 3$. Therefore, g_k of (6.74) changes the sign on (t_0,t_1) starting from $k \geq \max(3, k_0(|x_0|))$.

Lemma 1 is proved.

5.2 Proof of formula (6.33)

From (6.1), (6.22)-(6.25), (6.45), (6.48), (6.49) it follows that:

$$R_{W_0}f(s,\theta) = \int\limits_{x\theta=s} f(x)\,dx - G(s\theta,\theta)\sum_{k=3}^{\infty} k!\psi_{k-2}(|s|)\frac{\int\limits_{x\theta=s} f(x)f_k(x)dx}{H_k(s\theta,\theta)} \tag{6.80}$$

$$= \int\limits_{x\theta=s} f(x)\,dx - \int\limits_{x\theta=s} f(x)dx\sum_{k=3}^{\infty}\psi_{k-2}(|s|)\frac{\int\limits_{x\theta=s} f_k^2(x)dx}{\int\limits_{x\theta=s} f_k^2(x)\,dx} \tag{6.81}$$

$$= \int\limits_{x\theta=s} f(x)\,dx - \int\limits_{x\theta=s} f(x)dx\sum_{k=3}^{\infty}\psi_{k-2}(|s|) = 0,\ |s|>1/2,\ \theta\in\mathbb{S}^2. \tag{6.82}$$

Formula (6.33) is proved.

6 Proof of Lemma 2

Let

$$\Lambda_k := \{(x,\theta)\in\mathbb{R}^3\times\mathbb{S}^2 : |x\theta| \in (1-2^{-k+3}, 1-2^{-k+1})\}, k\in\mathbb{N},\ k\geq 4. \tag{6.83}$$

From (6.45) it follows that, for $k \geq 4$:

$$\operatorname{supp}\psi_{k-1} \subset (1-2^{-k+2}, 1-2^{-k}), \tag{6.84}$$

$$\operatorname{supp}\psi_{k-2} \subset (1-2^{-k+3}, 1-2^{-k+1}), \tag{6.85}$$

$$\operatorname{supp}\psi_{k-3} \subset (1-2^{-k+4}, 1-2^{-k+2}). \tag{6.86}$$

Formulas (6.48), (6.49), (6.84)-(6.86) imply the following expression for $W_0(x,\theta)$:

$$W_0(x,\theta) = 1 - G(x,\theta)\left((k-1)!f_{k-1}(x)\frac{\psi_{k-3}(|x\theta|)}{H_{k-1}(x,\theta)}\right.$$
$$+k!f_k(x)\frac{\psi_{k-2}(|x\theta|)}{H_k(x,\theta)} \tag{6.87}$$
$$\left.+(k+1)!f_{k+1}(x)\frac{\psi_{k-1}(|x\theta|)}{H_{k+1}(x,\theta)}\right),\ (x,\theta)\in\Lambda_k,\ k\geq 4.$$

Lemma 4. *There are positive constants c_1, c_2, k_1 depending on Φ, such that*

$$|f_k(x)| \leq c_1, \text{ for } k\in\mathbb{N}, \tag{6.88}$$
$$\left|\frac{\psi_{k-2}(|x\theta|)}{H_k(x,\theta)}\right| \leq c_2 2^k \quad \text{for } k\geq k_1 \text{ and } |x\theta|\leq 1-2^{-k+1}, \tag{6.89}$$
$$|G(x,\theta)| \leq c_1\frac{4^{-k}}{k!} \quad \text{for } k\geq 3 \text{ and } |x\theta|\geq 1-2^{-k}, \tag{6.90}$$
$$x\in\mathbb{R}^3,\ \theta\in\mathbb{S}^2, 1/2<|x\theta|<1,$$

where f_k, G, H_k are defined in (6.23), (6.49).

Lemma 4 is proved in Section 8.

From definition (6.83) and estimates (6.89), (6.90) it follows that

$$|G(x,\theta)| \leq c_1 4^{-k+3}/(k-3)!, \tag{6.91}$$
$$\left|\frac{\psi_{k-2}(|x\theta|)}{H_k(x,\theta)}\right| \leq c_2 2^k, \tag{6.92}$$
$$\text{for } (x,\theta)\in\Lambda_k,\ k\geq\max(4,k_1).$$

In addition, properties (6.84)-(6.86) and estimate (6.89) imply that:

$$\begin{cases}\psi_{k-1}(|x\theta|)=0,\\ \left|\dfrac{\psi_{k-3}(|x\theta|)}{H_{k-1}(x,\theta)}\right|\leq c_2 2^{k-1}\end{cases} \quad \text{if} \quad |x\theta|\in(1-2^{-k+3},1-2^{-k+2}), \tag{6.93}$$
$$\begin{cases}\psi_{k-2}(|x\theta|)=0,\\ \left|\dfrac{\psi_{k-1}(|x\theta|)}{H_{k+1}(x,\theta)}\right|\leq c_2 2^{k+1}\end{cases} \quad \text{if} \quad |x\theta|\in(1-2^{-k+2},1-2^{-k+1}), \tag{6.94}$$
$$\begin{cases}\psi_{k-1}(|x\theta|)=0,\\ \psi_{k-3}(|x\theta|)=0\end{cases} \quad \text{if} \quad |x\theta|=1-2^{-k+2}, \tag{6.95}$$

for $(x,\theta)\in\Lambda_k$, $k\geq\max(4,k_1)$.

Note that the condition $(x,\theta)\in\Lambda_k$ is splitted into the assumptions of (6.93), (6.94), (6.95).

Due to formulas (6.87), (6.91)-(6.95), we obtain the following estimates:

$$\begin{aligned}|1-W_0(x,\theta)| &= |G(x,\theta)|\left|(k-1)!f_{k-1}(x)\frac{\psi_{k-3}(|x\theta|)}{H_{k-1}(x,\theta)}+k!f_{k-2}(x)\frac{\psi_{k-2}(|x\theta|)}{H_k(x,\theta)}\right|\\ &\leq c_1 4^{-k+3}(c_1c_2(k-2)(k-1)2^{k-1}+c_1c_2(k-2)(k-1)k2^k)\\ &\leq 2^6 c_1^2 c_2 2^{-k}k^3 \quad \text{if} \quad |x\theta|\in(1-2^{-k+3},1-2^{-k+2}),\end{aligned} \tag{6.96}$$

$$
\begin{aligned}
|1-W_0(x,\theta)| &= |G(x,\theta)|\left|k!f_k(x)\frac{\psi_{k-2}(|x\theta|)}{H_k(x,\theta)}+(k+1)!f_{k+1}(x)\frac{\psi_{k-1}(|x\theta|)}{H_{k+1}(x,\theta)}\right| \\
&\le c_1 4^{-k+3}(c_1c_2 2^k(k-1)(k-2)+c_1c_2 2^{k+1}(k-2)(k-1)k(k+1)) \\
&\le 2^{12}c_1^2c_2 2^{-k}k^4 \quad \text{if} \quad |x\theta|\in(1-2^{-k+2},1-2^{-k+1}),
\end{aligned} \tag{6.97}
$$

$$
\begin{aligned}
|1-W_0(x,\theta)| &= |G(x,\theta)|\left|k!f_k(x)\frac{\psi_{k-2}(|x\theta|)}{H_k(x,\theta)}\right| \\
&\le 2^6c_1^2c_2 2^{-k}k^3 \quad \text{if} \quad |x\theta| = 1-2^{-k+2}.
\end{aligned} \tag{6.98}
$$

Estimates (6.96)-(6.98) imply that

$$
|1-W_0(x,\theta)|\le C\cdot 2^{-k}k^4,\ (x,\theta)\in\Lambda_k,\ k\ge\max(4,k_1). \tag{6.99}
$$

where C is a positive constant depending on c_1, c_2 of Lemma 4.

In addition, for $(x,\theta)\in\Lambda_k$ we have that $2^{-k+1}<\rho(|x\theta|)<2^{-k+3}$, which together with (6.99) imply (6.50).

Lemma 2 is proved.

7 Proof of Lemma 3

Let (e_1,e_2) be an orthonormal basis on $P_{(s,\theta)}\in\mathcal{P}$ and the origin of the coordinate system on $P_{(s,\theta)}$ is located at $s\theta\in P_{(s,\theta)}$.

By $u=(u_1,u_2)$, $u\in\mathbb{R}^2$, we denote the coordinates on $P_{(s,\theta)}$ with respect to (e_1,e_2).

Using Lemma 1 one can see that

$$
f|_{P_{(s,\theta)}}\in C_0^\infty(\mathbb{R}^2),\ f|_{P_{(s,\theta)}}(u)=f|_{P_{(s,\theta)}}(|u|),\ u\in\mathbb{R}^2. \tag{6.100}
$$

By our assumptions $f|_{P_{(s_0,\theta_0)}}(u)$ changes the sign.

Using this assumption and (6.100) one can see that there exist $\psi_{1,s_0},\psi_{2,s_0}$, such that:

$$
\psi_{1,s_0}\in C([0,+\infty)),\ \psi_{1,s_0}\ge 0, \psi_{2,s_0}(u):=\psi_{1,s_0}(|u|),\ u\in\mathbb{R}^2, \tag{6.101}
$$

$$
\int\limits_{P_{(s_0,\theta_0)}} f\psi_{2,s_0}\,d\sigma\neq 0. \tag{6.102}
$$

and if

$$
\int\limits_{P_{(s_0,\theta_0)}} f\,d\sigma\neq 0 \tag{6.103}
$$

then also

$$
\operatorname{sgn}\Big(\int\limits_{P_{(s_0,\theta_0)}} f\,d\sigma\Big)\operatorname{sgn}\Big(\int\limits_{P_{(s_0,\theta_0)}} f\psi_{2,s_0}\,d\sigma\Big)=-1, \tag{6.104}
$$

where $d\sigma=du_1\,du_2$ (i.e., σ is the standard Euclidean measure on $P_{(s,\theta)}$).

Let

$$
W_{f,s_0}(x,\theta)=1-\psi_{1,s_0}(|x-(x\theta)\theta|)\frac{\int\limits_{P_{(x\theta,\theta)}} f\,d\sigma}{\int_{P_{(x\theta,\theta)}} f\psi_{2,s_0}\,d\sigma},\ x\in\mathbb{R}^3,\ \theta\in\mathbb{S}^2, \tag{6.105}
$$

where $d\sigma = du_1\, du_2$ and (u_1, u_2) are the coordinates on $P_{(s,\theta)}$, $s = x\theta$, defined at the beginning of this proof.

Results of Lemma 1 and property (6.101) imply that

$$\int\limits_{P_{(x\theta,\theta)}} f\, d\sigma \text{ and } \int\limits_{P_{(x\theta,\theta)}} f\psi_{2,s_0}\, d\sigma \text{ depend only on } |x\theta|, \text{ where } x \in \mathbb{R}^3,\ \theta \in \mathbb{S}^2. \tag{6.106}$$

From (6.105), (6.106) it follows that W_{f,s_0} is rotation-invariant in the sense (6.16), (6.17).

Formulas (6.102), (6.105), (6.106) and properties of f and ψ_{2,s_0} of Lemma 1 and (6.101) imply that

$$\exists \varepsilon_1 > 0 : \int\limits_{P_{(x\theta,\theta)}} f\psi_{2,s_0}\, d\sigma \neq 0, \text{ for } (x,\theta) \in \Omega(\mathcal{J}_{s_0,\varepsilon_1}), \tag{6.107}$$

where the sets $\mathcal{J}_{s,\varepsilon}, \Omega(\mathcal{J})$ are defined in (6.13), (6.14), respectively.

In addition, using (6.105), (6.107), one can see that

$$W_{f,s_0} \text{ is continuous on } (x,\theta) \in \Omega(\mathcal{J}_{s_0,\varepsilon_1}). \tag{6.108}$$

In addition, from (6.100)-(6.106) it follows that

$$\begin{aligned} \text{if } |x\theta| = |s_0| \text{ then } W_{f,s_0}(x,\theta) &= 1 - \psi_{1,s_0}(|x - (x\theta)\theta|)\frac{\int\limits_{P_{(s_0,\theta)}} f\, d\sigma}{\int_{P_{(s_0,\theta)}} f\psi_{2,s_0}\, d\sigma} \\ &= 1 - \psi_{1,s_0}(|x - (x\theta)\theta|)\frac{\int\limits_{P_{(s_0,\theta_0)}} f\, d\sigma}{\int_{P_{(s_0,\theta_0)}} f\psi_{2,s_0}\, d\sigma} \geq 1. \end{aligned} \tag{6.109}$$

From properties of $f, \psi_{1,s_0}, \psi_{2,s_0}$ of Lemma 1 and (6.101) and from formulas (6.105), (6.106), (6.108), (6.109) it follows that

$$\exists \varepsilon_0 > 0\, (\varepsilon_0 < \varepsilon_1) : W_{f,s_0}(x,\theta) \geq 1/2, \text{ for } (x,\theta) \in \Omega(\mathcal{J}_{s_0,\varepsilon_0}), \tag{6.110}$$

which implies strict positiveness for W_{f,s_0} on $\Omega(\mathcal{J}_{s_0,\varepsilon})$.

Properties (6.106), (6.108), (6.110) imply item (ii) of Lemma 3 for $W_{f,s_0,\varepsilon} := W_{f,s_0}$, defined on $\Omega(\mathcal{J}_{s_0,\varepsilon_0})$.

From (6.1), (6.105), (6.107) it follows that

$$\begin{aligned} R_{W_{f,s_0}} f(s,\theta) &= \int\limits_{P_{(s,\theta)}} W_{f,s_0}(\cdot,\theta) f\, d\sigma \\ &= \int\limits_{P_{(s,\theta)}} f\, d\sigma - \frac{\int\limits_{P_{(s,\theta)}} f\, d\sigma}{\int_{P_{(s,\theta)}} f\psi_{2,s_0}\, d\sigma} \int\limits_{P_{(s,\theta)}} f\psi_{2,s_0}\, d\sigma = 0 \text{ for } s \in \mathcal{J}_{s_0,\varepsilon_0}, \theta \in \mathbb{S}^2. \end{aligned} \tag{6.111}$$

Item (i) of Lemma 3 follows from (6.111).

Lemma 3 is proved.

8 Proof of Lemma 4

8.1 Proof of estimate (6.88)

Estimate (6.88) follows from (6.23) and properties (6.24)-(6.26).

8.2 Proof of estimate (6.90)

From definitions (6.22), (6.49) we have that

$$G = \sum_{k=1}^{\infty} \frac{G_k}{k!}, \tag{6.112}$$

$$G_k(x,\theta) = \int\limits_{y\theta = x\theta} f_k(y)\, dy,\ x \in \mathbb{R}^3,\ \theta \in \mathbb{S}^2. \tag{6.113}$$

Parametrization of the points $y(r,\phi)$ on $P_{(s,\theta)} \in \mathcal{P}$, $s \in \mathbb{R}$, $\theta \in \mathbb{S}^2$, is given by the formula

$$y(r,\phi) = s\theta + r(e_1 \cos\phi + e_2 \sin\phi),\ r \in [0,+\infty),\ \phi \in [0,2\pi], \tag{6.114}$$

where (e_1, e_2) is some fixed orthonormal basis on $P_{(s,\theta)}$.

On the other hand,

$$r = r(\gamma) = |s| \tan(\gamma),\ \gamma \in [0, \pi/2), \tag{6.115}$$

where γ is the angle between $s\theta$ and the radius-vector $y(r,\phi)$ of (6.114).

It is convenient to rewrite $y(r,\phi)$ of (6.114) as $y = y(r(\gamma),\phi) \stackrel{\text{def}}{=} y(\gamma,\phi)$, $\gamma \in [0,\pi/2)$, $\phi \in [0,2\pi]$.

The standard Lebesgue measure σ on $P_{(s,\theta)}$ is given by the following formula:

$$\begin{aligned} d\sigma(\gamma,\phi) = r(\gamma,\phi) d\phi\, dr(\gamma) &= |s| \tan\gamma\, d\phi\, dr(\gamma) \\ &= |s|^2 \frac{\sin\gamma}{\cos^3\gamma}\, d\phi\, d\gamma. \end{aligned} \tag{6.116}$$

From (6.23), (6.113)-(6.116) we obtain

$$\begin{aligned} G_k(x,\theta) &= s^2 \int\limits_0^{2\pi} d\phi \int\limits_0^{\pi/2} \Phi\left(2^k\left(1 - \frac{|s|}{\cos\gamma}\right)\right) \cos\left(8^k \frac{|s|^2}{\cos^2\gamma}\right) \frac{\sin\gamma}{\cos^3\gamma}\, d\gamma \\ &= -2\pi|s|^2 \int\limits_0^{\pi/2} \Phi\left(2^k\left(1 - \frac{|s|}{\cos\gamma}\right)\right) \cos\left(8^k \frac{|s|^2}{\cos^2\gamma}\right) \frac{d(\cos\gamma)}{\cos^3\gamma} \\ &= \{t = \cos\gamma\} = -2\pi|s|^2 \int\limits_1^0 \Phi\left(2^k\left(1 - \frac{|s|}{t}\right)\right) \cos\left(8^k \frac{|s|^2}{t^2}\right) \frac{dt}{t^3} \\ &= \{u = \frac{1}{t^2}\} = \pi|s|^2 \int\limits_1^{+\infty} \Phi(2^k(1 - |s|\sqrt{u})) \cos(8^k|s|^2 u)\, du,\ s = x\theta. \end{aligned} \tag{6.117}$$

From (6.24)–(6.26), (6.117) it follows that

$$G_k(x,\theta) = 8^{-k}\pi \int\limits_1^{+\infty} \Phi(2^k(1-|s|\sqrt{u}))\, d\left(\sin(8^k|s|^2u)\right)$$

$$= 8^{-k}\pi \left(-\Phi(2^k(1-|s|))\sin(8^k|s|^2) - \int\limits_1^{+\infty} \left(\frac{d}{du}\Phi(2^k(1-|s|\sqrt{u}))\right)\sin(8^k|s|^2u)\, du \right), \tag{6.118}$$

$$|\Phi(2^k(1-|s|))\sin(8^k|s|^2)| \le 1, \tag{6.119}$$

$$\left| \int\limits_1^{+\infty} \left(\frac{d}{du}\Phi(2^k(1-|s|\sqrt{u}))\right)\sin(8^k|s|^2u)\, du \right| \le 2^k \max_{t\in\mathbb{R}} |\Phi'(t)| \int\limits_{\Lambda_{k,|s|}} du$$

$$\le 2^k \max_{t\in\mathbb{R}} |\Phi'(t)|, \tag{6.120}$$

$$\Lambda_{k,|s|} = \{u \ge 1 : 2^k(1-|s|\sqrt{u}) \in [4/5, 6/5]\}, \tag{6.121}$$

where $1/2 < |s| < 1$, $s = x\theta$, $k \in \mathbb{N}$.

Note that

$$|\Lambda_{k,|s|}| \le 1 \text{ for } 1/2 < |s| < 1, \tag{6.122}$$

where $|\Lambda|$ denotes the length of Λ.

Formulas (6.118)-(6.122) imply that

$$|G_k(x,\theta)| \le 4^{-k}\pi \max_{t\in\mathbb{R}} |\Phi'(t)| \text{ for } 1/2 < |s| < 1,\ s = x\theta,\ k \in \mathbb{N}. \tag{6.123}$$

Note that for $y \in P_{(s,\theta)}$, the following inequality holds:

$$2^k(1-|y|) \le 2^k(1-|s|) \le 2^{k-m} \le 4/5 \text{ for } 1-2^{-m} \le |s| < 1,\ k < m,\ m \ge 3. \tag{6.124}$$

Formulas (6.23), (6.24), (6.124) imply that

$$P_{(s,\theta)} \cap \operatorname{supp} f_k = \emptyset \text{ if } |s| \ge 1-2^{-m},\ k < m. \tag{6.125}$$

In turn, (6.113), (6.125) imply that

$$G_k(x,\theta) = 0 \text{ for } k < m,\ |x\theta| \ge 1-2^{-m}. \tag{6.126}$$

Due to (6.112), (6.123), (6.126) we have that:

$$|G(x,\theta)| \le \sum_{k=1}^{\infty} |G_k(x,\theta)|/k! = \sum_{k=m}^{\infty} |G_k(x,\theta)|/k!$$

$$\le \max_{t\in\mathbb{R}} |\Phi'(t)|\pi 4^{-m}/m! \sum_{k=0}^{\infty} 4^{-k} = c_1 \frac{4^{-m}}{m!},\ c_1 = \frac{4\pi}{3} \max_{t\in\mathbb{R}} |\Phi'(t)|$$

$$\text{for } |x\theta| \ge 1-2^{-m},\ m \ge 3. \tag{6.127}$$

Estimate (6.90) follows from (6.127).

8.3 Proof of estimate (6.89)

For each ψ_k from (6.45) we have that:

$$|\psi_k| \le 1. \tag{6.128}$$

Therefore, it is sufficient to show that

$$H_k \ge C_2 2^{-k} \text{ for } k \ge k_1,\ C_2 = c_2^{-1}. \tag{6.129}$$

Due to formula (6.49) and in a similar way with (6.117) we obtain

$$H_k(x,\theta) = |s|^2\pi \int\limits_1^\infty \Phi^2(2^k(1-|s|\sqrt{u}))\cos^2(8^k|s|^2u)\,du = H_{k,1}(x,\theta) + H_{k,2}(x,\theta),\ s = x\theta, \tag{6.130}$$

$$H_{k,1}(x,\theta) = \frac{\pi|s|^2}{2}\int\limits_1^{+\infty} \Phi^2(2^k(1-|s|\sqrt{u}))\,du, \tag{6.131}$$

$$H_{k,2}(x,\theta) = \frac{\pi|s|^2}{2}\int\limits_1^{+\infty} \Phi^2(2^k(1-|s|\sqrt{u}))\cos(2\cdot 8^k|s|^2u)\,du. \tag{6.132}$$

Note that

$$2^k(1-|s|) \ge 2^k\cdot 2^{-k+1} \ge 2 > 6/5 \text{ for } |s| \le 1-2^{-k+1},\ k \ge 3. \tag{6.133}$$

In turn, (6.24), (6.133) imply that

$$\Phi(2^k(1-|s|\sqrt{u})) = 0 \text{ for } u \le 1,\ |s| \le 1-2^{-k+1},\ k \ge 3. \tag{6.134}$$

Using (6.133) one can see that

$$\exists u_1 \ge 1, u_2 \ge 1,\ u_2 > u_1 \text{ such that } \begin{cases} 2^k(1-|s|\sqrt{u_1}) = 11/10, \\ 2^k(1-|s|\sqrt{u_2}) = 9/10, \end{cases} \tag{6.135}$$

$$|u_2-u_1| \ge (\sqrt{u_2}-\sqrt{u_1}) = \frac{2^{-k}}{5}|s|^{-1} \ge \frac{2^{-k}}{5}, \tag{6.136}$$

$$\text{for } 1/2 < |s| \le 1-2^{-k+1},\ k \ge 3.$$

Using (6.24), (6.26), (6.131), (6.134), (6.136) we obtain

$$H_{k,1}(x,\theta) \ge \frac{\pi}{8}\int\limits_{u_1}^{u_2} du \ge 2^{-k}\frac{\pi}{40}, \quad \text{for } \ 1/2 < |x\theta| < 1-2^{-k+1},\ k \ge 3. \tag{6.137}$$

On the other hand, using (6.24), (6.132), (6.134), in a similar way with (6.118)-(6.122),

we obtain

$$
\begin{aligned}
|H_{k,2}(x,\theta)| &= \frac{\pi|s|^2}{2}\left|\int\limits_1^{+\infty}\Phi^2(2^k(1-|s|\sqrt{u}))\cos(2\cdot 8^k|s|^2u)\,du\right| \\
&= \frac{\pi}{4}8^{-k}|s|^{-2}\left|\int\limits_1^{+\infty}\sin(2\cdot 8^k|s|^2u)\left(\frac{d}{du}\Phi^2(2^k(1-|s|\sqrt{u}))\right)du\right| \\
&\le \frac{\pi}{4}8^{-k}|s|^{-1}\max_{t\in\mathbb{R}}|\Phi(t)|\cdot\max_{t\in\mathbb{R}}|\Phi'(t)|\cdot 2^k\int\limits_{\Lambda_{k,|s|}}du \\
&\le \frac{\pi}{2}4^{-k}\max_{t\in\mathbb{R}}|\Phi(t)|\cdot\max_{t\in\mathbb{R}}|\Phi'(t)|,\ s=x\theta,
\end{aligned}
\tag{6.138}
$$

for $1/2<|x\theta|<1-2^{-k+1}$, $k\ge 3$.

From (6.130)-(6.132), (6.137), (6.138) it follows that

$$
\begin{aligned}
|H_k(x,\theta)| &\ge |H_{k,1}(x,\theta)|-|H_{k,2}(x,\theta)| \\
&\ge \frac{\pi}{40}2^{-k}-\frac{\pi}{2}4^{-k}\max_{t\in\mathbb{R}}|\Phi(t)|\cdot\max_{t\in\mathbb{R}}|\Phi'(t)| \\
&\ge C_2 2^{-k}\ \text{ for } 1/2<|x\theta|<1-2^{-k+1},\ k\ge k_1, \\
C_2 &= \frac{\pi}{40}-2^{-k_1}\frac{\pi}{2}\max_{t\in\mathbb{R}}|\Phi(t)|\max_{t\in\mathbb{R}}|\Phi'(t)|,
\end{aligned}
\tag{6.139}
$$

where k_1 is arbitrary constant such that $k_1\ge 3$ and C_2 is positive.

Estimate (6.89) follows from (6.139).

Lemma 4 is proved.

Acknowledgements

This work is partially supported by the PRC n° 1545 CNRS/RFBR: Équations quasi-linéaires, problèmes inverses et leurs applications. The authors are also grateful to the referee for remarks that have helped to improve the presentation.

Bibliography

[Be84] Beylkin, G., The inversion problem and applications of the generalized Radon transform. *Communications on pure and applied mathematics*, 37(5) : 579-599, 1984.

[Be85] Beylkin, G., Imaging of discontinuities in the inverse scattering problem by inversion of a causal generalized Radon transform *Journal of Mathematical Physics*, 26(1) : 99-108, 1985.

[BQ87] Boman, J., Quinto, E.T., Support theorems for real-analytic Radon transforms. *Duke Mathematical J.*, 55(4):943-948, 1987.

[Bo93] Boman, J., An example of non-uniqueness for a generalized Radon transform. *Journal d'Analyse Mathematique*, 61(1):395–401, 1993.

[MD92] Do Carmo, M. P., Riemannian Geometry. Birkhäuser Basel, 1992.

[Fi86] Finch, D., Uniqueness for the attenuated X-ray transform in the physical range. *Inverse problems*, 2(2), 1986.

[GN16] Goncharov, F.O., Novikov, R.G., An analog of Chang inversion formula for weighted Radon transforms in multidimensions. *Eurasian Journal of Mathematical and Computer Applications*, 4(2):23-32, 2016.

[Go17] Goncharov F. O., An iterative inversion of weighted Radon transforms along hyperplanes. *Inverse Problems* 33 124005, 2017.

[GN17] Goncharov F. O., Novikov R. G., An example of non-uniqueness for the weighted Radon transforms along hyperplanes in multidimensions. *Inverse Problems*, **34** 054001, 2018.

[GN17] Goncharov, F.O., Novikov, R.G., A breakdown of injectivity for weighted ray transforms in multidimensions. hal-01635188, version 1, 2017.

[GuN14] Guillement, J.-P., Novikov, R.G., Inversion of weighted Radon transforms via finite Fourier series weight approximations. *Inverse Problems in Science and Engineering*, 22(5):787–802, 2014.

[Ku92] Kunyansky, L., Generalized and attenuated Radon transforms: restorative approach to the numerical inversion. *Inverse Problems*, 8(5):809, 1992.

[LB73] Lavrent'ev, M. M., Bukhgeim, A. L., A class of operator equations of the first kind. *Functional Analysis and Its Applications*, 7(4):290-298, 1973.

[MQ85] Markoe, A., Quinto, E.T., An elementary proof of local invertibility for generalized and attenuated Radon transforms. *SIAM Journal on Mathematical Analysis*, 16(5):1114–1119, 1985.

[Na01] Natterer, F. The Mathematics of Computerized Tomography. SIAM, 2001.

[No11] Novikov, R.G., Weighted Radon transforms for which Chang's approximate inversion formula is exact. *Russian Mathematical Surveys*, 66(2):442–443, 2011.

[No14] Novikov, R.G., Weighted Radon transforms and first order differential systems on the plane. *Moscow Mathematical Journal*, 14(4):807–823, 2014.

[Qu83] Quinto, E.T., The invertibility of rotation invariant Radon transforms. *Journal of Mathematical Analysis and Applications*, 91(2):510–522, 1983.

[Qu83Err] Quinto, E.T., The invertibility of rotation invariant Radon transforms. Erratum. *Journal of Mathematical Analysis and Applications*, 94(2):602-603, 1983.

Article 5. A breakdown of injectivity for weighted ray transforms

F. O. Goncharov, R. G Novikov

We consider weighted ray-transforms P_W (weighted Radon transforms along straight lines) in $\mathbb{R}^d$, $d \geq 2$, with strictly positive weights W. We construct an example of such a transform with non-trivial kernel in the space of infinitely smooth compactly supported functions on $\mathbb{R}^d$. In addition, the constructed weight W is rotation-invariant continuous and is infinitely smooth almost everywhere on $\mathbb{R}^d \times \mathbb{S}^{d-1}$. In particular, by this construction we give counterexamples to some well-known injectivity results for weighted ray transforms for the case when the regularity of W is slightly relaxed. We also give examples of continuous strictly positive W such that $\dim \ker P_W \geq n$ in the space of infinitely smooth compactly supported functions on $\mathbb{R}^d$ for arbitrary $n \in \mathbb{N} \cup \{\infty\}$, where W are infinitely smooth for $d = 2$ and infinitely smooth almost everywhere for $d \geq 3$.

1 Introduction

We consider the weighted ray transforms P_W defined by

$$P_W f(x,\theta) = \int\limits_{\mathbb{R}} W(x+t\theta,\theta) f(x+t\theta)\, dt,\ (x,\theta) \in T\mathbb{S}^{d-1},\ d \geq 2, \tag{7.1}$$

$$T\mathbb{S}^{d-1} = \{(x,\theta) \in \mathbb{R}^d \times \mathbb{S}^{d-1} : x\theta = 0\}, \tag{7.2}$$

where $f = f(x)$, $W = W(x,\theta)$, $x \in \mathbb{R}^d$, $\theta \in \mathbb{S}^{d-1}$. Here, W is the weight, f is a test function on $\mathbb{R}^d$. In addition, we interpret $T\mathbb{S}^{d-1}$ as the set of all rays in $\mathbb{R}^d$. As a ray γ we understand a straight line with fixed orientation. If $\gamma = \gamma(x,\theta)$, $(x,\theta) \in T\mathbb{S}^{d-1}$, then

$$\begin{aligned} &\gamma(x,\theta) = \{y \in \mathbb{R}^d : y = x + t\theta,\ t \in \mathbb{R}\} \text{ (up to orientation)},\\ &\text{where } \theta \text{ gives the orientation of } \gamma. \end{aligned} \tag{7.3}$$

We assume that

$$W = \overline{W} \geq c > 0,\ W \in L^\infty(\mathbb{R}^d \times \mathbb{S}^{d-1}), \tag{7.4}$$

where $\overline{W}$ denotes the complex conjugate of W, c is a constant.

Note also that

$$P_W f(x,\theta) = \int\limits_{\gamma} W(x,\gamma) f(x)\, dx,\ \gamma = \gamma(x,\theta), \tag{7.5}$$

where

$$W(x,\gamma) = W(x,\theta) \text{ for } x \in \gamma,\ \gamma = \gamma(x,\theta),\ (x,\theta) \in T\mathbb{S}^{d-1}. \tag{7.6}$$

The aforementioned transforms P_W arise in various domains of pure and applied mathematics; see [LB73], [TM80], [Qu83], [Be84], [MQ85], [Fi86], [BQ87], [Sh92], [Ku92], [BQ93], [Bo93], [Sh93], [KLM95], [Pa96], [ABK98], [Na01], [No02a], [No02b], [BS04], [Ba09], [Gi10], [BJ11], [PG13], [No14], [Il16], [Ng17] and references therein.

In particular, the related results are the most developed for the case when $W \equiv 1$. In this case P_W is reduced to the classical ray-transform P (Radon transform along straight lines). The transform P arises, in particular, in the X-ray transmission tomography. We refer to [Ra17], [Jo38], [Co64], [GGG82], [He01], [Na01] and references therein in connection with basic results for this classical case.

At present, many important results on transforms P_W with other weights W satisfying (7.4) are also known; see the publications mentioned above with non-constant W and references therein.

In particular, assuming (7.4) we have the following injectivity results.

Injectivity 1 (see [Fi86]). Suppose that $d \geq 3$ and $W \in C^2(\mathbb{R}^d \times \mathbb{S}^{d-1})$. Then P_W is injective on $L^p_0(\mathbb{R}^d)$ for $p > 2$, where L^p_0 denotes compactly supported functions from L^p.

Injectivity 2 (see [MQ85]). Suppose that $d = 2$, $W \in C^2(\mathbb{R}^2 \times \mathbb{S}^1)$ and

$$0 < c_0 \leq W, \ \|W\|_{C^2(\mathbb{R}^2 \times \mathbb{S}^1)} \leq N, \tag{7.7}$$

for some constants c_0 and N. Then, for any $p > 2$, there is $\delta = \delta(c_0, N, p) > 0$ such that P_W is injective on $L^p(B(x_0, \delta))$ for any $x_0 \in \mathbb{R}^2$, where

$$L^p(B(x_0, \delta)) = \{f \in L^p(\mathbb{R}^2) : \operatorname{supp} f \subset \overline{B}(x_0, \delta)\},$$
$$\overline{B}(x_0, \delta) = \{x \in \mathbb{R}^2 : |x - x_0| \leq \delta\}.$$

Injectivity 3 (see [Qu83]). Suppose that $d = 2$, $W \in C^1(\mathbb{R}^2 \times \mathbb{S}^1)$ and W is rotation invariant (see formula (7.29) below). Then P_W is injective on $L^p_0(\mathbb{R}^2)$ for $p \geq 2$.

In a similar way with [Qu83], we say that W is rotation invariant if and only if

$$\begin{aligned} &W(x, \gamma) \text{ is independent of the orientation of } \gamma, \\ &W(x, \gamma) = W(Ax, A\gamma) \text{ for } x \in \gamma, \ \gamma \in T\mathbb{S}^{d-1}, \ A \in O(d), \end{aligned} \tag{7.8}$$

where $T\mathbb{S}^{d-1}$ is defined in (7.2), $O(d)$ denotes the group of orthogonal transformations of $\mathbb{R}^d$.

Note also that property (7.8) can be rewritten in the form (7.29), (7.30) or (7.31), (7.32); see Section 2.

Injectivity 4 (see [BQ87]). Suppose that $d = 2$, W is real-analytic on $\mathbb{R}^2 \times \mathbb{S}^1$. Then P_W is injective on $L^p_0(\mathbb{R}^2)$ for $p \geq 2$.

Injectivity 1 is a global injectivity for $d \geq 3$. Injectivity 2 is a local injectivity for $d = 2$. Injectivity 3 is a global injectivity for $d = 2$ for the rotation invariant case. Injectivity 4 is a global injectivity for $d = 2$ for the real-analytic case.

The results of Injectivity 1 and Injectivity 2 remain valid with C^α, $\alpha > 1$, in place of C^2 in the assumptions on W; see [Il16].

Injectivity 1 follows from Injectivity 2 in the framework of the layer-by-layer reconstruction approach. See [Fi86], [No02a], [Il16] and references therein in connection with the layer-by-layer reconstruction approach for weighted and non-abelian ray transforms in dimension $d \geq 3$.

The work [Bo93] gives a counterexample to Injectivity 4 for P_W in $C_0^\infty(\mathbb{R}^2)$ for the case when the assumption that W is real-analytic is relaxed to the assumption that W is infinitely smooth, where C_0^∞ denotes infinitely smooth compactly supported functions.

In somewhat similar way with [Bo93], in the present work we obtain counterexamples to Injectivity 1, Injectivity 2 and Injectivity 3 for the case when the regularity of W is slightly relaxed. In particular, by these counterexamples we continue related studies of [MQ85], [Bo93] and [GN18].

More precisely, in the present work we construct W and f such that

$$P_W f \equiv 0 \text{ on } T\mathbb{S}^{d-1},\ d \geq 2, \tag{7.9}$$

where W satisfies (7.4), W is rotation-invariant (i.e., satisfies (7.8)),

$$\begin{aligned} &W \text{ is infinitely smooth almost everywhere on } \mathbb{R}^d \times \mathbb{S}^{d-1} \text{ and} \\ &W \in C^\alpha(\mathbb{R}^d \times \mathbb{S}^{d-1}),\ \text{at least, for any } \alpha \in (0, \alpha_0),\ \text{where } \alpha_0 = 1/16; \end{aligned} \tag{7.10}$$

$$\begin{aligned} &f \text{ is a non-zero spherically symmetric infinitely smooth and} \\ &\text{compactly supported function on } \mathbb{R}^d; \end{aligned} \tag{7.11}$$

see Theorem 1 of Section 3.

These W and f directly give the aforementioned counterexamples to Injectivity 1 and Injectivity 3.

Our counterexample to Injectivity 1 is of particular interest (and is rather surprising) in view of the fact that the problem of finding f on $\mathbb{R}^d$ from $P_W f$ on $T\mathbb{S}^{d-1}$ for known W is strongly overdetermined for $d \geq 3$. Indeed,

$$\begin{aligned} &\dim \mathbb{R}^d = d,\ \dim T\mathbb{S}^{d-1} = 2d-2, \\ &d < 2d-2 \text{ for } d \geq 3. \end{aligned}$$

This counterexample to Injectivity 1 is also rather surprising in view of the aforementioned layer-by-layer reconstruction approach in dimension $d \geq 3$.

Our counterexample to Injectivity 3 is considerably stronger than the preceeding counterexample of [MQ85], where W is not yet continuous and is not yet strictly positive (i.e., is not yet separated from zero by a positive constant).

Using our W and f of (7.10), (7.11) for $d = 3$ we also obtain the aforementioned counterexample to Injectivity 2; see Corollary 1.1 of Section 3.

Finally, in the present work we also give examples of W satisfying (7.4) such that $\dim \ker P_W \geq n$ in $C_0^\infty(\mathbb{R}^d)$ for arbitrary $n \in \mathbb{N} \cup \{\infty\}$, where $W \in C^\infty(\mathbb{R}^2 \times \mathbb{S}^1)$ for $d = 2$ and W satisfy (7.10) for $d \geq 3$; see Theorem 2 of Section 3. To our knowledge, examples of W satisfying (7.4), where $\dim \ker P_W \geq n$ (for example in $L_0^2(\mathbb{R}^d)$) were not yet given in the literature even for $n = 1$ in dimension $d \geq 3$ and even for $n = 2$ in dimension $d = 2$.

In the present work we adopt and develop considerations of the famous work [Bo93] and of our very recent work [GN18].

In Section 2 we give some preliminaries and notations.

Main results are presented in detail in Sections 3.

Related proofs are given in Sections 4-9.

2 Some preliminaries

Notations. Let

$$\Omega = \mathbb{R}^d \times \mathbb{S}^{d-1}, \tag{7.12}$$
$$r(x,\theta) = |x - (x\theta)\theta|,\ (x,\theta) \in \Omega, \tag{7.13}$$
$$\Omega_0(\delta) = \{(x,\theta) \in \Omega : r(x,\theta) > \delta\}, \tag{7.14}$$
$$\Omega_1(\delta) = \Omega \backslash \Omega_0(\delta) = \{(x,\theta) \in \Omega : r(x,\theta) \le \delta\},\ \delta > 0, \tag{7.15}$$
$$\Omega(\Lambda) = \{(x,\theta) \in \mathbb{R}^d \times \mathbb{S}^{d-1} : r(x,\theta) \in \Lambda\},\ \Lambda \subset [0,+\infty), \tag{7.16}$$
$$T_0(\delta) = \{(x,\theta) \in T\mathbb{S}^{d-1} : |x| > \delta\}, \tag{7.17}$$
$$T_1(\delta) = \{(x,\theta) \in T\mathbb{S}^{d-1} : |x| \le \delta\},\ \delta > 0, \tag{7.18}$$
$$T(\Lambda) = \{(x,\theta) \in T\mathbb{S}^{d-1} : |x| \in \Lambda\},\ \Lambda \subset [0,+\infty), \tag{7.19}$$
$$\mathcal{J}_{r,\varepsilon} = (r-\varepsilon, r+\varepsilon) \cap [0,+\infty),\ r \in [0,+\infty),\ \varepsilon > 0. \tag{7.20}$$

The set $T_0(\delta)$ in (7.17) is considered as the set of all rays in $\mathbb{R}^d$ which are located at distance greater than δ from the origin.

The set $T_1(\delta)$ in (7.18) is considered as the set of all rays in $\mathbb{R}^d$ which are located at distance less or equal than δ from the origin.

We also consider the projection

$$\pi : \Omega \to T\mathbb{S}^{d-1}, \tag{7.21}$$
$$\pi(x,\theta) = (\pi_\theta x, \theta),\ (x,\theta) \in \Omega, \tag{7.22}$$
$$\pi_\theta x = x - (x\theta)\theta. \tag{7.23}$$

In addition, $r(x,\theta)$ of (7.13) is the distance from the origin $\{0\} \in \mathbb{R}^d$ to the ray $\gamma = \gamma(\pi(x,\theta))$ (i.e., $r(x,\theta) = |\pi_\theta x|$). The rays will be also denoted by

$$\gamma = \gamma(x,\theta) \stackrel{\text{def}}{=} \gamma(\pi(x,\theta)),\ (x,\theta) \in \Omega. \tag{7.24}$$

We also consider

$$P_W f(x,\theta) = P_W f(\pi(x,\theta)) \text{ for } (x,\theta) \in \Omega. \tag{7.25}$$

We also define

$$\begin{aligned} &B(x_0,\delta) = \{x \in \mathbb{R}^d : |x - x_0| < \delta\}, \\ &\overline{B}(x_0,\delta) = \{x \in \mathbb{R}^d : |x - x_0| \le \delta\},\ x_0 \in \mathbb{R}^d,\ \delta > 0, \end{aligned} \tag{7.26}$$
$$B = B(0,1),\ \overline{B} = \overline{B}(0,1). \tag{7.27}$$

For a function f on $\mathbb{R}^d$ we denote its restriction to a subset $\Sigma \subset \mathbb{R}^d$ by $f|_\Sigma$.

By C_0, C_0^∞ we denote continuous compactly supported and infinitely smooth compactly supported functions, respectively.

By $C^\alpha(Y)$, $\alpha \in (0,1)$, we denote the space of α-Hölder functions on Y with the norm:

$$\begin{aligned} &\|u\|_{C^\alpha(Y)} = \|u\|_{C(Y)} + \|u\|'_{C^\alpha(Y)}, \\ &\|u\|'_{C^\alpha(Y)} = \sup_{\substack{y_1,y_2 \in Y \\ |y_1 - y_2| \le 1}} \frac{|u(y_1) - u(y_2)|}{|y_1 - y_2|^\alpha}, \end{aligned} \tag{7.28}$$

where $\|u\|_{C(Y)}$ denotes the supremum of $|u|$ on Y.

Rotation invariance. Using formula (7.6), for positive and continous W, property (7.8) can be rewritten in the following equivalent form:

$$W(x,\theta) = U(|x-(x\theta)\theta|, x\theta),\ x \in \mathbb{R}^d,\ \theta \in \mathbb{S}^{d-1}, \tag{7.29}$$

for some positive and continuous U such that

$$U(r,s) = U(-r,s) = U(r,-s),\ r \in \mathbb{R},\ s \in \mathbb{R}. \tag{7.30}$$

In addition, symmetries (7.29), (7.30) of W can be also written as

$$W(x,\theta) = \tilde{U}(|x|, x\theta),\ (x,\theta) \in \Omega, \tag{7.31}$$

$$\tilde{U}(r,s) = \tilde{U}(-r,s) = \tilde{U}(r,-s),\ r \in \mathbb{R},\ s \in \mathbb{R}. \tag{7.32}$$

where $\tilde{U}$ is positive and continuous on $\mathbb{R} \times \mathbb{R}$. Using the formula $|x|^2 = |x\theta|^2 + r^2(x,\theta)$, one can see that symmetries (7.29), (7.30) and symmetries (7.31), (7.32) of W are equivalent.

Partition of unity. We recall the following classical result (see, e.g., Theorem 5.6 in [MD92]):
Let $\mathcal{M}$ be a C^∞-manifold, which is Hausdorff and has a countable base. Let also $\{U_i\}_{i=1}^\infty$ be an open locally-finite cover of $\mathcal{M}$.

Then there exists a C^∞-smooth locally-finite partition of unity $\{\psi_i\}_{i=1}^\infty$ on $\mathcal{M}$, such that

$$\operatorname{supp}\psi_i \subset U_i. \tag{7.33}$$

In particular, any open interval $(a,b) \subset \mathbb{R}$ and Ω satisfy the conditions for $\mathcal{M}$ of this statement. It will be used in Subsection 3.1.

3 Main results

Theorem 1. *There exist a weight W satisfying (7.4) and a non-zero function $f \in C_0^\infty(\mathbb{R}^d)$, $d \geq 2$, such that*

$$P_W f \equiv 0 \text{ on } T\mathbb{S}^{d-1}, \tag{7.34}$$

where P_W is defined in (7.1). In addition, W is rotation invariant, i.e., satisfies (7.29), and f is spherically symmetric with $\operatorname{supp} f \subseteq \overline{B}$. Moreover,

$$W \in C^\infty(\Omega \backslash \Omega(1)), \tag{7.35}$$

$$W \in C^\alpha(\mathbb{R}^d \times \mathbb{S}^{d-1}) \text{ for any } \alpha \in (0,\alpha_0),\ \alpha_0 = 1/16, \tag{7.36}$$

$$W \geq 1/2 \text{ on } \Omega \text{ and } W \equiv 1 \text{ on } \Omega([1,+\infty)), \tag{7.37}$$

$$W(x,\theta) \equiv 1 \text{ for } |x| \geq R > 1,\ \theta \in \mathbb{S}^{d-1}, \tag{7.38}$$

where Ω, $\Omega(1)$, $\Omega([1,+\infty))$ are defined by (7.12), (7.16), R is a constant.

The construction of W and f proving Theorem 1 is presented below in Subsections 3.1, 3.2. In addition, this construction consists of its version in dimension $d = 2$ (see Subsection 3.1) and its subsequent extension to the case of $d \geq 3$ (see Subsection 3.2).

Theorem 1 directly gives counterexamples to Injectivity 1 and Injectivity 3 of Introduction. Theorem 1 also implies the following counterexample to Injectivity 2 of Introduction:

Corollary 1.1. *For any $\alpha \in (0, 1/16)$ there is $N > 0$ such that for any $\delta > 0$ there are W_δ, f_δ satisfying*

$$W_\delta \geq 1/2,\ W_\delta \in C^\alpha(\mathbb{R}^2 \times \mathbb{S}^1),\ \|W_\delta\|_{C^\alpha(\mathbb{R}^2\times\mathbb{S}^1)} \leq N \tag{7.39}$$

$$f_\delta \in C^\infty(\mathbb{R}^2),\ f_\delta \not\equiv 0,\ \operatorname{supp} f_\delta \subseteq \overline{B}(0,\delta), \tag{7.40}$$

$$P_{W_\delta} f_\delta \equiv 0 \text{ on } T\mathbb{S}^1. \tag{7.41}$$

The construction of W_δ, f_δ proving Corollary 1.1 is presented in Subsection 5.1.

Theorem 2. *For any $n \in \mathbb{N} \cup \{\infty\}$ there exists a weight W_n satisfying (7.4) such that*

$$\dim \ker P_{W_n} \geq n \text{ in } C_0^\infty(\mathbb{R}^d),\ d \geq 2, \tag{7.42}$$

where P_W is defined in (7.1). Moreover,

$$W_n \in C^\infty(\mathbb{R}^2 \times \mathbb{S}^1) \text{ for } d = 2, \tag{7.43}$$

$$\begin{aligned} &W_n \text{ is infinitely smooth almost everywhere on } \mathbb{R}^d \times \mathbb{S}^{d-1} \text{ and} \\ &W_n \in C^\alpha(\mathbb{R}^d \times \mathbb{S}^{d-1}),\ \alpha \in (0, 1/16) \text{ for } d \geq 3, \end{aligned} \tag{7.44}$$

$$W_n(x,\theta) \equiv 1 \text{ for } |x| \geq R > 1,\ \theta \in \mathbb{S}^{d-1} \text{ for } n \in \mathbb{N},\ d \geq 2, \tag{7.45}$$

where R is a constant.

The construction of W_n proving Theorem 2 is presented in Section 4. In this construction we proceed from Theorem 1 of the present work for $d \geq 3$ and from the result of [Bo93] for $d = 2$. In addition, for this construction it is essential that $n < +\infty$ in (7.45).

3.1 Construction of f and W for $d = 2$

In dimension $d = 2$, the construction of f and W adopts and develops considerations of [Bo93] and [GN18]. In particular, we construct f, first, and then W (in this construction we use notations of Section 2 for $d = 2$). In addition, this construction is commented in Remarks 1-5 below.

Construction of f. The function f is constructed as follows:

$$f = \sum_{k=1}^{\infty} \frac{f_k}{k!}, \tag{7.46}$$

$$f_k(x) = \widetilde{f}_k(|x|) = \Phi(2^k(1-|x|))\cos(8^k|x|^2), x \in \mathbb{R}^2,\ k \in \mathbb{N}, \tag{7.47}$$

for arbitrary $\Phi \in C^\infty(\mathbb{R})$ such that

$$\operatorname{supp}\Phi = [4/5, 6/5], \tag{7.48}$$

$$0 < \Phi(t) \leq 1 \text{ for } t \in (4/5, 6/5), \tag{7.49}$$

$$\Phi(t) = 1, \text{ for } t \in [9/10, 11/10], \tag{7.50}$$

$$\begin{aligned} &\Phi \text{ monotonously increases on } [4/5, 9/10] \\ &\text{and monotonously decreases on } [11/10, 6/5]. \end{aligned} \tag{7.51}$$

Properties (7.48), (7.49) imply that functions $\widetilde{f}_k$ (and functions f_k) in (7.47) have disjoint supports:

$$\begin{aligned} &\operatorname{supp}\widetilde{f}_i \cap \operatorname{supp}\widetilde{f}_j = \emptyset \text{ if } i \neq j, \\ &\operatorname{supp}\widetilde{f}_k = [1 - 2^{-k}\left(\frac{6}{5}\right), 1 - 2^{-k}\left(\frac{4}{5}\right)],\ i,\ j,\ k \in \mathbb{N}. \end{aligned} \tag{7.52}$$

This implies the convergence of series in (7.46) for every fixed $x \in \mathbb{R}^2$.

Lemma 1. *Let f be defined by* (7.46)-(7.50). *Then f is spherically symmetric, $f \in C_0^\infty(\mathbb{R}^2)$ and* $\operatorname{supp} f \subseteq \overline{B}$. *In addition, if $\gamma \in T\mathbb{S}^1$, $\gamma \cap B \neq \emptyset$, then $f|_\gamma \not\equiv 0$ and $f|_\gamma$ has non-constant sign.*

Lemma 1 is similar to Lemma 1 of [GN18] and it is, actually, proved in Section 4.1 of [GN18].

Remark 1. Formulas (7.46)-(7.50) for f are similar to the formulas for f in [Bo93], where P_W was considered in $\mathbb{R}^2$, and also to the formulas for f in [GN18], where the weighted Radon transform R_W along hyperplanes was considered in $\mathbb{R}^3$. The only difference between (7.46)-(7.50) and the related formulas in [GN18] is the dimension $d = 2$ in (7.46)-(7.50) instead of $d = 3$ in [GN18]. At the same time, the important difference between (7.46)-(7.50) and the related formulas in [Bo93] is that in formula (7.47) the factor $\cos(8^k|x|^2)$ depends only on $|x|$, whereas in [Bo93] the corresponding factor is $\cos(3^k\phi)$ which depends only on the angle ϕ in the polar coordinates in $\mathbb{R}^2$. In a similar way with [Bo93], [GN18], we use the property that the restriction of the function $\cos(8^k|x|^2)$ to an arbitrary ray γ intersecting the open ball oscillates sufficiently fast (with change of the sign) for large k.

Construction of W. In our example W is of the following form:

$$\begin{aligned} W(x,\theta) &= \phi_1(x)\left(\sum_{i=0}^{N}\xi_i(r(x,\theta))W_i(x,\theta)\right)+\phi_2(x) \\ &= \phi_1(x)\left(\xi_0(r(x,\theta))W_0(x,\theta)+\sum_{i=1}^{N}\xi_i(r(x,\theta))W_i(x,\theta)\right)+\phi_2(x),\ (x,\theta)\in\Omega, \end{aligned} \tag{7.53}$$

where

$$\begin{aligned} &\phi_1 = \phi_1(|x|), \phi_2 = \phi_2(|x|) \text{ is a } C^\infty\text{-smooth partition of unity on } \mathbb{R}^2 \text{ such that,} \\ &\phi_1 \equiv 0 \text{ for } |x| \geq R > 1,\ \phi_1 \equiv 1 \text{ for } |x| \leq 1, \\ &\phi_2 \equiv 0 \text{ for } |x| \leq 1, \end{aligned} \tag{7.54}$$

$$\{\xi_i(s),\ s\in\mathbb{R}\}_{i=0}^N \text{ is a } C^\infty\text{- smooth partition of unity on } \mathbb{R}, \tag{7.55}$$

$$\xi_i(s) = \xi_i(-s),\ s\in\mathbb{R},\ i = \overline{0,N}, \tag{7.56}$$

$$\begin{aligned} &W_i(x,\theta) \text{ are bounded, continuous, strictly positive} \\ &\text{and rotation invariant (according to (7.29)), (7.32) on} \\ &\text{the open vicinities of } \operatorname{supp}\xi_i(r(x,\theta)),\ i = \overline{0,N},\ \text{respectively.} \end{aligned} \tag{7.57}$$

From the result of Lemma 1 and from (7.53), (7.54) it follows that

$$P_W f(x,\theta) = \xi_0(|x|)P_{W_0}f(x,\theta) + \sum_{i=1}^{N}\xi_i(|x|)P_{W_i}f(x,\theta),\ (x,\theta)\in T\mathbb{S}^1, \tag{7.58}$$

where W is given by (7.53). Here, we also used that $r(x,\theta) = |x|$ for $(x,\theta)\in T\mathbb{S}^1$.

From (7.53)-(7.57) it follows that W of (7.53) satisfies the conditions (7.4), (7.31), (7.32).

The weight W_0 is constructed in next paragraph and has the following properties:

$$W_0 \text{ is bounded, continuous and rotation invariant on } \Omega(1/2,+\infty), \tag{7.59}$$

$$\begin{aligned} &W_0 \in C^\infty(\Omega\,((1/2,1)\cup(1,+\infty))) \text{ and} \\ &W_0 \in C^\alpha(\Omega(1/2,+\infty)) \text{ for } \alpha \in (0,1/16), \end{aligned} \tag{7.60}$$

$$\begin{aligned} &\text{there exists } \delta_0 \in (1/2,1) \text{ such that:} \\ &\qquad W_0(x,\theta) \geq 1/2 \text{ if } r(x,\theta) > \delta_0, \\ &\qquad W_0(x,\theta) = 1 \quad \text{if } r(x,\theta) \geq 1, \end{aligned} \tag{7.61}$$

$$P_{W_0} f(x,\theta) = 0 \text{ on } \Omega((1/2,+\infty)), \tag{7.62}$$

where P_{W_0} is defined according to (7.1) for $W = W_0$, f is given by (7.46), (7.47).

In addition,

$$\operatorname{supp} \xi_0 \subset (-\infty,-\delta_0)\cup(\delta_0,+\infty), \tag{7.63}$$

$$\xi_0(s) = 1 \text{ for } |s| \geq 1, \tag{7.64}$$

where δ_0 is the number of (7.61).

In particular, from (7.61), (7.63) it follows that

$$W_0(x,\theta)\xi_0(r(x,\theta)) > 0 \text{ if } \xi_0(r(x,\theta)) > 0. \tag{7.65}$$

In addition,

$$\xi_i(r(x,\theta))W_i(x,\theta) \text{ are bounded, rotation invariant and } C^\infty \text{ on } \Omega, \tag{7.66}$$

$$W_i(x,\theta) \geq 1/2 \text{ if } \xi_i(r(x,\theta)) \neq 0, \tag{7.67}$$

$$P_{W_i} f(x,\theta) = 0 \text{ on } (x,\theta) \in T\mathbb{S}^1, \text{ such that } \xi_i(r(x,\theta)) \neq 0, \tag{7.68}$$

$$i = \overline{1,N},\ (x,\theta) \in \Omega.$$

Weights $W_1,\dots,W_N$ of (7.53) and $\{\xi_i\}_{i=0}^N$ are constructed in Subsection 3.1.

Theorem 1 for $d = 2$ follows from Lemma 1 and formulas (7.53)-(7.62), (7.65)-(7.68).

We point out that the construction of W_0 of (7.53) is substantially different from the construction of $W_1,\dots,W_N$. The weight W_0 is defined for the rays $\gamma \in T\mathbb{S}^1$ which can be close to the boundary ∂B of B which results in restrictions on global smoothness of W_0.

Remark 2. The construction of W summarized above in formulas (7.53)-(7.68) arises in the framework of finding W such that

$$P_W f \equiv 0 \text{ on } T\mathbb{S}^1 \text{ for } f \text{ defined in (7.46)-(7.51)}, \tag{7.69}$$

under the condition that W is strictly positive, sufficiently regular and rotation invariant (see formulas (7.4), (7.29), (7.30)). In addition, the weights W_i, $i = 0,\dots,N$, in (7.53) are constructed in a such a way that

$$P_{W_i} f = 0 \text{ on } V_i,\ i = 0,\dots,N, \tag{7.70}$$

under the condition that $W_i = W_i(x,\gamma)$ are strictly positive, sufficiently regular and rotation invariant for $x \in \gamma$, $\gamma \in V_i \subset T\mathbb{S}^1$, $i = 0,\dots,N$, where

$$\{V_i\}_{i=0}^N \text{ is an open cover of } T\mathbb{S}^1 \text{ and } V_0 = T_0(\delta_0), \tag{7.71}$$

$$V_i = T(\Lambda_i) \text{ for some open } \Lambda_i \subset \mathbb{R},\ i = 0,\dots,N, \tag{7.72}$$

where T_0 is defined in (7.17), δ_0 is the number of (7.61), $T(\Lambda)$ is defined in (7.19). In addition, the functions ξ_i, $i = 0, \dots, N$, in (7.53) can be interpreted as a partition of unity on $T\mathbb{S}^1$ subordinated to the open cover $\{V_i\}_{i=0}^N$. The aforementioned construction of W is a two-dimensional analog of the construction developed in [GN18], where the weighted Radon transform R_W along hyperplanes was considered in $\mathbb{R}^3$. At the same time, the construction of W of the present work is similar to the construction in [Bo93] with the important difference that in the present work f is spherically symmetric and W, W_i, $i = 0, \dots, N$, are rotation invariant.

Construction of W_0. Let $\{\psi_k\}_{k=1}^\infty$ be a C^∞ partition of unity on $(1/2, 1)$ such that

$$\operatorname{supp}\psi_k \subset (1 - 2^{-k+1}, 1 - 2^{-k-1}),\ k \in \mathbb{N}, \tag{7.73}$$

$$\text{first derivatives } \psi_k' \text{ satisfy the bounds: } \sup|\psi_k'| \le C2^k, \tag{7.74}$$

where C is a positive constant. Actually, functions $\{\psi_k\}_{k=1}^\infty$ satisfying (7.73), (7.74) were used in considerations of [Bo93].

Note that

$$1 - 2^{-(k-2)-1} < 1 - 2^{-k}(6/5),\ k \ge 3. \tag{7.75}$$

Therefore,

$$\text{for all } s_0,\ t_0 \in \mathbb{R}, s_0 \in \operatorname{supp}\psi_{k-2},\ t_0 \in \operatorname{supp}\Phi(2^k(1-t)) \Rightarrow s_0 < t_0,\ k \ge 3. \tag{7.76}$$

Weight W_0 is defined by the following formulas

$$W_0(x,\theta) = \begin{cases} 1 - G(x,\theta)\sum\limits_{k=3}^{\infty} k! f_k(x)\dfrac{\psi_{k-2}(r(x,\theta))}{H_k(x,\theta)},\ 1/2 < r(x,\theta) < 1, \\ 1,\ r(x,\theta) \ge 1 \end{cases}, \tag{7.77}$$

$$G(x,\theta) = \int\limits_{\gamma(x,\theta)} f(y)\,dy,\ H_k(x,\theta) = \int\limits_{\gamma(x,\theta)} f_k^2(y)\,dy,\ x \in \mathbb{R}^2,\ \theta \in \mathbb{S}^1, \tag{7.78}$$

where f, f_k are defined in (7.46), (7.47), respectively, rays $\gamma(x,\theta)$ are given by (7.24).

Formula (7.77) implies that W_0 is defined on $\Omega_0(1/2) \subset \Omega$.

Due to (7.47)-(7.50), (7.73), (7.76), in (7.78) we have that

$$H_k(x,\theta) \ne 0 \text{ if } \psi_{k-2}(r(x,\theta)) \ne 0,\ (x,\theta) \in \Omega, \tag{7.79}$$

$$\frac{\psi_{k-2}(r(x,\theta))}{H_k(x,\theta)} \in C^\infty(\Omega(1/2,1)), \tag{7.80}$$

where $r(x,\theta)$ is defined in (7.13), Ω, $\Omega(\cdot)$ are defined in (7.12), (7.16), $d = 2$.

Also, for any fixed $(x,\theta) \in \Omega$, $1/2 < r(x,\theta)$, the series in the right hand-side of (7.77) has only a finite number of non-zero terms (in fact, no more than two) and, hence, the weight W_0 is well-defined.

By the spherical symmetry of f, functions G, H_k in (7.77) are of the type (7.29) (and (7.31)). Therefore, W_0 is rotation invariant (in the sense of (7.29) and (7.31)).

Actually, formula (7.62) follows from (7.46), (7.47), (7.77), (7.78) (see Subsection 6.2 for details).

Using the construction of W_0 and the assumption that $r(x,\theta) > 1/2$ one can see that W_0 is C^∞ on its domain of definition, possibly, except points with $r(x,\theta) = 1$.

Note also that due to (7.46), (7.47), the functions f_k, G, H_k, used in (7.77), (7.78) can be considered as functions of one-dimensional arguments.

Formulas (7.59)-(7.61) are proved in Subsection 6.1.

Remark 3. Formulas (7.77), (7.78) given above for the weight W_0 are considered for the rays from $T_0(\delta_0)$ (mentioned in Remark 2) and, in particular, for rays close to the tangent rays to ∂B. These formulas are direct two-dimensional analogs of the related formulas in [GN18]. At the same time, formulas (7.77), (7.78) are similar to the related formulas in [Bo93] with the important difference that f, f_k are spherically symmetric in the present work and, as a corollary, W_0 is rotation invariant. Also, in a similar way with [Bo93], [GN18], in the present work we show that $G(x,\theta)$ tends to zero sufficiently fast as $r(x,\theta)\to 1$. This is a very essential point for continuity of W_0 and it is given in Lemma 3 of Subsection 6.1.

Construction of $W_1,\dots,W_N$ and $\xi_0,\dots,\xi_N$

Lemma 2. *Let $f\in C_0^\infty(\mathbb{R}^2)$ be spherically symmetric, $(x_0,\theta_0)\in T\mathbb{S}^1$, $f|_{\gamma(x_0,\theta_0)}\not\equiv 0$ and $f|_{\gamma(x_0,\theta_0)}$ changes the sign. Then there exist $\varepsilon_0>0$ and weight $W_{(x_0,\theta_0),\varepsilon_0}$ such that*

$$P_{W_{(x_0,\theta_0),\varepsilon_0}} f=0 \text{ on } \Omega(\mathcal{J}_{r(x_0,\theta_0),\varepsilon_0}), \tag{7.81}$$

$$\begin{aligned}&W_{(x_0,\theta_0),\varepsilon_0} \text{ is bounded, infinitely smooth,}\\ &\text{strictly positive and rotation invariant on } \Omega(\mathcal{J}_{r(x_0,\theta_0),\varepsilon_0}),\end{aligned} \tag{7.82}$$

where $\Omega(\mathcal{J}_{r,\varepsilon_0}),\mathcal{J}_{r,\varepsilon_0}$ are defined in (7.16) and (7.20), respectively.

Lemma 2 is proved in Section 7. This lemma is a two-dimensional analog of the related lemma in [GN18].

Remark 4. In Lemma 2 the construction of $W_{(x_0,\theta_0),\varepsilon_0}$ arises from

1. finding strictly positive and regular weight $W_{(x_0,\theta_0),\varepsilon}$ on the rays $\gamma=\gamma(x,\theta)$ with fixed $\theta=\theta_0$, where $r(x,\theta_0)\in\mathcal{J}_{r(x_0,\theta_0),\varepsilon}$ for some $\varepsilon>0$, such that (7.81) holds for $\theta=\theta_0$ and under the condition that
$$W_{(x_0,\theta_0),\varepsilon}(y,\gamma)=W_{(x_0,\theta_0),\varepsilon}(|y\theta_0|,\gamma),\ y\in\gamma=\gamma(x,\theta_0),\ r(x,\theta_0)\in\mathcal{J}_{r(x_0,\theta_0),\varepsilon}; \tag{7.83}$$
2. extending $W_{r(x_0,\theta_0),\varepsilon}$ to all rays $\gamma=\gamma(x,\theta)$, $r(x,\theta)\in\mathcal{J}_{r(x_0,\theta_0),\varepsilon}$, $\theta\in\mathbb{S}^1$, via formula (7.8).

We recall that $r(x,\theta)$ is defined in (7.13).

Let f be the function of (7.46), (7.47). Then, using Lemmas 1, 2 one can see that

$$\begin{aligned}&\text{for all } \delta\in(0,1) \text{ there exist } \{J_i=\mathcal{J}_{r_i,\varepsilon_i}, W_i=W_{(x_i,\theta_i),\varepsilon_i}\}_{i=1}^N\\ &\text{such that } J_i,\ i=\overline{1,N},\ \text{is an open cover of } [0,\delta] \text{ in } \mathbb{R},\\ &\text{and } W_i \text{ satisfy (7.81) and (7.82) on } \Omega(J_i),\ \text{respectively.}\end{aligned} \tag{7.84}$$

Actually, we consider (7.84) for the case of $\delta=\delta_0$ of (7.61).
Note that in this case $\{\Omega(J_i)\}_{i=1}^N$ for J_i of (7.84) is the open cover of $\Omega_1(\delta_0)$.
To the set $\Omega_0(\delta_0)$ we associate the open set

$$J_0=(\delta_0,+\infty)\subset\mathbb{R}. \tag{7.85}$$

Therefore, the collection of intervals $\{\pm J_i,\ i=\overline{0,N}\}$ is an open cover of $\mathbb{R}$, where $-J_i$ is the symmetrical reflection of J_i with respect to $\{0\}\in\mathbb{R}$.

We construct the partition of unity $\{\xi_i\}_{i=0}^N$ as follows:

$$\xi_i(s)=\xi_i(|s|)=\frac{1}{2}(\tilde{\xi}_i(s)+\tilde{\xi}_i(-s)),\ s\in\mathbb{R}, \tag{7.86}$$

$$\operatorname{supp}\xi_i\subset J_i\cup(-J_i),\ i=\overline{0,N}, \tag{7.87}$$

where $\{\tilde{\xi}_i\}_{i=0}^N$ is a partition of unity for the open cover $\{J_i \cup (-J_i)\}_{i=0}^N$ (see Section 2, Partition of unity, for $U_i = J_i \cup (-J_i)$).

Properties (7.63), (7.87) follow from (7.33) for $\{\tilde{\xi}_i\}_{i=0}^N$ with $U_i = J_i \cup (-J_i)$, the symmetry of $J_i \cup (-J_i)$, $i = \overline{1, N}$, choice of J_0 in (7.85) and from (7.86).

In turn, (7.64) follows from (7.85) and the construction of J_i, $i = \overline{1, N}$, from (7.84) (see the proof of Lemma 2 and properties (7.84) in Section 7 for details).

Properties (7.66)-(7.68) follow from (7.84) for $\delta = \delta_0$ and from (7.85)-(7.87).

This completes the description of $W_1, \dots, W_N$ and $\{\xi_i\}_{i=0}^N$.

Remark 5. We have that $J_i = \Lambda_i$, $i = 1, \dots, N$, where Λ_i are the intervals in formula (7.72) of Remark 2 and J_i are the intervals considered in (7.84), (7.85).

3.2 Construction of W and f for $d \geq 3$

Consider f and W of Theorem 1, for $d = 2$, constructed in Subsection 3.1. For these f and W consider $\tilde{f}$ and $\tilde{U}$ such that

$$f(x) = \widetilde{f}(|x|),\ W(x, \theta) = \tilde{U}(|x|, |x\theta|),\ x \in \mathbb{R}^2,\ \theta \in \mathbb{S}^1. \tag{7.88}$$

Proposition 1. *Let W and f, for $d \geq 3$, be defined as*

$$W(x, \theta) = \tilde{U}(|x|, |x\theta|),\ (x, \theta) \in \mathbb{R}^d \times \mathbb{S}^{d-1}, \tag{7.89}$$

$$f(x) = \tilde{f}(|x|),\ x \in \mathbb{R}^d, \tag{7.90}$$

where $\tilde{U}$, $\tilde{f}$ are the functions of (7.88). *Then*

$$P_W f \equiv 0 \text{ on } T\mathbb{S}^{d-1}. \tag{7.91}$$

In addition, weight W satisfies properties (7.35)-(7.38), *f is spherically symmetric infinitely smooth and compactly supported on $\mathbb{R}^d$, $f \not\equiv 0$.*

Proposition 1 is proved in Subsection 5.2.

This completes the proof of Theorem 1.

4 Proof of Theorem 2

4.1 Proof for $d \geq 3$

Let

W be the weight of Theorem 1 for $d \geq 3$, (7.92)

R be the number in (7.38) for $d \geq 3$, (7.93)

$\{y_i\}_{i=1}^\infty$ be a sequence of vectors in $\mathbb{R}^d$ such that $y_1 = 0$, $|y_i - y_j| > 2R$ for $i \neq j$, $i, j \in \mathbb{N}$, (7.94)

$\{\overline{B}_i\}_{i=1}^\infty$ be the closed balls in $\mathbb{R}^d$ of radius R centered at y_i (see (7.93), (7.94)). (7.95)

The weight W_n is defined as follows

$$W_n(x,\theta) = \begin{cases} 1 \text{ if } x \notin \bigcup\limits_{i=1}^{n} \overline{B}_i, \\ W(x-y_1,\theta) = W(x,\theta) \text{ if } x \in \overline{B}_1, \\ W(x-y_2,\theta) \text{ if } x \in \overline{B}_2, \\ ..., \\ W(x-y_k,\theta) \text{ if } x \in \overline{B}_k, \\ ..., \\ W(x-y_n,\theta) \text{ if } x \in \overline{B}_n, \end{cases} \tag{7.96}$$

$\theta \in \mathbb{S}^{d-1}$, $n \in \mathbb{N} \cup \{\infty\}$, $d \geq 3$,

where W is defined in (7.92), y_i and $\overline{B}_i$ are defined in (7.94), (7.95), respectively.

Properties (7.4), (7.44) and (7.45) for W_n, defined in (7.96), for $d \geq 3$, follow from (7.35)-(7.38), (7.92), (7.93).

Let

$$f_1(x) \stackrel{\text{def}}{=} f(x),\ f_2(x) \stackrel{\text{def}}{=} f(x-y_2), \ldots, f_n(x) \stackrel{\text{def}}{=} f(x-y_n),\ x \in \mathbb{R}^d,\ d \geq 3, \tag{7.97}$$

where y_i are defined in (7.94) and

$$f \text{ is the function of Theorem 1 for } d \geq 3. \tag{7.98}$$

One can see that

$$f_i \in C_0^\infty(\mathbb{R}^d),\ d \geq 3,\ f_i \not\equiv 0,\ \operatorname{supp} f_i \subset \overline{B}_i,\ \overline{B}_i \cap \overline{B}_j = \emptyset \text{ for } i \neq j, \tag{7.99}$$

where $\overline{B}_i$ are defined in (7.95), $i = 1, \ldots, n$.

The point is that

$$P_{W_n} f_i \equiv 0 \text{ on } T\mathbb{S}^{d-1},\ d \geq 3,\ i = 1, \ldots, n, \tag{7.100}$$

$$f_i \text{ are linearly independent in } C_0^\infty(\mathbb{R}^d),\ d \geq 3,\ i = 1, \ldots, n, \tag{7.101}$$

where W_n is defined in (7.96), f_i are defined in (7.97).

To prove (7.100) we use, in particular, the following general formula:

$$\begin{aligned} P_{W_y} f_y(x,\theta) &= \int\limits_{\gamma(x,\theta)} W(y'-y,\theta) f(y'-y)dy' \\ &= \int\limits_{\gamma(x-y,\theta)} W(y',\theta) f(y')dy' = P_W f(x-y,\theta),\ x \in \mathbb{R}^d,\ \theta \in \mathbb{S}^{d-1}, \end{aligned} \tag{7.102}$$

$$W_y(x,\theta) = W(x-y,\theta),\ f_y = f(x-y),\ x,\ y \in \mathbb{R}^d,\ \theta \in \mathbb{S}^{d-1}. \tag{7.103}$$

where W is an arbitrary weight satisfying (7.4), f is a test-function, $\gamma(x,\theta)$ is defined according to (7.24).

Formula (7.100) follows from formula (7.34), definitions (7.96), (7.97), (7.98), properties (7.99) and from formulas (7.102), (7.103).

Formula (7.101) follows from definitions (7.97), (7.98) and properties (7.99).

This completes the proof of Theorem 2 for $d \geq 3$.

4.2 Proof for $d = 2$

In [Bo93], there were constructed a weight W and a function f for $d = 2$, such that:

$$P_W f \equiv 0 \text{ on } T\mathbb{S}^1, \tag{7.104}$$
$$W = \overline{W} \geq c > 0,\ W \in C^\infty(\mathbb{R}^2 \times \mathbb{S}^1), \tag{7.105}$$
$$f \in C_0^\infty(\mathbb{R}^2),\ f \not\equiv 0,\ \text{supp} f \subset \overline{B}, \tag{7.106}$$

where c is a constant, $\overline{B}$ is defined in (7.27).

We define

$$\widetilde{W}(x,\theta) = c^{-1}\phi_1(x)W(x,\theta) + \phi_2(x),\ x \in \mathbb{R}^2,\ \theta \in \mathbb{S}^1, \tag{7.107}$$

where W is the weight of (7.104), (7.105), c is a constant of (7.105).

$$\begin{aligned}&\phi_1 = \phi_1(x), \phi_2 = \phi_2(x) \text{ is a } C^\infty\text{-smooth partition of unity on } \mathbb{R}^2 \text{ such that,}\\ &\phi_1 \equiv 0 \text{ for } |x| \geq R > 1,\ \phi_1 \equiv 1 \text{ for } |x| \leq 1,\ \phi_1 \geq 0 \text{ on } \mathbb{R}^2,\\ &\phi_2 \equiv 0 \text{ for } |x| \leq 1,\ \phi_2 \geq 0 \text{ on } \mathbb{R}^2,\end{aligned} \tag{7.108}$$

where R is a constant.

From (7.104)-(7.108) it follows that

$$P_{\widetilde{W}} f \equiv 0 \text{ on } T\mathbb{S}^1, \tag{7.109}$$
$$\begin{aligned}&\widetilde{W} \geq 1,\ \widetilde{W} \in C^\infty(\mathbb{R}^2 \times \mathbb{S}^1),\\ &\widetilde{W}(x,\theta) \equiv 1 \text{ for } |x| \geq R > 1,\ \theta \in \mathbb{S}^1.\end{aligned} \tag{7.110}$$

The proof of Theorem 2 for $d = 2$ proceeding from (7.106), (7.107), (7.109), (7.110) is completely similar to the proof of Theorem 2 for $d \geq 3$, proceeding from Theorem 1.

Theorem 2 is proved.

5 Proofs of Corollary 1.1 and Proposition 1

5.1 Proof of Corollary 1.1

Let

$$X_r = \{x_1 e_1 + x_2 e_2 + r e_3 : (x_1, x_2) \in \mathbb{R}^2\},\ 0 \leq r < 1, \tag{7.111}$$
$$S = X_0 \cap \mathbb{S}^2 = \{(\cos\phi, \sin\phi, 0) \in \mathbb{R}^3 : \phi \in [0, 2\pi)\} \simeq \mathbb{S}^1. \tag{7.112}$$

where (e_1, e_2, e_3) is the standard orthonormal basis in $\mathbb{R}^3$.

Without loss of generality we assume that $0 < \delta < 1$. Choosing r so that $\sqrt{1-\delta^2} \leq r < 1$, we have that the intersection of the three dimensional ball $B(0,1)$ with X_r is the two-dimensional disk $B(0,\delta')$, $\delta' \leq \delta$ (with respect to the coordinates (x_1, x_2) induced by basis (e_1, e_2) on X_r).

We define N, W_δ on $\mathbb{R}^2 \times \mathbb{S}^1$ and f_δ on $\mathbb{R}^2$ as follows:

$$N = \|W\|_{C^\alpha(\mathbb{R}^3 \times \mathbb{S}^2)}, \tag{7.113}$$
$$W_\delta := W|_{X_r \times S}, \tag{7.114}$$
$$f_\delta := f|_{X_r}, \tag{7.115}$$
$$\text{for } r = \sqrt{1-\delta^2},$$

where W and f are the functions of Theorem 1 for $d = 3$.

Due to (7.35)-(7.37), (7.113), (7.114) we have that

$$W_\delta \geq 1/2,\ \|W_\delta\|_{C^\alpha(\mathbb{R}^2\times\mathbb{S}^1)} \leq N. \tag{7.116}$$

Properties (7.116) imply (7.39).

In view of Lemma 1 for the function f of Theorem 1, we have that f_δ is spherically symmetric, $f_\delta \in C_0^\infty(B(0,\delta'))$, $f_\delta \not\equiv 0$.

Using (7.34), (7.114), (7.115) one can see that (7.41) holds.

This completes the proof of Corollary 1.1.

5.2 Proof of Proposition 1

Let

$$I(r) = \int\limits_{\gamma_r} \tilde{U}(|y|, r)\tilde{f}(|y|)\, dy,\ r \geq 0,\ \gamma_r = \gamma(re_2, e_1), \tag{7.117}$$

where $\gamma(x,\theta)$ is defined by (7.3), $(e_1, \dots, e_d)$ is the standard basis in $\mathbb{R}^d$.

Due to formula (7.34) of Theorem 1 for $d = 2$ and formulas (7.88), (7.117) we have that

$$I(r) = P_W f(re_2, e_1) = 0 \text{ for } r \geq 0. \tag{7.118}$$

Next, using (7.1), (7.88), (7.118) we have also that

$$P_W f(x,\theta) = \int\limits_{\gamma(x,\theta)} \tilde{U}(|y|, |y - (y\theta)\theta|)\tilde{f}(|y|)\, dy = I(|x|) = 0 \text{ for } (x,\theta) \in T\mathbb{S}^{d-1}, \tag{7.119}$$

where $\gamma(x,\theta)$ is defined in (7.3).

Formula (7.119) implies (7.91). Properties of W and f mentioned in Proposition 1 follow from properties (7.35)-(7.38) of W and of f of Theorem 1 for $d = 2$.

This completes the proof of Proposition 1.

6 Proofs of formulas (7.59)-(7.62)

6.1 Proof of formulas (7.59)-(7.61)

Lemma 3. *Let W_0 be defined by (7.77), (7.78). Then W_0 admits the following representation:*

$$W_0(x,\theta) = U_0(|x - (x\theta)\theta|, x\theta),\ (x,\theta) \in \Omega((1/2, +\infty)), \tag{7.120}$$

$$U_0(r,s) = \begin{cases} 1 - \widetilde{G}(r)\sum\limits_{k=3}^{\infty} k!\widetilde{f}_k((s^2+r^2)^{1/2})\dfrac{\psi_{k-2}(r)}{\widetilde{H}_k(r)},\ 1/2 < r < 1, \\ 1,\ r \geq 1 \end{cases}, \tag{7.121}$$

$$\widetilde{G}(r) \stackrel{\text{def}}{=} \int\limits_{\gamma_r} \widetilde{f}(|y|)\, dy,\ \widetilde{H}_k(r) \stackrel{\text{def}}{=} \int\limits_{\gamma_r} \widetilde{f}_k^2(|y|)\, dy,\ \widetilde{f} = \sum_{k=1}^{\infty} \frac{\widetilde{f}_k}{k!}, \tag{7.122}$$

$s \in \mathbb{R}$, $x \in \mathbb{R}^2$, γ_r *is an arbitrary ray in* $T(r)$, $r > 1/2$,

where $\widetilde{f}_k$ *are defined by* (7.47), $T(r)$ *is defined by* (7.19), $d = 2$. *In addition:*

$$U_0 \text{ is infinitely smooth on } \{(1/2, 1) \cup (1, +\infty)\} \times \mathbb{R}, \tag{7.123}$$

$$U_0(r, s) \to 1 \text{ as } r \to 1 \text{ (uniformly in } s \in \mathbb{R}), \tag{7.124}$$

$$U_0(r, s) = 1 \text{ if } s^2 + r^2 \geq 1, \tag{7.125}$$

$$|1 - U_0(r, s)| \leq C_0(1 - r)^{1/2} \log_2^4 \left(\frac{1}{1 - r}\right), \tag{7.126}$$

$$\text{for } 1/2 < r < 1,\ s \in \mathbb{R},$$

$$|U_0(r, s) - U_0(r', s')| \leq C_1|s - s'|^\alpha + C_1|r - r'|^\alpha, \tag{7.127}$$

$$\text{for } \alpha \in (0, 1/16),\ r, r' > 1/2,\ s, s' \in \mathbb{R},\ |r - r'| \leq 1,\ |s - s'| \leq 1,$$

where C_0, C_1 *are positive constants depending on* Φ *of* (7.48)-(7.50).

Lemma 3 is proved Section 8.

Lemma 3 implies (7.59)-(7.61) as follows.

The continuity and rotation invariancy of W_0 in (7.59) follow from (7.29), (7.30), (7.120), (7.127).

Due to (7.73), (7.120), (7.121), (7.122) we have also that

$$U_0 \text{ admits a continuous extension to } [1/2, +\infty) \times \mathbb{R}. \tag{7.128}$$

Properties (7.125), (7.128) imply the boundedness of W_0 on $\Omega_0(1/2)$, where $\Omega_0(\cdot)$ is defined in (7.14), $d = 2$. This completes the proof of (7.59).

Formula (7.60) follows from (7.120), (7.123), (7.127) and from the fact that $x\theta$, $|x - (x\theta)\theta|$ are infinitely smooth functions on $\Omega_0(1/2)$ and are Lipshitz in (x, θ) for $x \in \overline{B}(0, R)$, $R > 1$.

Formula (7.61) follows from (7.59), (7.120), (7.121), (7.124), (7.125).

This completes the proof of (7.59)-(7.61).

6.2 Proof of formula (7.62)

From (7.1), (7.46)-(7.49), (7.73), (7.77), (7.78) it follows that:

$$\begin{aligned} P_{W_0} f(x, \theta) &= \int\limits_{\gamma(x,\theta)} f(y)\, dy - G(x, \theta) \sum_{k=3}^{\infty} k! \psi_{k-2}(r(x, \theta)) \frac{\int\limits_{\gamma(x,\theta)} f(y) f_k(y) dy}{H_k(x, \theta)} \\ &= \int\limits_{\gamma(x,\theta)} f(y)\, dy - \int\limits_{\gamma(x,\theta)} f(y)\, dy \sum_{k=3}^{\infty} \psi_{k-2}(r(x, \theta)) \frac{\int\limits_{\gamma(x,\theta)} f_k^2(y) dy}{\int\limits_{\gamma(x,\theta)} f_k^2(y)\, dy} \\ &= \int\limits_{\gamma(x,\theta)} f(y)\, dy - \int\limits_{\gamma(x,\theta)} f(y)\, dy \sum_{k=3}^{\infty} \psi_{k-2}(r(x, \theta)) = 0 \text{ for } (x, \theta) \in \Omega_0(1/2), \end{aligned} \tag{7.129}$$

where $\gamma(x, \theta)$ is defined in (7.3), $\Omega_0(\cdot)$ is defined in (7.14), $d = 2$.

Formula (7.62) is proved.

7 Proof of Lemma 2

By $u \in \mathbb{R}$ we denote the coordinates on a fixed ray $\gamma(x, \theta)$, $(x, \theta) \in \Omega$, $d = 2$, taking into account the orientation, where $u = 0$ at the point $x - (x\theta)\theta \in \gamma(x, \theta)$; see notation (7.24).

Using Lemma 1, one can see that

$$f|_{\gamma(x,\theta)} \in C_0^\infty(\mathbb{R}),\ f|_{\gamma(x,\theta)}(u) = f|_{\gamma(x,\theta)}(|u|),\ u \in \mathbb{R}. \tag{7.130}$$

Using (7.130) and the assumption that $f|_{\gamma(x_0,\theta_0)}(u)$ changes the sign, one can see that there exists $\psi_{(x_0,\theta_0)}$ such that

$$\psi_{(x_0,\theta_0)} \in C_0^\infty(\mathbb{R}),\ \psi_{(x_0,\theta_0)} \geq 0,\ \psi_{(x_0,\theta_0)}(u) = \psi_{(x_0,\theta_0)}(|u|),\ u \in \mathbb{R}, \tag{7.131}$$

$$\int\limits_{\gamma(x_0,\theta_0)} f\psi_{(x_0,\theta_0)}\,d\sigma \neq 0, \tag{7.132}$$

and if

$$\int\limits_{\gamma(x_0,\theta_0)} f\,d\sigma \neq 0 \tag{7.133}$$

then also

$$\operatorname{sgn}(\int\limits_{\gamma(x_0,\theta_0)} f\,d\sigma)\operatorname{sgn}(\int\limits_{\gamma(x_0,\theta_0)} f\psi_{(x_0,\theta_0)}\,d\sigma) = -1, \tag{7.134}$$

where $d\sigma = du$ (i.e., σ is the standard Euclidean measure on $\gamma(x,\theta)$).

Let

$$W_{(x_0,\theta_0)}(x,\theta) = 1 - \psi_{(x_0,\theta_0)}(x\theta)\frac{\int\limits_{\gamma(x,\theta)} f\,d\sigma}{\int_{\gamma(x,\theta)} f\psi_{(x_0,\theta_0)}\,d\sigma},\ x \in \mathbb{R}^2,\ \theta \in \mathbb{S}^1, \tag{7.135}$$

where $d\sigma = du$, where u is the coordinate on $\gamma(x,\theta)$.

Lemma 1 and property (7.131) imply that

$$\int\limits_{\gamma(x,\theta)} f\,d\sigma \text{ and } \int\limits_{\gamma(x,\theta)} f\psi_{(x_0,\theta_0)}\,d\sigma \text{ depend only on } r(x,\theta),\ \text{where } (x,\theta) \in \Omega, \tag{7.136}$$

where $r(x,\theta)$ is defined in (7.13), Ω is defined in (7.12), $d = 2$.

From (7.131), (7.135), (7.136) it follows that $W_{(x_0,\theta_0)}$ is rotation-invariant in the sense (7.29).

Formulas (7.132), (7.135), (7.136), properties of f of Lemma 1 and properties of $\psi_{(x_0,\theta_0)}$ of (7.131) imply that

$$\exists \varepsilon_1 > 0 : \int\limits_{\gamma(x,\theta)} f\psi_{(x_0,\theta_0)}\,d\sigma \neq 0 \text{ for } (x,\theta) \in \Omega(\mathcal{J}_{r(x_0,\theta_0),\varepsilon_1}), \tag{7.137}$$

where sets $\Omega(\mathcal{J}_{s,\varepsilon})$, $\mathcal{J}_{s,\varepsilon}$ are defined in (7.16), (7.20), respectively.

In addition, using properties of f of Lemma 1 and also using (7.46), (7.52), (7.131), (7.135), (7.137), one can see that

$$W_{(x_0,\theta_0)} \in C^\infty(\Omega(\mathcal{J}_{r(x_0,\theta_0),\varepsilon_1})). \tag{7.138}$$

In addition, from (7.130)-(7.136) it follows that

$$\text{if } r(x,\theta) = r(x_0,\theta_0) \text{ then } W_{(x_0,\theta_0)}(x,\theta) = 1 - \psi_{(x_0,\theta_0)}(x\theta)\frac{\int\limits_{\gamma(x_0,\theta_0)} f\,d\sigma}{\int\limits_{\gamma(x_0,\theta_0)} f\psi_{(x_0,\theta_0)}\,d\sigma}$$

$$= 1 - \psi_{(x_0,\theta_0)}(x\theta)\frac{\int\limits_{\gamma(x_0,\theta_0)} f\,d\sigma}{\int\limits_{\gamma(x_0,\theta_0)} f\psi_{(x_0,\theta_0)}\,d\sigma} \geq 1, \tag{7.139}$$

where $r(x,\theta)$ is defined in (7.13), $d=2$.

From properties of f of Lemma 1, properties of $\psi_{(x_0,\theta_0)}$ of (7.131) and from formulas (7.135), (7.137), (7.138), (7.139) it follows that

$$\exists \varepsilon_0 > 0\,(\varepsilon_0 < \varepsilon_1) : W_{(x_0,\theta_0)}(x,\theta) \geq 1/2 \text{ for } (x,\theta) \in \Omega(\mathcal{J}_{r(x_0,\theta_0),\varepsilon_0}). \tag{7.140}$$

Let

$$W_{(x_0,\theta_0),\varepsilon_0} := W_{(x_0,\theta_0)} \text{ for } (x,\theta) \in \Omega(\mathcal{J}_{r(x_0,\theta_0),\varepsilon_0}), \tag{7.141}$$

where $W_{(x_0,\theta_0)}$ is defined in (7.135).

Properties (7.136), (7.138), (7.140) imply (7.82) for $W_{(x_0,\theta_0),\varepsilon_0}$ of (7.141).

Using (7.1), (7.135), (7.137), (7.141) one can see that

$$\begin{aligned} P_{W_{(x_0,\theta_0),\varepsilon_0}} f(x,\theta) &= \int\limits_{\gamma(x,\theta)} W_{(x_0,\theta_0)}(\cdot,\theta) f \, d\sigma \\ &= \int\limits_{\gamma(x,\theta)} f \, d\sigma \; - \frac{\int\limits_{\gamma(x,\theta)} f \, d\sigma}{\int\limits_{\gamma(x,\theta)} f\psi_{(x_0,\theta_0)} \, d\sigma} \int\limits_{\gamma(x,\theta)} f\psi_{(x_0,\theta_0)} \, d\sigma = 0 \text{ for } (x,\theta) \in \Omega(\mathcal{J}_{r(x_0,\theta_0),\varepsilon_0}), \end{aligned} \tag{7.142}$$

where $\Omega(\cdot)$ is defined in (7.16), $d=2$, $\mathcal{J}_{r,\varepsilon}$ is defined in (7.20). Formula (7.81) follows from (7.142).

Lemma 2 is proved.

8 Proof of Lemma 3

Proof of (7.120)-(7.122)**.** Using (7.13), (7.46), (7.47), (7.78), (7.122) we obtain

$$G(x,\theta) = \widetilde{G}(r(x,\theta)) = \int\limits_{\gamma(x,\theta)} f(x)\,dx, \tag{7.143}$$

$$H_k(x,\theta) = \widetilde{H}_k(r(x,\theta)) = \int\limits_{\gamma(x,\theta)} f_k^2(x)\,dx, \tag{7.144}$$

$$\widetilde{f}_k(|x|) = \widetilde{f}_k((|x\theta|^2 + |x-(x\theta)\theta|^2)^{1/2}),\ (x,\theta) \in \Omega_0(1/2), \tag{7.145}$$

where $\Omega_0(\cdot)$ is defined in (7.14), $d=2$, $\gamma(x,\theta)$ is defined as in (7.24).

Formulas (7.77), (7.78), (7.143)-(7.145) imply (7.120)-(7.122).

Proof of (7.123)**.** Let

$$\Lambda_k = (1-2^{-k+3}, 1-2^{-k+1}),\ k \in \mathbb{N},\ k \geq 4. \tag{7.146}$$

From (7.73) it follows that, for $k \geq 4$:

$$\operatorname{supp} \psi_{k-1} \subset (1-2^{-k+2}, 1-2^{-k}), \tag{7.147}$$

$$\operatorname{supp} \psi_{k-2} \subset (1-2^{-k+3}, 1-2^{-k+1}) = \Lambda_k, \tag{7.148}$$

$$\operatorname{supp} \psi_{k-3} \subset (1-2^{-k+4}, 1-2^{-k+2}). \tag{7.149}$$

Due to (7.121), (7.122), (7.147)-(7.149), we have the following formula for U_0:

$$U_0(r,s) = 1 - \widetilde{G}(r)\left((k-1)!\widetilde{f}_{k-1}((s^2+r^2)^{1/2})\frac{\psi_{k-3}(r)}{\widetilde{H}_{k-1}(r)}\right.$$
$$+k!\widetilde{f}_k((s^2+r^2)^{1/2})\frac{\psi_{k-2}(r)}{\widetilde{H}_k(r)} \tag{7.150}$$
$$\left.+(k+1)!\widetilde{f}_{k+1}((s^2+r^2)^{1/2})\frac{\psi_{k-1}(r)}{\widetilde{H}_{k+1}(r)}\right) \text{ for } r\in\Lambda_k,\ s\in\mathbb{R},\ k\geq 4.$$

From (7.122), (7.150) it follows that

$$\frac{\partial^n U_0}{\partial s^n}(r,s) = -\widetilde{G}(r)\left((k-1)!\frac{\partial^n \widetilde{f}_{k-1}((s^2+r^2)^{1/2})}{\partial s^n}\frac{\psi_{k-3}(r)}{\widetilde{H}_{k-1}(r)}\right.$$
$$+k!\frac{\partial^n \widetilde{f}_k((s^2+r^2)^{1/2})}{\partial s^n}\frac{\psi_{k-2}(r)}{\widetilde{H}_k(r)} \tag{7.151}$$
$$\left.+(k+1)!\frac{\partial^n \widetilde{f}_{k+1}((s^2+r^2)^{1/2})}{\partial s^n}\frac{\psi_{k-1}(r)}{\widetilde{H}_{k+1}(r)}\right),$$

$$\frac{\partial^n \widetilde{G}}{\partial r^n}(r) = \int_{-\infty}^{+\infty}\frac{\partial^n}{\partial r^n}\widetilde{f}((s^2+r^2)^{1/2})\,ds,\ \frac{\partial^n \widetilde{H}_m}{\partial r^n}(r) = \int_{-\infty}^{+\infty}\frac{\partial^n}{\partial r^n}\widetilde{f}_m^2((s^2+r^2)^{1/2})\,ds, \tag{7.152}$$
$$r\in\Lambda_k,\ s\in\mathbb{R},\ m\geq 1,\ n\geq 0,\ k\geq 4,$$

where $\widetilde{G}$, $\widetilde{H}_m$ are defined in (7.122).

Using Lemma 1 and formulas (7.46), (7.47), (7.73)-(7.80), (7.122) one can see that:

$$\begin{aligned}&\widetilde{f},\ \widetilde{f}_{m-2},\ \widetilde{G},\ \widetilde{H}_m \text{ belong to } C_0^\infty(\mathbb{R}),\\ &\frac{\psi_{m-2}}{\widetilde{H}_m} \text{ belongs to } C_0^\infty((1/2,1)) \text{ for any } m\geq 3.\end{aligned} \tag{7.153}$$

From (7.151)-(7.153) it follows that $U_0(r,s)$ has continuous partial derivatives of all orders with respect to $r\in\Lambda_k$, $s\in\mathbb{R}$. It implies that $U_0\in C^\infty(\Lambda_k\times\mathbb{R})$. From the fact that Λ_k, $k\geq 4$, is an open cover of $(1/2,1)$ and from definition (7.121) of U_0, it follows that $U_0\in C^\infty(\{(1/2,1)\cup(1,+\infty)\}\times\mathbb{R})$.

This completes the proof of (7.123).

Proof of (7.125)**.** From (7.47)-(7.50) it follows that

$$\widetilde{f}_k(|x|) = 0 \text{ if } |x|\geq 1 \text{ for } k\in\mathbb{N}. \tag{7.154}$$

Formula $|x|^2 = |x\theta|^2 + |x-(x\theta)\theta|^2$, $x\in\mathbb{R}^2$, $\theta\in\mathbb{S}^1$, and formulas (7.121), (7.154) imply (7.125).

Proofs of (7.126)**-**(7.127)**.**

Lemma 4. *There are positive constants c, k_1 depending on Φ of* (7.48)-(7.50)*, such that*

(i) for all $k \in \mathbb{N}$ the following estimates hold:

$$|\widetilde{f}_k| \le 1, \tag{7.155}$$

$$|\widetilde{f}_k'| \le c8^k, \tag{7.156}$$

where $\widetilde{f}_k'$ denotes the derivative of $\widetilde{f}_k$ defined in (7.122).

(ii) for $k \ge k_1$ and $1/2 < r \le 1$ the following estimates hold:

$$\left|\frac{\psi_{k-2}(r)}{\widetilde{H}_k(r)}\right| \le c2^k, \tag{7.157}$$

$$\left|\frac{d}{dr}\left(\frac{\psi_{k-2}(r)}{\widetilde{H}_k(r)}\right)\right| \le c2^{5k}, \tag{7.158}$$

where ψ_k are defined in (7.73), *$\widetilde{H}_k$ is defined in* (7.122).

(iii) for $k \ge 3$ and $r \ge 1 - 2^{-k}$ the following estimates hold:

$$|\widetilde{G}(r)| \le c\frac{(2\sqrt{2})^{-k}}{k!}, \tag{7.159}$$

$$\left|\frac{d\widetilde{G}}{dr}(r)\right| \le c\frac{8^k}{k!}, \tag{7.160}$$

where $\widetilde{G}$ is defined in (7.122).

Lemma 5. *Let U_0 be defined by* (7.121)-(7.122). *Then the following estimates are valid:*

$$\left|\frac{\partial U_0}{\partial s}(r,s)\right| \le \frac{C}{(1-r)^3}, \left|\frac{\partial U_0}{\partial r}(r,s)\right| \le \frac{C}{(1-r)^5} \text{ for } r \in (1/2,1),\ s \in \mathbb{R}, \tag{7.161}$$

where C is a constant depending only on Φ of (7.48)-(7.50).

Lemmas 4, 5 are proved in Subsections 9.1, 9.2, respectively.

Proof of (7.126)**.** From (7.157), (7.159) it follows that

$$|\widetilde{G}(r)| \le c(2\sqrt{2})^{-k+3}/(k-3)!, \tag{7.162}$$

$$\left|\frac{\psi_{k-2}(r)}{\widetilde{H}_k(r)}\right| \le c2^k, \tag{7.163}$$

$$\text{for } r \in \Lambda_k,\ k \ge \max(4, k_1),$$

where Λ_k is defined in (7.146).

Properties (7.147)-(7.149) and estimate (7.157) imply that

$$\begin{cases} \psi_{k-1}(r) = 0, \\ \left|\dfrac{\psi_{k-3}(r)}{\widetilde{H}_{k-1}(r)}\right| \le c2^{k-1} \end{cases} \quad \text{if} \quad r \in (1-2^{-k+3}, 1-2^{-k+2}), \tag{7.164}$$

$$\begin{cases} \psi_{k-2}(r) = 0, \\ \left|\dfrac{\psi_{k-1}(r)}{\widetilde{H}_{k+1}(r)}\right| \le c2^{k+1} \end{cases} \quad \text{if} \quad r \in (1-2^{-k+2}, 1-2^{-k+1}), \tag{7.165}$$

$$\begin{cases} \psi_{k-1}(r) = 0, \\ \psi_{k-3}(r) = 0 \end{cases} \quad \text{if} \quad r = 1-2^{-k+2}, \tag{7.166}$$

for $k \geq \max(4, k_1)$.

Note that the assumption that $r \in \Lambda_k$ is splitted into the assumptions on r of (7.164), (7.165), (7.166).

Using formulas (7.150), (7.162)-(7.166), we obtain the following estimates:

$$\begin{aligned} |1 - U_0(r,s)| &= |\widetilde{G}(r)| \left| (k-1)! \widetilde{f}_{k-1}((s^2+r^2)^{1/2}) \frac{\psi_{k-3}(r)}{\widetilde{H}_{k-1}(r)} + k! \widetilde{f}_k((s^2+r^2)^{1/2}) \frac{\psi_{k-2}(r)}{\widetilde{H}_k(r)} \right| \\ &\leq c(2\sqrt{2})^{-k+3}(c(k-2)(k-1)2^{k-1} + c(k-2)(k-1)k2^k) \\ &\leq 2^5\sqrt{2}c^2 2^{-k/2}k^3 \quad \text{if} \quad r \in (1-2^{-k+3}, 1-2^{-k+2}), \end{aligned} \tag{7.167}$$

$$\begin{aligned} |1 - U_0(r,s)| &= |\widetilde{G}(r)| \left| k! \widetilde{f}_k((s^2+r^2)^{1/2}) \frac{\psi_{k-2}(r)}{\widetilde{H}_k(r)} + (k+1)! \widetilde{f}_{k+1}((p^2+r^2)^{1/2}) \frac{\psi_{k-1}(r)}{\widetilde{H}_{k+1}(r)} \right| \\ &\leq c(2\sqrt{2})^{-k+3}(c2^k(k-2)(k-1)k + c2^{k+1}(k-2)(k-1)k(k+1)) \\ &\leq 2^{10}\sqrt{2}c^2 2^{-k/2}k^4 \quad \text{if} \quad r \in (1-2^{-k+2}, 1-2^{-k+1}), \end{aligned} \tag{7.168}$$

$$\begin{aligned} |1 - U_0(r,s)| &= |\widetilde{G}(r)| \left| k! \widetilde{f}_k((s^2+r^2)^{1/2}) \frac{\psi_{k-2}(r)}{\widetilde{H}_k(r)} \right| \\ &\leq 2^4\sqrt{2}c^2 2^{-k/2}k^3 \quad \text{if} \quad r = 1-2^{-k+2}, \end{aligned} \tag{7.169}$$

for $s \in \mathbb{R}$, $k \geq \max(4, k_1)$. Estimates (7.167)-(7.169) imply that

$$|1 - U_0(r,s)| \leq C\, 2^{-k/2}k^4,\ r \in \Lambda_k,\ s \in \mathbb{R},\ k \geq \max(4, k_1), \tag{7.170}$$

where C is a positive constant depending on c of Lemma 4.

In addition, for $r \in \Lambda_k$ we have that $2^{-k+1} < (1-r) < 2^{-k+3}$, which together with (7.170) imply (7.126).

This completes the proof of (7.126).

Proof of (7.127)**.** We consider the following cases of s, s', r, r' in (7.127):

1. Let
$$s, s' \in \mathbb{R} \text{ and } r, r' \geq 1. \tag{7.171}$$
Due to (7.121) we have that
$$U_0(r,s) = 1,\ U_0(r',s') = 1. \tag{7.172}$$
Identities in (7.172) and assumption (7.171) imply (7.127) for this case.

2. Let
$$s, s' \in \mathbb{R}, 1/2 < r < 1 \text{ and } r' \geq 1. \tag{7.173}$$
Then, due to (7.121), (7.126) we have that
$$|1 - U_0(r,s)| \leq C(1-r)^{1/3}, \tag{7.174}$$
$$U_0(r',s') = 1, \tag{7.175}$$

where s, s', r, r' satisfy assumption (7.173), C is a constant depending only on Φ. In particular, inequality (7.174) follows from (7.126) due to the following simple property of the logarithm:

$$\log_2^a\left(\frac{1}{1-r}\right) \le C(a,\varepsilon)(1-r)^{-\varepsilon} \text{ for any } \varepsilon > 0,\ r \in [0,1),\ a > 0, \tag{7.176}$$

where $C(a,\varepsilon)$ is some positive constant depending only on a and ε.

Due to (7.173), (7.174), (7.175) we have that

$$\begin{aligned} |U_0(r',s') - U_0(r,s)| &= |1 - U_0(r,s)| \le C(1-r)^{1/3} \\ &\le C|r-r'|^{1/3} \le C(|r-r'|^{1/3} + |s-s'|^{1/3}), \end{aligned} \tag{7.177}$$

where C is a constant depending only on Φ.

Estimate (7.177) and assumptions (7.173) imply (7.127) for this case. Note that the case when $s, s' \in \mathbb{R}$, $1/2 < r' < 1$ and $r \ge 1$ is completely similar to (7.173).

3. Let

$$s, s' \in \mathbb{R} \text{ and } r, r' \in (1/2, 1). \tag{7.178}$$

In addition, without loss of generality we assume that $r > r'$.

Next, using (7.123) one can see that

$$\begin{aligned} |U_0(r,s) - U_0(r',s')| &= |U_0(r,s) - U_0(r,s') + U_0(r,s') - U_0(r',s')| \\ &\le |U_0(r,s) - U_0(r,s')| + |U_0(r,s') - U_0(r',s')| \\ &\le \left|\frac{\partial U_0}{\partial s}(r,\hat{s})\right| |s-s'| + \left|\frac{\partial U_0}{\partial r}(\hat{r},s')\right| |r-r'|, \end{aligned} \tag{7.179}$$

for $s, s' \in \mathbb{R}$, $r, r' > 1/2$, and for appropriate $\hat{s}$, $\hat{r}$.

Note that $\hat{s}, \hat{r}$ belong to open intervals $(s,s'), (r',r)$, respectively.

Using (7.126), (7.161), (7.174), (7.179) and the property that $1/2 < r' < \hat{r} < r < 1$ we obtain

$$|U_0(r,s) - U_0(r',s')| \le C((1-r)^{1/3} + (1-r')^{1/3}), \tag{7.180}$$

$$|U_0(r,s) - U_0(r',s')| \le \frac{C}{(1-r)^5}(|s-s'| + |r-r'|), \tag{7.181}$$

where C is a constant depending only on Φ.

We have that

$$\begin{aligned} (1-r)^{1/3} + (1-r')^{1/3} &= (1-r)^{1/3} + ((1-r) + (r-r'))^{1/3} \\ &\le 2(1-r)^{1/3} + |r-r'|^{1/3} \\ &\le \begin{cases} 3|r-r'|^{1/3} \text{ if } 1-r \le |r-r'|, \\ 3(1-r)^{1/3} \text{ if } 1-r > |r-r'|, \end{cases} \end{aligned} \tag{7.182}$$

where r, r' satisfy (7.178). Note that in (7.182) we used the following inequality:

$$(a+b)^{1/m} \le a^{1/m} + b^{1/m} \text{ for } a \ge 0,\ b \ge 0,\ m \in \mathbb{N}. \tag{7.183}$$

In particular, using (7.180), (7.182) we have that

$$|U_0(r,s) - U_0(r',s')|^{15} \le 3^{15} C^{15} (1-r)^5 \text{ if } 1-r > |r-r'|, \tag{7.184}$$

where s, s', r, r' satisfy assumption (7.178), C is a constant of (7.180), (7.181).

Multiplying the left and the right hand-sides of (7.181), (7.184) we obtain

$$|U_0(r,s) - U_0(r',s')|^{16} \le 3^{15} C^{16} (|s-s'| + |r-r'|), \text{ if } 1-r > |r-r'|. \tag{7.185}$$

Using (7.180), (7.182) we obtain

$$|U_0(r,s) - U_0(r',s')| \le 3C|r-r'|^{1/3}, \text{ if } 1-r \le |r-r'|, \tag{7.186}$$

where C is a constant of (7.180), (7.181) depending only on Φ. Using (7.185) and (7.183) for $m = 16$, $a = |s-s'|$, $b = |r-r'|$, we have that

$$|U_0(r,s) - U_0(r',s')| \le 3C(|s-s'|^{1/16} + |r-r'|^{1/16}), \text{ if } 1-r > |r-r'|, \tag{7.187}$$

where s, s', r, r' satisfy assumption (7.178), C is a constant of (7.180), (7.181) which depends only on Φ.

Formulas (7.186), (7.187) imply (7.127) for this case.

Note that assumptions (7.171), (7.173), (7.178) for cases 1, 2, 3, respectively, cover all possible choices of s, s', r, r' in (7.127).

This completes the proof of (7.127).

This completes the proof of Lemma 3.

9 Proofs of Lemmas 4, 5

9.1 Proof of Lemma 4

Proof of (7.155)**,** (7.156)**.** Estimates (7.155), (7.156) follow directly from (7.47)-(7.50).

Proof of (7.159)**.** We will use the following parametrization of the points y on $\gamma(x,\theta) \in T\mathbb{S}^1$, $(x,\theta) \in \Omega$, $r(x,\theta) \ne 0$ (see notations (7.12), (7.13), (7.24) for $d = 2$):

$$y(\beta) = x - (x\theta)\theta + \tan(\beta) r(x,\theta)\, \theta,\ \beta \in (-\pi/2, \pi/2), \tag{7.188}$$

where β is the parameter.

We have that:

$$d\sigma(\beta) = r\, d(\tan(\beta)) = \frac{r\, d\beta}{\cos^2 \beta},\ r = r(x,\theta), \tag{7.189}$$

where σ is the standard Lebesgue measure on $\gamma(x,\theta)$.

From definitions (7.46), (7.122) it follows that

$$\widetilde{G}(r) = \sum_{k=1}^{\infty} \frac{\widetilde{G}_k(r)}{k!}, \tag{7.190}$$

$$\widetilde{G}_k(r) = \int\limits_{\gamma_r} \widetilde{f}_k(|y|)\, dy,\ \gamma_r \in T(r),\ r > 1/2, \tag{7.191}$$

where $T(r)$ is defined by (7.19).

Using (7.47), (7.188), (7.189), (7.191) we obtain the following formula for $\widetilde{G}_k$:

$$\begin{aligned}
\widetilde{G}_k(r) &= r \int\limits_{-\pi/2}^{\pi/2} \Phi\left(2^k\left(1-\frac{r}{\cos\beta}\right)\right)\cos\left(8^k\frac{r^2}{\cos^2\beta}\right)\frac{d\beta}{\cos^2\beta} \\
&= \{u=\tan(\beta)\} = 2\,r\int\limits_0^{+\infty}\Phi\left(2^k\left(1-r\sqrt{u^2+1}\right)\right)\cos\left(8^k r^2(u^2+1)\right)\,du \\
&= \{t=u^2\} = r\int\limits_0^{+\infty}\Phi\left(2^k\left(1-r\sqrt{t+1}\right)\right)\cos\left(8^k r^2(t+1)\right)\frac{dt}{\sqrt{t}} \\
&= r\cos(8^k r^2)\int\limits_0^{+\infty}\Phi(2^k(1-r\sqrt{t+1}))\frac{\cos(8^k r^2 t)}{\sqrt{t}}dt \\
&- r\sin(8^k r^2)\int\limits_0^{+\infty}\Phi(2^k(1-r\sqrt{t+1}))\frac{\sin(8^k r^2 t)}{\sqrt{t}}dt \\
&= 8^{-k/2}r^{-1}\cos(8^k r^2)\int\limits_0^{+\infty}\Phi_k(t,r)\frac{\cos(t)}{\sqrt{t}}dt \\
&- 8^{-k/2}r^{-1}\sin(8^k r^2)\int\limits_0^{+\infty}\Phi_k(t,r)\frac{\sin(t)}{\sqrt{t}}dt,\ r>1/2,
\end{aligned} \tag{7.192}$$

where

$$\Phi_k(t,r) = \Phi(2^k(1-r\sqrt{8^{-k}r^{-2}t+1})),\ t\geq 0,\ r>1/2,\ k\in\mathbb{N}. \tag{7.193}$$

For integrals arising in (7.192) the following estimates hold:

$$\left|\int\limits_0^{+\infty}\Phi_k(t,r)\frac{\sin(t)}{\sqrt{t}}dt\right| \leq C_1 < +\infty, \tag{7.194}$$

$$\left|\int\limits_0^{+\infty}\Phi_k(t,r)\frac{\cos(t)}{\sqrt{t}}dt\right| \leq C_2 < +\infty, \tag{7.195}$$

$$\text{for } 1/2 < r < 1,\ k\geq 1.$$

where Φ_k is defined in (7.193), C_1, C_2 are some positive constants depending only on Φ and not depending on k and r.

Estimates (7.194), (7.195) are proved in Subsection 9.3.

From (7.192)-(7.195) it follows that

$$|\widetilde{G}_k(r)| \leq 2\cdot 8^{-k/2}(C_1+C_2) \text{ for } r>1/2,\ k\in\mathbb{N}. \tag{7.196}$$

Note that for $y\in\gamma_r$, the following inequality holds:

$$\begin{aligned}
&2^k(1-|y|)\leq 2^k(1-r)\leq 2^{k-m}\leq 1/2<4/5 \\
&\text{for } 1-2^{-m}\leq r<1,\ k<m,\ m\geq 3,
\end{aligned} \tag{7.197}$$

where γ_r is a ray in $T(r)$ (see notations of (7.19), $d = 2$).

Formulas (7.47), (7.48), (7.122), (7.197) imply that

$$\gamma_r \cap \operatorname{supp} f_k = \emptyset \text{ if } r \geq 1 - 2^{-m},\ k < m, \tag{7.198}$$

In turn, (7.191), (7.198) imply that

$$\widetilde{G}_k(r) = 0 \text{ for } r \geq 1 - 2^{-m},\ k < m,\ m \geq 3. \tag{7.199}$$

Due to (7.190), (7.191), (7.196), (7.199) we have that:

$$\begin{aligned} |\widetilde{G}(r)| &\leq \sum_{k=m}^{\infty} |\widetilde{G}_k(r)|/k! \\ &\leq 2(C_1 + C_2)\frac{(2\sqrt{2})^{-m}}{m!}\sum_{k=0}^{\infty}(2\sqrt{2})^{-k} = c_1\frac{(2\sqrt{2})^{-m}}{m!}, \\ c_1 &= (C_1 + C_2)\frac{4\sqrt{2}}{2\sqrt{2}-1}, \\ &\text{for } r \geq 1 - 2^{-m},\ m \geq 3. \end{aligned} \tag{7.200}$$

This completes the proof of estimate (7.159).

Proof of (7.160)**.** Using (7.190), (7.191) we have that:

$$\left|\frac{d\widetilde{G}}{dr}(r)\right| \leq \sum_{k=1}^{\infty}\frac{1}{k!}\left|\frac{d\widetilde{G}_k(r)}{dr}\right|. \tag{7.201}$$

Formulas (7.47), (7.152) for $n = 1$, (7.156), (7.191) imply that

$$\begin{aligned} \left|\frac{d\widetilde{G}_k}{dr}(r)\right| &= \left|\int_{-\infty}^{+\infty}\frac{r\widetilde{f}_k'((s^2+r^2)^{1/2})}{\sqrt{r^2+s^2}}\,ds\right| \\ &\leq \int_{-\infty}^{+\infty}|\widetilde{f}_k'((s^2+r^2)^{1/2})|\,ds = \int_{\gamma_r}|\widetilde{f}_k'(|y|)|\,dy \leq c8^k\int_{\gamma_r\cap B(0,1)}dy \leq 2c8^k, \end{aligned} \tag{7.202}$$

where $B(0,1)$ is defined in (7.27), $d = 2$.
At the same time, formula (7.199) implies that

$$\frac{d\widetilde{G}_k(r)}{dr} = 0 \text{ for } r \geq 1 - 2^{-m},\ k < m,\ m \geq 3. \tag{7.203}$$

Formulas (7.201), (7.202), (7.203) imply the following sequence of inequalities:

$$\left|\frac{d\widetilde{G}(r)}{dr}\right| \leq \sum_{k=m}^{\infty}\frac{1}{k!}\left|\frac{d\widetilde{G}_k(r)}{dr}\right| \leq c\frac{8^m}{m!}\sum_{k=0}^{\infty}\frac{m!8^k}{(k+m)!},\ r \geq 1 - 2^{-m},\ m \geq 3. \tag{7.204}$$

The series in the right hand-side in (7.204) admits the following estimate:

$$\sum_{k=0}^{\infty}\frac{m!8^k}{(k+m)!} \leq \sum_{k=0}^{\infty}\frac{8^k}{k!} = e^8 \text{ and the estimate does not depend on } m. \tag{7.205}$$

Formulas (7.204), (7.205) imply (7.160).

Proof of (7.157)**.** For each ψ_k from (7.73) we have that

$$|\psi_k| \le 1. \tag{7.206}$$

Therefore, it is sufficient to show that

$$\widetilde{H}_k \ge C2^{-k} \text{ for } k \ge k_1,\ C = c^{-1}. \tag{7.207}$$

Proceeding from (7.122) and in a similar way with (7.192) we obtain the formulas

$$\widetilde{H}_k(r) = r \int\limits_0^{+\infty} \frac{\Phi^2(2^k(1-r\sqrt{t+1}))}{\sqrt{t}} \cos^2(8^k r^2(t+1))\, dt = \widetilde{H}_{k,1}(r) + \widetilde{H}_{k,2}(r),\ r > 1/2, \tag{7.208}$$

$$\widetilde{H}_{k,1}(r) = \frac{r}{2} \int\limits_0^{+\infty} \frac{\Phi^2(2^k(1-r\sqrt{t+1}))}{\sqrt{t}}\, dt, \tag{7.209}$$

$$\widetilde{H}_{k,2}(r) = \frac{r}{2} \int\limits_0^{+\infty} \frac{\Phi^2(2^k(1-r\sqrt{t+1}))}{\sqrt{t}} \cos(2\cdot 8^k r^2(t+1))\, dt. \tag{7.210}$$

In addition, we have that:

$$\text{supp}_t \Phi^2(2^k(1-r\sqrt{t+1})) \subset [0,3] \text{ for } 1/2 < r \le 1-2^{-k+1},\ k \ge 3, \tag{7.211}$$

where supp_t denotes the support of the function in variable t. Property (7.211) is proved below in this paragraph (see formulas (7.213)-(7.216)).

Note that

$$2^k(1-r) \ge 2^k \cdot 2^{-k+1} \ge 2 > 6/5 \text{ for } 1/2 < r \le 1-2^{-k+1},\ k \ge 3. \tag{7.212}$$

From (7.48), (7.49) and from (7.212) we have that:

$$\text{supp}_t \Phi^2(2^k(1-r\sqrt{t+1})) \subset [0,+\infty) \text{ for } 1/2 < r \le 1-2^{-k+1},\ k \ge 3. \tag{7.213}$$

We have that

$$\begin{aligned}
&\exists t_1^{(k)} = t_1^{(k)}(r) \ge 0, t_2^{(k)} = t_2^{(k)}(r) \ge 0,\ t_2^{(k)} > t_1^{(k)}, \text{ such that} \\
&\begin{cases} 2^k(1-r\sqrt{t_1^{(k)}+1}) = 11/10, \\ 2^k(1-r\sqrt{t_2^{(k)}+1}) = 9/10, \end{cases} \qquad (7.214) \\
&|t_2^{(k)} - t_1^{(k)}| \ge \left(\sqrt{t_2^{(k)}+1} - \sqrt{t_1^{(k)}+1}\right) = \frac{2^{-k}}{5} r^{-1} \ge \frac{2^{-k}}{5}, \qquad (7.215) \\
&\text{for } 1/2 < r \le 1-2^{-k+1},\ k \ge 3.
\end{aligned}$$

In addition, from (7.214) it follows that

$$\begin{aligned}
&t_1^{(k)} = \frac{(1-2^{-k}\frac{11}{10})^2}{r^2} - 1 \le 4(1-2^{-k}\frac{11}{10})^2 - 1 \le 3, \\
&t_2^{(k)} = \frac{(1-2^{-k}\frac{9}{10})^2}{r^2} - 1 \le 4(1-2^{-k}\frac{11}{10})^2 - 1 \le 3, \\
&\text{for } 1/2 < r \le 1-2^{-k+1},\ k \ge 3.
\end{aligned} \tag{7.216}$$

Using (7.48)-(7.50), (7.209), (7.211), (7.214)-(7.216) we have that

$$\widetilde{H}_{k,1}(r) \geq \frac{r}{2}\int\limits_{t_1^{(k)}}^{t_2^{(k)}} \frac{dt}{\sqrt{t}} \geq \frac{r}{2}\int\limits_{1+t_1^{(k)}}^{1+t_2^{(k)}} \frac{dt}{\sqrt{t}}$$
$$\geq r(\sqrt{t_2^{(k)}+1}-\sqrt{t_1^{(k)}+1}) \geq \frac{2^{-k}}{10} \text{ for } 1/2 < r \leq 1-2^{-k+1},\ k \geq 3. \tag{7.217}$$

On the other hand, proceeding from using (7.210) and, in a similar way with (7.192)-(7.196), we have

$$\begin{aligned}
|\widetilde{H}_{k,2}(r)| &= \frac{r}{2}\left|\int\limits_0^{+\infty} \frac{\Phi^2(2^k(1-r\sqrt{t+1}))}{\sqrt{t}}\cos(2\cdot 8^k r^2(t+1))\,dt\right| \\
&\leq \frac{r}{2}|\cos(2\cdot 8^k r^2)|\left|\int\limits_0^{+\infty}\Phi^2(2^k(1-r\sqrt{t+1}))\frac{\cos(2\cdot 8^k r^2 t)}{\sqrt{t}}dt\right| \\
&+ \frac{r}{2}|\sin(2\cdot 8^k r^2)|\left|\int\limits_0^{+\infty}\Phi^2(2^k(1-r\sqrt{t+1}))\frac{\sin(2\cdot 8^k r^2 t)}{\sqrt{t}}dt\right| \\
&\leq 8^{-k/2}\frac{r^{-1}}{2}\left|\int\limits_0^{+\infty}\Phi_k^2(t,r)\frac{\cos(2t)}{\sqrt{t}}dt\right| + 8^{-k/2}\frac{r^{-1}}{2}\left|\int\limits_0^{+\infty}\Phi_k^2(t,r)\frac{\sin(2t)}{\sqrt{t}}dt\right| \\
&\leq 8^{-k/2}C, \text{ for } 1/2 < r < 1-2^{-k+1},\ k \geq 3,
\end{aligned} \tag{7.218}$$

where $\Phi_k(t,r)$ is defined in (7.193), C is some constant depending only on Φ and not depending on k, r. In (7.218) we have also used that $\Phi^2(t)$ satisfies assumptions (7.48)-(7.50).

Note also that $\Phi^2(t)$ satisfies assumptions (7.48)-(7.50) for $\Phi(t)$.

Using (7.208)-(7.210), (7.217), (7.218) we obtain

$$\begin{aligned}
|\widetilde{H}_k(r)| &\geq |\widetilde{H}_{k,1}(r)| - |\widetilde{H}_{k,2}(r)| \\
&\geq \frac{2^{-k}}{10} - C'\cdot 8^{-k/2} \\
&\geq 2^{-k}\left(\frac{1}{10} - \frac{C'}{(\sqrt{2})^k}\right) \\
&\geq C\cdot 2^{-k} \text{ for } 1/2 < r < 1-2^{-k+1},\ k \geq k_1 \geq 3, \\
C &= \frac{1}{10} - C'(\sqrt{2})^{-k_1},
\end{aligned} \tag{7.219}$$

where C' depends only on Φ, k_1 is arbitrary constant such that $k_1 \geq 3$ and C is positive.

Formulas (7.157) follows from (7.73), (7.219).

This completes the proof (7.157).

Proof of (7.158)**.** The following formula holds:

$$\frac{d}{dr}\left(\frac{\psi_{k-2}(r)}{\widetilde{H}_k(r)}\right) = -\frac{\widetilde{H}_k'(r)\psi_{k-2}(r) - \widetilde{H}_k(r)\psi_{k-2}'(r)}{\widetilde{H}_k^2(r)},\ 1/2 < r < 1, \tag{7.220}$$

where $\widetilde{H}_k'$, ψ_{k-2}' denote the derivatives of $\widetilde{H}_k$, ψ_k, defined in (7.122), (7.73), respectively.

Using (7.47), (7.122), (7.152), $n = 1$, (7.155), (7.156) we have that

$$|\widetilde{H}_k'(r)| = 2\left|\int\limits_{-\infty}^{+\infty} \frac{r}{\sqrt{r^2+s^2}}\widetilde{f}_k(\sqrt{r^2+s^2})\widetilde{f}_k'(\sqrt{r^2+s^2})\,ds\right|$$
$$\leq 2\int\limits_{-\infty}^{+\infty}\left|\widetilde{f}_k(\sqrt{r^2+s^2})\widetilde{f}_k'(\sqrt{r^2+s^2})\right|\,ds = 2\int\limits_{\gamma_r}|\widetilde{f}_k(|y|)\widetilde{f}_k'(|y|)|\,dy \tag{7.221}$$
$$\leq 2c8^k\int\limits_{\gamma_r\cap B(0,1)} dy \leq 4c8^k,\ \gamma_r \in T(r),\ k \geq 3,\ r > 1/2,$$

where we use notations (7.19), (7.27), $d = 2$.

Using (7.73), (7.74), (7.157), (7.219)-(7.221) we have that

$$\left|\frac{d}{dr}\left(\frac{\psi_{k-2}(r)}{\widetilde{H}_k(r)}\right)\right| \leq C2^{2k}(|\widetilde{H}_k'(r)| + |\widetilde{H}_k(r)|\cdot|\psi_k'(r)|) \leq C'2^{5k}, \tag{7.222}$$
$$\text{for } 1/2 < r < 1 - 2^{-k+1},\ k \geq k_1 \geq 3,$$

where C' is a constant not depending on k and r and depending only on Φ.

This completes the proof of Lemma 4.

9.2 Proof of Lemma 5

It is sufficient to show that

$$\left|\frac{\partial U_0(r,s)}{\partial s}\right| \leq \frac{C}{(1-r)^3}, \tag{7.223}$$
$$\left|\frac{\partial U_0(r,s)}{\partial r}\right| \leq \frac{C}{(1-r)^5}, \tag{7.224}$$
$$\text{for } s \in \mathbb{R},\ r \in \Lambda_k,\ k \geq \max(4, k_1),$$

where C is a positive constant depending only on Φ of (7.47), Λ_k is defined in (7.146), k_1 is a constant arising in Lemma 4 and depending only on Φ.

Indeed, estimates (7.161) follow from (7.123), (7.223), (7.224) and the fact that Λ_k, $k \geq 4$, is an open cover of $(1/2, 1)$.

In turn, estimates (7.223), (7.224) follow from the estimates

$$\left|\frac{\partial U_0(r,s)}{\partial s}\right| \leq C\cdot 8^k, \tag{7.225}$$
$$\left|\frac{\partial U_0(r,s)}{\partial r}\right| \leq C\cdot (32)^k, \tag{7.226}$$
$$\text{for } s \in \mathbb{R},\ r \in \Lambda_k,$$

and from the fact that $2^{-k+1} < 1 - r < 2^{-k+3}$, $k \geq \max(4, k_1)$, for $r \in \Lambda_k$, where C is a positive constant depending only on Φ.

Estimate (7.225) follows from formula (7.151) for $n = 1$ and estimates (7.156), (7.157), (7.162)-(7.166).

Estimate (7.226) follows from (7.150), (7.155)-(7.158), (7.162)-(7.166) and from the estimates:

$$\left|\frac{d}{dr}\left(\frac{\psi_{k-i}(r)}{\widetilde{H}_{k-i+2}(r)}\right)\right| \le c2^{5(k+1)}, \tag{7.227}$$

$$\left|\frac{d\widetilde{G}(r)}{dr}\right| \le c\frac{8^{-k+3}}{(k-3)!}, \tag{7.228}$$

$$\text{for } r \in \Lambda_k,\ i \in \{1,2,3\},$$

where c is a constant arising in Lemma 4.

Estimate (7.227) follows from (7.158) (used with $k-1$, k, $k+1$ in place of k). Estimate (7.228) follows from (7.160) (used with $k-3$ in place of k).

This completes the proof of Lemma 5.

9.3 Proof of estimates (7.194), (7.195)

We use the following Bonnet's integration formulas (see, e.g., [Fic59], Chapter 2):

$$\int_a^b f_1(t)h(t)\,dt = f_1(a)\int_a^{\xi_1} h(t)\,dt, \tag{7.229}$$

$$\int_a^b f_2(t)h(t)\,dt = f_2(b)\int_{\xi_2}^b h(t)\,dt, \tag{7.230}$$

for some appropriate ξ_1, $\xi_2 \in [a,b]$, where

$$\begin{aligned} &f_1 \text{ is monotonously decreasing on } [a,b],\ f_1 \ge 0,\\ &f_2 \text{ is monotonously increasing on } [a,b],\ f_2 \ge 0,\\ &h(t) \text{ is integrable on } [a,b]. \end{aligned} \tag{7.231}$$

Let

$$g_1(t) = \frac{\sin(t)}{\sqrt{t}},\ g_2(t) = \frac{cos(t)}{\sqrt{t}},\ t > 0, \tag{7.232}$$

$$G_1(s) = \int_0^s \frac{\sin(t)}{\sqrt{t}}\,dt,\ G_2(s) = \int_0^s \frac{\cos(t)}{\sqrt{t}}\,dt,\ s \ge 0. \tag{7.233}$$

We recall that

$$\lim_{s\to+\infty} G_1(s) = \lim_{s\to+\infty} G_2(s) = \sqrt{\frac{\pi}{2}}. \tag{7.234}$$

From (7.232), (7.233), (7.234) it follows that

$$G_1, G_2 \text{ are continuous and bounded on } [0,+\infty). \tag{7.235}$$

Due to (7.48)-(7.51), (7.193) and monotonicity of the function $2^k(1 - r\sqrt{8^{-k}r^{-2}t+1})$ in t on $[0,+\infty)$ it follows that

$$\Phi_k(t,r) \text{ is monotonously decreasing on } [0,+\infty),\ \text{if } 2^k(1-r) \le 11/10, \tag{7.236}$$

$$\begin{aligned} &\Phi_k(t,r) \text{ is monotonously increasing on } [0,t_0] \text{ for some } t_0 > 0\\ &\quad \text{and is monotonously decreasing on } [t_0,+\infty),\ \text{if } 2^k(1-r) > 11/10. \end{aligned} \tag{7.237}$$

$$\text{for } r > 1/2,\ k \in \mathbb{N},$$

Moreover, due to (7.48)-(7.50), (7.193), for $T_k = 8^k$, $k \in \mathbb{N}$, we have that

$$\Phi_k(T_k, r) = \Phi(2^k(1 - r\sqrt{r^{-2}+1})) = \Phi(2^k(1-\sqrt{1+r^{-2}})) = 0, \tag{7.238}$$

$$\Phi_k(t, r) = 0 \text{ for } t \geq T_k, \tag{7.239}$$

$$|\Phi_k(t, r)| \leq 1 \text{ for } t \geq 0, \tag{7.240}$$

$$r > 1/2,\ k \in \mathbb{N}.$$

Using (7.193), (7.232)-(7.237), (7.239) and (7.229)-(7.231) we obtain

$$\int_0^{+\infty} \Phi_k(t,r) g_i(t)\,dt = \int_0^{T_k} \Phi_k(t,r) g_i(t)\,dt = \Phi_k(0,r) \int_0^{\xi} g_i(t)\,dt \tag{7.241}$$

$$= \Phi_k(0,r) G_i(\xi) \text{ for appropriate } \xi \in [0, T_k],\ \text{if } 2^k(1-r) \leq 11/10,$$

$$\int_0^{\infty} \Phi_k(t,r) g_i(t)\,dt = \int_0^{T_k} \Phi_k(t,r) g_i(t)\,dt = \int_0^{t_0} \Phi_k(t,r) g_i(t)\,dt + \int_{t_0}^{T_k} \Phi_k(t,r) g_i(t)\,dt$$

$$= \Phi_k(t_0,r) \int_{\xi'}^{t_0} g_i(t)\,dt + \Phi_k(t_0,r) \int_{t_0}^{\xi''} g_i(t)\,dt$$

$$= \Phi_k(t_0,r)(G_i(\xi'') - G_i(\xi')) \tag{7.242}$$

$$\text{for appropriate } \xi' \in [0, t_0],\ \xi'' \in [t_0, T_k],\ \text{if } 2^k(1-r) > 11/10,$$

where $i = \overline{1,2}$.

Estimates (7.194), (7.195) follow from (7.232), (7.233), (7.235), (7.240)-(7.242).

Bibliography

[ABK98] Arbuzov, E.V., Bukhgeim, A.L., Kazantsev, S. G., Two-dimensional tomography problems and the theory of A-analytic functions. *Siberian Adv. Math.*, 8:1-20, 1998.

[Ba09] Bal, G., Inverse transport theory and applications. *Inverse Problems*, 25(5), 053001 (48pp), 2009.

[BJ11] G. Bal, A. Jollivet, Combined source and attenuation reconstructions in SPECT. *Tomography and Inverse Transport Theory, Contemp. Math.*, 559, 13-27, 2011.

[Be84] Beylkin, G., The inversion problem and applications of the generalized Radon transform. *Communications on pure and applied mathematics*, 37(5):579-599, 1984.

[BQ87] Boman, J., Quinto, E.T., Support theorems for real-analytic Radon transforms. *Duke Mathematical J.*, 55(4):943-948, 1987.

[BQ93] Boman, J., Quinto, E. T., Support theorems for Radon transforms on real analytic line complexes in three-space. *Trans. Amer. Math. Soc.*, 335(2):877-890, 1993.

[Bo93] Boman, J., An example of non-uniqueness for a generalized Radon transform. *Journal d'Analyse Mathematique*, 61(1):395–401, 1993.

[BS04] Boman, J., Strömberg, J.-O., Novikov's inversion formula for the attenuated Radon transform—a new approach, *The Journal of Geometric Analysis*, 14(2): 185-198, 2004.

[Co64] Cormack, A.M., Representation of a function by its line integrals, with some radiological applications I, II. *J. Appl. Phys.* 34:2722–2727; 35:2908–2912, 1963-1964.

[MD92] Do Carmo, M. P., Riemannian Geometry. Birkhäuser Basel, 1992.

[Fic59] Fichtenholz, G.M., A course of differential and integral calculus, volume II, Moscow, 1959.

[Fi86] Finch, D., Uniqueness for the attenuated X-ray transform in the physical range. *Inverse Problems* 2(2), 1986.

[GGG82] Gel'fand, I. M., Gindikin, S. G., Graev, M. I., Integral geometry in affine and projective spaces. *Journal of Soviet Mathematics*, 18(2):39–167, 1982.

[Gi10] Gindikin, S., A remark on the weighted Radon transform on the plane. *Inverse Problems and Imaging*, 4(4):649-653, 2010.

[GN18] Goncharov F.O., Novikov, R.G. An example of non-uniqueness for Radon transforms with continuous positive rotation invariant weights. *The Journal of Geometric Analysis* 28(4): 3807-3828, 2018.

[He01] Helgason, S., Differential geometry and symmetric spaces. American Mathematical Soc., volume 341, 2001.

[Il16] Ilmavirta, J., Coherent quantum tomography. *SIAM Journal on Mathematical Analysis*, 48(5):3039–3064, 2016.

[Jo38] John, F., The ultrahyperbolic differential equation with 4 independent variables. *Duke Math. J.*, 4:300–322, 1938.

[KLM95] Kuchment, P., Lancaster, K., Mogilevskaya L., On local tomography. *Inverse Problems*, 11(3):571-589, 1995.

[Ku92] Kunyansky, L., Generalized and attenuated Radon transforms: restorative approach to the numerical inversion. *Inverse Problems*, 8(5):809-819, 1992.

[LB73] Lavrent'ev, M. M., Bukhgeim, A. L., A class of operator equations of the first kind. *Functional Analysis and Its Applications*, 7(4):290-298, 1973.

[MQ85] Markoe, A., Quinto, E.T., An elementary proof of local invertibility for generalized and attenuated Radon transforms. *SIAM Journal on Mathematical Analysis*, 16(5):1114–1119, 1985.

[Na01] Natterer, F., The Mathematics of Computerized Tomography. SIAM, 2001.

[Ng17] Nguyen, L. V., On the strength of streak artifacts in filtered back-projection reconstructions for limited angle weighted X-ray transform. *J. Fourier Anal. Appl.*, 23(3):712–728, 2017.

[No02a] Novikov, R.G., On determination of a gauge field on $\mathbb{R}^d$ from its non-abelian Radon transform along oriented straight lines. *Journal of the Institute of Mathematics of Jussieu*, 1(4), 559-629., 2002.

[No02b] Novikov, R.G., An inversion formula for the attenuated X-ray transformation. *Arkiv för matematik*, 40(1):145-167, 2002.

[No14] Novikov, R.G., Weighted Radon transforms and first order differential systems on the plane. *Moscow Mathematical Journal*, 14(4):807–823, 2014.

[Pa96] Palamodov, V.P., An inversion method for an attenuated x-ray transform. *Inverse Problems*, 12(5):717-729, 1996.

[PG13] Puro, A., Garin, A., Cormack-type inversion of attenuated Radon transform, *Inverse Problems*, 29(6), 065004 (14pp), 2013.

[Ra17] Radon, J., Uber die Bestimmung von Funktionen durch ihre Integralwerte längs gewisser Mannigfaltigkeiten. *Ber. Saechs Akad. Wiss. Leipzig, Math-Phys*, 69:262–267, 1917.

[Sh92] Sharafutdinov, V. A., On the problem of emission tomography for non-homogeneous media. *Dokl. Akad. Nauk.* 326:446-448, 1992 (Russian). English transl.: *Soviet Phys. Dokl.* 37: 469-470, 1992.

[Sh93] Sharafutdinov, V. A., Uniqueness theorems for the exponential X-ray transform. *Journal of Inverse and Ill-Posed Problems*, 1(4):355-372, 1993.

[TM80] Tretiak O.J., Metz, C., The exponential Radon transform. *SIAM J. Appl. Math.*, 39:341-354, 1980.

[Qu83] Quinto, E.T., The invertibility of rotation invariant Radon transforms. *Journal of Mathematical Analysis and Applications*, 91(2):510–522, 1983.

université PARIS-SACLAY | École doctorale de mathématiques Hadamard (EDMH)

Titre : Transformations de Radon pondérées et leurs applications

Mots Clefs : problèmes inverses, tomographie, transforamtions de Radon, géometrie integrale, analyse numérique

Résumé : Cette thèse est consacrée à l'étude des problèmes inverses des transformations de Radon pondérées dans les espaces euclidiens. D'une part, nos études sont motivées par l'application des transformations de Radon pondérées pour différentes tomographies, par exemple en tomographie d'émission (PET, SPECT), en tomographie de fluorescence et en tomographie optique. En particulier, nous développons une nouvelle approche de reconstruction pour les tomographies en 3D, où les données sont modélisées par des transformations des rayons pondérées le long des rayons parallèles à un plan fixe. A cet égard, nos résultats contiennent : des formules pour la réduction des transformées des rayons pondérées en transformées de Radon le long de plans en 3D ; un analogue de la formule d'inversion approximative de Chang et un analogue de l'algorithme d'inversion itératif de type Kunyansky pour les transformations de Radon pondérées en multidimension ; des reconstructions numériques à partir de données simulées et réelles. D'autre part, nos études sont motivées par des problèmes mathématiques liés aux transformations susmentionnées. Plus précisément, nous poursuivons l'étude de l'injectivité et de la non-injectivité des transformations de Radon et des transformations des rayons pondérées en multidimension et construisons une série de contre-exemples à l'injectivité de ces dernières. Ces contre-exemples sont intéressants et, dans un certain sens, inattendus parce qu'ils sont proches des cas où ces transformations deviennent injectives. En particulier, par l'une des nos constructions, nous donnons des contre-exemples à des théorèmes d'injectivité bien connus pour les transformations des rayons pondérées (Quinto (1983), Markoe, Quinto (1985), Finch (1986), Ilmavirta (2016)) lorsque les hypothèses de régularité des poids sont légèrement relaxées. Par ce résultat, nous montrons en particulier que les hypothèses de régularité sur les poids sont cruciales pour l'injectivité et qu'il y a une "brisure" de cette dernière si les hypothèses sont légèrement affaiblies.

Title : Weighted Radon transforms and their applications

Keys words : inverse problems, tomography, Radon transforms, integral geometry, numerical analysis

Abstract : This thesis is devoted to studies of inverse problems for weighted Radon transforms in euclidean spaces. On one hand, our studies are motivated by applications of weighted Radon transforms in different tomographies, for example, in emission tomographies (PET, SPECT), fluorescence tomography and optical tomography. In particular, we develop a new reconstruction approach for tomographies in 3D, where data are modeled by weighted ray transforms along rays parallel to some fixed plane. In this connection our results include : formulas for reduction of the aforementioned weighted ray transforms to weighted Radon transforms along planes in 3D ; an analog of Chang approximate inversion formula and an analog of Kunyansky-type iterative inversion algorithm for weighted Radon transforms in multidimensions ; numerical reconstructions from simulated and real data. On the other hand, our studies are motivated by mathematical problems related to the aforementioned transforms. More precisely, we continue studies of injectivity and non-injectivity of weighted ray and Radon transforms in multidimensions and we construct a series of counterexamples to injectivity for the latter. These counterexamples are interesting and in some sense unexpected because they are close to the setting when the corresponding weighted ray and Radon transforms become injective. In particular, by one of our constructions we give counterexamples to well-known injectivity theorems for weighted ray transforms (Quinto (1983), Markoe, Quinto (1985), Finch (1986), Ilmavirta (2016)) when the regularity assumptions on weights are slightly relaxed. By this result we show that, in particular, the regularity assumptions on weights are crucial for the injectivity and there is a breakdown of the latter if the assumptions are slightly relaxed.

Université Paris-Saclay
Espace Technologique / Immeuble Discovery
Route de l'Orme aux Merisiers RD 128 / 91190 Saint-Aubin, France